UNIVERSITY OF OKLAHOMA

GRADUATE COLLEGE

NONLINEAR DYNAMIC FINITE ELEMENT ANALYSIS OF STEEL FRAMES WITH SEMI-RIGID JOINTS

A DISSERTATION

SUBMITTED TO THE GRADUATE FACULTY

In partial fulfillment of the requirements for the

degree of

DOCTOR OF PHILOSOPHY

By

ALI ABOLMAALI

Norman, Oklahoma

1999

UMI Number: 9940293

NONLINEAR DYNAMIC FINITE ELEMENT ANALYSIS OF

STEEL FRAMES WITH SEMI-RIGID JOINTS

A DISSERTATION

APPROVED FOR THE SCHOOL OF CIVIL ENGINEERING

AND ENVIRONMENTAL SCIENCE

BY

A. R. Umberti

Benjamin Wallace

K. K. Muraleetharan

Luther White

[illegible]

Dedicated to:

My Teacher, Mentor, and Friend

Anant R. Kukreti

ACKNOWLEDGEMENTS

The author wishes to express his gratitude and appreciation to his teacher, mentor, and his sole graduate advisor throughout his graduate studies, Presidential Professor Anant R. Kukreti. Professor Kukreti, as an advisor and a friend, was available at all the times during this study, and he patiently educated the author for which he is thankful. Professor Kukreti's continuous support from the start to the end of this program will be remembered throughout the author's life. Without his knowledge, encouragement, and leadership, the completion of this study would have not been possible.

The author wishes to express his sincere gratitude to Professor Benjamin Wallace for his invaluable help in all phases of this study. The author would like to particularly thank him for the guidance he provided in the design and fabrication of the testing facilities. He was always available when troubles arose during testing. Special thanks also go to him to serve as a second reader of this dissertation.

Special thanks goes to Professor Luther White for his help and support during this study. His input during the development of mathematical models of this research was very valuable. The author also wishes to sincerely thank Professor Muraleetharan for his expert advise in the area of nonlinear dynamics. The author wishes to express his special appreciation to Professor Civan for accepting to serve in this committee at a short notice. His professionalism and understanding will be greatly remembered.

Special appreciation goes to Professor Thomas Bush for his expert opinions in interpretation of experimental results. The input, help, and encouragement provided by Professor N.C. Singhal of University of Rookee, India during his one-year stay at the University of Oklahoma will be remembered.

The author wishes to thank Mr. Mike Schmitz, the research and design technologist for the Fears Structural Engineering Laboratory, for his expertise and help in the experimental phase of this research.

Finally, the author is thankful to Mrs. Susan Wierimaa for her skillful typing of the final draft of this dissertation.

TABLE OF CONTENTS

LIST OF FIGURES

FIGURE **Page**

LIST OF TABLES

ABSTRACT

In this study a nonlinear dynamic analysis computer program for planar steel frames with semi-rigid connections is developed. The semi-rigid connections are modeled as a massless rotational spring element. This element has two nodes, one connected to the beam end, and the other to the column end. Its hysteresis behavior, under cyclic loads, is expressed by a moment-rotation relationship.

In order to develop rational moment rotation relationships, a total of 55 full-scale different types of commonly used semi-rigid connection specimens were tested to record their moment-rotation behavior under cyclic loads. These included double web angle (all bolted, and welded to beam web and bolted to column flange), top and seat angle, flush end-plate, and extended end-plate connections. Description of the test specimens fabricated, equipment used, and testing procedure are presented in detail. The failure modes observed are reported, which include either excessive rotation of the connection due to yielding or bolt fracture. Some of the all bolted double web angle connections failed due to beam web bearing failure. The moment-rotation hysteresis behavior of all connections was found to be nonlinear in nature.

To analytically describe this behavior for use in the computer program, the actual moment-rotation behavior was idealized by piecewise linear segments. For connections which failed due to either excessive connection rotation or bolt fracture, three types of linear segment models were constructed for each connection specimen tested. These included the elasto-plastic, bilinear, and modified bilinear models. These models differ in complexity and the way in which the connection yield moment is defined. In the elasto-plastic model, yielding in the connection is assumed to occur when the ultimate moment capacity (M_u) is reached, and then it is assumed to behave perfectly plastic until the ultimate rotation (θ_u) is reached. The bilinear model uses the transition moment (M_t) as the connections yield moment, which is defined as the moment at the intersection of the tangent drawn from the ultimate point, with coordinates (M_u, θ_u), to the peaks of the hysteresis loops in the first quadrant and the line of the initial stiffness (K_e). The modified bilinear model uses the characteristic moment (M_c) as the connection's yield moment, which is obtained by fitting a Ramberg-Osgood function to the experimental enveloping curve. This curve is defined as the curve passing through the peaks of the moment-rotation loops in the first quadrant, i.e., the loading portion. Comparing the experimental moment-rotation hysteresis loops recorded to those predicted by the analytical models, it is found that the modified bilinear model best idealized the behavior; however the elasto-plastic model is easiest to construct. For all bolted double web angle connections which failed due to beam web failure, a separate trilinear model is suggested.

In the dynamic analysis procedure presented, a Newton-Raphson iterative procedure is used to march along the moment-rotation curve for each connection spring element, and the dynamic equations of motion are solved using the constant acceleration method. No damping is considered in the analytical formulation, though due to the hysteresis behavior of the connection there will be some inherent damping. The computer program is shown to predict convergent solutions as the time step is refined to iteratively march the solution in the time domain. To further verify the computer program developed, results of a parametric study are also presented which investigate the effects of the connection moment-rotation model parameters, type of hysteresis model used, and different earthquake records on the sway response history of a frame. Actually, the dynamic computer program was an extension of a static analysis computer program developed for planar frames with semi-rigid connections. Details of this program are presented first. In this formulation the monotonic (static) moment-rotation behavior of the semi-rigid connection is modeled by an exponential function, and geometric nonlinearity (P-Δ effects) of the frame members is considered.

CHAPTER I

INTRODUCTION

1.1 General

Semi-rigid connections in steel frame structures have been in various phases of development for over 45 years. As the twentieth century draws to an end, semi-rigid connections appear to be at the genesis of utilization. It is believed that within the next few years there will be an international explosion of new uses and innovative applications of the semi-rigid approach. Today, there is a massive growing network of technology dedicated to an understanding of the influence of connections on the overall performance and stability of steel structures.

Conventional analysis and design of steel structures consider the actual behavior of a beam-to-column connection as either a rigid-joint or pinned-joint. In a perfectly rigid-joint, the full transfer of moment is assumed to occur between connected members, and the connection is modeled to rotate as a rigid body. In a pinned-joint, on the other hand, the joint is assumed to act as a frictionless hinge with no moment acting on the connection. In reality however, bolted connections are neither perfectly pinned nor totally rigid. In fact most connections exhibit semi-rigid deformation behavior that can contribute substantially to overall frame deflection (sway), and also to the internal force distribution in the connected members. The American Institute of Steel Construction (AISC) Load Resistance Factor Design (LRFD) Manual of Steel Construction (1994) defines the following three types of frame connections:

1. **Type I connection**, or " rigid" connection. A connection that exhibits greater than 90% rigidity is usually classified as a rigid connection, in which total transfer of moment from beam to column is assumed in the frame analysis.

2. **Type II construction**, or "simple" connection. In these types of connections, it is assumed that rigidity is less than 20% and hence, no transfer of moment from beam to column is assumed in the frame analysis.

3. **Type III construction**, or "semi-rigid" connection. The connections of these types offer some restraint between the members they connect and the moment between the beam and the column depend on the rotational stiffness of the connection. The rigidity of these connections varies over a wide range: 20 to 90% of fixity.

Figure 1.1 presents the monotonic (static) moment-rotation curves for a variety of commonly used semi-rigid connections. As it can be noticed, the single web-angle connection behaves as the most flexible connection and could be considered as pinned joint. On the other side is the T-stub connection, which is considered as the stiffest bolted connection and has a behavior that can be described as a rigid joint. In either case the moment-rotation relationship is nonlinear. Indeed, this nonlinear

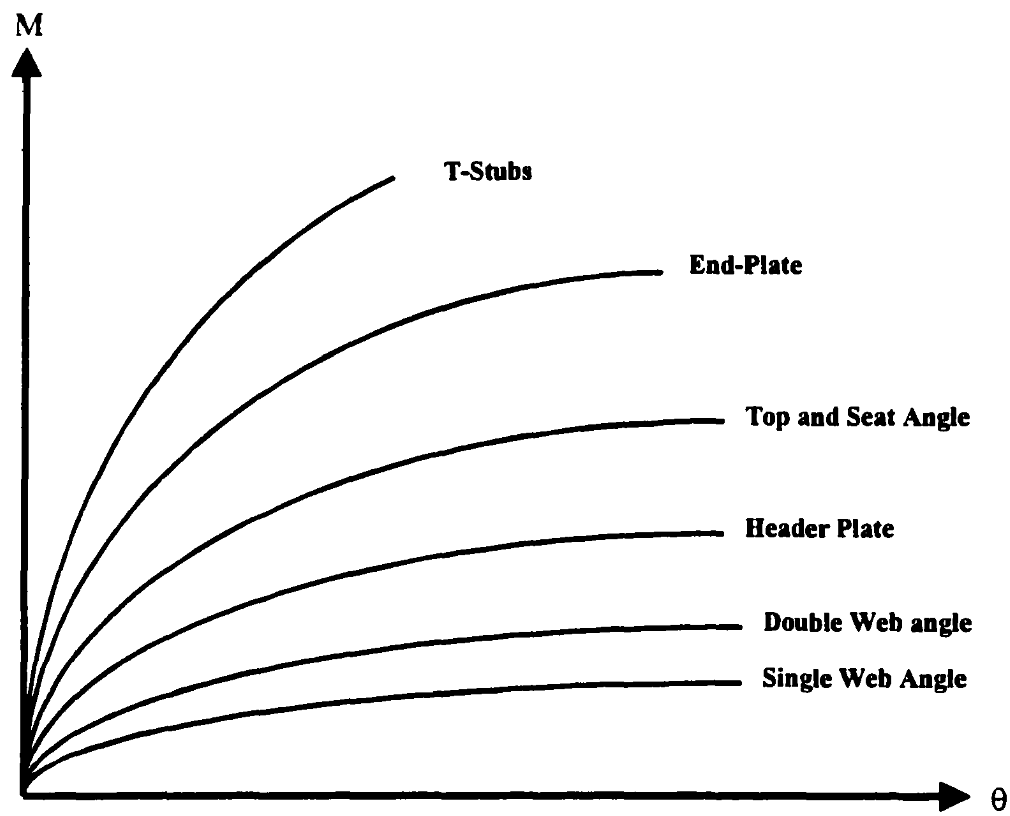

Fig. 1.1 Monotonic Moment–Rotation Curves of Typical Semi-Rigid Connections

behavior for certain types of connections, start at a very early stage of loading. Hence any analysis technique for frames with flexible joints calls for nonlinear analysis procedures, in which the nonlinear moment-rotation behavior for semi-rigid connections is treated as a classical material nonlinear problem. The AISC LRFD Manual of Steel Construction (1994) requires P-Delta analysis for steel building frames of Type III construction. (i.e., semi-rigid connections). The P-Delta analysis is a classical member geometric nonlinear problem, which needs to be coupled with the material nonlinearity of the connection, and that leads to a coupled nonlinear analysis procedure. Therefore, any static or dynamic analysis for frames with flexible joints, requires a coupled material (springs) and geometric (members) nonlinear frame analysis algorithm, which has been presently ignored by practitioners. In this research, it is intended to introduce such a coupled nonlinear procedure for static and dynamic analyses of steel frames with semi-rigid joints which make use of static and dynamic moment-rotation curves and hysteresis loops, respectively. Figure 1.2 shows typical static moment-rotation curve (Fig. 1.2 (a)) and cyclic moment moment-rotation hysteresis loops (Fig. 1.2 (b)), for a semi-rigid connection. As shown in this figure, the parameters defining monotonic moment-rotation curve or cyclic moment-rotation hysteresis loops of a typical semi-rigid connection, are: initial connection stiffness, K_e, ultimate moment carrying capacity, M_u, and corresponding ultimate rotation θ_u. Therefore, any attempt to predict the nonlinear material behavior of a certain semi-rigid connection, calls for predicting the aforementioned parameters defining the moment-rotation curve or hysteresis loops of a flexible connection.

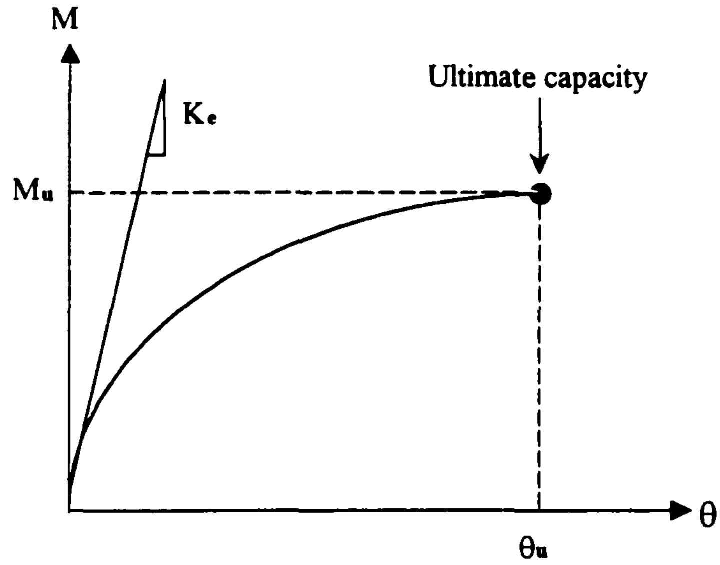

(a)

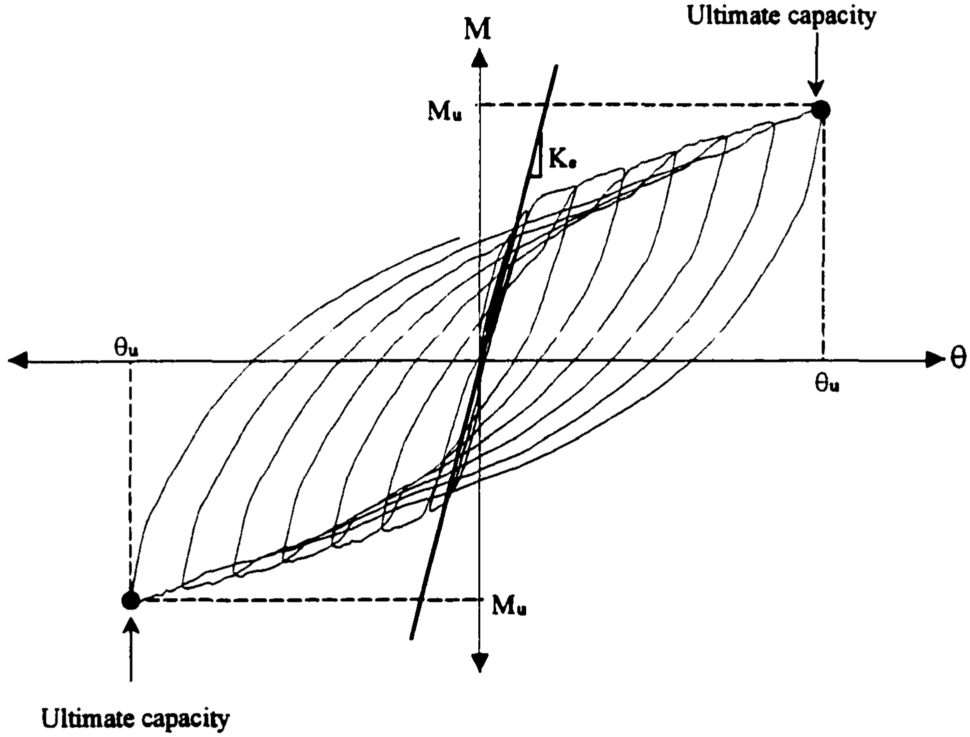

(b)

Fig. 1.2 Parameters Defining Non-linear Material Behavior of a Typical Semi-Rigid Connection: (a) Monotonic Moment-Rotation-Behavior; (b) Cyclic Moment-Rotation Hysteresis Behavior

1.2 Literature Review

Among studies reported for monotonic (static) semi-rigid frame analysis, Lui and Chen (1987) presented a methodology to analyze steel frames with flexible joints by expressing the column stiffness as a power series expansion, and slope deflection equations for the beam was modified to account for rotational springs which represented the semi-rigid connections. In this study, observations were made regarding the effects of flexible connections on the strength, deflection and internal force distribution of steel frame structures.

Goto and Chen (1987) followed the procedure described by Lui and Chen (1987) and implemented a secant modulus iterative procedure. In this research due to secant modulus formulation, the local variation of connection moment-rotation is not considered.

King and Chen (1993) proposed a practical LRFD-based analysis method for analysis of frames with semi-rigid connections. This method utilized a first order elastic analysis with a lateral load for the second order effects. In this report a simplified three-parameter model describing the tangential rotational stiffness of the semi-rigid connections under static loads is used.

Bhatti and Hingtegen (1995) examined the effect of certain parameters on serviceability limit-state of unbraced frames. In this study the monotonic (static) moment-rotation behavior of semi-rigid connections was modeled as elastic-perfectly plastic, described by its initial stiffness and ultimate moment capacity. In this research the connection plasticity was modeled and approximated by the reduced modulus technique.

Kukreti and Abolmaali (1999) presented a coupled nonlinear finite element methodology for steel frames with semi rigid connections in which iteration for material nonlinearity of the connection element was coupled with iteration for P-Delta effects. In this study an exponential function was introduced to represent moment-rotation behavior of the semi-rigid connections, which was differentiable and hence the tangential stiffness of the connection element is defined at each iteration cycle. This paper was a part of this research, which is introduced in detail in Chapter II of this dissertation.

Any study regarding frame analysis with flexible joints requires the moment-rotation behavior of the connection for monotonic studies and moment-rotation hysteresis behavior for dynamic studies. Hence, it would be desirable to conduct a search for previous studies including monotonic and cyclic experimental results and analytical models characterizing moment-rotation behavior of different classes of semi-rigid connections. These studies were first introduced by Rathbun (1936) and Hechtman and Johnston (1947). In these studies total fifteen experiments were conducted on top and seat angle connections using monotonic loading and rivets for fasteners. It was reported that top and seat angle connections will resist some end-moment of the beam, and therefore can be classified as partially restrained connections or semi-rigid connections.

Popov and Pinkley (1968) used Ramberg-Osgood function in modeling hysteresis loops obtained from experiments and it was concluded that using such models was in close agreement with the experimental loops of non-slip specimens.

Popov and Bertero (1973) conducted seven full-scale cyclic tests. These tests included all welded connections and connections with welded flanges and bolted webs. Moment-rotation hysteresis loops were reported for all test specimens and a skew-symmetric moment-rotation model was proposed for connections made by direct welding of flanges with or without connection plates.

Marley and Grestle (1982) reported results of a total of twenty-six tests on different types of semi-rigid connections. In this study the moment-rotation curves were obtained from extrapolation of the test results from the case of cyclic loading to the case of monotonically increasing moment versus rotation relationship.

Kishi and Chen (1986, 1987a, 1987b) proposed a three-parameter exponential model to describe moment-rotation characteristic of different types of semi-rigid connections.

Driscoll and Lu (1989) reported the results for six full-scale tests of large top and seat angle connections, in which the number of bolt rows, angle thickness, and bolt pretension were varied. All test specimens were cyclically loaded. In this study it was reported that a snug-tight connection behaved stiffer and stronger than its fully pretension counterpart. This conclusion by Driscoll and Lu (1989) was not confirmed in the research presented here and indeed it was contradicted. Driscoll and Lu (1989) also concluded that the snug-tight connection also reacted less adversely to load reversal, and its load-deformation response remained linear over a large range of loading.

Astaneh-Asl et al. (1989) investigated the cyclic behavior of double angle connections welded to beam webs and bolted to column flange. In this study, the moment-rotation hysteresis loops were presented and it was concluded that considerable moment could be transferred from beam to column. This could lead to plastic hinge formation in the column, since columns for this type of connection, are not designed for any moment transferred from beam via double web angle connections.

Mazroi (1990) investigated the monotonic moment-rotation behavior of the extended eight-bolt stiffened end-plate connections using 24 prototype connection tests and developed equations for parameters describing the moment-rotation curves of such connections. Furthermore, yield line analysis was used to analyze the column side of the connection. Finally, a design methodology for extended stiffened beam-to-column connection was proposed.

Mander et al. (1994) investigated the low cycle fatigue behavior of the top and seat angle connections by applying constant amplitude reverse cyclic load on specimens of the same geometrical properties. Their study showed that plastic moment capacity and connection stiffness were sensitive to how the bolts and nuts were oriented when tightened. The seismic fatigue ratio limited plastic rotation is suggested in the order of three percent.

Tsai et al. (1995) investigated the performance of ten cyclic beam-to-wide-flange-column moment connections. The connections were bolted-web welded-flange. This study concluded that supplemental web welds, but not supplemental web bolts, significantly enhance strength, ductility, and energy absorbing capacity of the connection. Experimental results indicate the cyclic rotational capacity of this type of connection ranges from 0.009 to 0.018 rad.

Vayas et al. (1995) conducted thirteen experiments to investigate the cyclic behavior of beam-to-column joints of steel frames made up of welded plate members with slender joint panels in the connection region. The performance of connections with respect to degree of rigidity and low cycle fatigue were examined. The behavior of a joint is divided into three actions: shear buckling of the pannel; tension field action; and frame action. This study concluded that a good performance can be achieved by properly selecting the dimensions of the web panel and surrounding flanges of the frame members.

Nader and Astaneh-Asl (1996) reported shaking table tests of top and seat with web angle connections and the results of these tests were compared with rigid and flexible connections tested on the shaking tables. This study reports that "a well–proportioned semi-rigid connection designed to behave in a more ductile manner can effectively participate in the nonlinear behavior of the structure, thus providing additional global structural ductility."

Sarraf and Bruneau (1996) conducted cyclic testing of riveted stiffened seat angle connections taken from a 83-year old building and the actual hysteresis behavior and potential moment resistance were investigated. It was concluded that these connections can develop considerable moment resistance, but due to pinching present in hysteresis loops, low energy dissipating capacity was observed. Two analytical models are suggested to predict the capacity of this connection, and two seismic retrofit strategies are suggested.

Also a literature search is necessary and justifiable for studies conducted on dynamic frame analysis up to date. Among the studies reported, Clough and Benuska

(1967) investigated the evaluation of ductility requirements imposed on the various members of a typical high-rise building when subjected to a relatively severe earthquake. In this study the principal subject of the investigation was a typical twenty-story, three-bay, open-frame building subjected to the El-Centro Earthquake. In this study, which considered rigid joints, both elastic and inelastic dynamic analysis was conducted. The inelastic analysis included member nonlinearity in which the nonlinear member deformations were expressed in terms of the member ductility ratio. This study concluded that the nonlinear lateral displacement due to earthquake response of tall buildings appeared to be similar in magnitude to the elastic displacement response. This research, also reported that the nonlinear member deformation tend to be concentrated in the girders, while columns remain elastic except in the top few stories.

Lionberger and Weaver (1969) investigated the dynamic response of frames with semi-rigid connections. In this study, rotational springs which represented flexible connections were treated as elastic supports in member stiffness matrices and element stiffness matrices were formulated using rotational springs. In this study, the axial strains were neglected and floor diaphragms were considered as rigid, such that the lumped mass idealization could be utilized. Damping was considered to be viscous in nature, and damping forces were assumed to be proportional to the relative lateral velocities between successive framing levels. Therefore, these types of damping were modeled as dashpots. The key load-time history was taken to be a triangular impulse loading similar to a blast loading. This study concluded that connection stiffness could influence both lateral displacement and member end moment to a large extent and flexible connections have appreciable effect on the overall flexibility of the structure.

1.3 Objectives and Scope

The overall objective of this study is to develop a dynamic analysis computer program for frames with semi-rigid connections and subjected to ground motion acceleration. This study is limited to planar frames; however, the basic concepts and principals are applicable to three-dimensional frames analysis. To achieve the aforementioned objective, this research was divided into four phases.

The first phase of this study deals with development of a monotonic (static) semi-rigid frame analysis source code that couples connection nonlinear (material) moment-rotation behavior with second order (P-Delta) effects (geometric nonlinearity). In this phase of the study, the semi-rigid beam-to-column connection is modeled as a "zero-length" rotational spring element of known moment-rotation behavior connected to two nodes with identical coordinates in space. These nodes are the beam-end node and the column-end node to which the spring element is connected to. The aforementioned nodes will have identical translational degrees-of-freedom, but different rotational degrees-of-freedom so that the connection's relative rotation is calculated as the difference in rotations of the aforementioned rotational degrees-of-freedoms. In this formulation, six degrees-of-freedoms are defined for each connection element for it to be consistent with the beam and column elements (members) in which the conventional frame elements are used. Since material nonlinearity of the connection element is defined by its corresponding moment-rotation curve, an exponential function, proposed by Mazroi (1990), is used to mathematically describe its behavior. This function is differentiable and hence the tangential stiffness of the connection is defined at each increment of the incremental procedure. An iterative Newton Raphson scheme is used to march along the moment-rotation curve of each connection as the load is incrementally applied. In each load increment, the initial tangential stiffness of the connection is used to start the analysis, which is corrected iteratively in cycles so as to satisfy equilibrium within acceptable error limits. In each load increment the nonlinear geometric stiffness matrix of each frame member due to P-Delta effects is iteratively determined. This requires the axial forces in the member to be known as a priori. The analysis for material nonlinear behavior of the spring elements and the geometric nonlinear behavior of the frame members is coupled. A detailed step-by-step procedure of this formulation is presented by Kukreti and Abolmaali, (1998) is also presented in Chapter II of this dissertation.

In order to develop rational moment-rotation relationships, in the second phase of this study an experimental program was conducted to obtain moment-rotation hysteresis loops for commonly used semi-rigid beam-to-column connections. The behavior of these semi-rigid connections was experimentally recorded when subjected to cyclic loads expected during an earthquake. The study included top and seat angle connections, all bolted double web angle connections, double web angle connections welded to the beam web and bolted to the column flange, flush-end plate connections, and four-bolt extended unstiffened end-plate connections. All test specimens consisted of a beam connected to a column by means of the semi-rigid connection. The columns used in the testing program were selected to be stiff enough such that they would not deform and hence, they would not contribute to the overall rotation of the connection. Also the beams are selected such that the failure would occur in the connection first. This enabled the behavior of the connection to be isolated, and therefore it was possible to directly record its moment-rotation hysteresis variation.

Development of mathematical models to idealize the moment-rotation hysteresis loops obtained from experimental studies followed the experimental program in the third phase of the study. Four different types of mathematical hysteresis models are developed for each type of connection studied. These hsyteresis models include the following: (1) elasto-plastic, (2) bilinear, (3) Ramberg-Osgood, and (4) modified bilinear model. The elasto-plastic and bilinear models, as shown in Figure 1.3 and Figure 1.4, respectively, belong to one class and both models unconservatively idealize the actual moment-rotation hysteresis behavior, but to a varying degree of accuracy. They also vary in level of complexity. The bilinear model is expected to more accurately model the moment-rotation behavior of the connection, whereas the elasto-plastic model will be a more simple to implement in a frame analysis computer program. Thus, both models have their own merits. The bilinear model is defined by four parameters, which are initial stiffness, K_e, ultimate moment capacity, M_u, ultimate rotation, θ_u, and transition moment, M_t. The transition moment M_t is defined as the moment at the intersection of the tangent line drawn from the ultimate point, with coordinates (M_u,θ_u), to the peaks of the hysteresis loops in the first quadrant and the initial stiffness slope line drawn at the origion. The

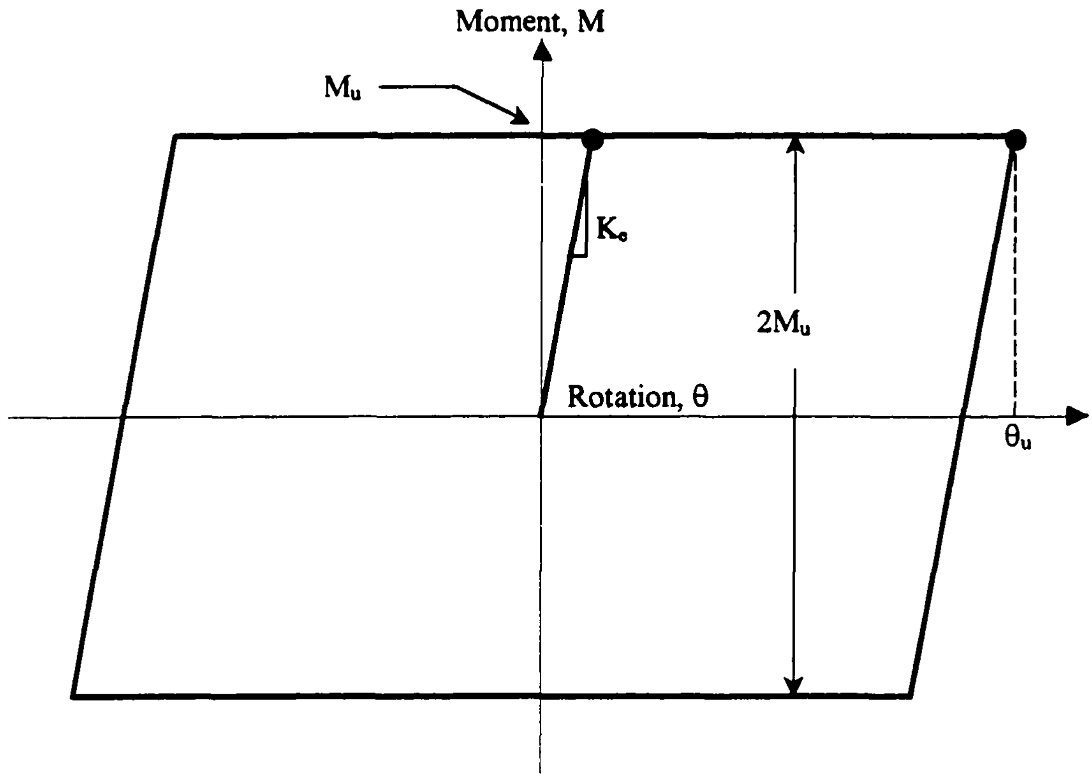

Fig. 1.3 Typical Elasto-Plastic Hysteresis Model

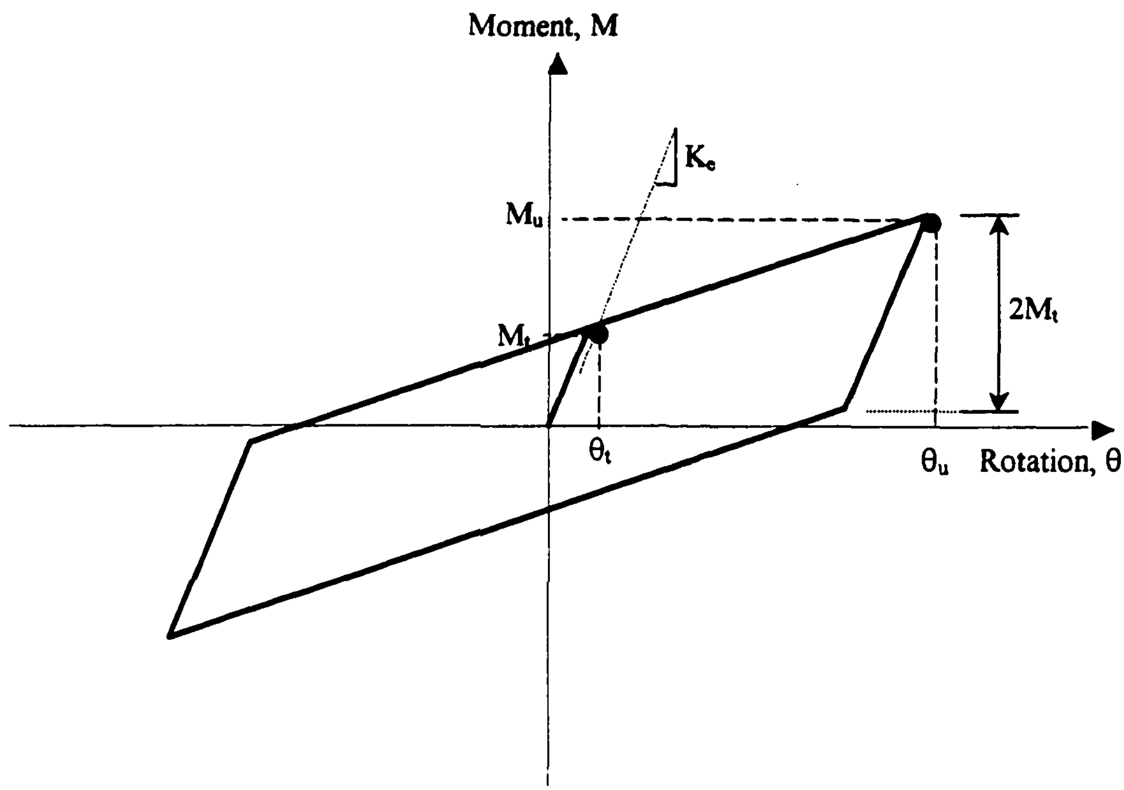

Fig. 1.4 Typical Bilinear Hysteresis Model

elasto-plastic model is a special case of the bilinear model, and, is described by only three parameters, which are K_e, M_u, and θ_u. The modified bilinear model uses the parameters defined for a Ramberg-Osgood hysteresis model. This model, as presented in Fig. 1.5, consists of three nonlinear portions, including a loading, an unloading (at some known moment level), and a reloading path. Ramberg and Osgood (1943) have proposed equations for these curves, which are defined in terms of two parameters, a characteristic moment, M_c, and a characteristic rotation, θ_c. It is important to note that Ramberg-Osgood function cannot model the pinching loops of the moment-rotation hysteresis loops and therefore, it should only be used for non-pinching portions. Finally, Fig. 1.6 shows the modified bilinear model, which is obtained in a similar fashion as the bilinear model with the exception that Ramberg-Osgood characteristic moment, M_c, and characteristic rotation, θ_c are used instead of transition moment, M_t, and transition rotation, θ_t. It should be pointed out that, the Ramberg-Osgood model is simply used to determine the characteristic moment and characteristic rotation required for the modified bilinear model; keeping this in mind, only three models are really developed for each connection. In addition, an attempt will also be made to suggest modifications to these three models if any connection fails in a unique failure mode, which is completely different than the others.

The final and fourth phase of this research is to develop a dynamic semi-rigid frame analysis algorithm and associated computer program by modifying the static semi-rigid frame analysis program of the first phase and using the mathematical models developed in the third phase of this study. For the dynamic frame analysis formulation, tangent stiffness is used to update the stiffness matrix of the nonlinear

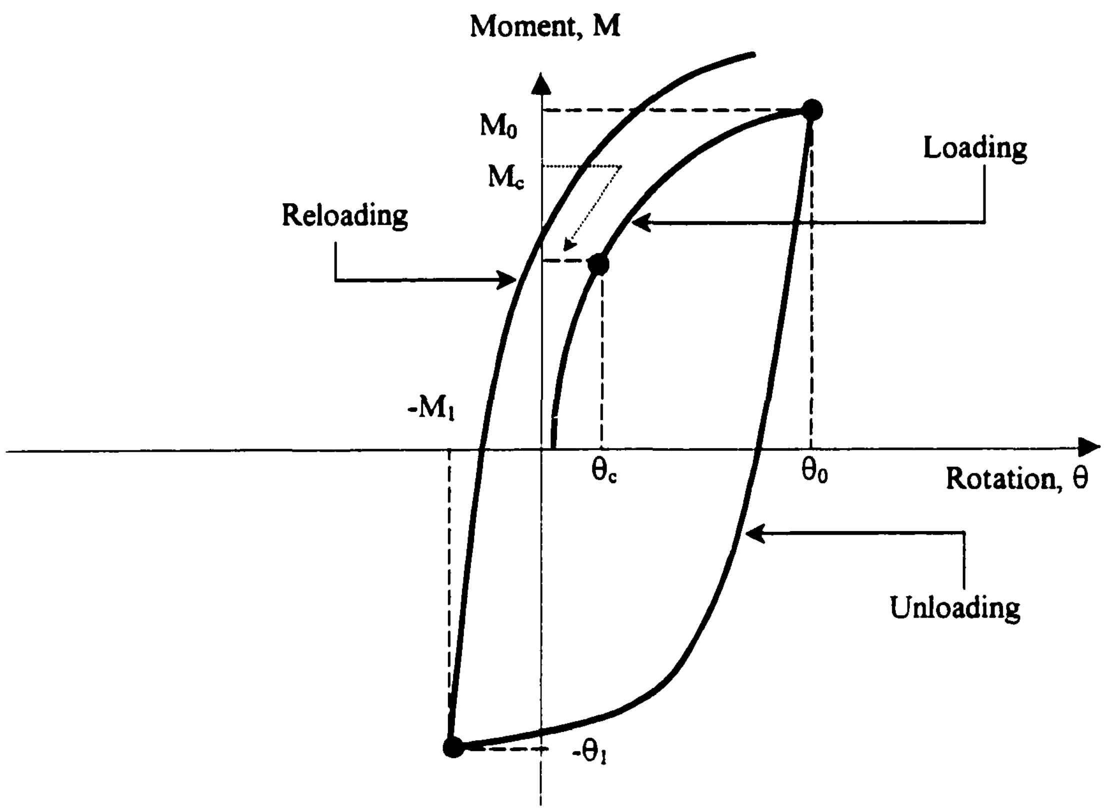

Fig. 1.5 Typical Ramberg-Osgood Hysteresis Model

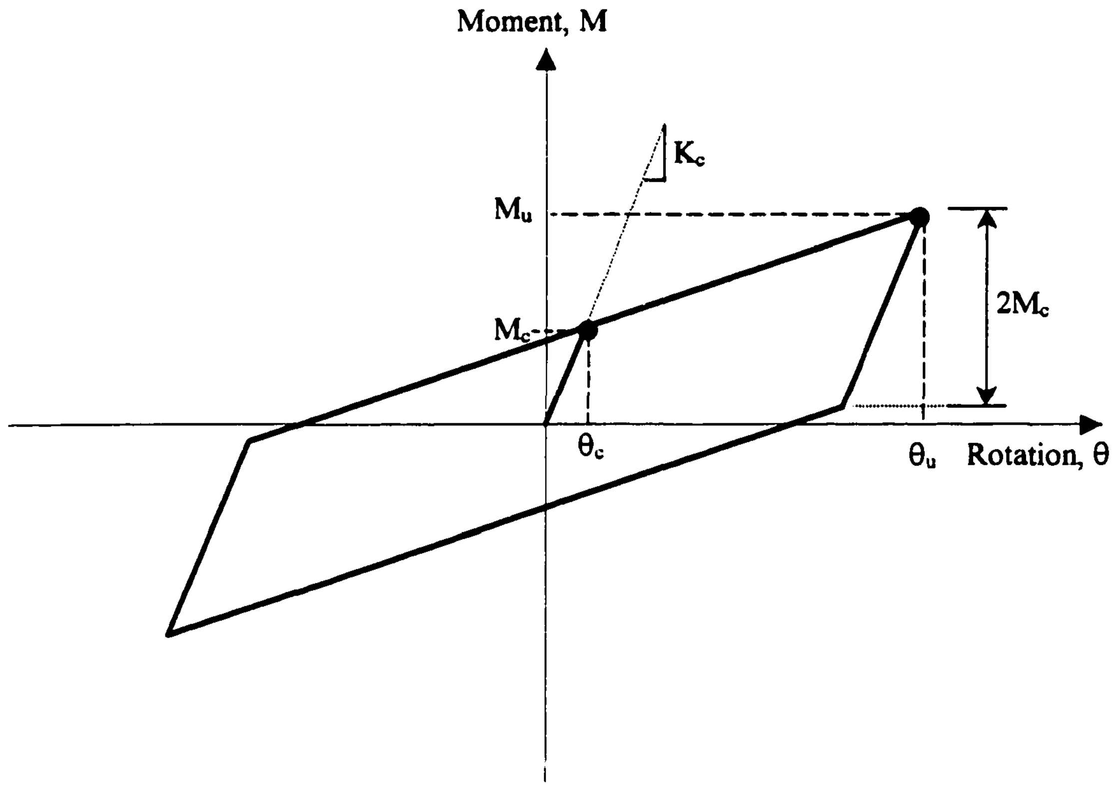

Fig. 1.6 Typical Modified Bilinear Hysteresis Model

connection elements. For time domain analysis a class of integration methods, based on assumed variations of nodal accelerations during each time step have been widely used. The method based on linear variation of acceleration with respect to time is known to be unstable in the presence of vibration modes with periods exceeding approximately one third of the time step, and hence, will not considered in this study. The alternative methods that are unconditionally stable include the constant variation of acceleration with respect to time step (Newmark-β method) and the linear variation of acceleration over an extended time step (Wilson-θ method), which is a modification of the conditionally stable linear acceleration method. Since it has been shown that the Wilson-θ method might introduce artificial damping in the system, the Newmark-β constant acceleration technique is adopted in this research. The moment-rotation hysteresis connection behavior will have some inherent damping, so no other form of damping is considered in this research. Furthermore, traditionally, damping matrices are linearly related to the mass and/or stiffness matrices, thus if needed, damping matrices can be easily added to the formulation later. The coupled mass (consistent mass) formulation for frame members is utilized in the formulation of the dynamic analysis algorithm.

CHAPTER II

MONOTONIC FINITE-ELEMENT SEMI-RIGID JOINT ANALYSIS PROGRAM

2.1 General

In conventional analysis and design of steel building frame structures the actual behavior of "rigid" beam-to-column connections is simplified by assuming each joint accommodates full transfer of moment, and the connection is assumed to rotate as a rigid body. In a pinned-joint, the joint is assumed to act as a frictionless hinge connection with no moments acting at the joint. However, the actual behavior of most bolted or a combination of bolted and welded connections used in steel building frame structures are indeed semi-rigid and are governed by a nonlinear relationship between the connection moment, M, and the relative rotation, θ, between the connected members, as shown in Fig. 2.1. Refer to Fig. 1.1 of Chapter I, in which the M-θ curves for some commonly used bolted connections are shown. This figure clearly demonstrates that, indeed, the behavior of a number of these connections falls in-between the aforementioned two conventional idealizations, and thus should be analyzed as a semi-rigid connection. The figure also shows that the amount of connection rigidity varies for different connections; a double-angle web

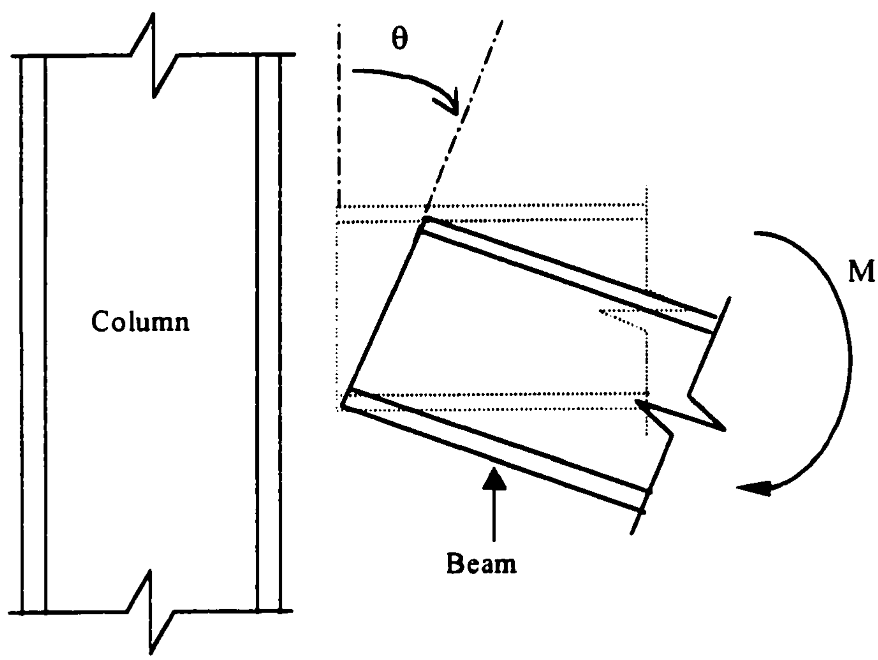

Fig. 2.1 Relative Rotation of Beam with Respect to Column

connection is much less rigid than a double-angle seated connection. For a particular connection, the stiffness would also vary by changing the geometric configuration of the connection elements (e.g., bolt diameter, bolt pitch, thickness of the plate elements connected, etc.). Thus, depending on the connection rigidity, the moment-rotation (M-θ) behavior of the semi-rigid beam-to-column connections in a steel building frame structure can significantly affect the lateral sway and internal member forces (primarily moments). If the connection rigidity is significantly overestimated (by assuming it to be rigid), the lateral drift or sway and member-end moments may significantly be under predicted. On the other extreme, if the connection rigidity is neglected (by assuming it to be pinned), the lateral drift may significantly be over predicted. As such, there is a need to develop frame analysis and design procedures and related software that more accurately considers the semi-rigid behavior of connections. In this chapter such an analysis procedure is presented, that not only considers the nonlinear moment-rotation behavior of connections but also the P-Delta (P-Δ) effect (i.e., nonlinear frame element geometric stiffness matrix). First, a general moment-rotation model for steel frame connections is presented in Section 2.2, as reported by Mazroi (1990). Second, the algorithm of the frame analysis procedure considering the moment-rotation curve of the connections and the P-Δ effect are presented in Sections 2.3 and 2.4, respectively. Third, to validate the analysis procedure presented, results from two example problems are presented in Section 2.5 and compared with results available in the literature considering other connection models. Fourth, results from a parametric study conducted to investigate the effect of the connection moment-rotation model parameters (which define the connection stiffness), and the frame geometry and loading on the frame story drifts and column moments are presented in Section 2.6. In this analysis, it is assumed that all loads are applied concurrently so no connection unloading is considered. It is understood that often in frames, the loads are applied sequentially; very often, gravity loads are already present when lateral loads (e.g., wind, earthquake, etc.) act. This type of loading is beyond the scope of the program developed.

2.2 Moment-Rotation (M-θ) Model for a Semi-Rigid Connection

The behavior of a semi-rigid connection can be described by the moment-rotation (M-θ) curve of the connection, which can either be obtained experimentally or analytically (by a finite element analysis of the connection domain). The best way to describe the nonlinear (M-θ) relationship for a semi-rigid connection is through a mathematical model based on experimental results. The nonlinear mathematical model selected must satisfy the following relationships:

1. The curve must pass through the origin, i.e.,

$$M = 0 \quad at \quad \theta = 0° \tag{2.1}$$

2. The slope of the curve at the origin must be equal to the initial elastic stiffness, K_e, of the connection, i.e.,

$$\frac{dM}{d\theta} = K_e \quad \text{at} \quad \theta = 0° \tag{2.2}$$

3. The model must possess a differential that represents the tangent stiffness, K_t, of the connection for any value of θ, i.e.,

$$\frac{dM}{d\theta} = K_t \qquad (2.3)$$

4. The tangent stiffness must decay as the connection elements yield and theoretically must approach zero as θ approaches to infinity. The connection moment at this stage represents the ultimate moment capacity of the connection, M_u, i.e.,

$$M = M_u \quad as \quad \theta \rightarrow \infty \qquad (2.4)$$

In view of the aforementioned points, and based on experimental test results on a number of different types of connections, the following mathematical model is selected for representing the M - θ behavior of a steel frame connection:

$$M = M_u \left(1 - e \, \frac{K_e \theta^{\alpha}}{M_u} \right) \qquad (2.5)$$

where "e" is the neparine number (=2.7813), and α is a rigidity parameter that will have a unique value for a particular connection. The higher the value of the parameter α, the more flexible the connection will be. The above model satisfies the conditions of Eqs. (2.1), (2.3) and (2.4) explicitly, and its tangential stiffness, K_t, is given by

$$K_t = \alpha K^e \, \theta^{(\alpha - 1)} \left(e^{\frac{K_e \theta^{\alpha}}{M_u}} \right) \qquad (2.6)$$

For α = 1, Eq. (2.6) satisfies the condition of Eq. (2.2) explicitly. However, for a value of α other than one, Eq. (2.6) does not have a bound at θ = 0°. On careful examination of the graphical plot of Eq. (2.5) for a range of possible values of K_e, M_u and α one finds that $K_t \approx K_e$ at an infinitesimal rotation away from the origin.

The value of θ at which $K_t \approx K_e$ will depend on M_u and α for a given K_e. For example, for $K_e = 10^5$ kip-in./rad, with M_u ranging from 500 kip-in. to 2,500 kip-in. and $\alpha = 0.5$ to 0.9, the value of θ at which $K_t \approx K_e$ for each case is presented in Table 2.1. As shown, the range of θ varies from 30×10^{-5} rad to 710×10^{-5} rad. It should be noted that determination of the exact value of the initial stiffness, K_e, even from physical tests, is not an easy task; usually a lower and upper bound on K_e is estimated based on loading history and precision of measuring rotation produced at very small load values. Barakat and Chen (1991) have also discussed this issue.

2.3 Frame Analysis Algorithm with Semi-Rigid Connections

2.3.1 Frame Element

A typical frame element is shown in Fig. 2.2. The stiffness analysis of such a frame element can be found in standard matrix structural analysis and finite element textbooks. In this sub-section, only key equations for the frame analysis that are used in the description of the algorithm are presented. The elastic stiffness matrix, $[K^e]$, of the frame element shown in Fig. 2.2 is given by

$$[K_e] = [K_a^e] + [K_b^e] \tag{2.7}$$

where $[K_a^e]$ = element axial stiffness matrix, and $[K_b^e]$ = element bending stiffness matrix, which are, respectively,

Table 2.1 Value of θ when $K_t \approx K_e$ for $K_e = 10^{-5}$ kip-in./rad

M_u (kip-in.)	**θ (rad)**				
	α				
	0.5	0.6	0.7	0.8	0.9
500	30×10^{-5}	64×10^{-5}	104×10^{-5}	140×10^{-5}	140×10^{-5}
1,000	81×10^{-5}	155×10^{-5}	235×10^{-5}	279×10^{-5}	269×10^{-5}
1,500	145×10^{-5}	257×10^{-5}	360×10^{-5}	435×10^{-5}	385×10^{-5}
2,500	300×10^{-5}	476×10^{-5}	635×10^{-5}	710×10^{-5}	600×10^{-5}

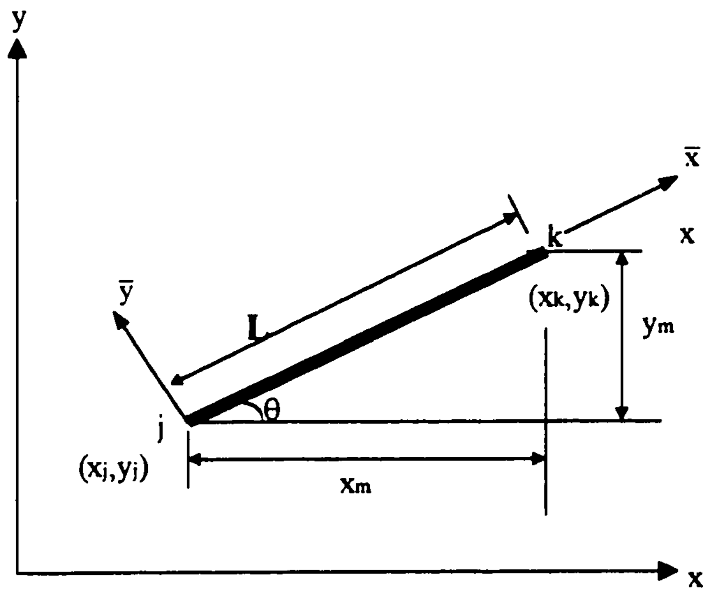

Element local coordinate system: $\bar{x}$, $\bar{y}$
Global coordinate system: x, y
Global coordinates of the near end: (x_j, y_j)
Global coordinate of the far end: (x_k, y_k)
$x_m = x_k - x_j$
$y_m = y_k - y_j$

$$L = (x_m^2 + y_m^2)^{1/2}$$

$$\text{Cos}\,\theta = c = x_m / L$$

$$\text{Sin}\,\theta = s = y_m / L$$

A = cross-sectional area
I = moment of inertia

Fig. 2.2 Typical Frame Element

$$
\left[K_a^e\right] = \frac{AE}{L}\begin{bmatrix} c^2 & cs & 0 & -c^2 & -cs & 0 \\ cs & s^2 & 0 & -cs & -s^2 & 0 \\ 0 & 0 & 0 & 0 & 0 & 0 \\ -c^2 & -cs & 0 & c^2 & cs & 0 \\ -cs & -s^2 & 0 & cs & s^2 & 0 \\ 0 & 0 & 0 & 0 & 0 & 0 \end{bmatrix} \tag{2.8}
$$

$$
\left[\mathrm{K}_a^c\right] = \frac{\mathrm{AE}}{\mathrm{L}}\begin{bmatrix} s^2 & -cs & -Ls/2 & -s^2 & cs & -Ls/2 \\ -cs & c^2 & Lc/2 & cs & -c^2 & Lc/2 \\ -Ls/2 & Lc/2 & L^2/3 & Ls/2 & -Lc/2 & L^2/6 \\ -s^2 & cs & Ls/2 & s^2 & -cs & -Ls/2 \\ cs & -c^2 & Lc/2 & -cs & c^2 & -Lc/2 \\ -Ls/2 & Lc/2 & L^2/6 & Ls/2 & -Lc/2 & L^2/3 \end{bmatrix} \tag{2.9}
$$

where L = element length, E = Young's modulus, A = area of cross-section, I = moment of inertia, and c and s are defined in Fig. 2.2.

2.3.2 Semi-Rigid Connection Element

A frame beam-to-column joint, representing a semi-rigid connection, is modeled by a nonlinear rotational spring, as shown in Fig. 2.3. The rotational spring is modeled to possess the M-θ curve given by Eq. (2.5). Such a beam-to-column joint is introduced in the frame analysis as a rotational spring, in which the end nodes of the spring have the same Cartesian coordinates. So, the connection between a beam- and column-end node is made by this spring element, which has zero length, and the ends of which experience, the same translation displacements along the global (x and y) Cartesian axis, but different rotations (refer to Fig. 2.3(a)). Thus, the degrees-of-freedom for both the end nodes of this spring element must be

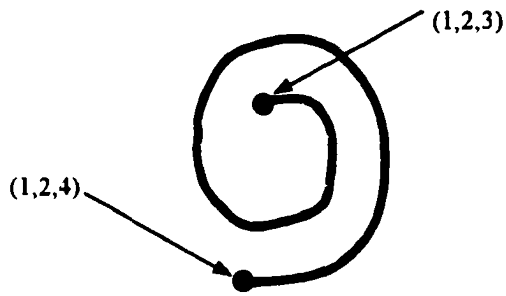

- *Zero length element*
- *Translational degrees-of-freedom (the first and second numbers in brackets) are equal*
- *Rotational degrees-of-freedom(the third number in brackets) are free*

(a)

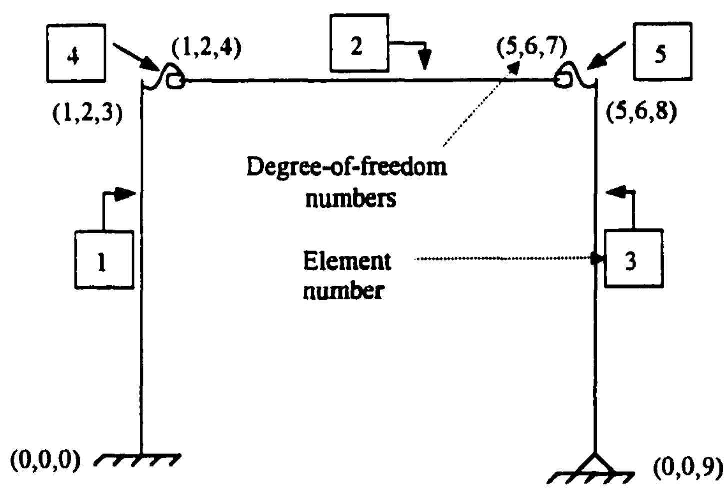

(b)

Fig. 2.3 Semi-Rigid Connection Model:
(a) Rotational Spring Element Configuration;
(b) Plane Frame Discrete Model with Semi-Rigid Connections

identical for the x and y translations, but different for rotational degrees-of-freedom. For example, for the node numbering scheme shown in Fig. 2.3(b), if the left column top-end node degrees-of-freedom numbers are *1, 2, 3;* then, the node number for the beam-end the degrees-of-freedom numbers will be *1, 2, 4.* The stiffness matrix, $[K^c]$, of such a nonlinear semi-rigid connection spring element is

$$[K^c] = \begin{bmatrix} 0 & 0 & 0 & 0 & 0 & 0 \\ 0 & 0 & 0 & 0 & 0 & 0 \\ 0 & 0 & K_0 & 0 & 0 & -K_0 \\ 0 & 0 & 0 & 0 & 0 & 0 \\ 0 & 0 & 0 & 0 & 0 & 0 \\ 0 & 0 & -K_0 & 0 & 0 & K_0 \end{bmatrix} \tag{2.10}$$

where the coefficient K_0 is equal to the initial elastic stiffness K_e, of the connection in the first step of the iterative analysis, and in subsequent iterations is equal to the tangent stiffness, K_t, of the connection, which is given by Eq. (2.6). It should be noted that the order of the semi-rigid connection spring stiffness matrix, $[K^c]$, is chosen to be 6x6, to be consistent with the size of the frame element axial and bending stiffness matrices, $[K_a^e]$ and $[K_b^e]$, to enable the logic of assembling stiffness matrices for all the element to be the same in the computer program.

2.3.3 Iterative Solution Algorithm for Frame Analysis with Semi-Rigid Joints

A Newton-Raphson procedure is used to model the nonlinear stiffness matrices of the semi-rigid joints (nonlinear springs) in the frame so as to iteratively force the solution to march along the M-θ curve of each beam-to-column connection. The step-by-step procedure is outlined below:

1. Using the elastic stiffness matrix, $[K^e]$, for each frame element and taking K_0 equal to the initial stiffness (i.e., $K_0 = K_e$) in Eq. (2.10) to formulate the stiffness matrix, $[K^c]$, of each semi-rigid beam-to-column joint, assemble the system stiffness matrix, $[K]$, for the entire frame using the conventional stiffness method of analysis.

2. Convert all element loads to equivalent nodal loads and assemble the system load vector, $\{F\}$. This load vector is decomposed into a force vector, $\{F_1\}$, containing all nodal direct forces (acting along the Cartesian x- and y-axis), and moment vectors, $\{M_1\}$, $\{M_2\}$,..., $\{M_{ns}\}$, one for each beam-to-column joint spring element containing the spring end moments only, such that

$$\{F\} = \{F_1\} + \{M_1\} + \{M_2\} + \ldots + \{M_{ns}\} \quad (2.11)$$

where ns = number of semi-rigid connection spring elements.

3. Solve the system equilibrium equation for system nodal displacement vector, $\{\delta\}$, such that

$$[F]\{\delta\} = \{F_1\} + \{M_1\} + \{M_2\} + \ldots + \{M_{ns}\} \quad (2.12)$$

4. From the system nodal displacement vector, $\{\delta\}$, for each semi-rigid connection spring element, compute the relative spring rotation, θ_i, for the i^{th} spring element from

$$\theta_i = \theta_{ig} - \theta_{il} \tag{2.13}$$

where subscript i = semi-rigid connection spring element number, θ_{ig} = rotation at the greater node number the spring is connected to, which will be the beam-end, and θ_{il} = rotation at the lesser node number the spring is connected to, which will be the column-end.

5. Substitute the rotation computed for each semi-rigid connection spring element using Eq. (2.13) into Eq. (2.5) for the value of θ and known value of α for the connection, and compute the connection moment, M_{ia}, which is given by

$$M_{ia} = M_u \left(1 - e \frac{K_e \theta_i^{\alpha}}{M_u} \right) \tag{2.14}$$

where M_u, for each semi-rigid connection, is computed using Eq. (2.7). When the total moment transferred (M_r) to the connection after converting the beam loads to equivalent joint loads is greater than M_u, some modification has to be made to simulate the rate of connection failure. In such a case, the connection moment is equal to M_u, and M_u/M_r scales the member stiffness matrices.

6. Substitute the rotation computed for each semi-rigid connection spring element using Eq. (2.13) into Eq. (2.6) for the value of θ, and compute the connection tangent stiffness, K_{ti}, which is given by

$$K_{ti} = \alpha K_e \theta^{(\alpha-1)} \left(e^{\frac{K_e \theta^{\alpha}}{M_u}} \right) \tag{2.15}$$

If K_{ti} for any connection element is less than 0.01 K_e, then the rotational degrees-of-freedom of both end nodes of spring element are set equal, and the relative connection rotation is set equal to zero. This would ensure that moment in the connection will remain as M_u for the remainder of the analysis.

7. If M_{ia} is less than M_u, then for each frame element compute the disbalanced moment vector, $\{M_i^{dis}\}^{(n)}$, from the following relationship:

$$\{M_i^{dis}\}^{(n)} = \{M_i\} - \{M_{ia}\}^{(n)} \qquad (2.16)$$

where the superscript (n) denotes the present correction iteration cycle number, vector $\{M_i\}$ contains the total incremental moment applied to the i^{th} semi-rigid connection spring element, the elements of the vector $\{M_{ia}\}^{(n)}$ for the i^{th} semi-rigid connection spring element is calculated using Eq. (2.14), and the vector $\{M_i^{dis}\}^{(n)}$ contains the disbalanced moment for the i^{th} semi-rigid connection spring element. Note that in the first iterative cycle, the vector $\{M_i\}$ for each frame element is defined by Eq. (2.11).

8. For each semi-rigid connection spring element taking $K_0 = K_{ti}$ in Eq. (2.10) to formulate the updated stiffness matrix, $[K^c]$, for each semi-rigid beam-to-column joint, and assemble the updated system stiffness matrix, $[K]^{(n)}$.

9. Compute the incremental system nodal displacement vector, $\{\Delta\delta\}^{(n)}$, from

$$[K]^{(n)}\{\Delta\delta\}^{(n)} = \{M_1^{dis}\}^{(n)} + \{M_2^{dis}\}^{(n)} + \ldots + \{M_{ns}^{dis}\}^{(n)} \qquad (2.17)$$

10. Find the corrected system nodal displacement vector, $\{\delta\}^{(n)}$, from

$$\{\delta\}^{(n)} = \{\delta\}^{(n+1)} + \{\Delta\delta\}^{(n)} \qquad (2.18)$$

where $\{\delta\}^{(n\text{-}1)}$ = system nodal displacement vector at the previous iterative cycle. It should be noted that for the first iterative cycle $\{\delta\}^{(1)}$ is the system nodal displacement vector obtained in Step 3.

11. To check convergence compute the error, ε_i, for each semi-rigid connection spring element using

$$\varepsilon_i = \left| \delta_i^{(n)} \quad \delta_i^{(n-1)} \right| \qquad (2.19)$$

If $\varepsilon_i = 1 \times 10^{-5}$, then the result obtained in Step 10 is acceptable, otherwise Steps 4 to 11 are repeated.

2.4 Modifications to the Solution Algorithm Considering *P*-Delta Effect

2.4.1 Modifications for P-Delta Effect Only

When a frame subjected to lateral (e.g., wind or seismic) loads is also subjected to gravity loads, the lateral drift of the structure increases. This phenomenon is known as the P-Delta (*P-Δ*) effect, where "*P*" represents the axial force in a frame element (column) and "Delta" or *Δ* represents the story drift. The

AISC LRFD Manual of Steel Construction (1994) requires that this effect must be considered in the frame analysis with semi-rigid connections. To consider the *P-Δ* effect, the frame analysis solution procedure presented in the previous section needs to be modified. The frame element stiffness matrix needs to incorporate the so-called element geometric stiffness matrix, $[K_g^e]$, which in the element global coordinate (shown as *x*- and *y*-axis in Fig. 2.2) system is given by Willems and Lucas (1978) as:

$$\left[K_g^e\right] = \frac{P}{L}\begin{bmatrix} 6s^2/5 & -6cs/5 & -sL/10 & -6s^2/5 & 6cs/5 & -sL/10 \\ -6cs/5 & 6c^2/5 & cL/10 & 6cs/5 & -6c^2/5 & cL/10 \\ -sL/10 & cL/10 & 2L^2/15 & sL/10 & -cL/10 & -L^2/30 \\ -6s^2/5 & 6cs/5 & sL/10 & 6s^2/5 & -6cs/5 & sL/10 \\ 6cs/5 & -6c^2/5 & -cL/10 & -6cs/5 & 6c^2/5 & -cL/10 \\ -sL/10 & cL/10 & -L^2/30 & sL/10 & -cL/10 & -2L^2/15 \end{bmatrix} \tag{2.20}$$

where the axial force in the element, *P*, is related to the element local nodal displacements (i.e., along $\bar{x}$-axis shown in Fig. 2.2) by

$$P = \frac{EA}{L}\left(\bar{u}_k - \bar{u}_j\right) \tag{2.21}$$

where $\bar{u}_k$ = displacement along local $\bar{x}$-axis at node *k* (greater node number), and = $\bar{u}_j$ displacement along local $\bar{y}$-axis at node *j* (lesser node number). The total stiffness matrix, $[K_T^e]$, of a frame element is obtained from

$$\left[K_T^e\right] = \left[K^e\right] + \left[K_g^e\right] \tag{2.22}$$

where the matrix $[K^e]$, is the standard elastic element stiffness matrix of a frame element given by Eq. (2.7). It should be noted that the elements of the matrix $[K_g^e]$, require the element nodal displacements to be known as a priori, thus suggesting that an iterative process has to be used to determine the system stiffness matrix, $[K]$, and the system nodal displacements for given loading acting on the frame. Also, it should be noted that if the axial load obtained from Eq. (2.21) for a frame element is compressive (i.e., P is negative), there will be a reduction in the total stiffness of the system obtained when the results of Eq. (2.22) are assembled into the system stiffness matrix. Similarly, if the axial load obtained from Eq. (2.21) for a frame element is tensile (i.e., P is positive), there will be an increase in the total stiffness of the system obtained when the results of Eq. (2.22) are assembled into the system stiffness matrix. The step-by-step solution algorithm to incorporate the P-Δ effects for a frame with rigid joints is as follows:

1. Find the elastic stiffness matrix, $[K^e]$, of each frame element, and assemble them to obtain the system stiffness matrix, $[K]$. For given loads, also assemble the system load vector, $\{F\}$. Find the system nodal displacements, $\{\delta\}$, by solving

   $$[K]\{\delta\} = \{F\} \tag{2.23}$$

   Thus, in this step the geometric stiffness matrix of each element is assumed to be a null matrix.

2. From the system nodal displacement vector, $\{\delta\}$, extract the element nodal displacement vector, $\{\delta\}_i$, for each frame element, and transform each to correspond to the local coordinate system of the element. Substitute the local element nodal displacements corresponding to the two axial degrees-of-freedom into Eq. (2.21),

and compute the axial force (P) in each frame element. Using Eq. (2.22), formulate the geometric stiffness matrix of each frame element, and substituting the element stiffness matrices, $[K^e]$ and $[K_g^e]$, into Eq. (2.22), obtain the total updated system stiffness matrix. Let this matrix be denoted as $[K]^{(n)}$, where the superscript (n) denotes the current iterative cycle.

3. Solve again the updated system stiffness equilibrium equation for system nodal displacement vector, $\{\delta\}^{(n)}$,

$$\left[K^{(n)}\right]\{\delta\}^{(n)} = \{F\}^{(n)} \tag{2.24}$$

4. Compute error, ε_i, using the following equation to check if the computed nodal displacements have converged:

$$\varepsilon_i = \left| \left(\delta_i^{(n)} - \delta_i^{(n-1)}\right) \div \left(\delta_i^{(n)}\right) \right| \tag{2.25}$$

If $\varepsilon_i = 1 \times 10^{-5}$, then the result obtained in Step 4 is acceptable, otherwise Steps 2 to 4 are repeated.

2.4.2 Algorithm Coupling the Semi-Rigid Joint Behavior and P-Delta Effect

In this section, an algorithm is presented to analyze a planar frame with semi-rigid joints, in which the P-Δ effect is also considered. This algorithm basically couples the two algorithms presented earlier. The step-by-step procedure is as follows:

1. **Same as Step 1** of frame analysis with semi-rigid joints.
2. **Same as Step 2** of frame analysis with semi-rigid joints.
3. **Same as Step 3** of frame analysis with semi-rigid joints.

4. From the system nodal displacement vector, $\{\delta\}$, extract the element nodal displacement vector, $\{\delta\}_i$, for each frame element, and transform each to correspond to the local coordinate system of the element. Substitute the local element nodal displacements corresponding to the two axial degrees-of-freedom into Eq. (2.21), and compute the axial force (P) in each frame element.

5. Calculate the geometric stiffness matrix, $[K_g^e]^{(n)}$, of each frame element using the value of axial force calculated in Step 4. *The iteration to model P-Δ effect starts now.* The superscript *(n)* denotes the present iteration cycle number.

6. **Same as Step 4** of frame analysis with semi-rigid joints. *The iteration to model the nonlinear behavior of each semi-rigid beam-to-column joint starts now.*

7. **Same as Step 5** of frame analysis with semi-rigid joints.

8. **Same as Step 6** of frame analysis with semi-rigid joints.

9. **Same as Step 7** of frame analysis with semi-rigid joints.

10. For each semi-rigid connection spring element take $K_0 = K_n$ in Eq. (2.10) to formulate the updated stiffness matrix, $[K^c]^{(n)}$, for each semi-rigid beam-to-column joint.

11. Formulate the updated total element stiffness matrix, $[K_T^e]^{(n)}$, by adding the element elastic stiffness matrix, $[K^e]$, computed in Step 1 and the element geometric stiffness matrix, $[K_g^e]^{(n)}$, computed in Step 5, as given in Eq. (2.22).

12. Assemble the updated total element stiffness matrix, $[K_T^e]^{(n)}$, computed for each frame element in Step 11 above and the stiffness matrix, $[K^c]^{(n)}$, computed for each semi-rigid beam-to-column joint in Step 10 above, into the system stiffness matrix, and obtain the updated system stiffness matrix denoted as $[K]^{(n)}$.

13. **Same as Step 9** of frame analysis with semi-rigid joints. Note: In this step the system stiffness matrix, $[K]^{(n)}$, computed in Step 12 above is used along with the disbalanced spring moments computed in Step 9 above.

14. **Same as Step 10** of frame analysis with semi-rigid joints.

15. **Same as Step 11** of frame analysis with semi-rigid joints.

16. If the requirement of Step 15 above is not satisfied, Steps 6 to 15 are repeated until convergence is achieved. ***This terminates the iteration to model the nonlinear behavior of each semi-rigid beam-to-column joint.***

17. Using the system nodal displacement vector, $\{\delta\}^{(n)}$, computed in Step 14 above, formulate the element nodal displacement vector, $\{\delta\}_i^{(n)}$, for each frame element, and transform each to correspond to the local coordinate system of the element. Using the local element nodal displacements corresponding to the two axial degrees-of-freedom, compute the axial deformation, $\Delta u_i^{(n)}$, for each frame element from

$$\Delta u_i^{(n)} = \bar{u}_k^{(n)} - \bar{u}_j^{(n)} \tag{2.26}$$

where, as defined earlier, $\bar{u}_k^{(n)}$ = displacement along local $\bar{x}$-axis at node k (greater node number of the element), $\bar{u}_j^{(n)}$ = displacement along local $\bar{x}$-axis at node j (lesser node number of the element), and subscript i denotes frame element number.

18. To check for P-Δ convergence, compute the error, ε_i, for each frame element using

$$\varepsilon_i = \left|\Delta u_i^{(n)} / \Delta u_i^{(n-1)}\right| \tag{2.27}$$

where $\Delta u_i^{(n-1)}$ = element axial deformation computed at the previous iterative cycle. If $\varepsilon_i = 1 \times 10^{-5}$, then the results obtained in Step 16 above are acceptable, otherwise Steps 5 to 18 above are repeated.

2.5 Validation of the Frame Analysis Algorithms Presented

In order to verify the results obtained from the frame analysis algorithms presented in this chapter, two example frame problems, shown in Figs. 2.4 and 2.5, are analyzed. These problems have also been analyzed by King and Chen (1993) and Bhatti and Hingtegen (1995). The frames are analyzed assuming all connections to be rigid and semi-rigid, with and without P-Δ effects for each case. For all analyses E = 29,000 *ksi* is assumed, and the following values for the initial stiffness and ultimate moment capacity of the connections are used: K_i = 786,732 kip-in./rad and M_u = 1,989 kip-in. The following values for the loading shown in Figs. 2.4 and 2.5 are used: for Example 1, P = 100 kip and H = 10 kip; and for Example 2, w = 0.15 kip/in. and H = 7 kip. It should be noted that in Example 1 there are no distributed loads acting on the beams, so no Newton-Raphson iterations

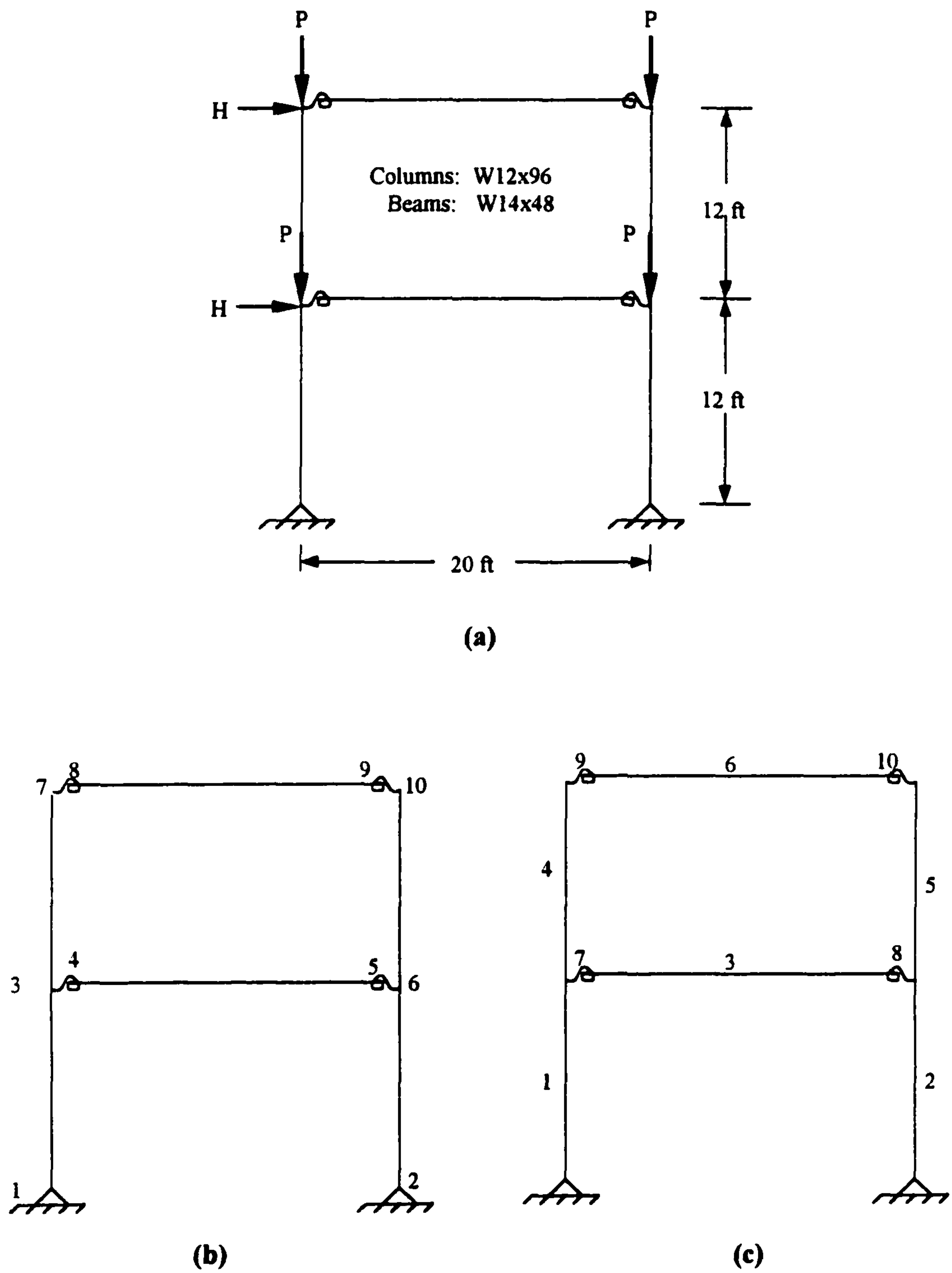

Fig. 2.4 Example 1—Planar Frame:
(a) Frame Model; (b) Node Numbers; (c) Element Numbers

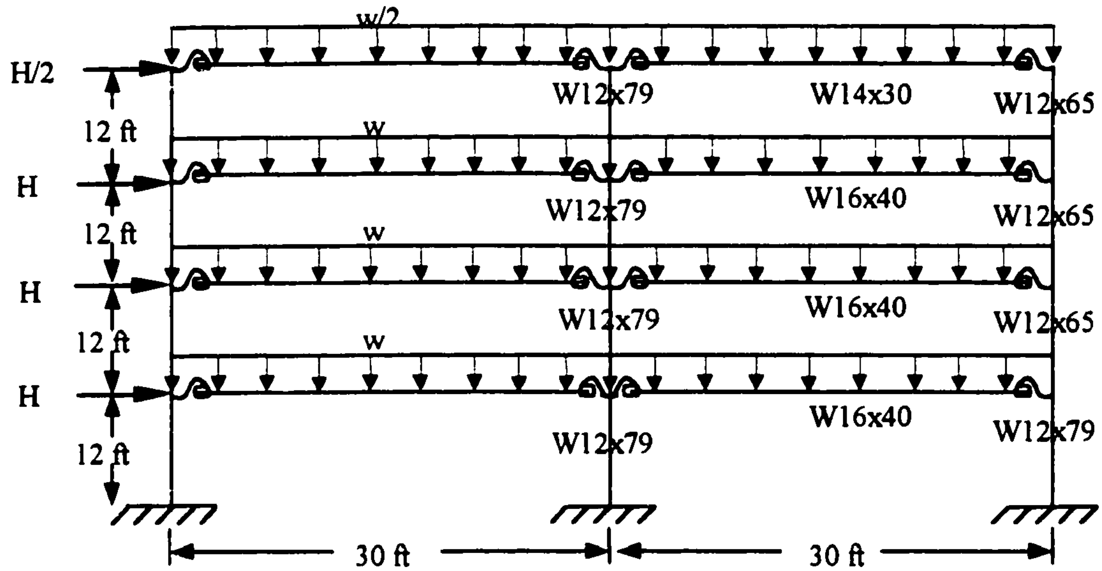

(a)

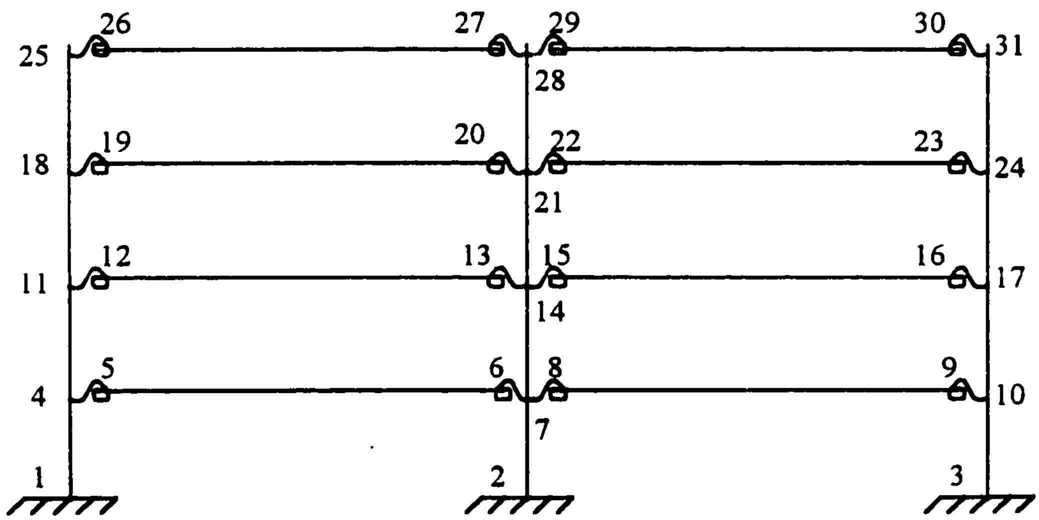

(b)

Fig. 2.5 Example 2—Planar Frame:
(a) Frame Model; (b) Node Numbers; (c) Element Numbers

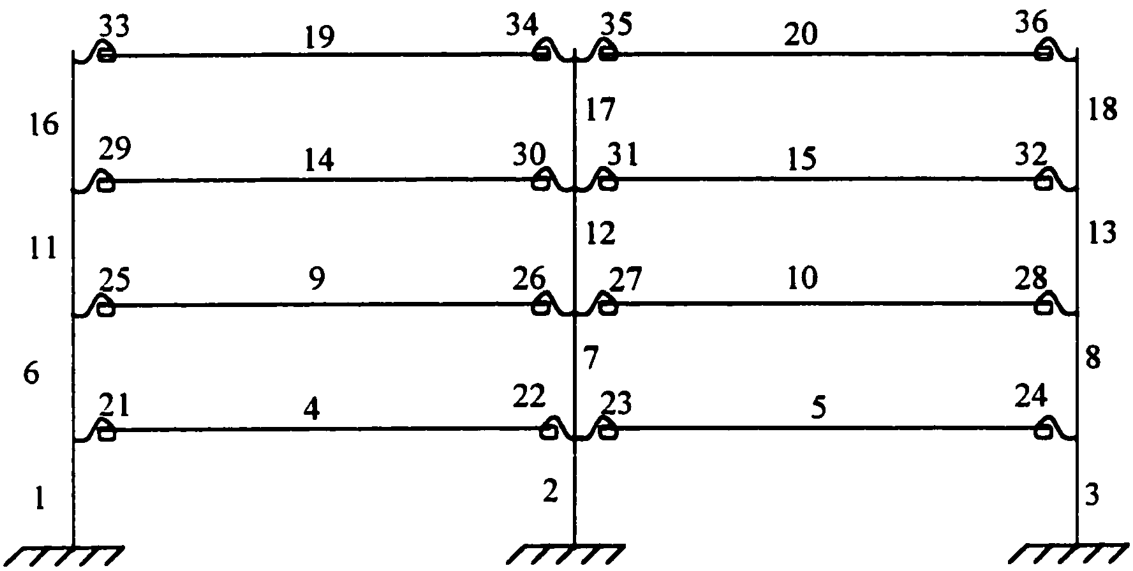

(c)

Fig. 2.5 Example 2—Planar Frame:
(a) Frame Model; (b) Node Numbers; (c) Element Numbers (Continued)

are required to balance the connection spring moments; but the connection springs will magnify the *P-Δ* effects. The results obtained for story drifts and column moments are summarized in Tables 2.2 and 2.3. Also, results of the spring moments for Examples 1 and 2 are presented in Table 2.4. As shown, when all joints in the frame are actually considered rigid, identical results are obtained with those reported by King and Chen (1993) and Bhatti and Hingtegen (1995). However, that is not the case when the joints are modeled as semi-rigid connections. The frame analysis results presented in Tables 2.2 and 2.3 use the moment-rotation function of Eq. (2.5) with the values of α = 0.8, 0.9, and 1.0 in columns (6), (7), and (8) of these tables, respectively. As indicated from the values reported in these tables, as the value of α increases, the maximum lateral sway increases, showing that the connection becomes more flexible as α is increased. To further illustrate this, Fig. 2.6 shows a plot of the exponential function (Eq. (2.5)) for the same initial stiffness, K_e, and ultimate moment capacity, M_u, used in frames of Examples 1 and 2 (K_e = 786,732 kip-in./rad and M_u = 1,989 kip-in.) for values of α = 0.8, 0.9, and 1.0. The results of Tables 2.2 and 2.3 are consistent with the moment-rotation plots of Fig. 2.6, since lateral sway increases with increasing connection flexibility with maximum lateral sway obtained using α = 1.0. As indicated in Table 2.2, the values of absolute maximum moment in columns increase by increasing the rigidity parameter α from 0.8 to 1.0. In order to investigate the effect of these parameters on the frame with a uniform distributed load (now Newton-Raphson iteration applies), the maximum bending moment in the three lower level columns (i.e., element numbers 1, 2, and 3) increases as the rigidity parameter, α, is increased and the moment in other columns

Table 2.2 Results for Frame of Example 1

Maximum lateral displacement (in.)									
		Rigid connection with P-Δ			Semi-rigid connection with P-Δ				
					Present study				
Node No. (1)	Rigid no P-Δ (2)	Present Study (3)	Bhatti & Hingtegen[13] (4)	King & Chen[12] (5)	α = 0.8 (6)	α = 0.9 (7)	α = 1.0 (8)	Bhatti & Hingtegen[13] (9)	King & Chen[12] (10)
3	1.011	1.168	1.168	1.16	1.09	1.20	1.35	1.477	2.02
7	1.509	1.731	1.731	1.82	1.62	1.78	2.10	2.292	3.26

Absolute maximum bending moments in columns (kip-in.)									
		Rigid connection with P-Δ			Semi-rigid connection with P-Δ				
					Present study				
Element No. (1)	Rigid no P-Δ (2)	Present Study (3)	Bhatti & Hingtegen[13] (4)	King & Chen[12] (5)	α = 0.8 (6)	α = 0.9 (7)	α = 1.0 (8)	Bhatti & Hingtegen[13] (9)	King & Chen[12] (10)
1	1,443	1,703	1,677	1,670	1,706	1,708	1,730	1,739	1,837
2	1,437	1,701	1,699	1,644	1,701	1,705	1,723	1,731	1,834
4	711	800	794	794	854	889	902	902	1,116
5	711	802	795	794	854	889	902	902	1,116

Table 2.3 Results for Frame of Example 2 (Continued)

(a) Maximum lateral displacement (in.)									
		Rigid connection with P-Δ			Semi-rigid connection with P-Δ				
					Present study				
Node No.	Rigid no P-Δ	Present Study	Bhatti & Hingtegen[13]	King & Chen[12]	α = 0.8	α = 0.9	α = 1.0	Bhatti & Hingtegen[13]	King & Chen[12]
(1)	(2)	(3)	(4)	(5)	(6)	(7)	(8)	(9)	(10)
4	0.260	0.269	0.269	0.270	0.40	0.42	0.44	0.304	0.400
11	0.639	0.663	0.663	0.660	0.60	0.72	0.85	0.771	1.070
18	0.909	0.941	0.941	0.940	1.09	1.12	1.23	1.116	1.610
25	1.070	1.109	1.109	1.110	1..21	1.42	1.65	1.328	1.950

Table 2.3 Results for Frame of Example 2

(b) Absolute maximum bending moments in columns (kip-in.)

Element No.	Rigid no P-Δ	Rigid connection with P-Δ			Semi-rigid connection with P-Δ				
					Present study				
		Present Study	Bhatti & Hingtegen[13]	King & Chen[12]	α = 0.8	α = 0.9	α = 1.0	Bhatti & Hingtegen[13]	King & Chen[12]
(1)	(2)	(3)	(4)	(5)	(6)	(7)	(8)	(9)	(10)
1	510	534	534	534	615	632	648	619	843
2	932	957	957	958	1,108	1,115	1,250	1,016	1,170
3	1,117	1,202	1,202	1,202	1,212	1,349	1,440	1,254	1,397
6	467	455	455	455	280	212	98	404	291
7	631	657	657	656	622	612	593	649	596
8	1,087	1,102	1,102	1,101	1,212	983	1,025	1,064	1,044
11	616	615	615	615	621	454	491	591	559
12	458	473	474	473	440	581	530	496	542
13	1,020	1,029	1,029	1,029	1,102	1,051	1,108	1,005	996
16	701	703	704	02	683	593	478	687	705
17	195	200	200	200	215	342	228	225	313
18	815	818	820	818	795	753	885	812	846

Table 2.4 Connection Spring Moments for Frames of Example 1 and 2 (Continued)

(a) For the frames of Example 1						
Spring No.	Moment (kip-in.)			Rotation (rad)		
	$\alpha = 0.8$	$\alpha = 0.9$	$\alpha = 1.0$	$\alpha = 0.8$	$\alpha = 0.9$	$\alpha = 1.0$
4	1,989	1,989	1,989	0.009	0.021	0.025
5	1,989	1,989	1,989	0.003	0.011	0.017
8	1,989	1,989	1,989	0.003	0.011	0.017
9	1,989	1,989	1,989	0.009	0.021	0.025

Table 2.4 Connection Spring Moments for Frames of Example 1 and 2

(b) For the frames of Example 2						
Spring No.	Moment (kip-in.)			Rotation (rad)		
	$\alpha = 0.8$	$\alpha = 0.9$	$\alpha = 1.0$	$\alpha = 0.8$	$\alpha = 0.9$	$\alpha = 1.0$
21	1,989	1,989	1,989	0.003	0.010	0.015
22	1,989	1,989	1,989	0.016	0.020	0.022
23	1,989	1,989	1,989	0.005	0.012	0.022
24	1,989	1,989	1,989	0.012	0.023	0.030
25	1,989	1,989	1,989	0.004	0.015	0.022
26	1,989	1,989	1,989	0.010	0.019	0.022
27	1,989	1,989	1,989	0.002	0.011	0.021
28	1,989	1,989	1,989	0.010	0.020	0.050
29	1,989	1,989	1,989	0.006	0.014	0.020
30	1,989	1,989	1,989	0.009	0.017	0.023
31	1,989	1,989	1,989	0.007	0.015	0.020
32	1,989	1,989	1,989	0.008	0.015	0.020
33	1,989	1,989	1,989	0.002	0.007	0.009
34	1,989	1,989	1,989	0.004	0.009	0.023
35	1,989	1,989	1,989	0.002	0.009	0.018
36	1,989	1,989	1,989	0.003	0.012	0.022

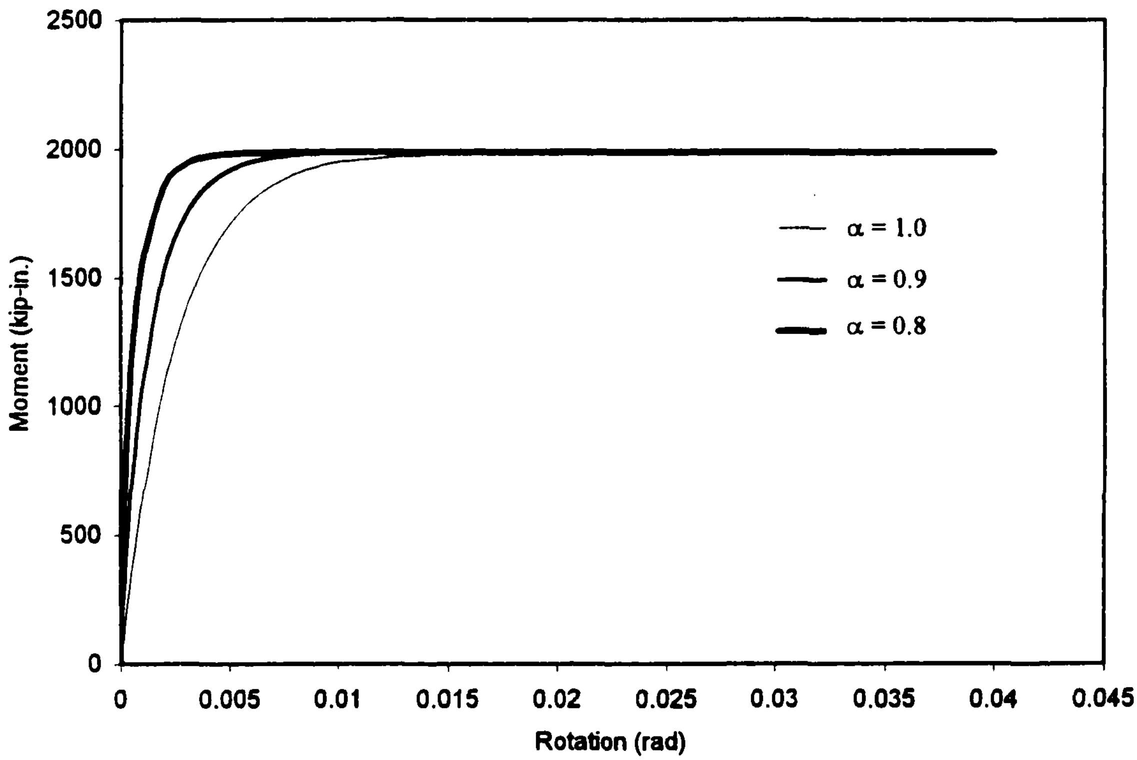

Fig. 2.6 Exponential Moment-Rotation Function Plot with Rigidity Parameters, $\alpha = 0.8$, $\alpha = 0.9$, and $\alpha = 1.0$

decreases or increases due to semi-rigid behavior, which causes redistribution of moments. The results obtained in column (6) for α = 0.8 of Tables 2.2 and 2.3 are close to that reported by Bhatti and Hingtegen (1995). This is due to the fact that the exponential function used for these examples (M_u = 1,989 kip-in., K_e = 786,732 kip-in./rad and α = 0.8) models the connection behavior being close to an elastic-perfectly-plastic model, which is similar to the connection model used by Bhatti and Hingtegen (1995). This model is much stiffer than that used by King and Chen (1993). The exponential function presented in this study can model a variety of moment-rotation curves using an appropriate value for the rigidity parameter, α. For the same connection initial stiffness and ultimate moment capacity, a value of α = 0.8 represents a stiffer connection and a value of α = 1.0 represents a more flexible connection, as shown in Fig. 2.6. The exponential function, Eq. (2.5), along with the coupled nonlinear frame analysis program algorithm presented in this chapter, uses a marching scheme in which the solution advances along the moment-rotation curve of the semi-rigid connection element. To check this, the results for connection spring moments along with the corresponding connection rotations obtained for Examples 1 and 2 are presented in Tables 2.4. From this table it can be seen that for the frames of Examples 1 and 2 as the rigidity parameter, α, is increased, the connection rotations also increases. The results of Table 2.4 also show that for the frame of Example 1, the lower-level springs (elements 4 and 9) are the most highly stressed springs (i.e., θ = 0.025 rad for α = 1.0) and the upper level springs (elements 5 and 8) are the least stressed springs (θ = 0.017 rad for α = 1.0). Plots of moment-rotation curves obtained from the frame analysis program are compared with the exponential function, Eq. (2.5), in Figs. 2.7(a and b) with the rigidity parameter, $\alpha = 1.0$, for the least and the most stressed springs of Example 1, respectively. As this figure demonstrates, the moment-rotation curves obtained from frame analysis programs are identical to the exponential function, Eq. (2.5).

2.6 Parametric Study

The connection model suggested in this chapter is described by the following three parameters: initial stiffness, K_e, ultimate moment capacity, M_u, and rigidity parameter α. In order to investigate the effect of these parameters on the frame behavior, a typical unbraced frame of an office building, as shown in Fig. 2.8, is used. This frame has also been used by Bhatti and Hingtegen (1995). The frame consists of three bays and four stories, and the following data is used to compute the loads: dead load = 75 psf (6 in. slab), live load = 100 psf, wind load = 25 psf (on vertical area), and frame spacing = 25 ft. The beam and column sections used are shown in Fig. 2.8. By varying the values of K_e, M_u, and α, basically different types of connections are assumed to be used for the frame, and their effect on the frame response is compared. In this parametric study, the influence of these parameters, as they are varied one-at-a-time from a low to a high value, on the lateral drift of the response quantity in evaluating its performance. Thus, the sway or drift of the frame is considered as the main response quantity in evaluating its performance. The ultimate strength is not considered in this study. The values chosen are such that the moment generated in the spring representing the semi-rigid connection is not allowed to exceed the plastic moment capacity of the beam cross-section. Also,

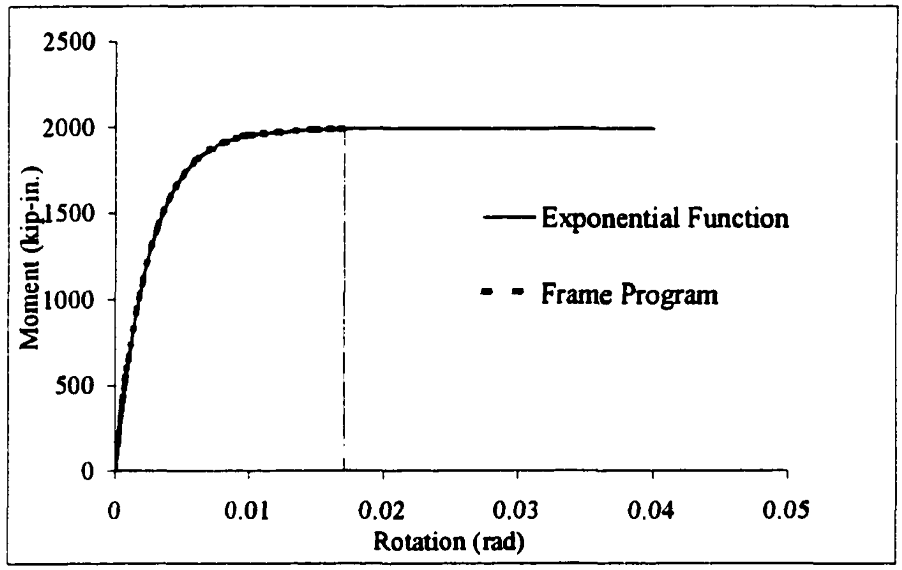

(a)

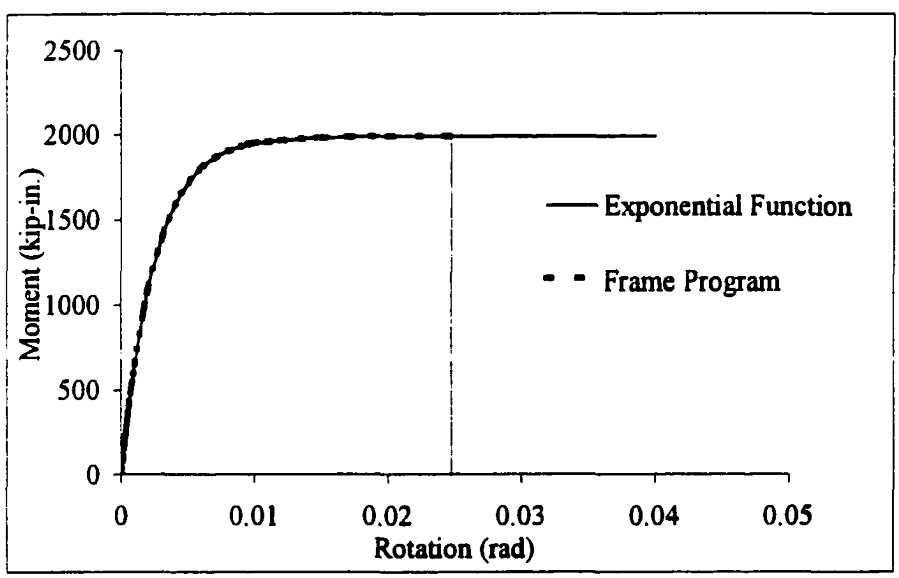

(b)

Fig. 2.7 Comparison of Moment-Rotation Plot Obtained from Frame Analysis Program with Theoretical Moment-Rotation Plot----Example 1: (a) Least Stressed Spring; (b) Most Stressed Spring

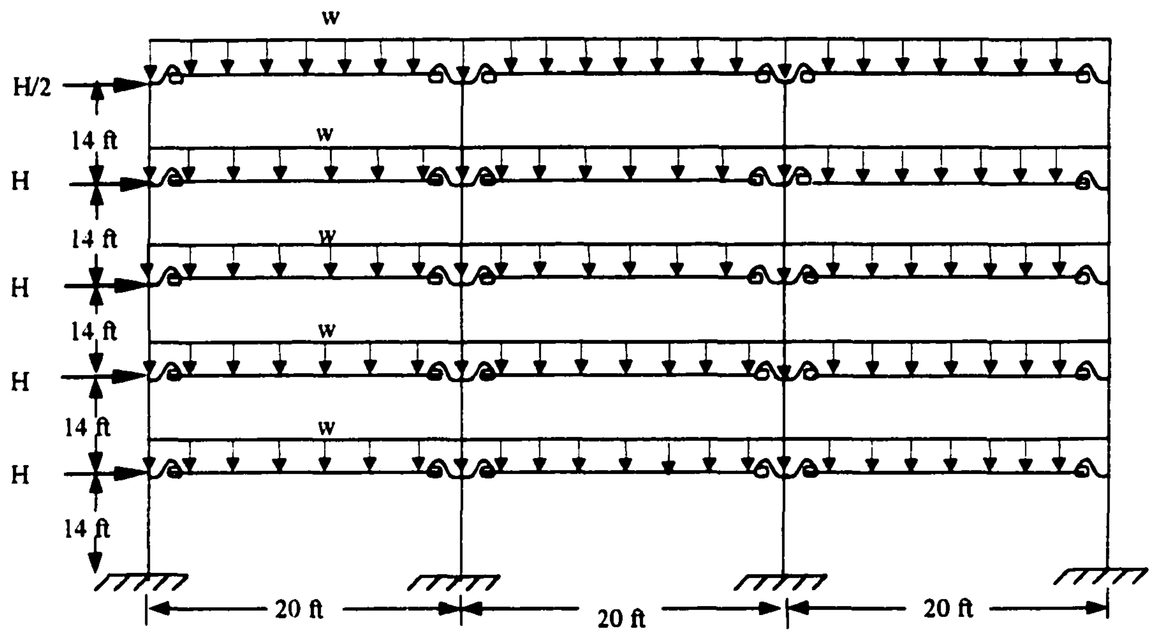

Columns: Levels 1 and 2 are W14×90
Levels 3, 4 and 5 are W14×61
Beams: All are W24×76

Fig. 2.8 Planar Frame Used for the Parametric Study

when varying one variable, the others were held constant to a selected value, generally chosen as an average value. The results obtained are presented in the sub-sections that follow.

2.6.1 Effect of Connection Initial Stiffness

The effect of initial stiffness, K_i, on the frame maximum drift is shown in Fig. 2.9, both without and with *P-Δ* effect considered in the frame analysis. In this study, M_u and α were taken to be 2,000 kip-in. and 1.0, respectively. From Fig. 2.9, it can be seen that for very small values of K_e, the connection behaves basically like a pinned-connection with little to no transfer of moments. The lateral loads are completely resisted by columns, which behave as cantilever beams over their full height. It should be noted that *P-Δ* effect magnifies the lateral drift of the frame for low values of K_e. However, for high values of K_e the *P-Δ* effect makes no difference. Also for very high values of K_e (i.e., $K_e > 10^7$ kip-in./rad), the frame behaves as one with rigid connections and with the value of maximum lateral sway being much less than H/400 = 840/400 = 2.1 in., which is a typical design value used for frames with rigid joints.

2.6.2 Effect of Connection Ultimate Moment Capacity

The effect of the connection ultimate moment capacity on the sway response of the parametric study frame is investigated. Figure 2.10 shows the lateral sway versus connection ultimate moment capacity, M_u, for two different values of connection initial stiffness (i.e., $K_e = 10^5$ kip-in./rad and $K_e = 10^6$ kip-in./rad). For a

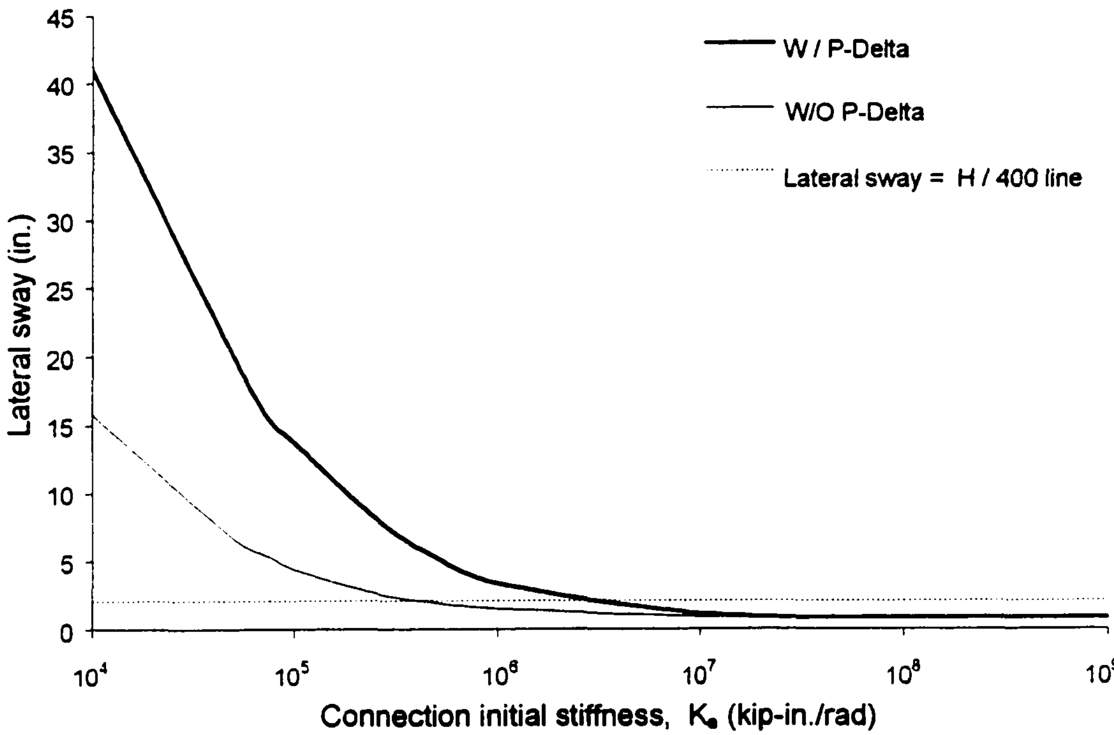

Fig. 2.9 Effect of Connection Stiffness on Lateral Sway

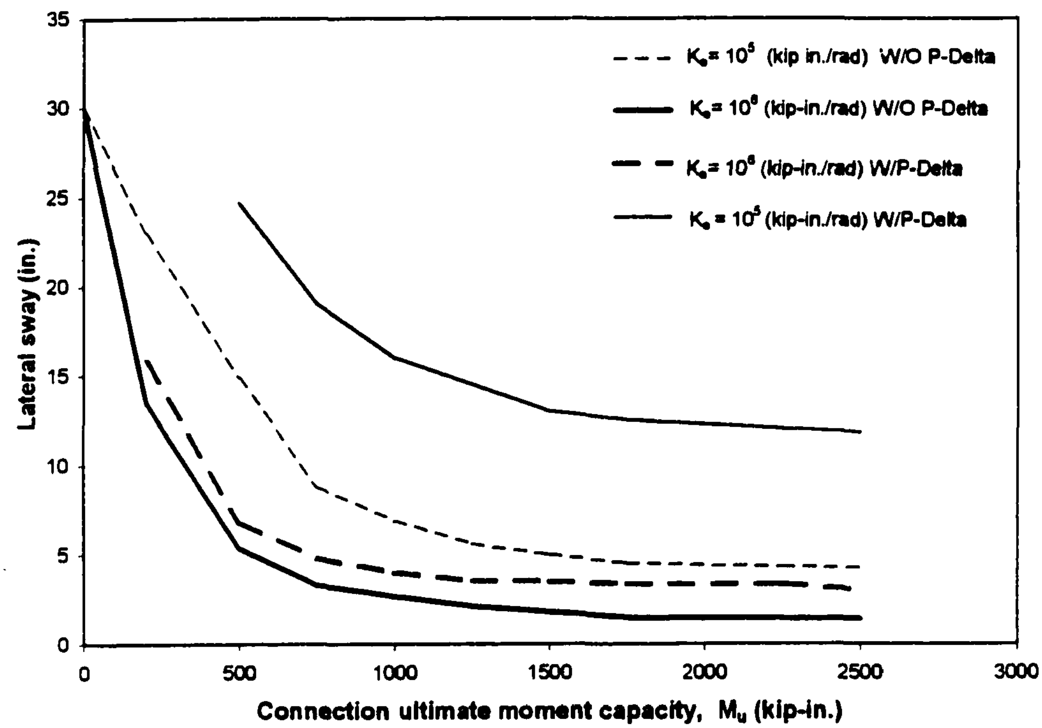

Fig. 2.10 Effect of Connection Strength and Stiffness on Frame Sway

very low connection moment capacity, the frame would behave like a shear connection frame without lateral braces, which results in high lateral sway. As connection moment capacity increases, lateral sway would decrease as a function of initial connection stiffness with higher lateral drift for lower initial connection stiffness. In all cases shown in Fig. 2.10, the lateral sway is magnified when the P-Δ analysis is performed.

2.6.3 Effect of Connection Rigidity

The effect of varying the connection rigidity parameter, α, of the exponential model, Eq. (2.9), is investigated and presented in Fig. 2.11. In this part of the study, the ultimate moment capacity of the connection, M_u, was kept constant at a value of M_u = 2,000 kip-in. and the rigidity parameter, α, was varied from a low value of α = 0.5 to a high value of α = 1.0. The connection initial stiffness, K_e, was varied from a low value of $K_e = 5 \times 10^4$ (kip-in./rad) to a high value of $K_e = 10^6$ (kip-in./rad). Figure 2.11(a) shows the effect of connection rigidity, α, in absence of P-Δ effects and Fig. 2.11(b) shows the effect of connection rigidity including P-Δ effects. In both cases as the connection rigidity parameter, α, increases, the sway would increase with magnified sway in presence of P-Δ effects. It should be noted, as expected, for low values of α (i.e., α < 0.6) similar sway is obtained for all values of K_e, with and without P-Δ effects.

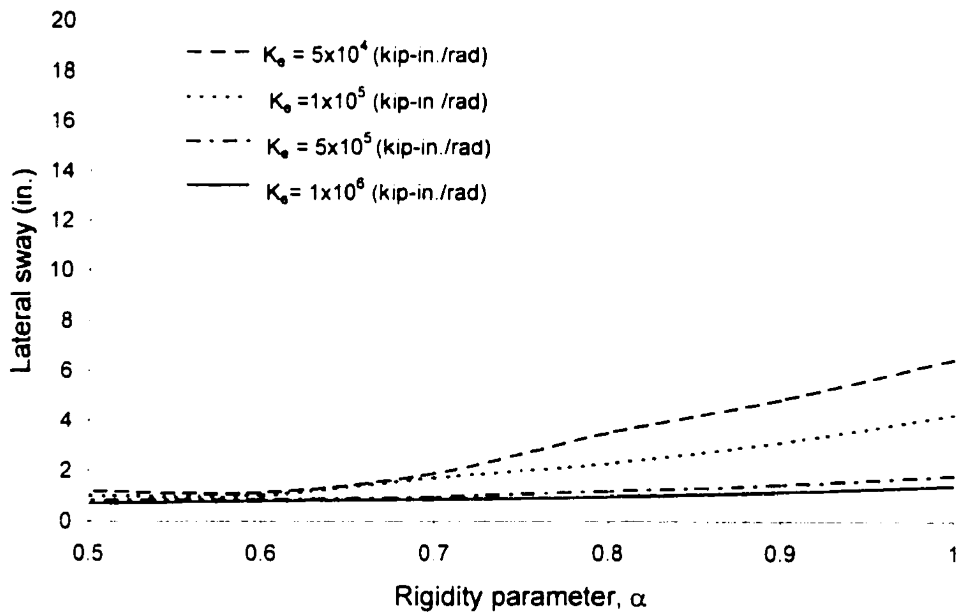

(a)

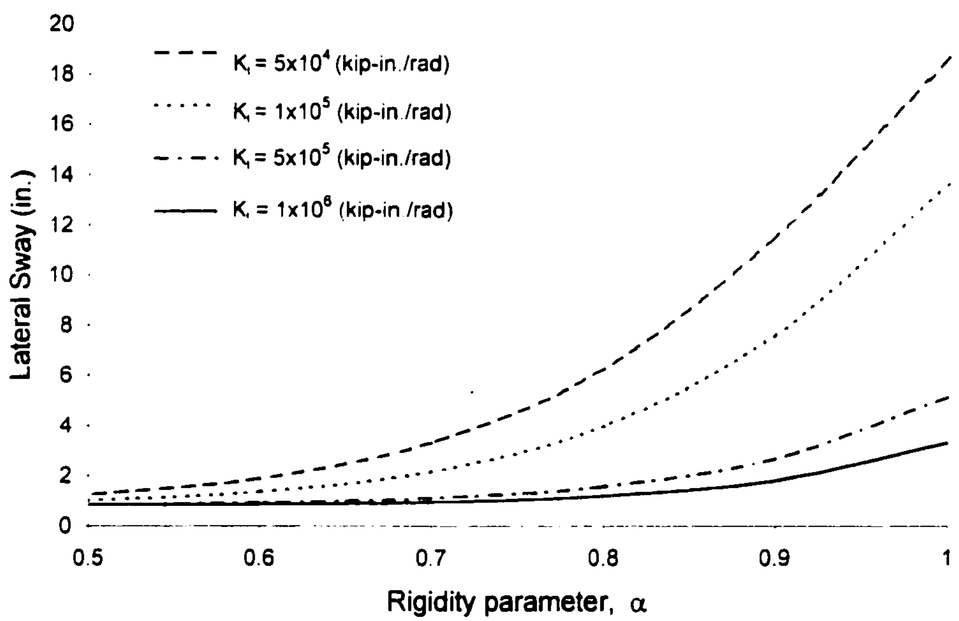

(b)

Fig. 2.11 Effect of Connection Rigidity on Lateral Sway: (a) W/O P-Delta; (b) With P-Delta

2.7 Effect of Decay of Tangential Stiffness

To show the effect of rate of decay of the tangent stiffness of the connection spring elements on lateral sway, Fig. 2.12 shows the graphical plot of lateral sway versus tangential sway for the most and least stressed spring elements of Example 1 with $K_e = 10^6$ kip-in./rad, M_u = 2,000 kip-in. and α = 1.0. As shown in this figure, for low values of sway the tangent stiffness of the most and least stressed connection are about equal (up to about $K_t = 6\times10^5$ kip-in./rad). But, as sway increases, the rate of decay of the most stressed spring is much more rapid occurs due to the coupled P-Δ effect. The tangent stiffness of the least stressed connection also decays, but at a slower rate as demonstrated from the values shown in Fig. 2.12. It should also be noted in Fig. 2.12 that when K_t approaches to zero (when the spring moment is equal to ultimate moment), the sway rapidly increases. This happens because the connection behaves as an elastic-perfectly-plastic element. This example clearly demonstrates that when semi-rigid connection behavior is coupled with P-Δ effect, the sway predicted is significantly magnified.

2.8 Chapter Summary

A finite element analysis computer program algorithm is developed for planar frames with semi-rigid beam-to-column connections (joints), in which the connections are modeled as nonlinear rotational spring elements with material nonlinearity of these spring elements being described by an exponential moment-rotation function. This moment-rotation function uses three connection parameters, the initial elastic stiffness, K_e, ultimate moment capacity, M_u, and rigidity parameter,

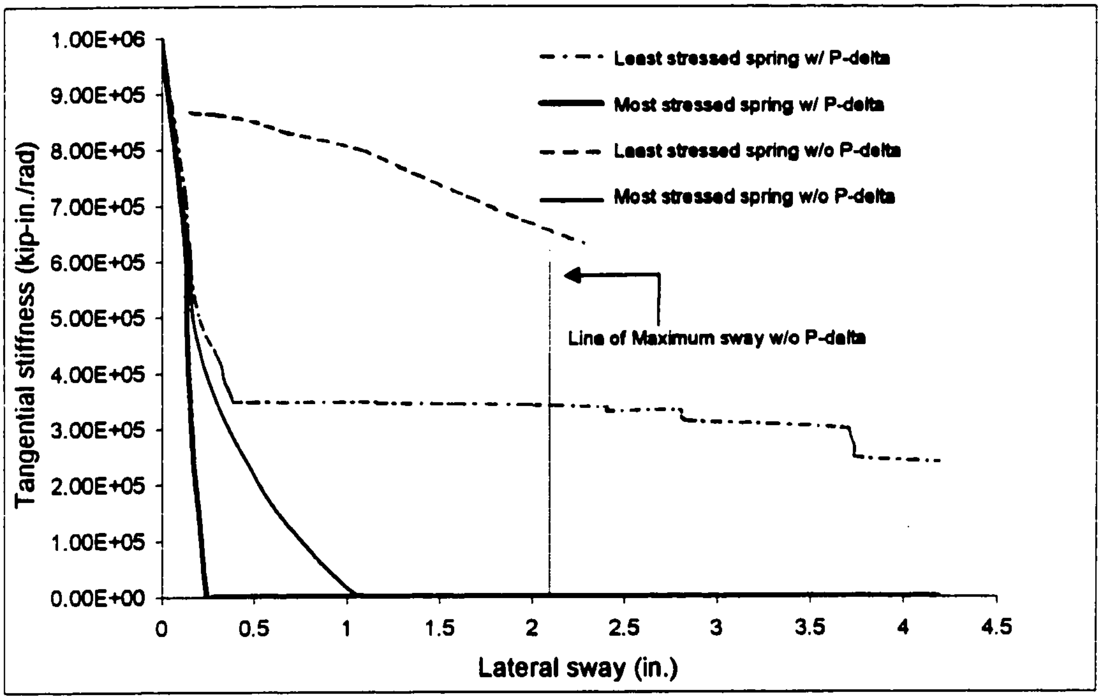

Fig. 2.12 Decay of Tangential Stiffness with Lateral Sway for the Frame of Parametric Study

α, to define the shape of the curve. These spring elements are zero length elements and are treated as point elements in between the beam and column member ends. A Newton-Raphson technique is used to march along the exponential moment-rotation function, which uses the updated tangent stiffness of the connection in each iteration cycle to compute the unbalanced load needed to be applied to satisfy equilibrium. Since for the exponential moment-rotation function the tangent stiffness at the origin (at $\theta = 0°$) is not bounded, it is proposed to compute its value at an infinitesimal rotation ($\theta = 10^{-6}$ rad) away from the origin. This value of tangent stiffness will be approximately equal to the initial elastic stiffness of the connection. The iteration for $P\text{-}\Delta$ is coupled with the iteration for nonlinear spring elements in the Newton-Raphson procedure.

Two frame examples were selected as those used by King and Chen (1993) and Bhatti and Hingtegen (1995). The results obtained for lateral sway and column end-moments were validated by comparing with those reported in these references. The results obtained by using $\alpha = 0.8$ for the value of rigidity parameter were in close agreement with those reported by Bhatti and Hingtegen (1995), because the exponential model used in these examples modeled the connection moment-rotation curve closer to an elasto-plastic model, which is the moment-rotation model used by Bhatti and Hingtegen (1995)

A parametric study was conducted to investigate the effect of the three parameters, K_e, M_u, and α, defining the moment-rotation function on the response of the frame (i.e., lateral sway). The result of this study indicated that as the connection initial stiffness, K_e, increases, the frame behaves like a frame with rigid joints and in which the maximum lateral sway is less than $H/400$, where H is the inter-story lateral load. For a low value of the connection moment capacity, M_u, the frame behaves as a shear connection frame with no lateral braces, and in which the lateral load is primarily resisted by columns acting as cantilever beams. As the ultimate moment of the connection was increased, the frame sway decreased depending on the value of the initial elastic stiffness, K_e, and rigidity parameter, α, used. For low values of α (i.e., $\alpha = 0.5$), the results are similar to a frame with rigid joints; whereas for high values of α (i.e., $\alpha = 0.9$ to 1.0), the results are similar to a frame with semi-rigid joints analyzed using the algorithm presented in this chapter. The effect of rate of decay of tangent stiffness of connection elements on the lateral sway was also investigated.

CHAPTER III

EXPERIMENTAL PROGRAM

3.1. General

Dynamic analysis of semi-rigid frames requires the moment-rotation hysteresis behavior of the beam-to-column connection mechanism to be known. Then, the connections can be modeled as a rotational spring with this known moment-rotation hysteresis relationship. This type of analysis and modeling technique was presented in Chapter II for static analysis of semi-rigid frames subjected to monotonic loads. Actually, the moment-rotation hysteresis behavior of a semi-rigid beam-to-column connection can only be obtained through experimental testing. In this study, the moment-rotation hysteresis relationship was obtained by testing connection geometries in which the failure occurs in the connection rather than in the members it is connected to. As done for the static loading study, which was described in Chapter II, the column sizes were chosen such that the column element deformation did not contribute significantly towards the total connection rotation. Of course, as pointed out in Chapter II, this is a limitation of the study, but it is considered to be a first important step toward hysteresis models for some of the commonly used beam-to-column semi-rigid connections.

This chapter presents experimental testing procedures and results used to obtain the moment-rotation hysteresis loops for a wide range of semi-rigid connections, some of which were shown in Fig. 1.1 of Chapter I. Referring to Fig.1.1, the end-plate connections are categorized as being the most rigid and can be used to transfer significant moment between the members connected. On the other hand, double web angle connections are the most flexible and are often classified as simple (shear) connections, which are modeled as incapable of transferring any significant moment between the connecting members. This figure also shows that the top and seat angle connections are in between these two extremes. This chapter reports moment-rotation hysteresis test results for semi-rigid connections in which the connection stiffness and moment capacity vary from low to intermediate to high values. In particular, test results for the following semi-rigid connections are presented:

1. Double web angle connections, bolted both to the beam web and the column flange, and those which are welded to the beam web and bolted to the column flange, as shown in Fig. 3.1(a) and Fig. 3.1(b), respectively.
2. Top and seat angle connections, bolted both to the beam and the column flange, as shown in Fig. 3.1(c).
3. Four-bolt flush end-plate connections of the type, as shown in Fig. 3.1(d)
4. Four-bolt extended unstiffened end-plate connections of the type, as shown in Fig. 3.1(e).

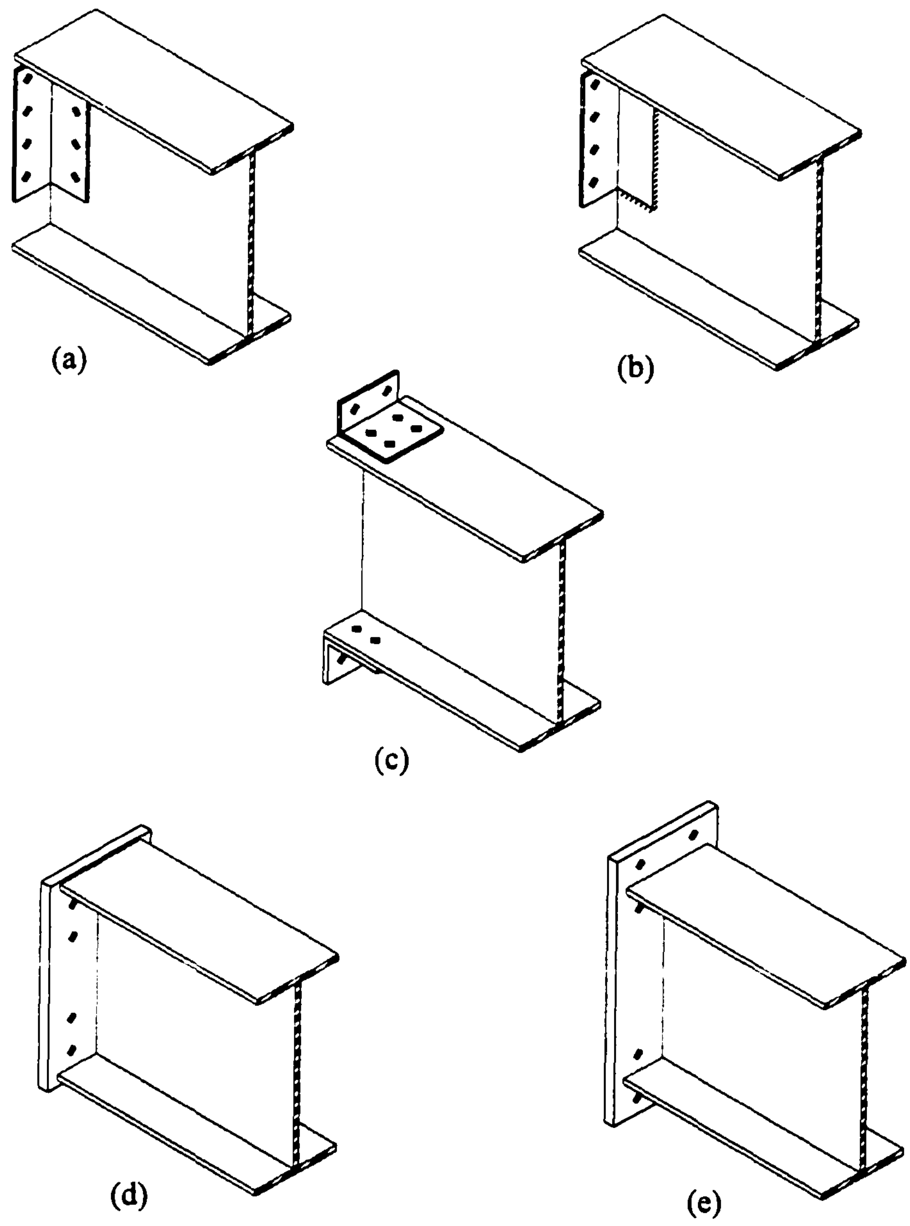

Fig. 3.1 Typical Connection Types Studied: (a) Type I Double Web Angle; (b) Type II Double Web Angle; (c) Top and Seat Angle; (d) Flush End-Plate; (e) Extended End-Plate Connections

3.2 Selection of Test Cases for Semi-Rigid Connections Studied

3.2.1 Types of Double Web Angle Connections Studied

The two types of double web angle connections considered are designated as follows:

1. The double web angle connection, bolted to both the beam web and the column flange, as shown in Fig 3.1(a), will be referred to as a " Type I" double web angle from this point forward
2. The double web angle connection, welded to the beam web and bolted to the column flange, as shown in Fig. 3.1(b), will be referred to as a "Type II" double web angle from this point forward.

3.2.1.1 "Type I" Double Web Angle Connections

The geometric variables describing the configuration of a typical "Type I" double web angle connection configuration are shown in Fig. 3.2. As shown in this figure, the geometric variables are: d_b= bolt diameter; G = angle gauge, distance from the heel of the angle to the center of bolt line; g_c = column gauge, distance between the centerline of the bolts connected to the column flange; t = angle thickness; ℓ = length of the angle leg; k = distance from the heel of the angle to the toe of the filet; and N = number of bolt rows. Also, other variables that need to be considered when fabricating a "Type I" double web angle connection are: d = beam depth; and b_f= column flange width. It should also be noted, that a typical 3 in. bolt spacing was used in all specimens of this study.

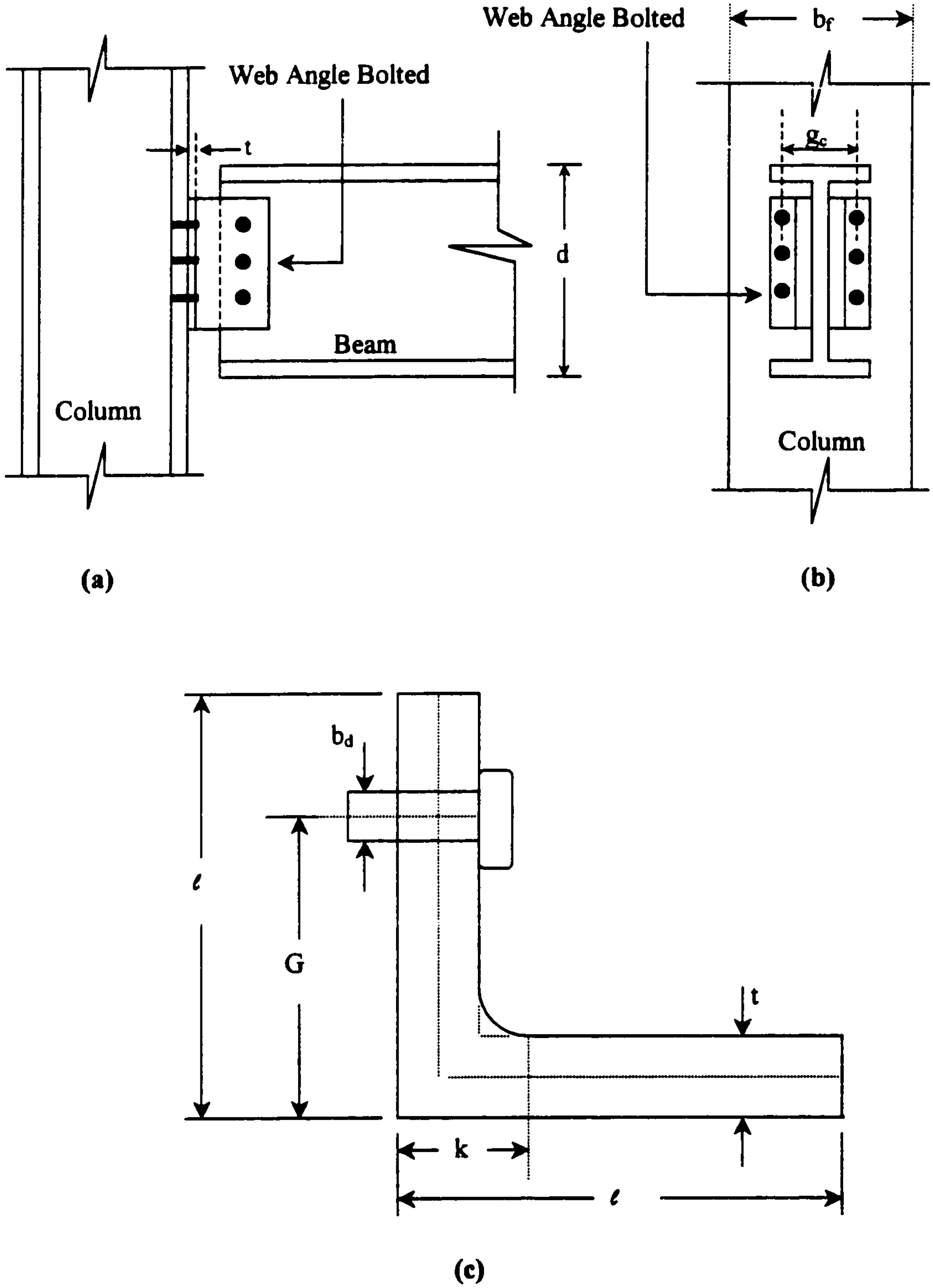

Fig. 3.2 Geometric Variables for a "Type I" Double Web Angle Connection: (a) Side View; (b) Front View; (c) Geometric Variables of Angle

In selecting the test cases for this connection, the aforementioned geometric variables were varied considering current design and fabrication practices (AISC LRFD Manual of Steel Construction 1994), and these variations are presented in columns (3) through (7) of Table 3.1. As shown in column (3) of this table, two lengths of angle legs were considered in this research that are 4 and 5 in. As shown in column (4) of Table 3.1, four values of angle thickness were considered, varying from a low value of 1/4 in., to intermediate values of 1/2 and 1 5/8 in., to a high value of 3/4 in. The reason that more cases of angle thickness variations were considered than the other geometric variables was based on a previous study conducted by Kukreti and Abolmaali (1999), which reported that the angle thickness effects the connection stiffness and strength the most. As shown in column (5) of Table 3.1, the variation of bolt diameter was limited to 5/8 and 3/4 in. As shown in column (6) of Table 3.1, only one value of column gauge (4½ in.) was used for all test specimens, due to budget limitations of the testing program. The author is well aware of the importance of varying column gauge in bolted connections, as reported by Kukreti and Abolmaali (1999) for the top and seat angle connections. As shown in column (7) of Table 3.1, 3, 4, 5, and 6 bolt rows were considered; more bolts were considered for deeper beams. This range of variation is highly important since the number of bolt rows is related to the length of the angle. Therefore, a larger number of bolt rows requires longer angles, resulting in more stiffness and strength of the connection assembly. As shown in column (8) of Table 3.1, three different beam depth sizes (16, 21, and 24 in.) were considered, corresponding to beam sections W16x42, W21x65, and W24x68. In columns (9) and (10) of Table 3.1, the

Table 3.1 Test Cases Selected for "Type I" Double Web Angle Connections

Test No. (1)	Test Designation DW-I-ℓ-t-b_d-g_c-N-d (2)	ℓ (in.) (3)	t (in.) (4)	b_d (in.) (5)	g_c (in.) (6)	N (7)	d (in.) (8)	K_e (kip-in./rad) (9)	M_u (kip-in.) (10)
1	DW-I-4-1/4-3/4-4½-3-16	4	1/4	3/4	4½	3	16	1,949	31
2	DW-I-4-1/4-3/4-4½-4-16	4	1/4	3/4	4½	4	16	1,949	31
3	DW-I-4-5/8-3/4-4½-4-16	4	5/8	3/4	4½	4	16	103,147	117
4	DW-I-5-1/2-3/4-4½-4-21	5	1/2	3/4	4½	4	21	98,143	134
5	DW-I-4-1/4-3/4-4½-5-21	4	1/4	3/4	4½	5	21	1,949	31
6	DW-I-4-3/8-3/4-4½-5-21	4	3/8	3/4	4½	5	21	28,773	57
7	DW-I-4-3/8-3/4-4½-3-16	4	3/8	3/4	4½	3	16	28,773	57
8	DW-I-4-3/8-3/4-4½-4-16	4	3/8	3/4	4½	4	16	28,773	57
9	DW-I-5-1/2-5/8-4½-5-24	5	1/2	5/8	4½	5	24	32,372	83
10	DW-I-5-3/4-3/4-4½-5-24	5	3/4	3/4	4½	5	24	1,444,402	255
11	DW-I-4-1/2-3/4-4½-4-24	4	1/2	3/4	4½	4	24	32,372	83
12	DW-I-5-3/8-5/8-4½-4-24	5	3/8	5/8	4½	4	24	24,917	87
13	DW-I-5-3/8-5/8-4½-6-24	5	3/8	5/8	4½	6	24	24,917	87

monotonic (static) values for initial connection stiffness, K_o, and ultimate moment capacity, M_u for each test specimen selected are reported, as obtained from the empirical equations presented in Kishi and Chen (1987b). These equations were developed using experimental results for double web angle connections subjected to static loads, and in which the bolts were snug-tight as per rules specified in the AISC LRFD Manual of Steel Construction (1994). These values are compared to the values obtained when the connections are subjected to cyclic loads, and the bolts are fully pre-tensioned. It appears to the author, that the formulae presented by Kishi and Chen (1987b) predicts the angle's stiffness and strength, rather than stiffness and strength of the connection assembly. This can be observed by comparing the stiffness values (column (9)) and the strength values (column (10)) reported in Table 3.1 for Test Specimens (1) and (2). The equations presented by Kishi and Chen (1987b) predict the same values of stiffness and strength for both test cases, while the difference between Test Specimens (1) and (2) is in the number of bolt rows used. Test Specimen (1) uses less angle material than Test Specimen (2), therefore, the value of stiffness and strength should be higher than that for Test Specimen (2). The equations presented by Kishi and Chen (1987b) does not account for this difference.

The test cases selected for the study and reported in column (2) of Table 3.1 are designated by **DW-I-ℓ-t-b_d-g_c-N-d**, where: **DW** represents the Double Web angle connection, **I** represents the "Type I" connection, and the other variables were defined earlier. Therefore, Test Specimen (1) in Table 3.1, which is designated as DW-I-4-1/4-3/4-4½-3-16, denotes a double angle test specimen that is bolted to both the beam web and the column flange, and consists of 4x4x1/4 angles with three ¾ in. diameter bolts at a column gauge of 4½ in. The depth of the beam used in this test specimen is 16 in., which corresponded to a depth of a W16x42 section.

3.2.1.2 "Type II" Double Web Angle Connections

The geometrical variables describing the configuration of a typical "Type II" double web angle connection are shown in Fig. 3.3. As shown in this figure, the geometric variables are: d_b = bolt diameter; G = angle gauge, distance from the heel of the angle to center of the bolt line; g_c = column gauge, distance between centerline of the bolts connected to the column flange; t = angle thickness; ℓ = length of the angle leg; k = distance from the heel of the angle to the toe of the fillet; and N = number of bolt rows. Other variables that need to be considered when fabricating "Type II" double web angle connections are: d = beam depth; and b_f = column flange width. As in the "Type I" connections, all bolts were located on 3 in. spacing.

In selecting the test cases for this connection, the aforementioned variables were varied considering current design and fabrication practices (AISC LRFD Manual of Steel Construction 1994), and these variations are presented in columns (3) through (7) of Table 3.2. As shown the column (3) of Table 3.2, the following different lengths of angle legs were considered: 3, 4, 5, and 6 in. As shown in column (4) of Table 3.2, the following values of angle thickness were considered: 1/4, 3/8, 1/2, 5/8, and 3/4 in. As shown in column (5) of Table 3.2, the following sizes of bolt diameters were considered: 1/2, 5/8, 3/4, and 7/8 in. As shown in

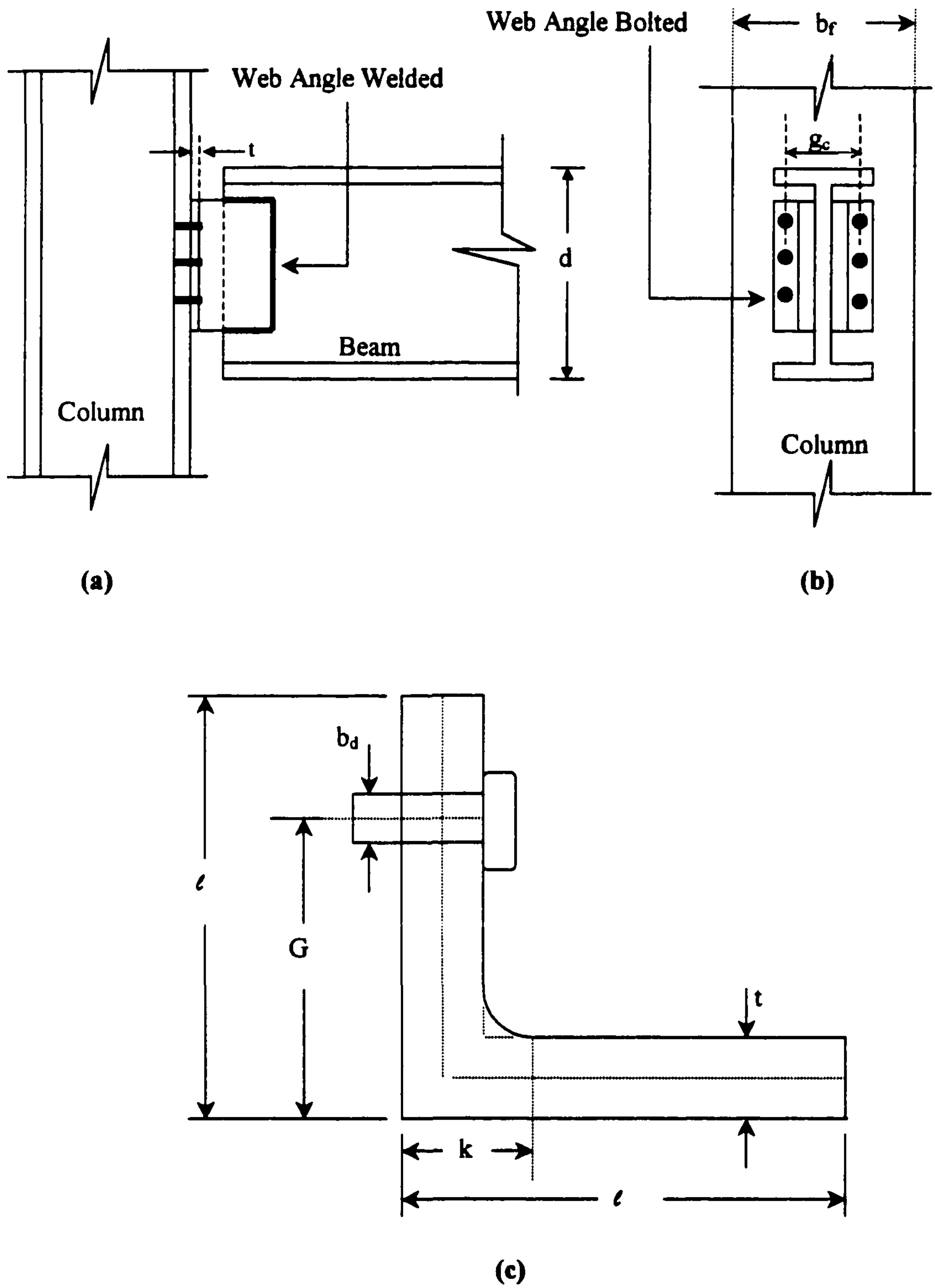

Fig. 3.3 Geometric Variables for a "Type II" Double Web Angle Connection: (a) Side View; (b) Front View; (c) Geometric Variables of Angle

Table 3.2 Test Cases Selected for "Type II" Double Web Angle Connections

Test No. (1)	Test Designation DW-II-ℓ-t-b_d-g_c-N-d (2)	ℓ (in.) (3)	t (in.) (4)	b_d (in.) (5)	g_c (in.) (6)	N (7)	d (in.) (8)	K_e (kip-in./rad) (9)	M_u (kip-in.) (10)
1	DW-II-3-1/4-1/2-2½-3-24	3	1/4	1/2	2½	3	24	10,825	391
2	DW-II-3-1/2-3/4-3½-4-24	3	1/2	3/4	3½	4	24	66,474	1,673
3	DW-II-4-5/8-3/4-3½-5-24	4	5/8	3/4	3½	5	24	83,059	4,026
4	DW-II-4-3/8-3/4-3½-4-24	4	3/8	3/4	3½	4	24	25,834	1,167
5	DW-II-5-3/4-3/4-5½-4-24	5	3/4	3/4	5½	4	24	47,801	2,394
6	DW-II-5-1/2-5/8-4½-6-24	5	1/2	5/8	4½	6	24	61,590	4,288
7	DW-II-6-3/4-3/4-7½-5-24	6	3/4	3/4	7½	5	24	28,773	3,810
8	DW-II-6-1/2-7/8-5½-6-24	6	1/2	7/8	5½	6	24	36,791	4,018

column (6) of Table 3.2, the following column gauges were considered: 2½, 3½, 4½, 5½, and 7½ in. Unlike the "Type I" double web angle connection, the column section selected for this series of experiments was a W14x159, which has a flange width of 15½ in. to accommodate the aforementioned column gauges. As shown in column (7) of Table 3.2, the following numbers of bolt rows were considered: 3, 4, 5, and 6. This actually means that different angle lengths were considered, as was done for "Type I" double web angle connections. Only one beam depth, d = 24 in., was used in all test specimens, which corresponded to the depth of a W24x68 section. However, to be consistent with Table 3.1, this is mentioned as a variable in column (8) of Table 3.2.

Test cases selected for the study and reported in column (2) of Table 3.2 are designated by **DW-II-ℓ-t-b_d-g_c-N-d**, where **II** represents "Type II" connections; all other variables have previously been defined. Therefore, Test Specimen (1) of Table 3.2, which is designated by DW-II-3-1/4-1/2-2½-3-24, denotes a double angle test specimen that is bolted to the beam web and welded to the column flange, and consists of 3x3x1/4 angles with three 1/2 in. diameter bolts at a column gauge of 2½ in.

In columns (9) and (10) of Table 3.2, values of monotonic initial stiffness, K_e, and ultimate moment capacity, M_u, are presented as obtained from the formulae reported by Bhatti and Hingtegen (1995). As shown, K_e varies from a low value of 10,825 kip-in./rad to a high value of 83,059 kip-in./rad, and M_u varies from a low value of 391 kip-in. to a high value of 4,288 kip-in. It should be noted that the values reported in columns (9) and (10) are obtained from empirical equations developed from static test results in which snug-tight bolts were used. However, in this research the bolts were pre-tensioned to 70% of their tensile strength (proof load), and the connections were subjected to cyclic loads. Hence, the values of stiffness and strength obtained with fully pre-tensioned bolts and cyclic loads are expected to differ from those reported in columns (9) and (10) of Table 3.2.

3.2.2 Top and Seat Angle Connections

The geometric variables describing the configuration of a typical top and seat angle are shown in Fig. 3.4. As shown, the angle is connected to the beam flange by two rows of bolts, and to the column flange using by one row of bolts. The geometric variables are: ℓ_v = length of vertical angle leg (the shorter dimension in this study); ℓ_h = length of horizontal angle legs (the longer dimension in this study); d_b = bolt diameter; G = distance from the heel of the angle to the column bolt row; and g_c = column gauge, distance between centerline of the bolts connected to the column flange. Also, other variables that need to be considered when fabricating a top and seat angle connection are: d = depth of the beam; and b_f = width of the column flange.

In selecting the test cases for this connection, the aforementioned variables were varied considering current design and fabrication practices (ASIC LRFD Manual of Steel Construction 1994), and those variations are presented in columns (3) through (8) of Table 3.3. Kishi and Chen (1987b) have presented analytical equations, based on a cantilever model theory and static loads, to calculate the initial stiffness and ultimate moment capacity of a top and seat angle connection. These

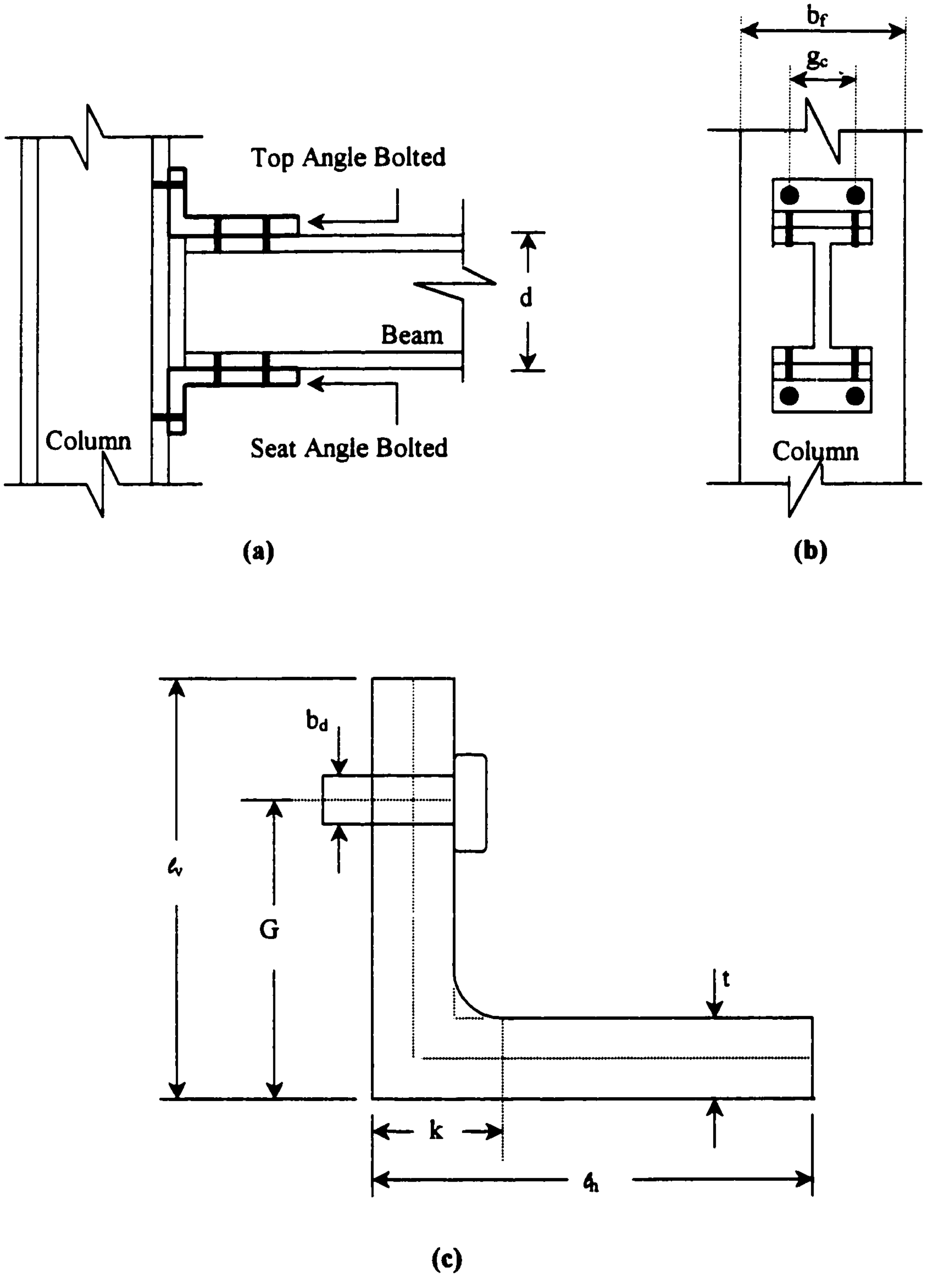

Fig. 3.4 Geometric Variables for a Top and Seat Angle Connection: (a) Side View; (b) Front View; (c) Geometric Variables of Angle

Table 3.3 Test Cases Selected for Top and Seat Angle Connections

Test No. (1)	Test Designation TS-ℓ_h-ℓ_v-t-b_d-G-g_c-d (2)	ℓ_h (in.) (3)	ℓ_v (in.) (4)	t (in.) (5)	b_d (in.) (6)	G (in.) (7)	g_c (in.) (8)	d (in.) (9)	K_e (kip-in./rad) (10)	M_u (kip-in.) (11)
1	TS-6-4-3/4-5/8-2½-5-14	6	4	3/4	5/8	2½	5	14	532,000	752
2	TS-6-6-3/8-5/8-4½-5-14	6	6	3/8	5/8	4½	5	14	8,800	92
3	TS-6-6-3/4-5/8-3½-5-14	6	6	3/4	5/8	3½	5	14	204,000	699
4	TS-6-6-3/4-5/8-4½-4-16	6	6	3/4	5/8	4½	4	16	109,000	516
5	TS-6-4-3/4-3/4-2½-5-14	6	4	3/4	3/4	2½	5	14	627,000	779
6	TS-6-4-1/2-3/4-2½-5-14	6	4	1/2	3/4	2½	5	14	157,000	367
7	TS-6-4-3/4-3/4-2½-4-16	6	4	3/4	3/4	2½	4	16	864,000	902
8	TS-6-4-1/2-3/4-2½-4-16	6	4	1/2	3/4	2½	4	16	218,000	426
9	TS-6-6-3/4-3/4-3½-4-16	6	6	3/4	3/4	3½	4	16	313,000	844
10	TS-6-4-3/4-7/8-2½-4-16	6	4	3/4	7/8	2½	4	16	1,026,000	931
11	TS-6-6-3/4-7/8-2½-4-16	6	6	3/4	7/8	2½	4	16	1,538,000	1,389
12	TS-6-6-3/4-7/8-4½-4-16	6	6	3/4	7/8	4½	4	16	128,000	554

values are reported in columns (10) and (11) of Table 3.3. As shown in column (10) of Table 3.3, when based on static behavior equations, the initial stiffness, K_e, for test specimens selected varied from a low value of 8,800 kip-in./rad for Test Specimen (2) to a high value of 1,538,000 kip-in./rad for Test Specimen (11). Similarly, ultimate moment capacity, M_u, varied from a low value of 92 kip-in. for Test Specimen (2) to a high value of 1,389 kip-in. for Test Specimen (11), as shown in column (11) of Table 3.3.

Test cases selected for study and reported in column (2) of Table 3.3 are designated by **TS-ℓ_h-ℓ_v-t-b_d-G-g_c-d**, where **TS** represents the top and seat angle connections; all other variables have been previously defined. Therefore, a test specimen identified as TS-6-4-3/4-5/8-2½-5-14 denotes a top and seat angle connection fabricated from an angle with a horizontal leg length of 6 in., a vertical leg length of 4 in., and a thickness of 3/4 in. (i.e., L6x4x3/4 in.). This angle is connected to the beam and column flanges by 5/8 in. diameter A-325 bolts, where the distance, G, from the heel of the angle to the centerline of the first column row is 2½ in. The column gauge for this test specimen is 5 in., and the beam depth used is 16 in. It should be noted, that in column (3) of Table 3.3 only one size of horizontal angle length was considered: 6 in.; whereas, two sizes of vertical angle lengths were considered: 4 and 6 in., as shown in column (4). Thus, two angle sizes were used in selection of test cases—L6x6xt and L6x4xt in. As shown in column (5) of Table 3.3, the angle thickness considered varied from a low value of 3/8 in., to an intermediate value of 1/2 in., and a high value of 3/4 in. As shown in column (6) of Table 3.3, bolt diameters were limited to three sizes: 5/8, 3/4, and 7/8 in. Three values of distance were used: 2½, 3½, and 4½ in. Two values of the column gauge, g_c, were used: 4 and 5 in., as shown in column (8) of Table 3.3. Finally, as shown in column (9) of Table 3.3, two values of beam depth, d, were used: 14 and 16 in., corresponding to the depth of W14x43 and W16x45 sections, respectively.

3.2.3 Flush End-Plate Connections

A flush end-plate connection is a special class of end-plate connection in which the end-plate does not extend beyond the beam flange. The geometric variables describing the configuration typical of a flush end-plate connection are shown are shown in Fig. 3.5. As shown in this figure, two rows of bolts are used both above and below the beam flanges. The geometric variables are: b_p = end-plate width; d_p = end-plate depth; t_p = end-plate thickness; p_f = flange pitch, the distance from top of the flange to first row of bolts; p_b = bolt pitch, the vertical distance between the centerline of bolts in either compression or tension side of connection; b_d = bolt diameter; and g_c = column gauge. Beam depth is not considered as a separate geometric parameter for the flush end-plate connection because it is equal to end-plate depth.

The selection of the test specimens for the flush end-plate connections reported in this study was done by Hartman (1999) and based on the end-plate connections commonly used and identified by the Star Building Systems (sponsor of the study). Table 3.4 summarizes the values of the geometric variables for the selected twelve test specimens. Each test specimen was tested twice to validate the experimental findings reported. The flush end-plate test specimens selected and

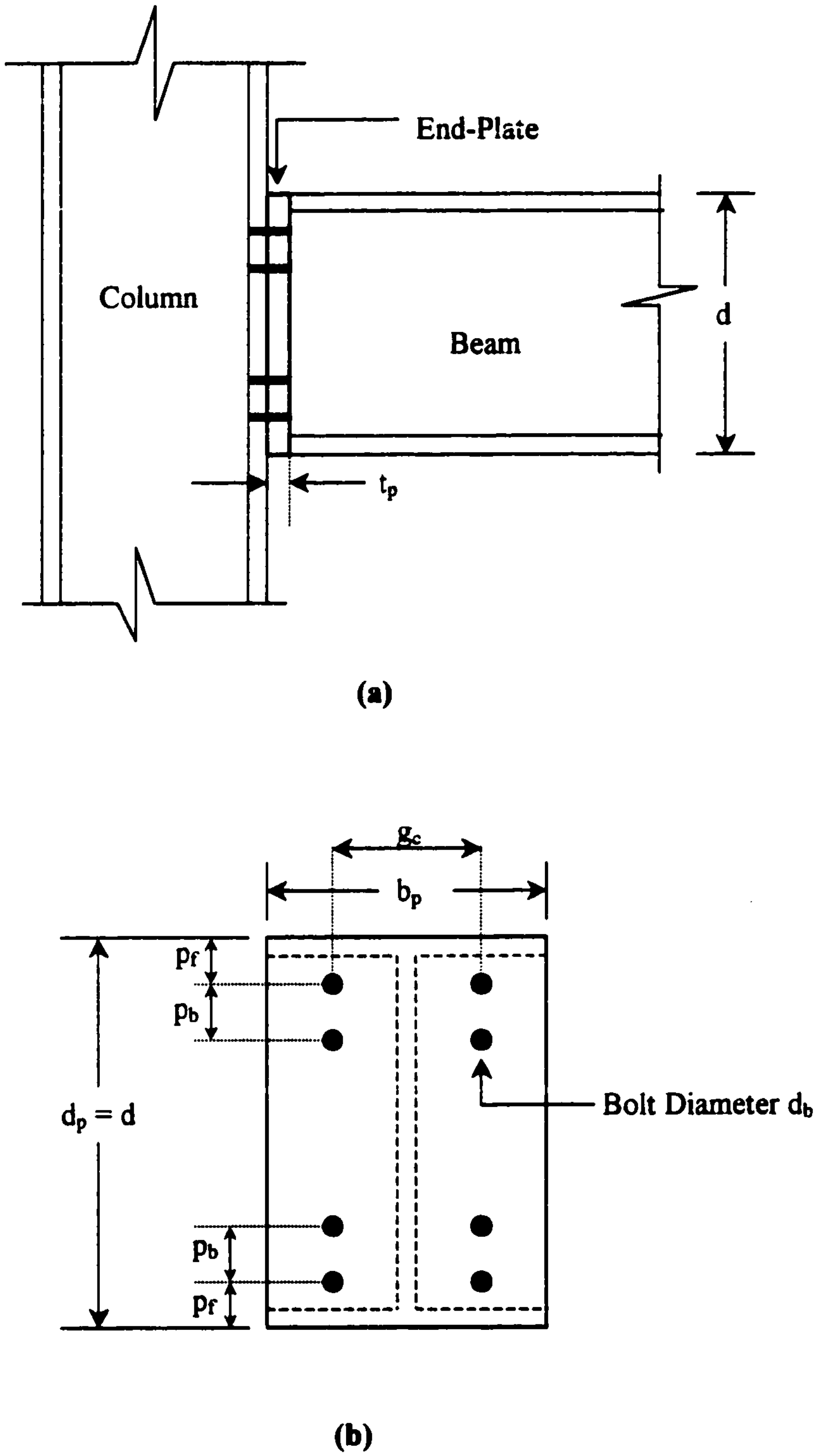

Fig. 3.5 Geometric Variables for a Flush End-Plate Connection: (a) Typical Side View; (b) Typical Front View

Table 3.4 Test Cases Selected for Flush End-Plate Connections

Test No. (1)	Test Designation FEP-II-b_p-d_p-t_p-b_d-p_f-p_b-g_c (2)	b_p (in.) (3)	d_p (in.) (4)	t_p (in.) (5)	b_d (in.) (6)	p_f (in.) (7)	p_b (in.) (8)	g_c (in.) (9)
1	FEP-II-6-18-3/8-3/4-1⅝-3-3	6	18	3/8	3/4	1⅝	3	3
2	FEP-II-6-18-1/2-3/4-1⅝-3-3	6	18	1/2	3/4	1⅝	3	3
3	FEP-II-6-18-5/8-3/4-1⅝-3-3	6	18	5/8	3/4	1⅝	3	3
4	FEP-II-8-18-3/8-1-1⅞-3½ -3½	8	18	3/8	1	1⅞	3½	3½
5	FEP-II-8-18-1/2-1-1⅞-3½ -3½	8	18	1/2	1	1⅞	3½	3½
6	FEP-II-8-18-3/4-1-1⅞-3½ -3½	8	18	3/4	1	1⅞	3½	3½
7	FEP-II-6-22-3/8-3/4-1⅝-3-3	6	22	3/8	3/4	1⅝	3	3
8	FEP-II-6-22-1/2-3/4-1⅝-3-3	6	22	1/2	3/4	1⅝	3	3
9	FEP-II-6-22-5/8-3/4-1⅝-3-3	6	22	5/8	3/4	1⅝	3	3
10	FEP-II-8-22-3/8-1-1⅞-3½ -3½	8	22	3/8	1	1⅞	3½	3½
11	FEP-II-8-22-1/2-1-1⅞-3½ -3½	8	22	1/2	1	1⅞	3½	3½
12	FEP-II-8-22-3/4-1-1⅞-3½ -3½	8	22	3/4	1	1⅞	3½	3½

reported in column (2) of Table 3.4 are designated by **FEP-II-b_p-d_p-t_p-b_d-p_f-p_b-g_c**, where **FEP** represents the flush end-plate connection and **II** represents two rows of bolts on both sides of beam flanges; all other variables were previously defined. Hence, a test specimen designated as FEP-II-6-18-3/8-3/4-1 5/8-3-3 is interpreted as a flush end-plate connection with two rows of bolts on both sides of the beam flanges with: b_p = 6 in., d_p = 18 in., t_p = 3/8 in., d_b = 3/4 in., p_f = 1 5/8 in., p_b = 3 in., and g_c = 3 in.

As shown in column (3) of Table 3.5, two end-plate widths were considered: 6 and 8 in. The variation of end-plate depth was limited to values of 18 and 22 in. Column (5) of this table shows that four different values of plate thickness were considered: 3/8, 1/2, 5/8, and 3/4 in. As shown in column (6) of Table 3.4, two A-325 bolt sizes were considered: 3/4 and 1 in., and as shown in column (7), two values of flange pitch were considered: 1 5/8 and 1 7/8 in. As presented in columns (8) and (9) of Table 3.4, two values of bolt pitch and column gauge were considered: 3 and 3 1/2 in. It is interesting to note that the same values of the column gauge, g_c, and bolt pitch, p_b, were used in each specimen, which was fabricated to produce a square bolt pattern in tension and compression sides of the connection. It should also be noted that in these specimens the plate width, bolt pitches, and bolt gauge were correlated to bolt diameter.

3.2.4 Extended Unstiffened End-Plate Connections

The geometric variables describing the configuration of a typical extended end-plate connection is shown in Fig. 3.6. As shown in this figure, the end-plate

Table 3.5 Test Cases Selected for Extended End-Plate Connections

Test No. (1)	Test Designation EEP-b_p-d_p-t_p-b_d-p_f-g_c (2)	b_p (in.) (3)	d_p (in.) (4)	t_p (in.) (5	b_d (in.) (6	p_f (in.) (7)	g_c (in.) (8)
1	EEP-7-22½-1/2-3/4-1⅜-3½	7	22½	1/2	3/4	1⅜	3½
2	EEP-8-22½-5/8-7/8-1½-5½	8	22½	5/8	7/8	1½	5½
3	EEP-9-22½-1/2-1⅛-1⅞-3½	9	22½	1/2	1⅛	1⅞	3½
4	EEP-10-22½-1/2-7/8-1⅜-4½	10	22½	1/2	7/8	1⅜	4½
5	EEP-9-31-7/8-1-1¾-3½	9	31	7/8	1	1¾	3½
6	EEP-10-31-3/4-1⅛-1¼-7½	10	31	3/4	1⅛	1¼	7½
7	EEP-9-31-5/8-1-1⅞-7½	9	31	5/8	1	1⅞	7½
8	EEP-10-31-1/2-1⅛-1⅛-3½	10	31	1/2	1⅛	1⅛	3½

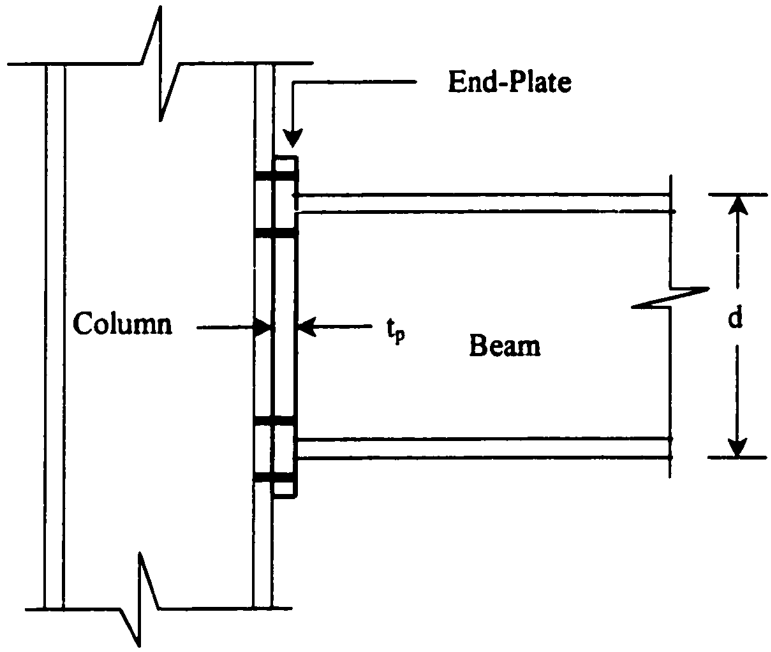

(a)

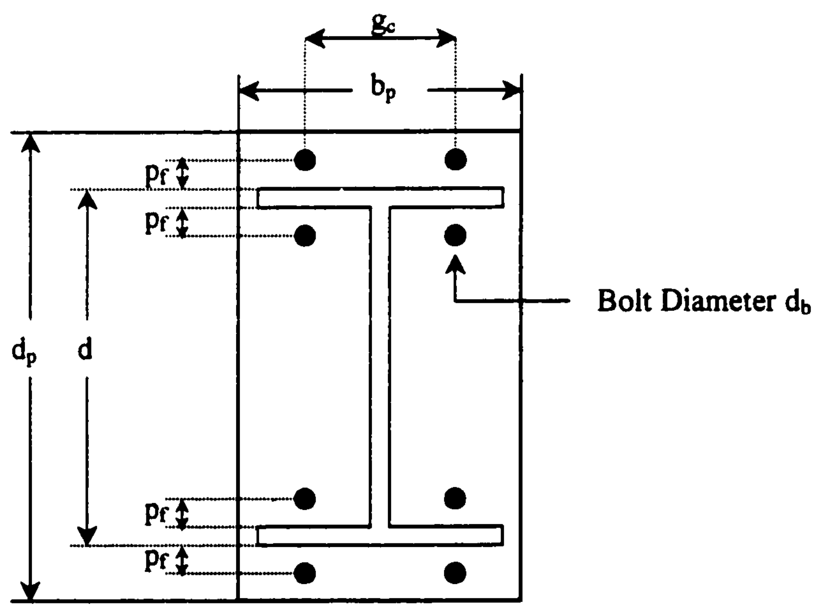

(b)

Fig. 3.6 Geometric Variables for an Extended End-Plate Connection: (a) Typical Side View; (b) Typical Front View

extends beyond the beam flange, and consists of one row of two bolts on either sides of the beam flange. Hence, there are four bolts on either side of a beam flange. This connection is commonly referred to as the extended unstiffened four-bolt end-plate connection. The extended end-plate connection is fabricated by an end-plate welded to the beam-end and bolted to the column flange. The geometric variables defining the connection configuration are shown in Fig. 3.5, and include: b_p = end-plate width; d_p = end-plate depth; t_p = end-plate thickness; p_f = flange pitch, the distance from the top or bottom side of the flange to the first row of bolts; d_b = bolt diameter; and g_c = column gauge. The aforementioned geometric variables were varied within the range, as shown in Table 3.5, and includes values for eight test cases selected. Column (2) of this table shows the test cases designated by **EEP-b_p-d_p-t_p-b_d-p_f-g_c**, where **EEP** represents the extended end-plate connection; all other variables have been previously defined. Therefore, a test specimen designated as EEP-7-22 $\frac{1}{2}$-1/2-3/4-1 $\frac{3}{8}$-3 $\frac{1}{2}$ identifies an extended end-plate connection with: b_p = 7 in., d_p = 22 $\frac{1}{2}$ in., and t_p = 1/2 in. The end-plate of this test specimen is connected to the column flange by bolts with diameter, b_d = 3/4 in., at a flange pitch, p_f = 1 $\frac{3}{8}$ in., and a column gauge, g_c = 3 $\frac{1}{2}$ in.

The varied range of geometric variables in the test specimens selected is presented in columns (3) through (7) of Table 3.5. Column (3) shows four different values of end-plate widths were considered: 7, 8, 9, and 10 in. column (4) shows two end-plate depths were considered: 22 $\frac{1}{2}$ and 31 in. It is important to note that the depth of the end-plate for an extended end-plate connection can actually be related to the beam depth, flange pitch, and bolt edge distance, using specifications presented in the AISC LRFD Manual of Steel Construction (1994). Therefore, the depth of the beam is not considered as an independent geometric variable for this connection. Column (5) shows that the end-plate thickness varied from a low value of 1/2 in. to a high value of 7/8 in., and two intermediate values of 5/8 and 3/4 in. Column (6) shows that four different bolt diameters were considered: 3/4, 7/8, 1, and $1\frac{1}{8}$ in. For the flange pitch, p_f, which is one the most important variables that influence the rigidity of the end-plate (Kukreti et al. 1990), six different values were considered with a low value of $1\frac{1}{8}$ in. to a high value of $1\frac{7}{8}$ in. Finally, as shown in column (8), four values of commonly used column gauge were considered: $3\frac{1}{2}$, $4\frac{1}{2}$, $5\frac{1}{2}$, and $7\frac{1}{2}$ in.

3.3 Typical Test Specimens

A typical test specimen consisted of a beam, which was connected to a stub-column by means of the semi-rigid connection considered. The stub-column section was attached to a reaction frame that extended to the base of the laboratory floor. Typical configurations of the test specimens for double web angle, top and seat angle, flush end-plate, and extended end-plate connections are shown in Figs. 3.7, 3.8, 3.9, and 3.10, respectively. The instrumentation of the test specimen was kept identical with the only difference being the location of the two linear variable displacement transducers (LVDTs). The location of the LVDTs was dependent on the type of semi-rigid connection used, as shown in Figs. 3.7 through 3.10, which will be explained later in this chapter. The stub-column differed for each type of semi-rigid connection tested; but in all test specimens, the column sections selected

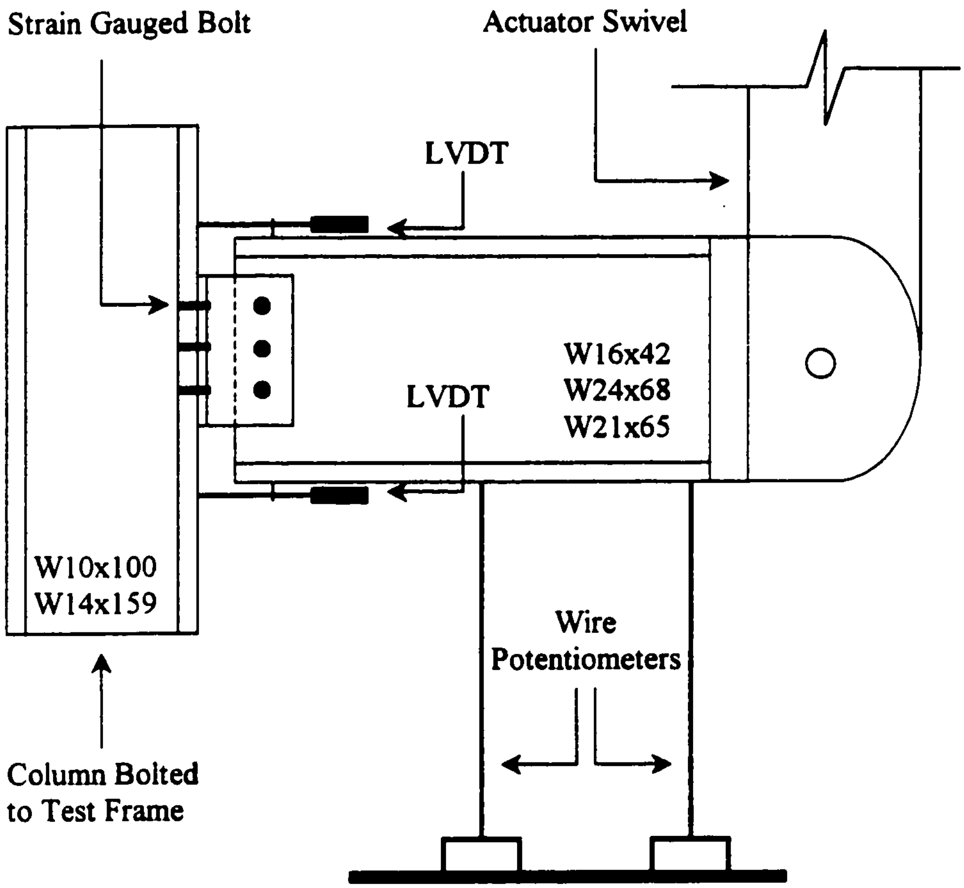

Fig. 3.7 Typical Test Set Up for Double Web Angle Connections

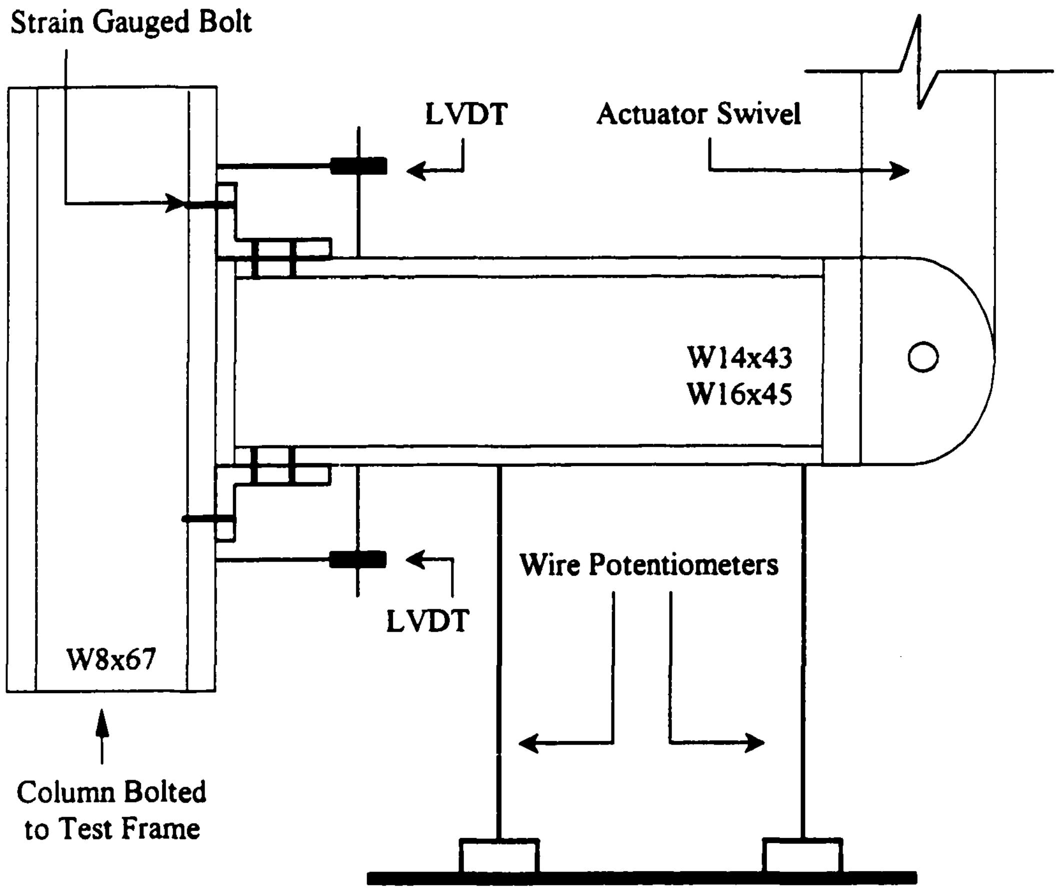

Fig. 3.8 Typical Test Specimen for Top and Seat Angle Connections

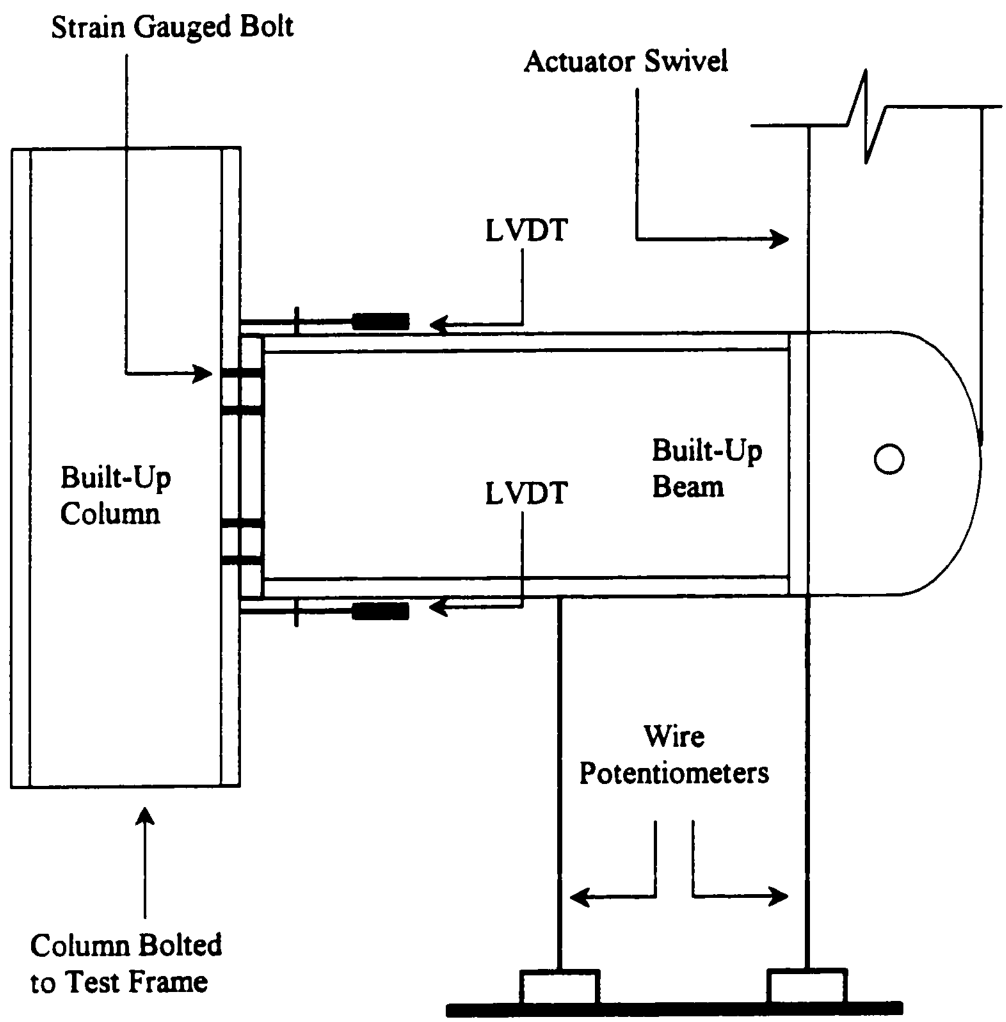

Fig. 3.9 Typical Test Specimen for Flush End-Plate Connections

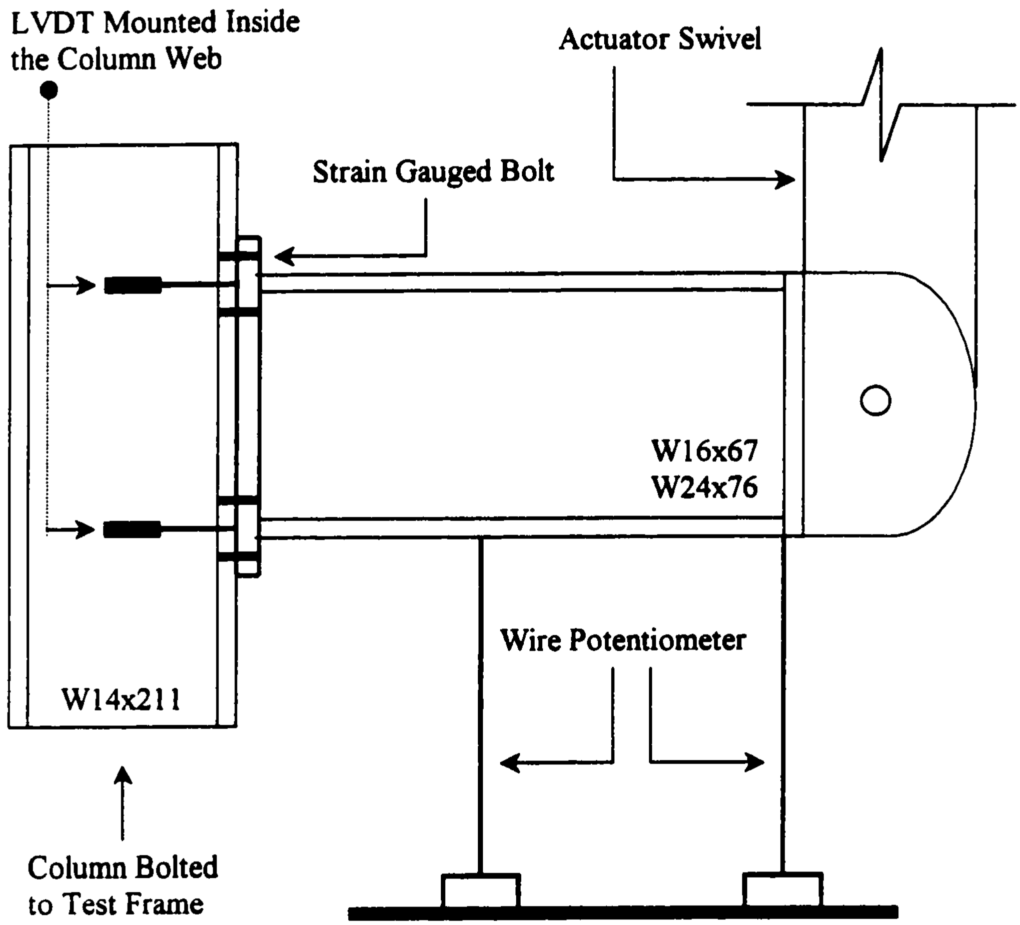

Fig 3.10 Typical Test Specimen for Extended End Plate Connections

had a column flange thickness of 1 in. or greater, which basically provided a rigid column that did not contribute significantly toward the total connection rotation. The column sections selected for different types of connection tested are as follows:

1. For the "Type I" double web angle connection, a W10x100 section with t_f = 1.120 in. was selected.
2. For the "Type II" double web angle connection, a W14X159 section with t_f = 1.190 in. was selected.
3. For the top and seat angle connection, a W8x67 section with t_f = 0.935 in. was selected.
4. For the four-bolt flush end-plate connection, a built-up column with b_f = 8 in., t_f = 1 in., d = 12 in., t_w = 3/8 in., and overall length, L = 60 in. was used.
5. For the four-bolt extended unstiffened end-plate connection, a W14x211 section with t_f = 1.560 in. was selected.

The beams used in the experimental testing program presented in this research were different, based on the type of semi-rigid connection tested. However, all the beams were selected to remain elastic and to ensure that the inelastic (yielding) behavior only occurs in the connection elements. The beam sections selected for the five types of semi-rigid connections tested are as follows:

1. For "Type I" double-web angle connection, two sizes of beams were considered, W16x42 and W21x65, which provided beam depths of 16 and 21 in., respectively.
2. For "Type II" double web-angle connection, one size of beam was considered, W24x68, with a beam depth of 24 in.

3. For the top and seat angle connection, two sizes of beams were considered, W14x43 and W16x45, which provided beam depths of 14 and 16 in., respectively.

4. For the flush end-plate connection, four different built-up beams were considered. For Specimens Tests (1) through (3), the beam dimensions were: $b_f = 6$ in., $t_f = 1/2$ in., $d = 18$ in., $t_w = 1/4$ in., and overall beam length, $L = 84$ in. For Specimens Tests (4) through (6), the beam dimensions were: $b_f = 8$ in., $t_f = 1/2$ in., $d = 18$ in., $t_w = 1/4$ in., and overall beam length, $L = 84$ in. For Specimens Tests (7) through (9), the beam dimensions were: $b_f = 6$ in., $t_f = 1/2$ in., $d = 22$ in., $t_w = 1/4$ in., and overall beam length, $L = 84$ in. Finally, for Specimens Tests (10) through (12), the beam dimensions were: $b_f = 8$ in., $t_f = 1/2$ in., $d = 22$ in., $t_w = 1/4$ in., and overall beam length, $L = 84$ in.

5. For the four-bolt extended unstiffened end-plate connections studied, two different beam sizes, W16x67 and W24x76, were considered providing beam depths of 16 and 24 in., respectively.

The bolts used in all the test specimens were SC-type (slip critical) A-325 high strength bolts. All bolts were pre-tensioned to a level of 70% of their minimum tensile strength (proof load). In each type of connection tested, two-to-three bolts were strain gauged so that the bolt force variation could be observed. Also, this allowed determination of the torque corresponding to proof load level, and the same torque was used to tighten the other (non-strain gauged) bolts. This procedure ensured the same pre-tension force level in all the bolts without the need to strain-gauged all the bolts in the test specimen.

For all tests, bolt forces were measured by bolt gauges, which were placed inside holes drilled in the bolt shanks. The holes were drilled in a manner so that the strain gauges could be centered within the tension area. Referring to Fig. 3.11, the length of the drill distance, d_l, is calculated using the following expressions:

$$d_l = T_l / 2 + SG_l / 2 + W_{bh} \qquad (3.1)$$

where d_l = the length of the hole drilled; T_l = the length of the bolt tension area; SG_l = length of the bolt strain gauge; and W_{bh} = the width of the bolt head. The bolts were drilled from the bolt head to a distance of d_l, given by Eq. (3.1). After drilling, each bolt was cleaned using a special conditioner fluid; and blown dry with a special machine in the laboratory. Then, the wires were soldered to the two wires of the strain gauges in order to connect the gauges to the data acquisition system. The photograph of the data acquisition control console is shown in Fig. 3.12(a). To calibrate the bolts, a voltmeter, Baldwin Universal Testing Machine, shown in Fig. 3.12(c), and an amplifier were used. The bolts were placed in the Baldwin Universal Testing Machine and an increasing monotonic tensile load was applied to the bolts at increments of 1 kip, and the corresponding voltage was recorded. A plot was prepared of voltage (vertical axis) versus load (horizontal axis). Using the method of least squares, a best-fit straight line was passed through these points. The slope of this line is the calibration factor for each bolt. For the tests where the bolt forces were recorded, the tensile force in the bolt was computed by measuring the voltage signal received from the bolt strain gauge and multiplying it by the

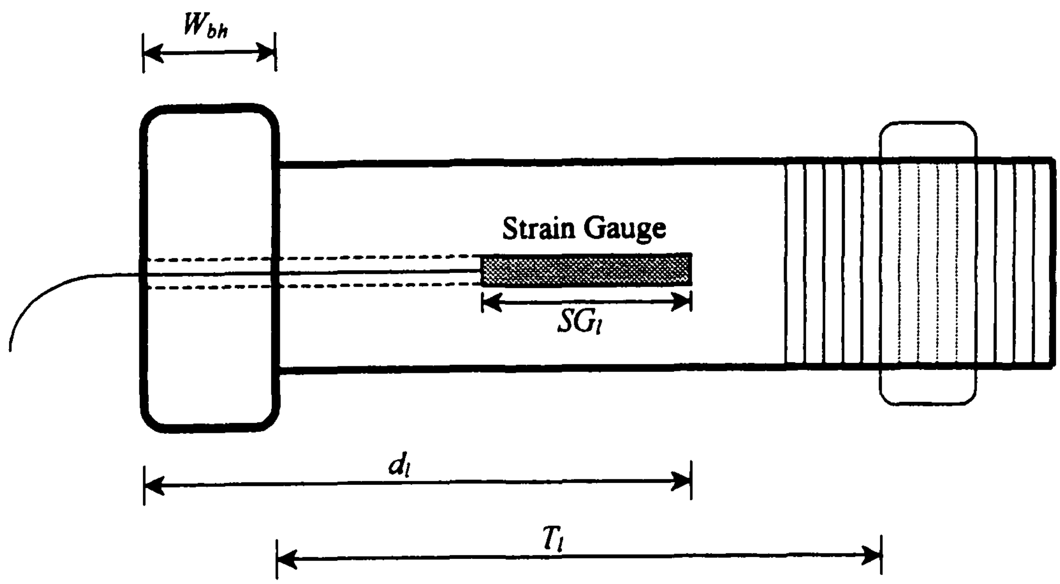

Fig. 3.11 Geometric Details of a Bolt Strain Gauge

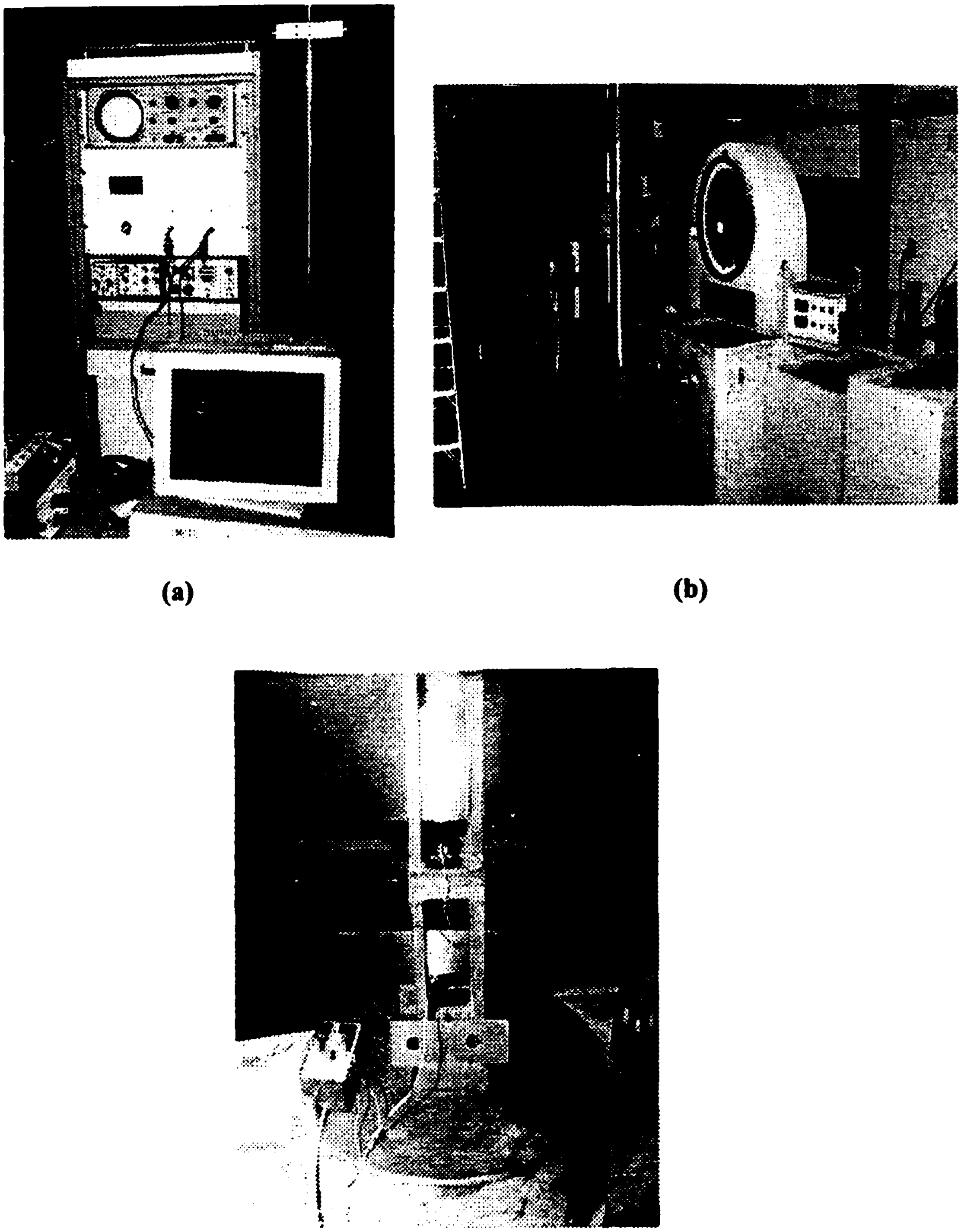

(a) (b)

(c)

Fig. 3.12 Laboratory Equipment Used: (a) Data Acquisition System; (b) Baldwin Testing Machine; (c) Bolt Calibration Set Up

calibration factor. The photograph of the set up for bolt calibration is shown in Fig. 3.12(b).

3.4. Typical Test Set Up and Instrumentation

The basic configuration of the test set up used in this research for all types of connections tested is shown in Fig. 3.13, though this figure shows the test set up for a top and seat angle connection. This test set up consisted of: (1) an actuator to apply the force; (2) a beam of a reaction frame to support the actuator; and (3) a column of a reaction frame to support the column in a typical test specimen. The whole reaction frame was bolted to the laboratory floor, and the column of the test specimen was connected to the column of the reaction frame. Lateral braces were provided at the beam end connected to the actuator swivel to prevent out-of-plane buckling of the test specimen. A photograph of lateral braces is shown in Fig. 3.14. The instrumentation used in the test specimens for double web angle, top and seat angle, flush end-plate, and extended end-plate connections are shown schematically in Figs. 3.7 through 3.10, respectively. This instrumentation consisted of two LVDTs to calculate the relative connection rotation, two wire potentiometers to measure displacements at two points along the beam specimen span, and strain gauged bolts to measure bolt forces. In addition, a load cell and displacement transducers were installed in the actuator to measure the cyclic load applied to the beam-end and the actuator stroke (displacement), respectively. Depending on the type of connection, the two LVDTs were placed close to the top and bottom flanges of the beam, such that the LVDTs tips touched the column flange. The actual

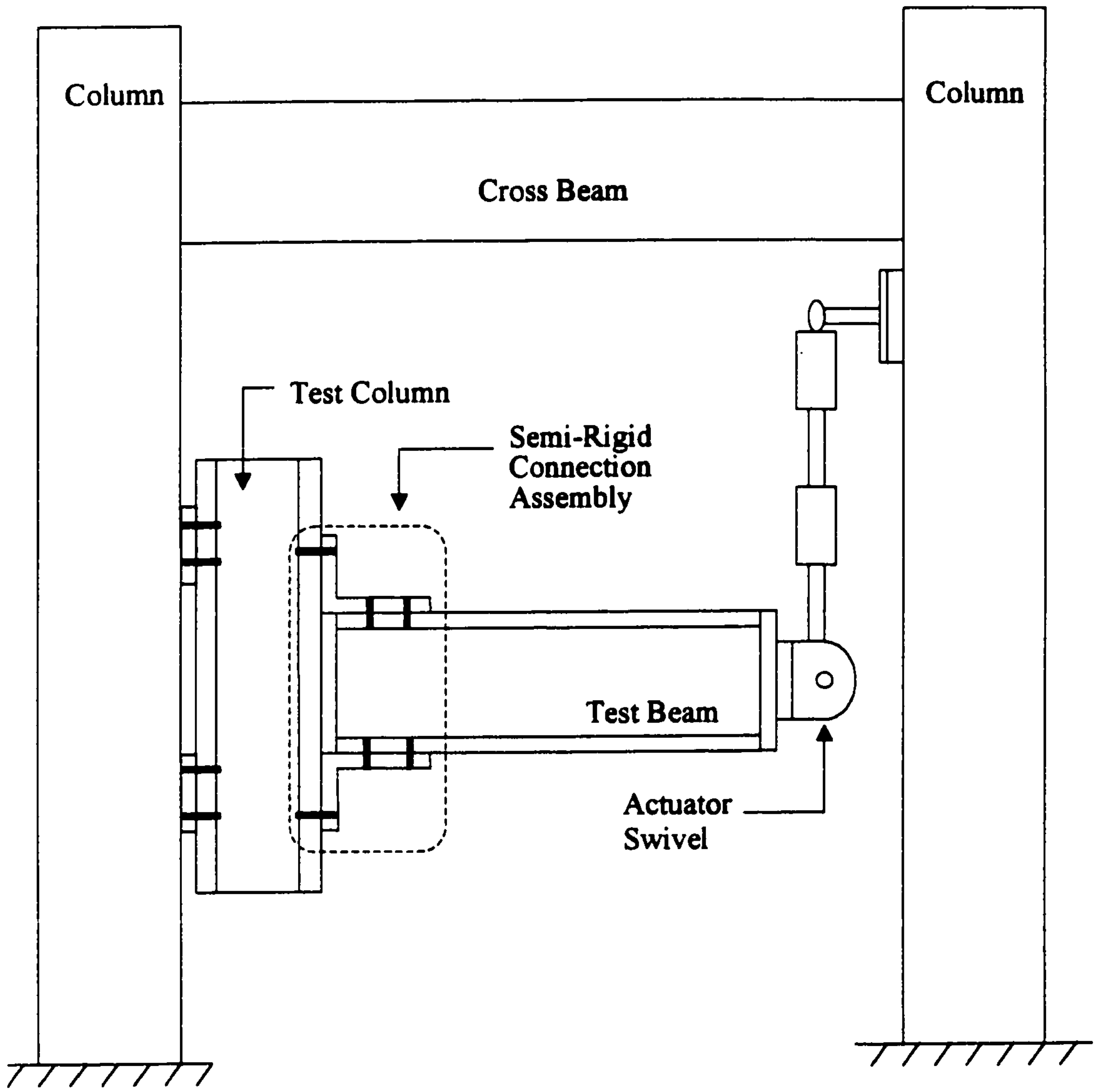

Fig. 3.13 Typical Test Set Up

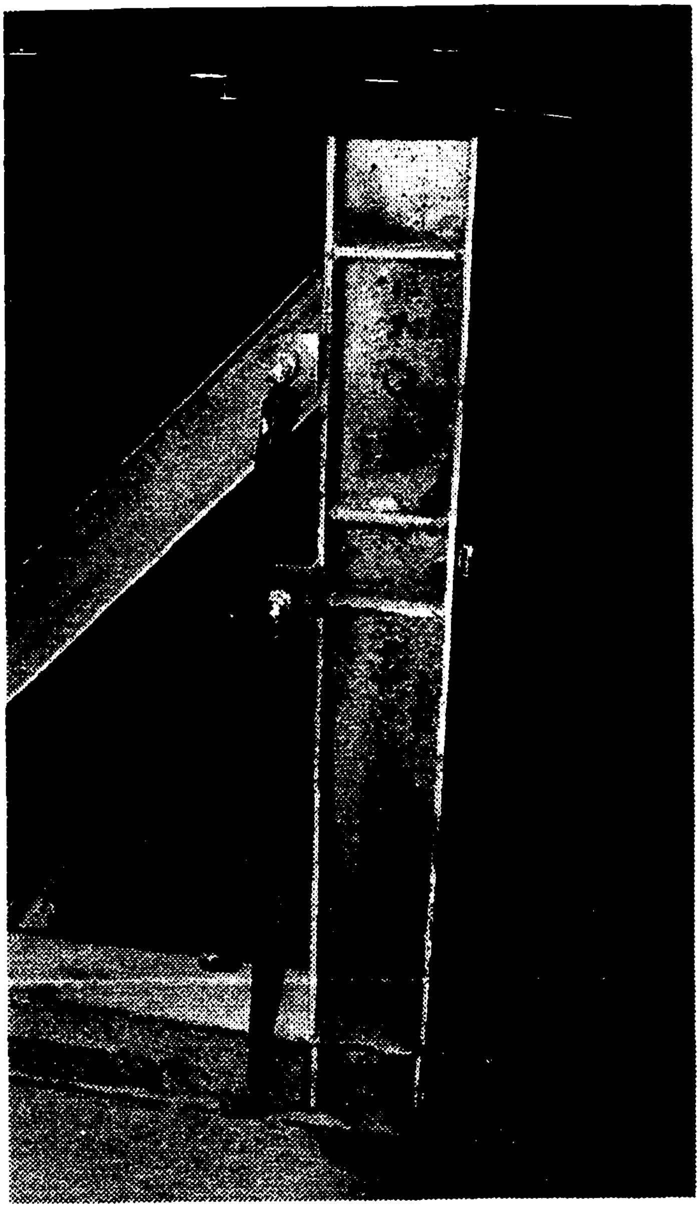

Fig. 3.14 Photograph of Lateral Braces

location of the LVDT tips for the different types of connections tested were as follows:

1. Just above and below the top and bottom beam flanges, respectfully, as shown in Fig. 3.7 for the two types of double web angle connection test specimens (Type I and Type II).
2. Just above and below the top and seat angle, respectively, as shown in Fig. 3.8 for the top and seat angle connection test specimens.
3. Just above and below the top and bottom beam flanges, respectively, as shown in Fig. 3.9 for the four-bolt flush end-plate connection test specimens.
4. At the centerlines of the top and bottom beam flanges by drilling two holes from back of the column flange and mounting LVDTs in the beam column web, as shown in Fig. 3.10.

The relative displacements measured of the two LVDTs, divided by the vertical distance between the their tips, give the local rotation of the connection test specimen. The global rotation of the connection was calculated by dividing the vertical displacement recorded by each wire potentiometer by the distance of the wire potentiometer from the face of the specimen column flange. Hence, the connection rotation at every load level was measured in two independent ways: using LVDT readings and wire potentiometer readings, and the two results were compared for consistency. The moment on the connection applied was calculated by multiplying the force recorded by the actuator load cell by the distance from the center of the actuator to the face of the column. This distance for the different types of connections tested were as follows:

1. For the “Type I” double web angle connection, test specimens = 38.5 in.
2. For the “Type II” double web angle connection, test specimens = 69.5 in.
3. For the top and seat angle connection, test specimens = 44.5 in.
4. For the four-bolt flush end-plate connection, test specimens = 69.5.in.
5. For the four-bolt extended unstiffened end-plate connection, test specimens = 71.0 in.

The typical test set up and instrumentation described were used for all five types of semi-rigid connections studied. However, minor changes were made for “Type II” double web angle connection, where the actuator was bolted to the top of the beam rather than on the beam end. Also, for the case of the extended end-plate connection, two load cells, with a capacity of 50 kip each, were used to obtain the higher moment capacity required.

3.5 Typical Loading History

The loading history used was aimed at duplicating the expected behavior during an earthquake. The initial portion of the loading history used in all tests is shown in Fig. 3.15. As shown in this figure, the specimen was first loaded to a one-kip load applied by the actuator in tension. Then, the specimen was unloaded and reverse loading was applied to a negative value of one-kip actuator load in compression, and finally reloaded to zero. This process was defined as the one-kip loop. For each specimen, three cycles of such one-kip loops were applied at the beginning of the test. Next, the specimen was subjected to three cycles of two-kip loops. The third load step consisted of applying three cycles of three-kip loops,

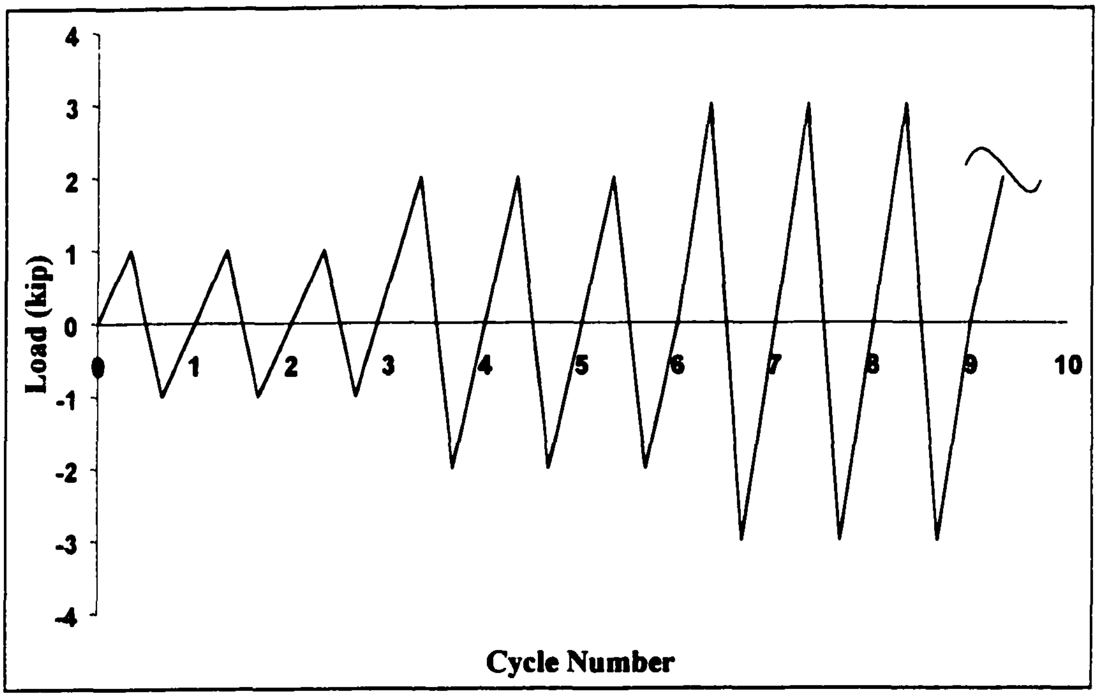

Fig. 3.15 Typical Loading History

followed by two cycles of four-kip loops. This process was repeated during the early stages of the test, and during this stage load feedback was used to control the actuator. The initial stiffness, K_e, was computed from the recorded moment-rotation history for these elastic cycles. The load control was continued until a significant difference in the rotation at peak values in tension and compression was noted. At this point, the control was switched to displacement control, and the displacement was incremented at 0.1 in. intervals. This increment of 0.1 in. continued until a 1 in. displacement value was reached, then the increment was changed to 0.2 in. This displacement increment continued until either bolt failure or excessive connection rotation was observed.

3.6 Typical Testing Procedure

The same test procedure was followed for all the specimens. Each specimen was assembled with all the bolts tightened to their proof load, including the shear connections (double web angle and top and seat angle connections) tested in this study. Next, white wash was applied to the connection region to detect yielding in different components of the connection assembly. The previously calibrated LVDTs were placed properly, depending on the type of semi-rigid connection test specimens used, as described in Section 3.3. The two previously calibrated wire potentiometers were installed, and the actuator was then bolted to the beam. The wire potentiometer, actuator load, and displacement transducers were connected to an automated data acquisition system to record and process the data, and the whole experiment was computer controlled. After the bolts were tightened and the actuator was connected, the cyclic loading was applied through the actuator, following the loading history described in Section 3.5 until either bolt failure or excessive rotation occurred. The connection rotation and moment were recorded as the testing was in progress.

3.7 Test Results

In this section the results for the different semi-rigid connections tested are presented. It is important to mention that the bolts in all connections were pre-tensioned to their proof load, even for the connections that traditionally are considered as shear connections. The test results presented in this section include the failure mode observed for each semi-rigid connection tested, and its moment-rotation hysteresis plot until failure. The test results are first presented for the most flexible connection, which was the double web angle connection, followed by connections with increasing rigidity, and ends with the extended end-plate connection, which was the least flexible.

3.7.1 Double Web Angle Connections

3.7.1.1 "Type I" Double Web Angle Connections

Thirteen tests were conducted for "Type I" double web angle connections, geometric details of which were presented in Table 3.1. Two failure modes were observed to occur, either excessive rotation or beam web bearing failure. Excessive rotation occurs due to excessive yielding of the angle material, beyond acceptable rotation limits for semi-rigid connections. In previous literature, Chen and Lui

(1991), this limit is set at a value of connection rotation of $\theta = 0.03$ rad. When a connection is about to reach the ultimate rotation, significant loss in stiffness occurs. Ultimate rotation in testing was said to occur when any further increase in load cycles did not result in much significant gain in strength (i.e., moment), but it lead to a very rapid increase in rotation. The test was then stopped. The other type of failure observed for "Type I" double web angle connections was beam web bearing failure. This type of failure occurred on test specimens with angle thickness, $t > 3/8$ in. The reason for this failure is that as angle thickness increases, the moment resistance of the connection increases. The resulting larger moment causes larger forces to be transferred to the beam web bolts as shear forces. This transfer of higher bolt shear forces cause the beam web material around the bolt holes to fail in bearing, which can be observed by the holes becoming oval shaped. Photographs of bolts holes "egging" are shown in Fig. 3.16 for Tests (2) and (9) of "Type I" double angle connections tested.

Table 3.6 summarizes the values of initial connection stiffness, K_o, ultimate moment capacity, M_u, and associated failure modes for the twelve test specimens; no data was recorded for one test due to equipment malfunction (Test Specimen (4)). The results presented in column (2) show that the lowest connection stiffness was obtained for Test Specimen (1), 16,721 kip-in./rad, and the highest connection stiffness was obtained for Test Specimen (10), 314,000 kip-in./rad. Comparing Test Specimens (1) and (10), reveals that Test Specimen (1) has the lowest value of angle thickness, $t = 1/4$ in., whereas Test Specimen (10) has the highest value of angle thickness, $t = 3/4$ in. Therefore, some of this difference can be attributed to

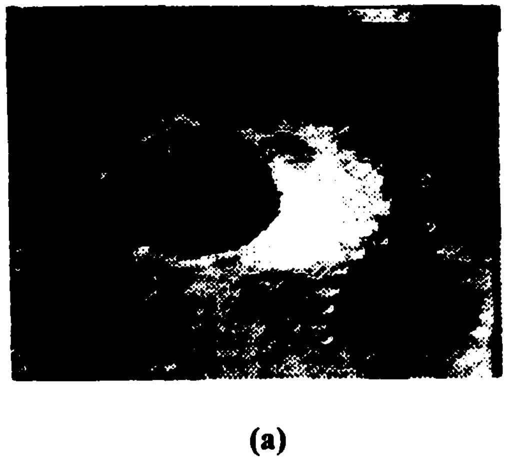

(a)

(b)

Fig. 3.16 Photograph of Bolts "Egging":
(a) For Test (2); (b) For Test (9)

Table 3.6 Test Results for "Type I" Double Web Angle Connections

Test No. (1)	Test Designation DW-I-ℓ-t-b_d-g_c-N-d (2)	Initial Stiffness K_e (kip-in./rad) (3)	Ultimate Moment M_u (kip-in.) (4)	Ultimate Rotation θ_u (rad) (5)	Failure Mode (6)
1	DW-I-4-1/4-3/4-4½-3-16	16,721	105	0.05	Angle Yielding
2	DW-I-4-1/4-3/4-4½-4-16	26,251	184	0.05	Angle Yielding
3	DW-I-4-5/8-3/4-4½-4-16	165,033	561	0.05	Web Bearing
4	DW-I-5-1/2-3/4-4½-4-21	-	-	-	-
5	DW-I-4-1/4-3/4-4½-5-21	99,000	288	0.05	Angle Yielding
6	DW-I-4-3/8-3/4-4½-5-21	194,604	540	0.05	Angle Yielding
7	DW-I-4-3/8-3/4-4½-3-16	53,755	166	0.05	Angle Yielding
8	DW-I-4-3/8-3/4-4½-4-16	122,230	342	0.05	Angle Yielding
9	DW-I-5-1/2-5/8-4½-5-24	170,517	707	0.045	Web Bearing
10	DW-I-5-3/4-3/4-4½-5-24	314,000	814	0.044	Web Bearing
11	DW-I-4-1/2-3/4-4½-4-24	108,000	442	0.044	Web Bearing
12	DW-I-5-3/8-5/8-4½-4-24	50,356	325	0.044	Yielding/bearing
13	DW-I-5-3/8-5/8-4½-6-24	158,000	900	0.048	Angle Yielding

the angle thickness. Also, in Test Specimen (10) the number of bolt rows, N=5, were noted, whereas the number of bolt rows decreased, N=3, in Test Specimen (1). Also, the beam depth was increased from d = 16 in. in Specimen (1) to d = 24 in. in Test Specimen (10). Both these factors contributed to an increase in connection stiffness in Specimen (10). However, earlier studies (Kukreti and Abolmaali, 1999) showed that the angle thickness is the most important variable effecting connection initial stiffness. The results presented in column (4) of Table 3.6 shows that the value of ultimate moment is lowest for Test Specimen (1), 105 kip-in., and highest for Test Specimen (13), 900 kip-in./rad.

Comparing the angle thickness for the following Test Specimens: (1), t = 1/4 in.; (10), t = 3/4 in.; and (13), t = 3/8 in. to the ultimate moment capacities obtained for these test cases (M_u = 105, 814, and 900 kip-in., respectively, for Specimens (1), (10) and (13)), it can be concluded that increase in angle thickness alone has increased the connection's ultimate moment capacity. Comparing the number of bolt rows, N, used in Test Specimens (1), (10) and (13), it is observed that N = 3, 5, and 6, respectively. Also the beam depth, d, is increased from d = 16 in. in Test Specimen (1) to d = 24 in. in Test Specimens (10) and (13). Thus, it appears that N and d (both are actually inter-related; larger N requires larger d) may have more effect on the strength of the connection.

The results presented in columns (5) and (6) of Table 3.6 summarize the ultimate connection rotation and failure modes, respectively. Column (5) of this table shows that the ultimate rotation recorded for the test specimens varied from of 0.045 rad to 0.05 rad. Test Specimens (1), (2) through (8), and (13) exhibited angle yielding, indicating that the failure was governed by excessive yielding of the angle material, resulting in excessive rotation. In Test Specimens (9) through (11), the failure of the connections was bearing failure of beam web material due to bolt bearing against the beam web and causing egging of the bolt holes. In Test Specimen (12), a mixed failure mode was observed. The overall shape of the moment-rotation hysteresis loops for the two different failure modes were quite distinct, as will be discussed later in this chapter. As stated earlier, no data was reported for Test Specimen (4) due to instrumentation malfunction.

The moment–rotation hysteresis loops for Test Specimens (1) through (13) are presented in Figs. A-1(a) through A-1(*l*) of Appendix A, respectively. As can be seen from the overall shapes of hysteresis loops obtained, all tests exhibit significant cyclic yielding resulting in increasing rotation with increasing load and varying degrees of pinching. Pinching results from permanent deformation caused in the yielded materials, which is unrecoverable during load reversal. Both the angle material and bolt shank yield in the connection as the load cycles are increased. Due to excessive yielding of the angle material, the surface area of contact between the angle leg and the column flange would decrease in subsequent load reversals. This would lead to an increase in bolt forces connecting the angle leg to the column flange, and ultimately caused yielding in the bolt shanks. This would then lead to unrecoverable permanent deformation in the bolt shank and a misfit (or gap) in the connection.

The paragraphs that follow describe the behavior of each test specimen tested for the "Type I" double web angle connection.

Test Specimen (1). This test specimen consisted of a W16x45 beam attached to a W10x100 column using L4x4x1/4 web angles with three rows of 3/4 in. diameter A-325 bolts with a column gauge of 4 ¼ in. The moment-rotation hysteresis plot obtained for this test specimen is shown in Fig. A-1(a) of Appendix A. As shown in this figure, the moment-rotation behavior exhibits slight pinching. The initial stiffness, K_e, of this test specimen is 16,700 kip-in./rad obtained by averaging the result obtained for the first nine elastic loops. The ultimate moment, M_u, of this test specimen is recorded as 105 kip-in. The testing was stopped at an ultimate rotation of 0.05 rad. The overall behavior of this test specimen was yielding of the angle material, mostly pronounced along the bolt rows connected to the column flange and along the heel of the angle. Visible separation of the angle leg from the column flange was observed when the wire potentiometer reading was measured at 0.7 in., corresponding to a global rotation of 0.0022 rad.

Test Specimen (2). This test specimen consisted of a W16x45 beam attached to a W10x100 column using L4x4x1/4 web angles with four rows of 3/4 in. diameter A-325 bolts with a column gauge of 4 ¼ in. The only difference between this test specimen and that of Test Specimen (1) is that one row of bolts was added. The moment-rotation hysteresis plot obtained for this test specimen is shown in Fig. A-1(b) of Appendix A. As shown in this figure, much less pinching occurs in this test specimen than Test Specimen (1), which is attributed to less angle deformation due to the use of a longer angle leg to accommodate the one additional row of bolts. The initial stiffness, K_e, of this test specimen is 26,251 kip-in./rad obtained by averaging the first nine elastic loops. The ultimate moment, M_u, of this test specimen is recorded as 184 kip-in. The testing was stopped at an ultimate rotation of 0.05 rad. Plastic hinges formed along the column flange bolt line and the toe of the fillet on both legs of the angle. Visible separation of the angle leg from the column flange was observed when the wire potentiometer reading was measured at 0.2 in. corresponding, to a global rotation of 0.00014 rad.

Test Specimen (3). This test specimen consisted of a W16x45 beam attached to a W10x100 column using L4x4x5/8 web angles with four rows of 3/4 in. diameter A-325 bolts with a column gauge of 4 1/4 in. The moment-rotation hysteresis plot obtained for this test specimen is shown in Fig. A-1(c) of Appendix A. As shown in this figure, the pinching of the moment-rotation hysteresis loops is well pronounced and starts in the very early stages of loading. This is due to beam web bearing failure, which resulted in looseness in the connection due to egging of the beam web bolt holes. It seems that the bolts moved freely at a constant load level in the oval-shaped holes during the load reversal. Once the bolts again touched the beam web material on the other side, the connection once again starts resisting additional load. The behavior of this test specimen was such that no distinct plastic hinges formed and no yield line patterns were observed. The initial stiffness, K_e, of this test specimen is 165,033 kip-in./rad, obtained by averaging the first nine elastic loops. The ultimate moment, M_u, of this test specimen is recorded as 561 kip-in. The testing was stopped at an ultimate rotation of 0.05 rad. The connection failed due to web angle slippage when the wire potentiometer deflection reached 1.9 in., corresponding to a global ultimate rotation of 0.057 rad.

Test Specimen (4). This test specimen consisted of a W21x62 beam attached to a W10x100 column using L5x5x1/2 web angles with four rows of 3/4 in. diameter A-325 bolts with a column gauge of 4¼ in. The moment-rotation hysteresis plot for this test specimen is not presented due to loss of data caused by instrumentation malfunction. However, visual inspection during the testing process indicated that no yielding of the angle occurred. Also, inspection of the bolt holes at the end of the testing showed that the shape of the bolt holes in the beam web was oval shaped, indicating that beam web material bearing failure occurred.

Test Specimen (5). This test specimen consisted of a W21x62 beam attached to a W10x100 column using L4x4x1/4 web angles with four rows of 3/4 in. diameter A-325 bolts with a column gauge of 4¼ in. The moment-rotation hysteresis plot obtained for this test specimen is shown in Fig. A-1(d) of Appendix A. As shown in this figure, pinching of the moment-rotation hysteresis loops is less pronounced than that observed for tests in which beam web material bearing failure occurred. In this test specimen, the yield line patterns were observed along the bolt line on the side of the angle attached to the column flange. Additional plastic hinges were also observed along the fillet of the angle on the beam and column side. Initial separation of the angle from the column flange was observed when the wire potentiometer deflection was measured at 0.08 in., corresponding to a global rotation of 0.00253 rad. Indentations around the bolt holes on the column side of the angle leg, caused by the bolt heads, were more pronounced on the bolt holes on the extreme ends of the angle leg. The failure of this test specimen was well-defined since excessive angle deformations, caused by yielding of the angle material, occurred. The initial stiffness, for this test specimen was 99,000 kip-in./rad, and the ultimate moment capacity was 288 kip-in. The testing was stopped at an ultimate rotation of 0.05 rad.

Test Specimen (6). This test specimen consisted of a W21x62 beam attached to a W10x100 column using L4x4x3/8 web angles with five rows of 3/4 in. diameter A-325 bolts with a column gauge of 4 1/4 in. The moment-rotation hysteresis plot obtained for this test specimen is shown in Fig. A-1(e) of Appendix A. As shown in this figure, pinching of the moment-rotation hysteresis loops is less pronounced than that observed for tests in which the beam web material bearing failure occurred. In this test specimen, the yield line patterns were observed along the bolt line on the side of the angle attached to the column flange. Additional plastic hinges were also observed along the fillet of the angle on the beam and column side. Initial separation of the angle from the column flange was observed when the wire potentiometer deflection was measured at 0.4 in., corresponding to a global rotation of 0.0119 rad. This separation became more pronounced at 0.7 in. deflection (global rotation = 0.021 rad). Indentations around bolt holes in the angles on the column side of the angle leg, caused by the bolt heads, were more pronounced on the bolt holes at the extreme ends of the angle leg. The failure of this test specimen was well-defined since excessive angle deformations, caused by yielding of the angle materials, occurred. The initial connection stiffness for this test specimen was 194,604 kip-in./rad, and the ultimate moment was 540 kip-in. The connection failed due to excessive rotation caused by significant angle yielding.

Test Specimen (7). This test specimen consisted of a W16x45 beam attached to a W10x100 column using L4x4x3/8 web angles with three rows of 3/4 in. diameter A-325 bolts with a column gauge of 4 ¼ in. The moment-rotation hysteresis plot obtained for this test specimen is shown in Fig. A-1(f) of Appendix A. As shown in this figure, pinching of the moment-rotation hysteresis loops is less pronounced than that observed for tests in which the beam web material bearing failure occurred. In this test specimen the yield line patterns were observed along the bolt line on the side of angle attached to the column flange. Additional plastic hinges were also observed along the fillet of the angle on the beam and column side. Initial separation of angle from the column flange was observed when the wire potentiometer deflection was measured at 0.5 in., corresponding to a global rotation of 0.0153 rad. Yield lines were first observed when the wire potentiometer deflection reached a value of 0.55 in., corresponding to a global rotation of 0.0164 rad. Indentations around the bolt holes on the column side of the angle leg, caused by the bolt heads, were more pronounced on the bolt holes on the extreme ends of the angle leg. Testing was concluded when the wire potentiometer deflection reached 1.6 in. (global rotation = 0.051 rad). The failure of this test specimen was well-defined since excessive angle deformations occurred, caused by yielding of the angle materials. The initial connection stiffness for this test specimen was K_o, = 53,755 kip-in./rad, and the ultimate moment was M_u = 166 kip-in. The failure mode for this connection was clearly excessive rotation of the connection due to angle yielding.

Test Specimen (8). This test specimen consisted of a W16x45 beam attached to a W10x100 column using L4x4x3/8 web angles with four rows of 3/4 in. diameter A-325 bolts with a column gauge of $4\frac{1}{4}$ in. The moment-rotation hysteresis plot obtained for this test specimen is shown in Fig. A-1(g) of Appendix A. As shown in this figure, pinching of the moment-rotation hysteresis loops is less pronounced than that observed for tests in which the beam web material bearing failure occurred. In this test specimen, the yield line patterns were observed along the bolt line on the side of the angle attached to the column flange. Additional plastic hinges were also observed along the fillet of the angle on the beam and column side. Initial separation of the angles from the column flange was observed when the wire potentiometer deflection was measured at 0.45 in., corresponding to a global rotation of 0.0141 rad. Yield lines were first observed when the wire potentiometer deflection reached a value of 0.40 in., corresponding to a global rotation of 0.0137 rad. Indentations around the bolt holes on the column side of the angle leg, caused by the bolt heads, were more pronounced on the bolt holes on the extreme ends of the angle leg. Testing was concluded when the wire potentiometer deflection reached 1.6 in. (global rotation = 0.054 rad). The initial connection stiffness for this test specimen was 122,230 kip-in./rad, and the ultimate moment was 342 kip-in. The failure mode for this connection was excessive rotation of the connection due to angle yielding.

Test Specimen (9). This test specimen consisted of a W24x63 beam attached to a W14x159 column using L5x5x1/2 web angles with five rows of 5/8 in. diameter A-325 bolts with a column gauge of $4\frac{1}{4}$ in. The moment-rotation hysteresis plot obtained for this test specimen is shown in Fig. A-1(h) of Appendix A. As shown in this figure, pinching of the moment-rotation hysteresis loops is well pronounced and started in very early stages of the loading. This is attributed to the fact that this test specimen experienced beam web material bearing failure. For this test, no yield line pattern and, hence, no distinct plastic hinges were observed. The initial stiffness of this test specimen was 170,157 kip-in./rad, and the ultimate moment of this test specimen was 707 kip-in. The testing process was stopped at the rotation of 0.045 rad.

Test Specimen (10). This test specimen consisted of a W24x63 beam attached to a W14x159 column using L5x5x3/4 web angles with five rows of 3/4 in. diameter A-325 bolts with a column gauge of 4¼ in. The moment-rotation hysteresis plot observed for this test specimen is shown in Fig. A-1(i) of Appendix A. As shown in this figure, significant pinching is observed in this test specimen. This is due to the fact that angle thickness for this test specimen was the highest (t = 3/4 in.). When angle thickness is large, flexure of the outstanding legs of the angles does not limit the forces to less than the bolt bearing capacity at the beam web, thus causing a beam web bearing failure. The initial stiffness of this test specimen was 314,000 kip-in./rad, and the ultimate moment of this test specimen was 814 kip-in. The testing process was stopped at the rotation of 0.044 rad.

Test Specimen (11). This test specimen consisted of a W24x63 beam attached to a W14x159 column using L4x4x1/2 web angles with four rows of 3/4 in. diameter A-325 bolts with a column gauge of 4¼ in. The moment-rotation hysteresis plot obtained for this test specimen is shown in Fig. A-1(j) of Appendix

A. As shown in this figure, the moment-rotation hysteresis loops of this connection exhibited pinching, but much less in comparison to that observed for Test Specimen (10). This may be due to the fact that the angle thickness used in this test specimen was t = 1/2 in., which is less than the angle thickness of t = 3/4 in. used in Test Specimen (10). The failure mode in this test specimen was beam web bearing failure, as obtained for Test Specimen (10). The initial stiffness of this test specimen was 108,000 kip-in./rad, and the ultimate moment of this test specimen was 442 kip-in. The testing process was stopped at the rotation of 0.044 rad.

Test Specimen (12). This test specimen consisted of a W24x63 beam attached to a W14x159 column using L5x5x3/8 web angles with four rows of 5/8 in. diameter A-325 bolts with a column gauge of 4 1/4 in. The moment-rotation hysteresis plot obtained for this test specimen is shown in Fig. A-1(k) of Appendix A. As shown in this figure, the moment-rotation hysteresis loops of this connection exhibited some pinching, but unlike that obtained for Test Specimens (4), (9), (10) and (14), the pinching observed did not create pronounced flat portions in the beginning cycles, but it increased as failure was approached. Initiation of beam web material bearing failure was observed to occur after the test assembly was dismantled. However, the primary mode of failure was due to angle deformation; yield lines were observed along the bolt lines connected to the column flange and along the heel of the angle. Thus, in Table 3.6, the failure mode is indicated as a combined yielding and bearing failure. The angle separation from the column flange was observed at the wire potentiometer deflection corresponding to 0.6 in., corresponding to a global rotation of 0.002 rad. The testing was terminated at a global rotation of 0.044 rad. The initial stiffness of the connection was 50,356 kip-in./rad, and the ultimate moment corresponding to an ultimate rotation of 525 kip-in.

Test Specimen (13). This test specimen consisted of a W24x63 beam attached to a W14x159 column using L5x5x3/8 web angles with six rows of 5/8 in. diameter A-325 bolts with a column gauge of 4 1/4 in. The moment-rotation hysteresis plot obtained for this test specimen is shown in Fig. A-1(*l*) of Appendix A. As shown in this figure, moment-rotation hysteresis loops of this connection are similar to those tests that exhibited failure mode due to excessive rotation and angle yielding. Some pinching was observed at final load levels, when angles had yielded excessively and had separated away from the column flange. The initial stiffness of the connection was 158,000 kip-in./rad, and this test specimen had the highest ultimate moment, 900 kip-in., corresponding to an ultimate rotation of 0.048 rad. It is interesting to note, that this test specimen was fabricated with six rows of bolts (highest number of bolt rows); thus, a much longer angle was used. This contributed to the higher ultimate moment capacity. Also of interest in this connection, is that even though the angle thickness was less than that for Test Specimen (10), it was still able to resist a higher moment (900 kip-in. versus 814 kip-in.).

Finally, it should be noted that the failure mode, observed in the series of testing conducted for "Type I" double web angle connections, can be detected from a visual inspection of the moment-rotation hysteresis loops recorded. For the failure mode defined by the excessive rotation of the connection due to angle yielding, the hysteresis loops do not show a well-defined flat plateau. However, as shown in Fig.

3.17, the hysteresis loops obtained for the test specimens where failure was due to beam web material bearing, a well-defined flat plateau is obtained. The width of this flat plateau depends on the angle thickness. With increasing angle thickness, more force would transfer as shear force to the beam web, resulting in this type of failure. Due to egging of the bolt holes in this failure mode, the bolts will slide in the holes at a constant load level until contact by the bolt shank is made again with the beam web. Then the connection once again starts resisting load. This can be observed when comparing the hysteresis loops of Test Specimen (10) with those recorded for Test Specimens (4), (9), and (11).

3.7.1.2 "Type II*" Double Web Angle Connections*

For "Type II" double web angle connections eight test specimens were considered, geometric details of which were presented in Table 3.2. The failure modes observed were either excessive rotation caused by angle yielding or bolt fracture. Table 3.7 summarizes the values of the initial connection stiffness, K_e, and the ultimate moment capacity, M_u, obtained for these eight tests. This table shows that the range of initial stiffness varied from a low value of 47,841 kip-in./rad to a high value of 484,064 kip-in./rad. It is worthwhile to note that this high value of stiffness, 484,064 kip-in./rad, for the "Type II" double web angle connection (which is classified as a shear connection by the AISC LRFD Manual of Steel Construction 1994), is usually expected to be observed for end-plate connections (classified as moment connections). The same level of initial stiffness was obtained for one of the flush end-plate connections tested in this study. For example, an initial stiffness of

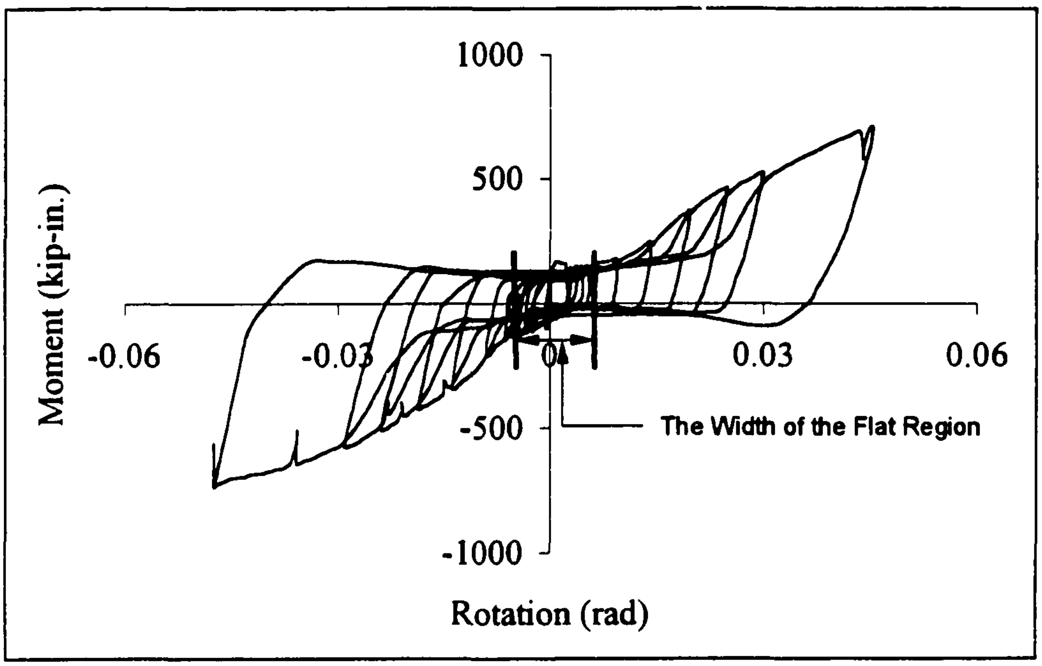

Fig. 3.17 Typical Moment-Rotation Hysteresis Loops for "Type I" Double Web Angle Connections with Beam Web Bearing Failure

Table 3.7 Test Results for "Type II" Double Web Angle Connections

Test No. (1)	Test Designation DW-II-ℓ-t-b_d-g_c-N-d (2)	Initial Stiffness K_e (kip-in./rad) (3)	Ultimate Moment M_u (kip-in.) (4)	Ultimate Rotation θ_u (rad) (5)	Failure Mode (6)
1	DW-II-3-1/4-1/2-2½-3-24	47,841	253	0.03156	Angle Yielding/ Bolt Fracture
2	DW-II-3-1/2-3/4-3½-4-24	252,551	1,061	0.03696	Angle Yielding
3	DW-II-4-5/8-3/4-3½-5-24	484,064	2,236	0.02289	Bolt Fracture
4	DW-II-4-3/8-3/4-3½-4-24	285,513	819	0.03953	Angle Yielding
5	DW-II-5-3/4-3/4-5½-4-24	143,839	1,255	0.03957	Angle Yielding
6	DW-II-5-1/2-5/8-4½-6-24	394,685	1,819	0.03209	Angle Yielding
7	DW-II-6-3/4-3/4-7½-5-24	276,138	1,807	0.03762	Angle Yielding
8	DW-II-6-1/2-7/8-5½-6-24	402,151	1,792	0.03517	Angle Yielding

458,357 kip-in./rad was obtained for a flush end-plate connection (Test Specimen (2) reported in Table 3.9 later). The values reported in Table 3.7 also show that the value of the ultimate moment capacity, M_u, ranged from a low value of 253 kip-in. to a high value of 2,236 kip-in. Again this high value of connection strength, 2,236 kip-in., is comparable to the value obtained for Test Specimen (2) flush end-plate connection, for which the ultimate moment was 2,209 kip-in., as reported in Table 3.9 later. This is an interesting observation, which shows that a double web connection can be designed to provide a stiffness and strength as some of the moment connections. Furthermore, the ultimate rotation reported for Test Specimen (3) in Table 3.7 is 0.02289 rad; whereas the value reported in Table 3.9 for Test Specimen (2) flush end-plate connection was 0.01217 rad. This indicates that Test Specimen (3) double web angle connection is more ductile than the Test Specimen (2) flush end-plate connection. Thus, leading to the conclusion that Test Specimen (3) double web angle connection provides a similar stiffness and strength as one of the test specimens tested for the flush end-plate connection, and in addition provides more ductility. The paragraphs that follow in this section describe the specific observation for each test specimen.

Test Specimen (1). This test specimen consisted of a W24x68 beam attached to a W14x159 column using L3x3x1/4 web angles welded to the beam web using 70 ksi tensile strength weld, and bolted to the column flange using three rows of 1/2 in. diameter A-325 bolts with a column gauge of 2½ in. The moment-rotation hysteresis plot obtained for this test specimen is shown in Fig. A-2(a) of Appendix A. As shown in this figure, the moment-rotation hysteresis behavior shows no pinching and exhibits a very ductile behavior. The initial connection stiffness was 47,841 kip-in./rad, obtained by averaging the slopes of the initial few loops. The ultimate moment recorded for this test specimen was 253 kip-in. The initial angle separation from the column flange occurred at a rotation of 0.005 rad. At a rotation of 0.01 rad, the yield lines began to form at the bolted angle leg at the top and progressed towards the first bolt. During rotation cycles of 0.02 to 0.024 rad, the yield lines began to spread around each of the bolts. The deformation of the angle was pronounced and significant angle yielding occurred. At a rotation of 0.03156 rad, the bottom bolt fractured in tension, an this rotation was recorded as the ultimate rotation, θ_u. Thus, a mixed mode of failure occurred in this test specimen, which was excessive rotation due to angle yielding and bolt fracture.

Test Specimen (2). This test specimen consisted of a W24x68 to the beam attached to a W14x159 column using L3x3x1/2 web angles welded to the beam web using 70 ksi tensile strength weld, and bolted to the column flange using four rows of 3/4 in. diameter A-325 bolts with a column gauge of 3 ½ in. The moment-rotation hysteresis plot observed for this test specimen is shown in Fig. A-2(b) of Appendix A. As shown in this figure, the moment-rotation hysteresis plots a ductile behavior with some pinching at higher load levels. The initial connection stiffness was 252,551 kip-in./rad, obtained by averaging the slopes of the initial few loops. The ultimate moment recorded for this test specimen was 1,061 kip-in. At a rotation of 0.003 rad, the fillet of the angles began to show small yield lines at the top and bottom portions of the angles. The initial angle separation from the column flange occurred at a rotation of 0.004 rad. At this rotation, the yield lines began to form in the bolted angle leg at the top and progressed down towards the first bolt hole. Simultaneously, similar yield lines formed at the bottom of the angle leg. During the rotation cycle of 0.007 rad, complete yield lines formed along the bolt line. The failure mode of this test specimen was excessive yielding of the angle material, resulting in excessive rotation of the connection.

Test Specimen (3). This test specimen consisted of a W24x68 beam attached to a W14x159 column using L4x4x5/8 web angles welded to the beam web using 70 ksi tensile strength weld, and bolted to the column flange using five rows of 3/4 in. diameter A-325 bolts with a column gauge of 3 ½ in. The moment-rotation hysteresis plot obtained for this test specimen is shown in Fig. A-2(c) of Appendix A. As shown in this figure, the moment-rotation hysteresis plots depict a significant ductile behavior. The initial connection stiffness was 484,064 kip-in./rad, obtained by averaging the slopes of the initial few loops. The ultimate moment recorded for this test specimen was 2,236 kip-in. At a rotation of 0.006 rad, yield lines formed in the bolted angle along the top two holes and bottom two holes. The initial angle separation from the column flange occurred at a rotation of 0.004 rad. At a rotation of 0.009 rad, complete yield lines formed along the bolt line. The test was terminated when the top bolt fractured in tension at a rotation of 0.02289 rad.

Test Specimen (4). This test specimen consisted of a W24x68 beam attached to a W14x159 column using L4x4x5/8 web angles welded to the beam web using 70 ksi tensile strength weld, and bolted to the column flange using four rows of 3/4 in. diameter A-325 bolts with a column gauge of 3 ½ in. The moment-rotation hysteresis plot obtained for this test specimen is shown in Fig. A-2(d) of Appendix A. As shown in this figure, the moment-rotation hysteresis plots depict a ductile behavior. The initial connection stiffness was 285,513 kip-in./rad, obtained by averaging the slopes of the initial few loops. The ultimate moment recorded for this test specimen was 819 kip-in. At a rotation of 0.003 rad, yield lines formed in the bolted angle along the top two holes and bottom two holes. The initial angle separation from the column flange occurred at a rotation of 0.003 rad. The yield lines were formed along the angle line at a rotation of 0.005 rad. At a rotation of 0.009 rad, distinct yield lines formed along the bolt line. The failure of this connection is categorized as excessive yielding of the angle material resulting in excessive rotation.

Test Specimen (5). This test specimen consisted of a W24x68 beam attached to a W14x159 column using L5x5x3/4 web angles welded to the beam web using 70 ksi tensile strength weld, and bolted to the column flange using four rows of 3/4 in. diameter A-325 bolts with a column gauge of 5 ½ in. The moment-rotation hysteresis plot obtained for this test specimen is shown in Fig. A-2(e) of Appendix A. As shown in this figure, the moment-rotation hysteresis plots depict a ductile behavior with pinching at higher load levels. The initial connection stiffness was 143,839 kip-in./rad, obtained by averaging the slopes of the initial few loops. The ultimate moment recorded for this test specimen was 1,255 kip-in. The initial angle separation from the column flange occurred at a rotation of 0.008 rad. At a rotation of 0.014 rad, faint yield lines formed in the bolted angle legs at the top of the angles by the bolt heads. During the rotation cycle of 0.026 rad, a distinct yield line was formed along the bolt line. The testing was terminated at a rotation corresponding to 0.03957 rad. The mode of failure of this test specimen was excessive yielding of angle material resulting in excessive connection rotation.

Test Specimen (6). This test specimen consisted of a W24x68 beam attached to a W14x159 column using L5x5x1/2 web angles welded to the beam web using 70 ksi tensile strength weld, and bolted to the column flange using six rows of 5/8 in. diameter A-325 bolts at a column gauge of 4½ in. The moment-rotation hysteresis plot obtained for this test specimen is shown in Fig. A-2(f) of Appendix A. As shown in this figure, the moment-rotation hysteresis plots depict a significant ductile behavior. The initial connection stiffness was 394,685 kip-in./rad., obtained by averaging the slopes of the initial few loops. The ultimate moment recorded for this test specimen was 1,819 kip-in. At a rotation of 0.004 rad, separation of the angle leg from the column face occurred. At the same rotation, faint yield lines were formed in the bolted angle leg at the top of the angles by the bolt heads. During rotation cycle of 0.008 rad, distinct yield lines formed along the bolt lines. The failure mode of this test specimen was excessive yielding of the angle material at an ultimate rotation of 0.03209 rad.

Test Specimen (7). This test specimen consisted of a W24x68 beam attached to a W14x159 column using L6x6x3/4 web angles welded to the beam web using 70 ksi tensile strength weld, and bolted to the column flange using five rows of 3/4 in. diameter A-325 bolts with a column gauge of 7½ in. It should be noted that this specimen has the highest column gauge. The moment-rotation hysteresis plot obtained for this test specimen is shown in Fig. A-2(g) of Appendix A. As shown in this figure, the moment-rotation hysteresis plots depict a ductile behavior with pinching at high load levels. The initial connection stiffness was 276,138 kip-in./rad, obtained by averaging the slopes of the initial few loops. The ultimate moment recorded for this test specimen was 1,807 kip-in. At a rotation of 0.002 rad, separation of the angle leg from the column face occurred. At a rotation of 0.006 rad, faint yield lines formed in the bolted angle leg at the top and bottom of the angles by the outer bolt heads. During rotation cycles of 0.014 rad, a distinct yield line formed along the bolt line. At a rotation of 0.022 rad, the yield line along the bolt line was observed to be complete. The mode of failure for this test specimen was excessive angle yielding at an ultimate rotation of 0.03762 rad.

Test Specimen (8). This test specimen consisted of a W24x68 beam attached to a W14x159 column using L6x6x1/2 web angles welded to the beam web using 70 ksi tensile strength weld, and bolted to the column flange using six rows of 7/8 in. diameter A-325 bolts with a column gauge of 5 ½ in. The moment-rotation hysteresis plot obtained for this test specimen is shown in Fig. A-2(h) of Appendix A. As shown in this figure, the moment-rotation hysteresis plots depict a significant ductility behavior, with pinching at higher load levels. The initial connection stiffness was 402,151 kip-in./rad, obtained by averaging the slopes of the initial few loops. The ultimate moment recorded for this test specimen was 1,792 kip-in. At a rotation of 0.004 rad, separation of the angle leg from the column face occurred. The faint yield lines were formed at a rotation of 0.001 rad, in the bolted angle leg at the top and bottom portions of the angle by the outer bolt heads. During rotation cycle of 0.002 rad, a distinct yield line formed along the bolt line. At a rotation of

0.004 rad, the yield line along the bolt line was complete. The failure of this connection specimen was determined to be excessive angle yielding at an ultimate rotation of 0.03517 rad.

3.7.2 Top and Seat Angle Connections

For top and seat angle connections, twelve tests were conducted, and in one test equipment malfunction occurred (Test Specimen (7)). Table 3.8 presents the stiffness, strength, and mode of failure test results for each test specimen. The primary failure modes observed were excessive yielding of the angles or fracture of the bolts in tension. This table shows that the value of the connection initial stiffness varies from a low value of 73,000 kip-in./rad to a high value of 629,219 kip-in./rad. The ultimate moment capacity varies from a low value of 219 kip-in. to a high value of 1,792 kip-in. Once again, these high values of connection stiffness and strength, 629,219 kip-in./rad and 1,792 kip-in., respectively, are comparable to those reported for flush end-plate connections in Table 3.9; for example, K_e = 616,329 kip-in./rad for Test Specimen (8) and M_u = 1,979 kip-in. for Test Specimen (1) flush end-plate connections. Thus, certain top and seat angle connection geometries can provide equivalent stiffness and/or strength as some flush end-plate moment connections, and at the same time more ductility. The ultimate rotation at which the testing was terminated due to the connection failure is shown in column (5) of Table 3.8. A rotation of about 0.045 rad corresponded to a connection failure due to angle yielding, whereas an ultimate rotation less than α = 0.042 rad

Table 3.8 Test Results for Top and Seat Angle Connections

Test No. (1)	Test Designation TS-ℓ_h-ℓ_v-t-b_d-G-g_c-d (2)	Initial Stiffness K_e (kip-in./rad) (3)	Ultimate Moment M_u (kip-in.) (4)	Ultimate Rotation θ_u (rad) (5)	Failure Mode (6)
1	TS-6-4-3/4-5/8-2½-5-14	247,063	791	0.0229	Bolt Failure
2	TS-6-6-3/8-5/8-4½-5-14	73,000	219	0.0450	Angle Yielding
3	TS-6-6-3/4-5/8-3½-5-14	168,732	840	0.0420	Bolt Failure
4	TS-6-6-3/4-5/8-4½-4-16	177,621	745	0.0450	Angle Yielding
5	TS-6-4-3/4-3/4-2½-5-14	428,796	1,221	0.0340	Bolt Failure
6	TS-6-4-1/2-3/4-2½-5-14	192,226	813	0.0450	Angle Yielding
7	TS-6-4-3/4-3/4-2½-5-16	-	-	-	-
8	TS-6-4-1/2-3/4-2½-4-16	533,178	901	0.0450	Angle Yielding
9	TS-6-6-3/4-3/4-3½-4-16	239,845	1,164	0.0440	Angle Yielding
10	TS-6-4-3/4-7/8-2½-4-16	602,379	1,665	0.0380	Bolt Failure
11	TS-6-6-3/4-7/8-2½-4-16	629,219	1,792	0.0450	Angle Yielding
12	TS-6-6-3/4-7/8-4½-4-16	190,132	920	0.0450	Angle Yielding

corresponded to a bolt failure. The paragraphs that follow present the configuration details of each test specimen and observations made during the experimental testing.

Test Specimen (1). This test specimen consisted of a W14x43 beam with top and seat angles of L6x6x3/4, and used A-325 high strength bolts with a 5/8 in. diameter. The distance from the heel of the angle to the first bolt row, G, of the outstanding leg was $2\frac{1}{2}$ in. The spacing, g_c, between the bolts in either leg of the angles was 5 in. The deformed geometry and the yield line patterns observed for this specimen test indicated a small amount of deformation in the leg of the angle connected to the beam flange. This deformation was more noticeable in the portion of the angle leg connected to the beam flange between the heel of the angle and the first bolt row. The yield surface line pattern observed in this test started in the first bolt row of the angle leg connected to the beam flange and progressed along this line over the whole length of the angle. The bolts ruptured in tension at a moment of 791 kips-in. at a rotation of 0.0229 rad. This moment and rotation were defined to be the ultimate values. The moment-rotation hysteresis loops obtained for this test are shown in Fig. A-3(a) of the Appendix A. The initial stiffness of the connection was 247,063 kips-in./rad. The excessive pinching shown in this figure occurs due to bolt fracture failure.

Test Specimen (2). This test specimen consisted of a W14x43 beam with top and seat angles of L6x6x3/8, and used A-325 high strength bolts with a 5/8 in. diameter. The distance from the heel of the angle to the centerline of the first bolt row, G, of the outstanding leg was 4.5 in. The spacing, g_c, between the bolts in either leg of the angles was 5 in. The differences between this and Test Specimen

(1) included an increase in the angle length, and a decrease in angle thickness. Yield lines were observed to form in the rows of bolts on the angle leg connected to the beam flange, as well as the angle leg connected to the column flange. Also, yield line patterns were noticed in the vicinity of the intersection of the two angle legs. Thus, the deformed configuration of the top and seat angle, and the yielding observed in both the angle legs indicated that the connection exhibited a significant ductile behavior. The moment-rotation hysteresis loops obtained for this specimen are shown in Fig. A-3(b) of the Appendix A. As shown in this figure, this connection possessed a low moment capacity with no pinching. The value of the initial connection stiffness, K_e, the ultimate moment capacity of the connection, M_u, and the ultimate rotation, θ_u, were 73,000 kips-in./rad, 219 kips-in., and 0.045 rad, respectively. The failure mode for this test specimen was excessive rotation due to angle yielding.

Test Specimen (3): The test specimen chosen for this test was basically the same as that used for Test Specimen (2) with the exceptions that the angle thickness was increased from 3/8 to 3/4 in. and the value of G was decreased from 4.5 to 3.5 in. Comparing the failed specimen of this test with that for Test Specimen (2), it was observed that the deformation of the angle leg connected to the column flange in this specimen was much less, because the angle thickness was increased and the distance G was decreased. The yield lines occurred along the bolt line connected to the column flange, as well as those connected to the beam flange. The moment-rotation hysteresis behavior obtained for this test specimen is shown in Fig. A-3(c) of Appendix A, drawn to the same scale as that of Test Specimens (1) and

(2). Comparing the results reveals that this test specimen is stiffer, but has less ultimate moment capacity than Test Specimen (1). Also, more pinching occurred. The value of the initial stiffness, K_e, the ultimate moment capacity of the connection, M_u, and the ultimate rotation, θ_u were 168,732 kips-in./rad, 840 kips-in., and 0.042 (rad.), respectively. The failure in this test specimen occurred when one of the bolts failed in tension.

Test Specimen (4). In this test specimen, the depth of the beam was larger than that used for Test Specimens (1) through (3). The beam selected was W16x45, and the top and seat angles and bolts were the same as that used for Test Specimen (3). The distance G was kept at 4.5 in., the same used for Test Specimen (2). In this test specimen, yielding started at the bolt row of the angle leg connected to the beam flange and extended toward the heel of the angle as the cyclic loading continued. Also, yield lines formed along the row of bolts in the angle leg connected to the column flange. On the failed specimen two plastic hinges were seen to have formed on either side of the heel in two angle legs. The moment-rotation hysteresis loops obtained for this test specimen are shown in Fig. A-3(d) of Appendix A. Pinching was observed due to angle separation from the column flange as a result of excessive yielding in the angles. The values of the initial connection stiffness, K_e, the ultimate moment capacity of the connection, M_u, and ultimate rotation, θ_u, were 177,621 kips-in./rad, 745 kips-in., and 0.045 rad, respectively. The failure mode for this test specimen was excessive yielding of the angle material, which resulted in excessive rotation.

Test Specimen (5). This test specimen is similar to Test Specimen (1), with the exception that the bolt diameter was increased from 5/8 to 3/4 in. In this test, yielding started at the heel in the angle leg connected to the beam flange, and gradually extended towards the first row of bolts on this leg as the cyclic load continued. Also, some yielding was seen to occur in the outstanding leg of the angles, particularly in the vicinity of the heel of the angle. In the failed specimen, one plastic hinge seemed to have formed at the heel of the angle leg connected to the beam flange. The moment-rotation hysteresis behavior obtained for this test is shown in Fig. A-3(e) of Appendix A. As can be seen in this figure, significant pinching occurs. Also, comparing this variation with Fig. A-3(a) of Appendix A for Test Specimen (1), it is evident that this test specimen is much stiffer. The ultimate moment capacity, M_u, for this specimen is 54.4% greater than that obtained for Test Specimen (1). The initial stiffness, K_e, the ultimate moment capacity of the connection, M_u, and the ultimate rotation, θ_u, of this test specimen were 428,796 kips-in./rad, 1,221 kips-in. and 0.034 rad, respectively. The failure mode for this connection, was bolt fracture failure.

Test Specimen (6). This test specimen was similar to Test Specimen (5), with the exception that angle thickness was reduced from 3/4 to 1/2 in., the depth of the beam was increased from 14 to 16 in., and bolt spacing in each bolt row was decreased from 5 to 4 in. Yielding occurred in the two angle legs on either side of the heel, and then extended towards the bolt row in the outstanding leg connected to the column flange as the cyclic load continued. Also, some yielding occurred along the first bolt row in the angle leg connected to the beam flange. In the failed specimen, three hinges seem to have formed, one on each angle leg on either side of the heel, and one at the bolt head on the outstanding leg. The moment-rotation hysteresis behavior obtained for this specimen is shown in Fig. A-3(f) of Appendix A. As shown in this figure, pinching occurs at higher load levels. The values of initial stiffness, K_e, the ultimate moment capacity of the connection, M_u, and ultimate rotation, θ_u, of this test specimen were 192,226 kips-in./rad, 813 kips-in., and 0.045 rad, respectively. The failure mode of this specimen was excessive rotation of the connection assembly.

Test Specimen (7). This test specimen was similar to Test Specimen (5), with the exception that the beam depth was increased from 14 to 16 in. and bolt spacing in each bolt row was decreased from 5 to 4 in. Yielding occurred at the heel of the angle leg connected to the beam flange and gradually extending toward the first row of bolts on this leg as the cyclic load continued. Some yielding was also noticed between the bolts in the outstanding leg of the angle connected to the column flange. In the failed specimen, a plastic hinge was observed to have formed at the heel of the angle leg connected to the beam flange. The moment-rotation hysteresis loops obtained for this specimen are shown in Fig. A-3(g) of Appendix A. As shown in this figure, significant pinching was observed. The values of initial stiffness, K_e, and the ultimate moment capacity, M_u, and ultimate rotation, θ_u, of this test specimen were 707,523 kips-in./rad, 1,296 kips-in. and 0.023 rad, respectively. The failure mode for this connection was bolt fracture failure. The value of K_e obtained from this seems to be in error; a lower initial stiffness was expected. This could be attributed to instrumentation malfunction during the testing. Therefore, the results for this test specimen were not reported in Table 3.8.

Test Specimen (8). This test specimen was similar to the Test Specimen (7), with the exception that the angle thickness was reduced from 3/4 to 1/2 in. This reduction in angle thickness greatly increases the connection flexibility, as explained by Kukreti and Abolmaali (1999). The effect of the reduction of the angle thickness also resulted in much more yielding in the angle legs. Yielding started in the two angle legs on either side of the heel and gradually extended towards the nearest bolt line as the cyclic load continued. The moment-rotation hysteresis loops obtained for this test specimen are shown in Fig. A-3(h) of the Appendix A. As shown in this figure, some pinching was observed to occur, but not significant. Comparing this moment-rotation hysteresis behavior with that obtained for Test Specimen (7), it is clear that this connection had a lower moment capacity, but much more ductility. The values of initial stiffness, K_e, ultimate moment capacity of the connection, M_u, and ultimate rotation, θ_u, were 533,178 kips-in./rad, 901 kips-in. and 0.045 rad, respectively. For this test specimen, the failure mode was excessive rotation.

Test Specimen (9). This test specimen was assembled using a W16x45 beam, L6x6x3/4 in. top and seat angle, 3/4 in. A-325 high strength bolts, G equal to 3.5 in., and a column gauge of 4 in. For this test specimen, excessive deformation of the outstanding angle leg occurred, which seemed to govern the behavior. Yielding initiated in both angle legs on either side of the heel, and propagated towards the nearest bolt row as the cyclic loading continued. The moment-rotation hysteresis loops obtained for this test are shown in Fig A-3(i) of Appendix A. The mode of failure in this test was bolt failure in tension; however, the moment-rotation hysteresis loops of Fig. A-3(i) of Appendix A indicates that this particular test specimen showed enough ductility up to the failure rotation of about 0.044 rad. Therefore, it was concluded that the mode of failure in this connection was a mixed mode failure due to a combination of excessive rotation of the connection assembly and bolt fracture failure. This mixed mode of failure is a result of high angle thickness (3/4 in.) and a high value of G (3.5 in.). For this test specimen, the values of the initial stiffness, K_e, the ultimate moment capacity of the connection, M_u, and the ultimate rotation, θ_u, were 239,845 kips-in./rad, 1,164 kips-in. and 0.044 rad, respectively.

Test Specimen (10). This test specimen was similar to Test Specimen (8), with the exception that the angle thickness was increased from 1/2 in. to 3/4 in., and the bolt diameters were increased from 3/4 in. to 7/8 in. For this test specimen, yielding was initiated in the two angle legs on either side of the heel, and propagated, but not significantly, towards the nearest bolt as the cyclic load continued. Comparing the yield pattern observed for Test Specimen (10) with that of Test Specimen (8), it was concluded that less yielding occurred in Test Specimen (10) due to an increase in the angle thickness. The moment-rotation hysteresis loops obtained for this test are shown in Fig A-3(j) of Appendix A. As shown in this figure, significant pinching was observed. The values of the initial stiffness, K_e, and the ultimate moment capacity, M_u, and the ultimate rotation, θ_u, of this test specimen were 602,379 kips-in./rad, 1,665 kips-in. and 0.038 rad, respectively. The failure mode of this test specimen was bolt failure.

Test Specimen (11). This test specimen was identical to Test Specimen (10), except the length of the outstanding angle leg was increased from 4 to 6 in. Hence, the angles used in this specimen were L6x6x3/4. Yielding was observed to occur first at the heels of both angle legs and gradually propagated towards the bolt line in the outstanding leg connected to the column flange as the cyclic load continued. The moment-rotation hysteresis loops obtained for this connection are shown in Fig. A-3(k) of Appendix A. As shown in this figure, significant pinching was observed to occur. The values of the initial stiffness, K_o, the ultimate moment capacity of the connection, M_u, and the ultimate rotation, θ_u, of this test specimen were 629,219 kips-in./rad, 1,792 kips-in. and 0.045 rad, respectively. The failure mode for this connection was excessive rotation due to angle yielding.

Test Specimen (12). This test specimen was identical to Test Specimen (11), except the distance G was increased from 2.5 to 4.5 in. The deformation of the angles indicated that yielding was initiated at the heels of the two angle legs and propagated towards the bolt line in the outstanding leg. The moment-rotation hysteresis loops obtained for this test are shown in Fig. A-3(*l*) of Appendix A. Comparing these with the hysteresis loops obtained for Test Specimen (11), it can be seen that by increasing G the moment-rotation hysteresis loops for this test specimen become more flat, indicating a lesser initial stiffness and moment capacity of the connection. This shows that by increasing G the pinching effect was reduced. The moment-rotation hysteresis loops for this test specimen shows a ductile behavior. The values of the initial stiffness, K_e, the ultimate moment capacity of the connection, M_u, and the ultimate rotation, θ_u, of this test specimen were 190,132 kips-in./rad, 920 kips-in. and 0.045 rad, respectively. The failure mode for this connection was excessive rotation due to angle yielding.

3.7.3 Flush End-Plate Connections

For flush end-plate connections, twelve tests were conducted. The test specimens for this series of tests were selected and conducted by Hartman (1999). These test specimens were based on the standards adopted by Star Building Systems, the sponsor for the study. Column (2) of Table 3.9 presents stiffness, strength, and failure mode test results for each test specimen. This table shows that the initial stiffness varies from a low value of 458,357 kip-in./rad to a high value of 1,311,543 kip-in./rad. It is important to mention that no value of initial stiffness for Test Specimen (1), FEP-II-6-18-3/8-3/4-1 $\frac{5}{8}$-3-3, was reported because the stiffness value obtained was not meaningful when compared to other tests (lower initial stiffness should have been obtained). As reported in Table 3.9, the values of the ultimate moment capacity for the flush end-plate test specimens varied from 1,979 kip-in. to 4,622 kip-in. As shown in column (5) of Table 3.9, the maximum rotation observed for flush end-plate specimens was θ_u = 0.01217 rad for Test Specimen (2). Comparing this value of ultimate rotation with those observed in the case of double web angle and top and seat angle connections, it is evident that a much smaller ultimate rotation was obtained in comparison to that reported earlier for other connections. This was expected, since flush end-plate connections are much stiffer

Table 3.9 Test Results for Flush End-Plate Connections

Test No. (1)	Test Designation FEP-II-b_p-d_p-t_p-b_d-p_f-p_b-g_c (2)	Initial Stiffness K_e (kip-in./rad) (3)	Ultimate Moment M_u (kip-in.) (4)	Ultimate Rotation θ_u (rad) (5)	Failure Mode (6)
1	FEP-II-6-18-3/8-3/4-1⅝-3-3	NMV*	1,979	0.0116	Plate Rupture
2	FEP-II-6-18-1/2-3/4-1⅝-3-3	458,357	2,209	0.01217	Bolt Fracture
3	FEP-II-6-18-5/8-3/4-1⅝-3-3	498,330	2,228	0.00707	Bolt Fracture
4	FEP-II-8-18-3/8-1-1⅞-3½ -3½	699,191	2,257	0.01518	Plate Rupture
5	FEP-II-8-18-1/2-1-1⅞-3½ -3½	935,306	3,434	0.01880	Bolt Failure
6	FEP-II-8-18-3/4-1-1⅞-3½ -3½	NMV	4,036	0.02031	Bolt Failure
7	FEP-II-6-22-3/8-3/4-1⅝-3-3	599,077	2,227	0.00982	Plate Rupture
8	FEP-II-6-22-1/2-3/4-1⅝-3-3	616,329	2,766	0.01083	Bolt Fracture
9	FEP-II-6-22-5/8-3/4-1⅝-3-3	725,965	2,892	0.00842	Bolt Fracture
10	FEP-II-8-22-3/8-1-1⅞-3½ -3½	915,236	2,870	0.00970	Weld-Failure
11	FEP-II-8-22-1/2-1-1⅞-3½ -3½	973,722	UM**	UM	Plate Rupture
12	FEP-II-8-22-3/4-1-1⅞-3½ -3½	1,311,543	4,906	0.0140	Bolt Fracture

* No Meaningful value was obtained

** Ultimate Moment was not reached due to testing apparatus malfunction than double web angle and top and seat angle connections, as shown in Fig. 1.1 of Chapter I. Finally, the failure modes for these test specimens are listed as either plate rupture or bolt fracture in column (6) of Table 3.9. In this research, the plate rupture is defined to occur when the end-plate yields and ultimately tears off along the weld line of the beam web. The failure categorized as bolt fracture is bolt rupture in tension. The bolt fracture for all the flush end-plate test specimens was accompanied by end-plate yielding as well. The paragraphs that follow present configuration details of each test specimen, and observations made during testing.

Test Specimen (1). This test specimen consisted of a built-up beam with the following geometric properties: b_f = 6 in., t_f = 1/2 in., d = 18 in., and t_w = 1/4 in. with an overall length, L = 84 in.; and a built-up column with the following geometric properties: b_f = 8 in., t_f = 1 in., d = 12 in., and t_w = 3/8 in. with an overall length, L = 60 in. A 6 in. wide, 18 in. deep, and 3/8 in. thick end-plate was used, with A-325 high strength 3/4 in. diameter bolts at a flange pitch of $1\frac{5}{8}$ in., a bolt pitch of 3 in., and a column gauge of 3 in. As the loading continued, the end-plate separation at the beam flange level occurred at a rotation of 0.001 rad. Yield lines around the top and bottom bolts formed at a rotation of 0.0035 rad. The plate ruptured along the weld line in the beam web. The moment-rotation hysteresis loops obtained for this test specimen are shown in Fig. A-4(a) of Appendix A. As shown in this figure, the hysteresis loops clearly represent a ductile behavior with pinching at higher load levels. The ultimate moment capacity recorded for this test specimen was 1,979 kip-in. at a rotation of 0.01160 rad. The value of the connection initial stiffness obtained for this test specimen was not reported. This is due to the fact that upon comparison of this test specimen (with t_p = 3/8 in.) with other test specimens (e.g., Test Specimen (2) with t_p = 1/2 in.), lower initial stiffness for this test specimen was expected, while higher stiffness was obtained. This was attributed to initial lack of fit due to initial bowing in the end-plate, which is an important factor that can effect the initial stiffness, as discussed by Davison et al. (1987). The mode of failure for this test specimen was end-plate rupture, since the end-plate tore off along the weld line of the beam web.

Test Specimen (2). This test specimen consisted of a built-up beam with the following geometric properties: b_f = 6 in., t_f = 1/2 in., d = 18 in., and t_w = 1/4 in. with an overall length, L = 84 in.; and a built-up column of the following geometric properties: b_f = 8 in., t_f = 1 in., d = 12 in., and t_w = 3/8 in. with an overall length, L = 60 in. A 6 in. wide, 18 in. deep, and 5/8 in. thick end-plate was used, with A-325 high strength 3/4 in. diameter bolts at a flange pitch of 1 ⅝ in., a bolt pitch of 3 in., and a column gauge of 3 in. As the loading continued, the yield lines started to form between the top and bottom bolts at a rotation of about 0.003 rad. Yielding around the bolts occurred at 0.004 rad, and the end-plate started to separate from the column flange at a rotation of 0.005 rad. As cyclic loading continued, the end-plate started to bend above the bolts. At a rotation of 0.014 rad, the bottom bolt failed in tension at a rotation of 0.016 rad. The moment-rotation hysteresis loops obtained for this test specimen are shown in Fig. A-4(b) of Appendix A. As shown in this figure, the hysteresis loops show pinching at higher load levels. The connection initial stiffness obtained was 458,357 kip-in./rad. The ultimate moment capacity recorded for this test specimen was 2,209 kip-in. at a rotation of 0.01217 rad. The failure mode for this test specimen was recorded as bolt fracture. However, end-plate deformation and yielding existed prior to bolt fracture.

Test Specimen (3). This test specimen consisted of a built-up beam with the following geometric properties: $b_f = 6$ in., $t_f = 1/2$ in., $d = 18$ in., and $t_w = 1/4$ in. with an overall length, $L = 84$ in.; and a built-up column of the following geometric properties: $b_f = 8$ in., $t_f = 1$ in., $d = 12$ in., and $t_w = 3/8$ in. with an overall length, $L = 60$ in. A 6 in. wide, 18 in. deep, and 5/8 in. thick end-plate was used, with A-325 high strength 3/4 in. diameter bolts at a flange pitch of $1^5/_8$ in., a bolt pitch of 3 in., and a column gauge of 3 in. Observations during this testing indicated that the separation of the end-plate at the top and bottom occurred at a rotation of 0.001 rad. Yielding around the bolts in the end-plate was detected at a rotation of 0.004 rad. End-plate yielding continued until top bolt fractured at a rotation of 0.00707 rad. The moment-rotation hysteresis loops obtained for this test specimen are shown in Fig. A-4(c) of Appendix A. As shown in this figure, the hysteresis loops show some yielding. Due to higher plate thickness, the energy dissipation capacity of this end-plate is lower than that of Test Specimens (1) and (2), as evident from the hysteresis loops presented. The connection initial stiffness obtained was 498,330 kip-in./rad. The ultimate moment capacity recorded for this test specimen was 2,228 kip-in. at a rotation of 0.007 rad. As expected, due to increased end-plate thickness, the ultimate rotation for this test specimen is less than the ultimate rotations for Test Specimens (1) and (2). The failure mode for this test specimen was recorded as bolt fracture. However, some end-plate deformation and yielding existed prior to bolt failure. The yielding for this test specimen was less than yielding for Test Specimens (1) and (2).

Test Specimen (4). This test specimen consisted of a built-up beam with the following geometric properties: b_f = 8 in., t_f = 1/2 in., d = 18 in., and t_w = 1/4 in. with an overall length, L = 84 in.; and a built-up column of the following geometric properties: b_f = 8 in., t_f = 1 in., d = 12 in., and t_w = 3/8 in. with an overall length, L = 60 in. A 8 in. wide, 18 in. deep, and 3/8 in. thick end-plate was used, with A-325 high strength 1 in. diameter bolts at a flange pitch of $1^7/_8$ in., a bolt pitch of 3½ in., and a column gauge of 3½ in. The moment-rotation hysteresis loops obtained for this test specimen are presented in Fig. A-4(d) of Appendix A. In this test specimen, initial yielding in the end-plate occurred around the bolts closest to the beam flange at a rotation of 0.0037 rad. The end-plate started to separate from the column flange at the beam flange level at a rotation of 0.0053 rad. Yielding in the end-plate propagated from the bolts closest to the beam flange to the bolts farthest from the beam flange. At a rotation of 0.0110 rad, the end-plate had yielded around all the bolts. The value of connection initial stiffness was 699,191 kip-in./rad, and the ultimate moment capacity was recorded as 2,257 kip-in. For this test specimen, the mode of failure was end-plate rupture at an ultimate rotation of 0.01518 rad.

Test Specimen (5). This test specimen consisted of a built-up beam with the following geometric properties: b_f = 8 in., t_f = 1/2 in., d = 18 in., and t_w = 1/4 in. with an overall length, L = 84 in.; and a built-up column of the following geometric properties: b_f = 8 in., t_f = 1 in., d = 12 in., and t_w = 3/8 in. with an overall length, L = 60 in. A 8 in. wide, 18 in. deep, and 1/2 in. thick end-plate was used, with A-325 high strength 1 in. diameter bolts with a flange pitch of 1 ⅞ in., a bolt pitch of 3 ½ in., and a column gauge of 3 ½ in. The moment-rotation hysteresis loops obtained for this test specimen are presented in Fig. A-4(e) of Appendix A. For this test specimen, yielding in the end-plate was first observed at a rotation of 0.0055 rad. This yielding, which started around the bolts closest to the beam flange, extended towards the bolts farthest to the beam flange at a rotation of 0.0128 rad. The end-plate started to separate from the column flange at the beam flange level at a rotation of 0.0146 rad. The end-plate for this test specimen also separated from the column flange at mid-depth of the beam. The value of connection initial stiffness for this test specimen was 935,306 kip-in./rad, and the value of the ultimate moment was recorded as be 3,434 kip-in. Bolt fracture occurred at a rotation of 0.0188 rad. Even though the failure mode for this test specimen was reported as bolt fracture, the end-plate experienced pronounced yielding.

Test Specimen (6). This test specimen consisted of a built-up beam with the following geometric properties: b_f = 8 in., t_f = 1/2 in., d = 18 in., and t_w = 1/4 in. with an overall length, L = 84 in.; and a built-up column of the following geometric properties: b_f = 8 in., t_f = 1 in., d = 12 in., and t_w = 3/8 in. with an overall length, L = 60 in. A 8 in. wide, 18 in. deep, and 3/4 in. thick end-plate was used, with A-325 high strength 1 in. diameter bolts at a flange pitch of 1 ⅞ in., a bolt pitch of 3 ½ in., and a column gauge of 3 ½ in. The moment-rotation hysteresis loops obtained for this test specimen are presented in Fig. A-4(f) of Appendix A. For this test specimen, the yielding in the end-plate was observed at the vicinity of the bolts closest to the beam flange at a rotation of 0.01 rad. The end-plate separated from the column flange at the beam flange level at a rotation of 0.0182 rad. Yielding in the end-plate extended to the bolts farthest from the beam flange at a rotation of 0.019 rad. For this test specimen, the connection initial stiffness obtained was not recorded because the value of initial stiffness for this test specimen was not meaningful when compared to other test specimens of Table 3.9, and the ultimate moment capacity was recorded as 4,036 kip-in. at a rotation of 0.02031 rad. For this test specimen, the mode of failure was bolt fracture.

Test Specimen (7). This test specimen consisted of a built-up beam with the following geometric properties: b_f = 6 in., t_f = 1/2 in., d = 22 in., and t_w = 1/4 in. with an overall length, L = 84 in.; and a built-up column of the following geometric properties: b_f = 8 in., t_f = 1 in., d = 12 in., and t_w = 3/8 in. with an overall length, L = 60 in. A 6 in. wide, 22 in. deep, and 3/8 in. thick end-plate was used, with A-325 high strength 3/4 in. diameter bolts at a flange pitch of 1 $\frac{3}{8}$ in., a bolt pitch of 3 in., and a column gauge of 3 in. This test specimen exhibited slight initial separation at the mid-depth and top of the end-plate before testing. As a result of cyclic loading, initial end-plate separation occurred at 0.0025 rad. The yield line formation initiated at 0.004 rad along the bolt line. As cyclic load continued, the plate yielding continued until the plate ruptured along the weld line in the web of the beam. The moment-rotation hysteresis loops obtained for this test specimen are presented in Fig. A-4(g) of Appendix A. As shown in this figure, pinching was observed to occur. The value of connection initial stiffness for this test specimen was 599,077 kip-in./rad, the ultimate rotation was observed to be 0.00982 rad, and the corresponding ultimate moment was 2,227 kip-in. The failure mode for this test specimen was yielding of the end-plate, resulting in end-plate rupture.

Test Specimen (8). This test specimen consisted of a built-up beam with the following geometric properties: b_f = 6 in., t_f = 1/2 in., d = 22 in., and t_w = 1/4 in. with an overall length, L = 84 in.; and a built-up column of the following geometric properties: b_f = 8 in., t_f = 1 in., d = 12 in., and t_w = 3/8 in. with an overall length, L = 60 in. A 6 in. wide, 22 in. deep, and 3/8 in. thick end-plate was used, with A-325 high strength 3/4 in. diameter bolts at a flange pitch of 1 $^{3}/_{8}$ in., a bolt pitch of 3 in., and a column gauge of 3 in. For this test specimen, the first yield lines in the end-plate occurred around the top and bottom bolts at a rotation of 0.003 rad. The first separation of the end-plate at the beam flange level occurred at the rotation of 0.0048 rad. At a rotation of 0.005 rad, yielding along the bolt lines was initiated. At the rotation of 0.008 rad, the mid-depth of the end-plate separated from the column flange. The testing was terminated due to bottom bolt fracture at a rotation of 0.01083 rad. The moment-rotation hysteresis loops obtained for this test specimen are presented in Fig. A-4(h) of the Appendix A. The value of the connection initial stiffness for this test specimen was 616,329 kip-in./rad, the ultimate moment was 2,766 kip-in., and the corresponding ultimate rotation was 0.01083 rad.

Test Specimen (9). This test specimen consisted of a built-up beam with the following geometric properties: b_f = 6 in., t_f = 1/2 in., d = 22 in., and t_w = 1/4 in. with an overall length, L = 84 in.; and a built-up column of the following geometric properties: b_f = 8 in., t_f = 1 in., d = 12 in., and t_w = 3/8 in. with an overall length, L

= 60 in. A 6 in. wide, 22 in. deep, and 3/8 in. thick end-plate was used, with A-325 high strength 3/4 in. diameter bolts at a flange pitch of 1 ⅝ in , a bolt pitch of 3 in., and a column gauge of 3 in. During the cyclic loading of this test specimen, the yielding was first observed in the end-plate around the top and bottom bolts. The end-plate separated from the column flange at the beam flange level at a rotation of 0.0022 rad. The testing was terminated due to bolt fracture at 0.00842 rad. The moment-rotation hysteresis loops obtained for this test specimen are presented in Fig. A-4(i) of Appendix A. As shown in this figure, the hysteresis behavior of this test specimen is similar to those obtained for other ductile specimens with pinching occurring at higher load levels. The value of connection initial stiffness for this test specimen obtained was 725,965 kip-in./rad, the ultimate moment capacity was 2,892 kip-in., and the ultimate rotation was recorded as 0.00842 rad. The failure mode for this connection was bolt fracture accompanied with yielding of end-plate material.

Test Specimen (10). This test specimen consisted of a built-up beam with the following geometric properties: b_f = 8 in., t_f = 1/2 in., d = 22 in., and t_w = 1/4 in. with an overall length, L = 84 in.; and a built-up column of the following geometric properties: b_f = 8 in., t_f = 1 in., d = 12 in., and t_w = 3/8 in. with an overall length, L = 60 in. A 8 in. wide, 22 in. deep, and 3/8 in. thick end-plate was used, with A-325 high strength 1 in. diameter bolts at a flange pitch of 1 ⅞ in., a bolt pitch of 3 ½ in., and a column gauge of 3 ½ in. At the start of the testing, a gap between the end-plate and the column flange was observed, which occurred during the pre-tensioning of the bolts. The initial yield patterns in the end-plate material around the bolt holes was observed at 0.003 rad. The separation of the end-plate from the column flange at the beam flange level was recorded at 0.0035 rad. Also yield lines formed along the bolt line, in the end-plate, at the rotation 0.004 rad, and mid-depth of the end-plate separated from the column flange at a rotation of 0.007 rad. The moment-rotation hysteresis loops obtained for this test specimen are presented in Fig. A-4(j) of Appendix A. The mode of failure for this test specimen was end-plate rupture along the weld line in the beam web, including excessive end-plate deformation. The value of the initial connection stiffness obtained was 915,236 kip-in./rad. The values of the ultimate rotation and ultimate moment were 0.00970 rad and 2,870 kip-in., respectfully.

Test Specimen (11). This test specimen consisted of a built-up beam with the following geometric properties: $b_f = 8$ in., $t_f = 1/2$ in., $d = 22$ in., and $t_w = 1/4$ in. with an overall length, $L = 84$ in.; and a built-up column of the following geometric properties: $b_f = 8$ in., $t_f = 1$ in., $d = 12$ in., and $t_w = 3/8$ in. with an overall length, $L = 60$ in. A 8 in. wide, 22 in. deep, and 3/8 in. thick end-plate was used, with A-325 high strength 1 in. diameter bolts at a flange pitch of $1\frac{7}{8}$ in., a bolt pitch of $3\frac{1}{2}$ in., and a column gauge of $3\frac{1}{2}$ in. Initial yielding in the end-plate occurred around the top and bottom bolts at a rotation of 0.0018 rad. The end-plate separated from the column flange at the beam flange level at a rotation of 0.0025 rad. Yielding along the line of the inner bolt row was initiated at a rotation 0.0053 rad. This test specimen behaved more rigid compared to other test specimens, i.e., less ductility was observed in this test specimen. The moment-rotation hysteresis behavior obtained for this test specimen is presented in Fig. A-4(k) of Appendix A. Comparison of moment-rotation hysteresis loops of this figure with those presented for other test specimens confirms the above statement regarding the low ductility of this test specimen. The value of the initial connection stiffness obtained for this test specimen was 973,722 kip-in./rad. The value of the ultimate rotation was 0.00813 rad, at an ultimate moment capacity of 3,445 kip-in. The mode of failure for this test specimen was end-plate yielding and rupture.

Test Specimen (12). This test specimen consisted of a built-up beam with the following geometric properties: $b_f = 8$ in., $t_f = 1/2$ in., $d = 22$ in., and $t_w = 1/4$ in. with an overall length, $L = 84$ in.; and a built-up column of the following geometric properties: $b_f = 8$ in., $t_f = 1$ in., $d = 12$ in., and $t_w = 3/8$ in. with an overall length, $L = 60$ in. A 8 in. wide, 22 in. deep, and 3/8 in. thick end-plate was used, with A-325 high strength 1 in. diameter bolts at a flange pitch of $1\frac{7}{8}$ in., a bolt pitch of $3\frac{1}{2}$ in., and a column gauge of $3\frac{1}{2}$ in. Initiation of yield lines in the end-plate occurred around the outer bolts at a rotation of 0.0059 rad. As cyclic load continued, the end-plate separated from the column flange at the beam flange level at a rotation of 0.0079 rad. The yield lines in the end-plate around the outer bolts became more pronounced at the rotation of 0.015 rad, and bolt failure occurred at a rotation of 0.00823 rad, corresponding to an ultimate moment of 4,622 kip-in. The moment-rotation hysteresis loops obtained for this test specimen are presented in Fig. A-4(*l*) of Appendix A. As shown in this figure, more pinching occurred in this specimen than Test Specimen (11), but at higher load levels. The value of the initial connection stiffness for this test specimen was 1,311,543 kip-in./rad, which was the highest value obtained. The mode of failure for this test specimen was end-plate yielding and rupture.

3.7.4 Extended Unstiffened End-Plate Connections

For extended end-plate connections, eight tests were conducted. The stiffness, strength and failure mode results for these tests are presented in Table 3.10. As noted in this table, experiments could not be completed for Test Specimens (5) through (7) since the actuator capacity was reached before the test specimen failure occurred. Therefore, the values of the ultimate moment and the ultimate rotations for these tests are not reported. This table shows that the values of the connection initial stiffness, available for all the test specimens, varied from a low value of 1,200,516 kip-in./rad to a high value of 4,857,958 kip-in./rad. It is interesting to note that the lowest value of initial stiffness, 1,200,516 kip-in./rad is in the same range as the highest initial stiffness, 1,311,543 kip-in./rad, reported in Table 3.9 for flush end-plate connection test specimens. The values of the ultimate moment for the extended end-plate tests reported in Table 3.10 varies from a low value of 2,758 kip-in. to a high value of 6,218 kip-in. The values of the ultimate rotation vary from a low value of 0.0044 rad to a high value of 0.0134 rad. The paragraphs that follow present the configuration details of each test specimen, and observations made during testing.

Test Specimen (1). This test specimen consisted of a W16x68 beam connected to a W14x159 column using a 7 in. wide, 22 ½ in. high, and 1/2 in. thick end-plate, with four A-325 high strength 3/4 in. diameter bolts at a pitch of 1 ⅜ in., and a column gauge of 3 ½ in. In this test specimen an initial plate separation of 0.048 in. was present at the midpoint of the end-plate due to bowing that occurred

Table 3.10 Test Results for Extended End-Plate Connections

Test No. (1)	Test Designation EEP-b_p-d_p-t_p-b_d-p_f-g_c (2)	Initial Stiffness, K_e (kip-in./rad) (3)	Ultimate Moment M_u (kip-in.) (4)	Ultimate Rotation θ_u (rad) (5)	Failure Mode (6)
1	EEP-7-22½-1/2-3/4-1⅜-3½	1,129,937	2,758	0.0084	End-Plate Yielding
2	EEP-8-22½-5/8-7/8-1½-5½	2,035,000	3,535	0.0093	End-Plate Yielding
3	EEP-9-22½-1/2-1⅛-1⅞-3½	1,200,516	3,460	0.0134	End-Plate Yielding
4	EEP-10-22½-1/2-7/8-1⅜-4½	2,058,229	3,165	0.0132	Bolt Failure
5	EEP-9-31-7/8-1-1¾-3½	3,470,945	N/A	N/A	No Failure
6	EEP-10-31-3/4-1⅛-1¼-7½	4,857,958	N/A	N/A	No Failure
7	EEP-9-31-5/8-1-1⅞-7½	1,675,542	N/A	N/A	No Failure
8	EEP-10-31-1/2-1⅛-1⅛-3½	3,235,654	6,218	0.0145	End-Plate Yielding

during welding. During the testing, the beam flange force caused permanent plate deformation at a rotation of 0.003 rad. It was shortly thereafter that pinching occurred as visible in the hysteresis loops presented in Fig. A-5(a) of Appendix A. Yielding was also detected in the end-plate around one of the inner bolts, which later failed. There were some indications of bolt yielding, which resulted in bolt elongation, bent threads, and slightly bent bolts. The ultimate moment was reached due to excessive end-plate deformation. Although bolt rupture occurred shortly thereafter, it was not considered the main mode of failure, since the end-plate had already shown reduced moment capacity.

Test Specimen (2). This test specimen consisted of a W16x68 beam connected to a W14x159 column using a 8 in. wide, 22 ½ in. high, and 5/8 in. thick end-plate, with four A-325 high strength 7/8 in. diameter bolts at a pitch of 1 ½ in., and a column gauge of 5 ½ in. As the cyclic load was applied, it was observed that bolt forces began to drop when end-plate yielded at a rotation of 0.0015 rad. End-plate yielding around the bolt holes was also observed first, and the yield lines extended radically outward from the bolt and followed the lines of maximum moment, indicating that gauge may have had an effect on failure mode in this test. The moment-rotation hysteresis loops obtained for this test specimen are shown in Fig. A-5(b) of Appendix A. After end-plate yielding, a reduction in the stiffness slope was observed in the hysteresis loops. Figure A-5(b) does not include the last two loops because of missing information due to a LVDT malfunction. Failure occurred as a result of excessive end-plate yielding, determined by reduced moment capacity with increasing rotation.

Test Specimen (3). This test specimen consisted of a W16x68 beam connected to a W14x159 column using a 9 in. wide, 22 ½ in. high, and 1/2 in. thick end-plate, with four A-325 high strength 7/8 in. diameter bolts at a pitch of 1 ⅞ in., and a column gauge of 3 ½ in. For this test specimen, visible end-plate separation occurred at a rotation of 0.003 rad. The moment-rotation hysteresis loops obtained for this test specimen are shown in Fig. A-5(c) of Appendix A. Yielding occurred around the bolt holes late in the testing at a rotation of 0.012 rad. Failure for this test specimen was reached due to excessive end-plate deformation.

Test Specimen (4). This test specimen consisted of a W16x68 beam connected to a W14x159 column using a 10 in. wide, 22 ½ in. high, and 1/2 in. thick end-plate, with four A-325 high strength 7/8 in. diameter bolts at a pitch of 1 ⅜ in., and a column gauge of 4 ½ in. As the cyclic load was continued, it was observed that the end-plate started to yield at a rotation of 0.002 rad. Significant yielding occurred in the end-plate and around the bolt holes at an approximate rotation of 0.006 rad. The moment-rotation hysteresis loops obtained for this test specimen are presented in Fig. A-5(d) of Appendix A, which indicates that pinching started to occur near the end of the test. Testing was concluded when an inner bolt fracture occurred.

Test Specimen (5). This test specimen consisted of a W24x76 beam connected to a W14x159 column using a 9 in. wide, 31 in. high, and 7/8 in. thick end-plate, with four A-325 high strength 1 in. diameter bolts at a pitch of 1 ¾ in., and a column gauge of 3 ½ in. The bolts were pre-tensioned to 45 kips, slightly lower than the desired value for fully tensioned bolts. Local yielding occurred on the top and bottom of the beam web at a rotation of 0.002 rad. This was due to the fact that high end-plate thickness forced the failure to occur in the beam web. Also, some end-plate deformation occurred at the beam flange level, creating a permanent separation of 0.014 in. Some lateral movement was observed during testing, and was subsequently corrected for. The actuators reached their capacity before a failure mode occurred; hence, a value for ultimate moment capacity could not be obtained. The moment-rotation hysteresis loops obtained for this test specimen are presented in Fig. A-5(e) of Appendix A. The value of connection initial stiffness obtained was 70,945 kip-in./rad.

Test Specimen (6). This test specimen consisted of a W24x76 beam connected to a W14x159 column using a 10 in. wide, 31 in. high, and 3/4 in. thick end-plate, with four A-325 high strength 1 1/8 in. diameter bolts at a pitch of 1 1/4 in., and a column gauge of 7 1/2 in. For this test specimen, some end-plate yielding occurred around the bolts at a rotation of 0.005 rad. Some local yielding occurred in the beam flanges. Again, a failure mode was not reached due to the limited actuator loading capacity. The connection remained elastic throughout testing. The moment-rotation hysteresis loops obtained for this test specimen was presented in Fig. A-5(f) of Appendix A. The value of the connection initial stiffness of 4,857,958 kip-in./rad was obtained by averaging the moment-rotation slopes for all values where significant displacement was recorded.

Test Specimen (7). This test specimen consisted of a W24x76 beam connected to a W14x159 column using a 9 in. wide, 31 in. high, and 5/8 in. thick end-plate, with four A-325 high strength 1 in. diameter bolts at a pitch of 1 7/8 in., and a column gauge of 7 ½ in. There was an initial plate gap of 0.025 in. at the midpoint of the end-plate for this test specimen due to bowing that occurred after welding. At a rotation of 0.003 rad, yielding occurred around the inner bolts from top flange. Once testing was concluded, yielding was visible around all the bolts. End-plate separation was visible at the beam flange level at a rotation of 0.04 rad. The separation was as high as 0.3 in. at the upper flange during maximum downward loading. A malfunction occurred in one of the transducers early during the testing, probably due to jarring that occurred during testing. Moment measurement was affected, and accurate hysteresis loops and bolt force plots could not be obtained. The moment-rotation hysteresis loops obtained for this test specimen are shown in Fig. A-5(g) of Appendix A. However, the value of the connection initial stiffness, K_e, could be calculated based on the early loops obtained before the malfunction occurred, and a value of 599,077 kip-in./rad was obtained.

Test Specimen (8). This test specimen consisted of a W24x76 beam connected to a W14x159 column using a 10 in. wide, 31 in. high, and 1/2 in. thick end-plate, with four A-325 high strength 1 ⅛ in. diameter bolts at a pitch of 1 ⅛ in., and a column gauge of 3 ½ in. For this test specimen, initially, the end-plate was not in contact on the extended sides of the outer bolts due to warping caused by welding, so there was limited prying forces in the early stages of the testing. At a rotation of 0.00165 rad, yielding was observed around the bolt holes, and end-plate separation was visible at the beam flange level. Also a weld crack was initiated on the upper side of the beam flange that caused the upper flange to act as a hinge. The connection reached an ultimate moment capacity of 6,218 kip-in. The moment-rotation hysteresis loops, as shown in Fig. A-5(h) of Appendix A became flatter at this point, indicating that yielding did occur. Pinching that occurred during testing may have been due to insufficient pre-tensioning of the bolts, which caused bolt slippage.

3.8 Chapter Summary

The experimental program presented in this chapter included the cyclic testing of the following four types of semi-rigid connections: (1) two types of double web angle (all bolted, and welded to beam web and bolted to column flange), (2) top and seat angle, (3) flush end-plate, and (4) extended-end-plate connections. A similar loading history, as described in Section 3.5, was applied to all the test specimens. The moment-rotation hysteresis loops were recorded for all test specimens. The behavior of each test specimen is discussed, and the values of the connection initial stiffness, ultimate moment capacity, ultimate rotation capacity, and failure mode are presented. The general observations made for type semi-rigid connections studied in this research are summarized in the paragraphs that follow.

"Type I" Double Web Angle Connection. In this connection, angles were bolted to both the beam web and the column flange. All bolts were pre-tensioned to full proof load level. Two failure modes were observed, including excessive rotation due to yielding of the angle and beam web bearing failure. The excessive rotation failure mode was observed for those specimens with an angle thickness, $t \leq 3/8$ in., while the beam web bearing failure was identified for those test specimens with an angle thickness, $t > 3/8$ in. The ultimate rotation for the former failure mode was about 0.05 rad and for the latter about 0.045 rad. The moment-rotation hysteresis loops for this type of connection exhibited pinching for both failure modes. For the case of beam web bearing failure, the pinching for hysteresis loops had a very well-defined flat portion, where deformation occurs under constant moment, followed by a sloping region where rotation increases due to an increase in moment. The width of this flat plateau was larger for higher values of angle thickness. The overall behavior of these connections, where the bolts were pre-tensioned to proof load, showed that these connections are capable of dissipating energy and for certain combinations of geometric variables significant moment transfer across the connection is possible before failure.

"Type II" Double Web Angle Connections. In this connection, the angles are welded to the beam web and bolted to the column flange. The moment-rotation hysteresis loops of these type connections showed significant ductility and pinching at higher load levels. The failure modes were either excessive yielding of angles or tensile failure of bolts connected to the column flange. Ultimate moment capacity as high as 2,236 kip-in. and initial stiffness as high as 484,064 kip-in./rad were recorded in Test Specimen (3), which compared to the strength and stiffness values recorded for Test Specimen (2) of flush end-plate connections. However, a comparison between the ultimate rotation of 0.02289 rad, recorded for Test Specimen (3) of "Type II" double web angle connection, and an ultimate rotation of 0.00707 rad recorded for Test Specimen (2) for flush end-plate connection, shows that the former connection provides the same stiffness and strength, but possesses better ductility. This characteristic will be more desirable for energy dissipation in seismic regions. Therefore, it might be worthwhile for future studies to research the ductility behavior of certain shear connections with fully pre-tensioned bolts, which can offer similar strength and stiffness as traditional moment connections.

Top and Seat Angle Connections: The top and seat angle connections studied in this research were of the type in which top and seat angles were bolted to the beam flange using two rows of bolts and bolted to the column flange using one row of bolts. The moment-rotation hysteresis loops for these connections showed pinching at higher cyclic load levels. The modes of failure observed were excessive angle yielding and tensile bolt failure. The connection initial stiffness for certain test specimens, e.g., Test Specimen (11), were as high as 629,219 kip-in./rad, comparable to the value of 616,329 kip-in./rad obtained for certain flush end-plate connections tested (Test Specimen (8)). Again, as in the case of "Type II" double web angle connection, the ultimate rotation for Test Specimen (11) of the top and seat angle connection was 0.045 rad, whereas the ultimate rotation for Test Specimen (8) of flush end-plate connection was 0.01083 rad. This indicates that certain top and seat angle connections with fully pre-tension bolts could provide high stiffness as some traditional moment connections and also possess more ductility.

Flush End-Plate Connections: The flush end-plate connections studied in this research were of the type with one row of bolts on either side of both beam flanges. All bolts were pre-tensioned to full proof load level. The test specimens for this series of testing were selected based on the standards used by Star Building Systems (sponsor of the study). The primary modes of failure for these connections were end-plate yield failure, rupture of the end-plate, and bolt fracture. The ductility observed in the moment-rotation hysteresis loops was not as desirable as those observed for shear connections tested with fully pre-tensioned bolts with similar strength and stiffness. One of the flush end-plate connections, Test Specimen (12), which had an initial stiffness of 1,311,543 kip-in./rad, an ultimate rotation capacity of 0.00823 rad, and an ultimate moment capacity of 4,622 kip-in., compared with the stiffness and strength of an extended end-plate connection tested, Test Specimen (1), which possessed an initial stiffness of 1,129,937 kip-in./rad, an ultimate rotation capacity of 0.00840 rad, and an ultimate moment capacity of 2,758 kip-in. It is interesting to note that the values of ultimate rotation and initial stiffness are very close (almost the same) for the two aforementioned test specimens, Test Specimen.(1) end-plate connection offers slightly more ductility because the value of ultimate moment is higher for this test specimen, but the ultimate moment capacity of the flush end-plate specimen is significantly higher. This shows that with proper choice of geometric variables, it is possible to design a semi-rigid connection to possess sufficient stiffness and moment capacity as some moment-type connections, but still possess higher ductility desirable in seismic conditions. This aspect needs to be further studied.

Extended End-Plate Connections: The extended end-plate connections studied in this research were four-bolt unstiffened extended end-plate connections. All bolts were pre-tensioned to full proof load level. During testing for some of these connections, the actuator capacity was reached before the ultimate conditions could be reached. This included Test Specimens (5) through (7). The failure modes for the remaining five test specimens were excessive end-plate yielding and bolt fracture. The moment-rotation hysteresis loops for these test specimens showed that energy dissipation existed in the connection assembly. This type of connections was the stiffest connection studied in this research. The failure of most of the test specimens, which were tested to failure, was governed by excessive yielding of the end-plate rather than bolt fracture.

CHAPTER IV

DEVELOPMENT OF MATHEMATICAL HYSTERESIS MODELS

4.1 General

In this chapter, different mathematical models are developed to idealize the experimentally recorded moment-rotation hysteresis loops for semi-rigid connections. Four mathematical models are proposed, which include the elasto-plastic, bilinear (which uses the Ramberg-Osgood function on parameters), modified bilinear and trilinear models. The first three models are used for semi-rigid connections in which the failure under cyclic loads is caused by excessive yielding, with or without bolt fracture. These models are shown to vary in degree of accuracy when idealizing the actual moment-rotation hysteresis behavior. The trilinear model is proposed for double web angle connections in which the failure considers the egging of the bolt holes caused by bearing failure of the beam web material. The model parameters, which need to be specified to construct the four proposed mathematical models, are identified in Section 4.2, and using test data for each connection the values of the model parameters are presented in Sections 4.3 to 4.6. Comparisons between the predicted mathematical models and the experimentally recorded moment-rotation hysteresis loops are also presented in these sections. At the end of the chapter, in Section 4.7, important conclusions are summarized.

4.2. Mathematical Models

The first step towards formulating a mathematical hysteresis model for a semi-rigid connection is to define the parameters that are needed to geometrically construct the moment-rotation hysteresis loops. Based on test results presented in Chapter III, two primary modes of failures were observed for the four different types of semi-rigid connections tested. These failure modes include excessive yielding of the connection elements, with or without bolt fracture failure, and beam web material bearing failure. The majority of the semi-rigid connections tested in this study exhibited the former mode of failure, and the typical moment-rotation hysteresis loops obtained are of the form shown in Fig. 4.1(a). As shown in this figure, the main parameters defining the shape of the enveloping loop are initial stiffness, K_e, ultimate moment capacity, M_u, ultimate rotation capacity, θ_u, and a connection yield moment, M_y. Since determination of the connection assembly's yield moment is not an easy task, it will be shown later in this chapter that a proposed transition moment, M_t, or the Ramberg-Osgood characteristic moment, M_c can be used to idealize the moment levels at which yielding is initiated. The moment-rotation hysteresis loops observed for the Type I (all bolted) double web angle connection in which beam web material bearing failure occurred, are shown in Fig. 4.1(b). As shown in this figure, the parameters defining hysteresis loops are: K_e, M_u, θ_u, and the dimensions of the rectangular box formed around the origin of moment and rotation axes, which

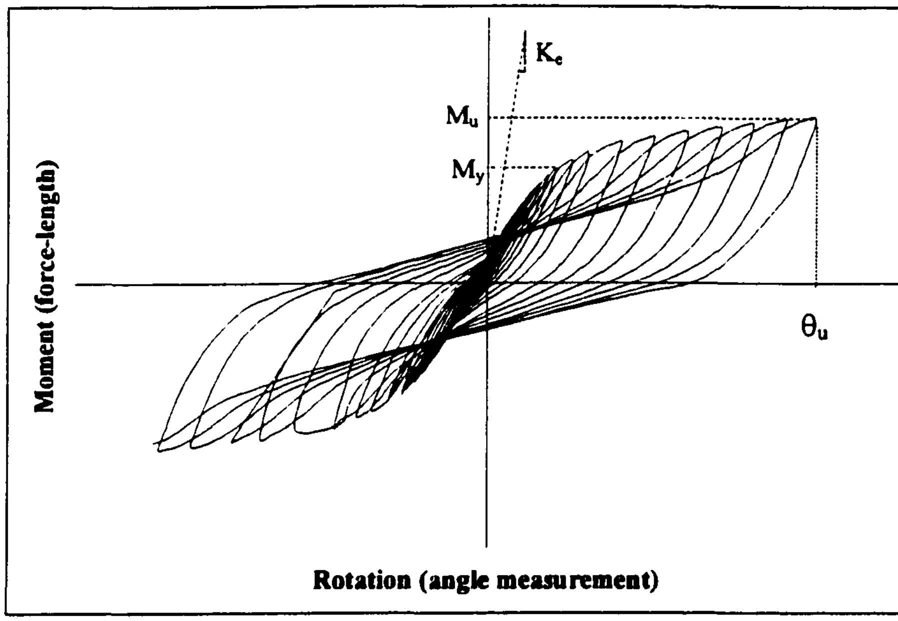

(a)

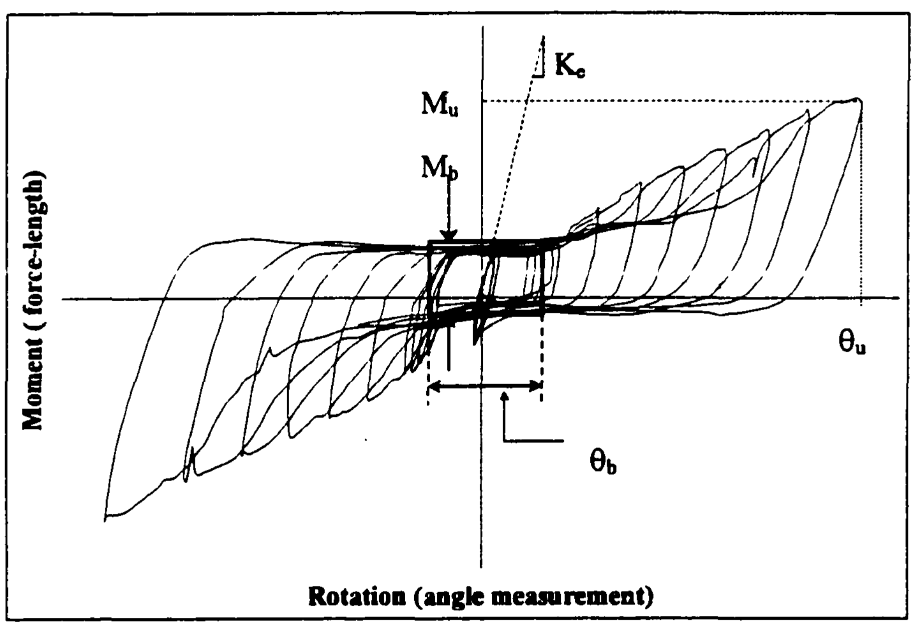

(b)

Fig. 4.1 Moment Rotation Hysteresis Parameters:
(a) Angle Yielding Behavior; (b) Beam Web Bearing Behavior

represents the region in which slippage occurs due to egging of the beam web bolt holes caused by web bearing failure. The width of this rectangular region, which is seen to increase as the angle thickness is increased (as explained in Chapter III) for the same beam web thickness, is denoted as bearing rotation, θ_b, and the height of this rectangle is denoted as bearing moment, M_b, of the connection. The subsections that follow present the procedure to geometrically construct the different mathematical hysteresis models using the aforementioned mathematical hysteresis models.

4.2.1 Elasto-Plastic Model

The first mathematical model proposed to idealize the experimentally recorded moment-rotation hysteresis loops is the elasto-plastic model. This model uses K_e, M_u, and θ_u, as shown in Figure 4.2. The model is constructed as follows:

1. Draw a straight line from the origin to point (1), with coordinates of (M_u/K_e, M_u). Therefore, point (1) is the intersecting point of a linear line of slope K_e:1 (vertical : horizontal) drawn from origin and a line of zero slope drawn from point (2) with coordinates of (θ_u, M_u). In this model, point (1) represents the yield point of the connection mechanism and yield moment in this model is assumed to be equal to the ultimate moment of the connection.
2. Draw a straight line from point (1) to point (2) with coordinates of (θ_u, M_u). This line, which has a zero slope, represents the post-stiffness of the semi-rigid connection mechanism after yielding. The behavior is assumed to remain perfectly plastic until the loading reverses.

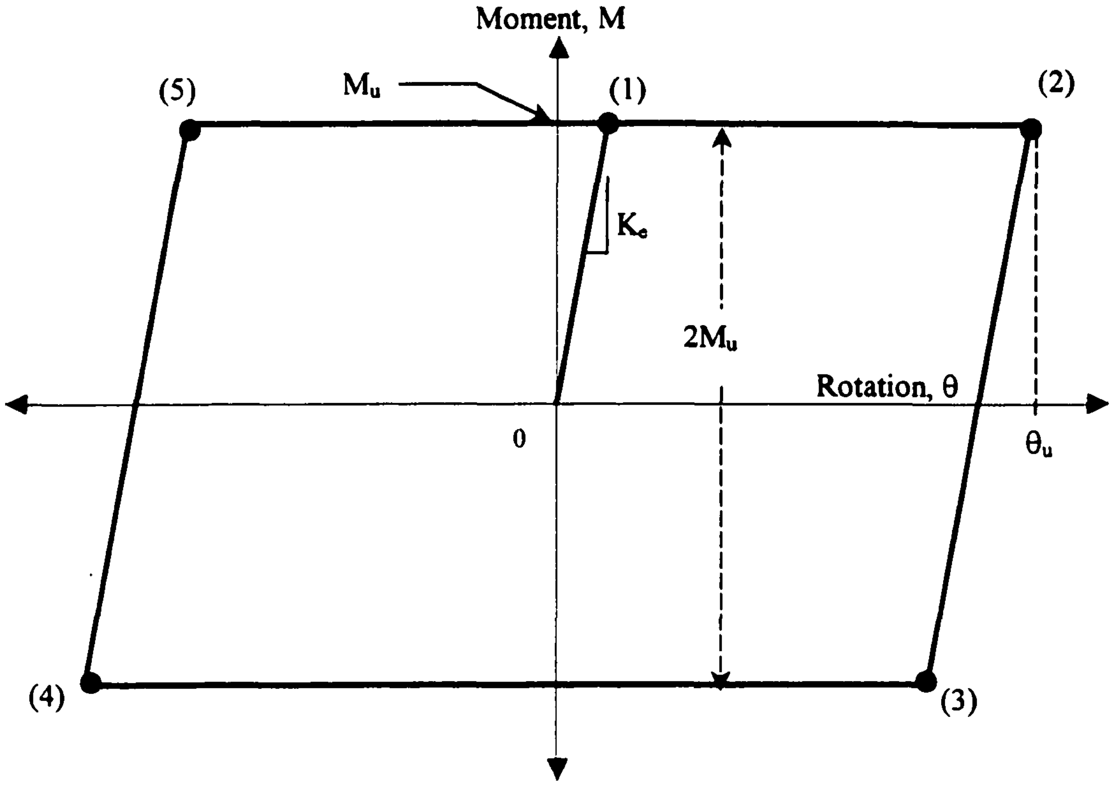

Fig. 4.2 Typical Elasto-Plastic Hysteresis Model

3. Locate point (3), which has a coordinate of (θ_u-2M_u/K_e, -M_u) and draw a straight line from point (2) to point (3). In locating point (3), the directional anisotropy is considered. In other words, it is assumed that the yielding in reverse loading occurs at (2M_u) measured from point of unloading (2).

4. Draw a straight line of zero slope from point (3) to point (4), which has coordinates of (-θ_u, -M_u). This line, which is a line of zero slope, represents the post-stiffness of the connection mechanism after yielding in the reverse cycle occurs.

5. Draw a straight line from point (4) to point (5), which has a coordinate of (-θu+2M_u/K_e, M_u). In locating point (5), as done for point (3), the directional anisotropy is considered as the cyclic loading changes direction from negative to positive or unloading to reloading.

6. Draw a straight line from point (5) to point (1) to complete the model.

Since the elasto-plastic model requires three independent hysteresis parameters (K_e, M_u, and θ_u) to describe it, is a three-parameter model, and is the simplest model to construct. However, this model is expected to be the least conservative model among the models presented in this chapter.

4.2.2 Bilinear Model

The bilinear moment-rotation hysteresis model proposed to idealize the experimentally recorded moment-rotation hysteresis loops is shown in Figure 4.3. The idealized yield moment for this model is called the transition moment, M_t, which

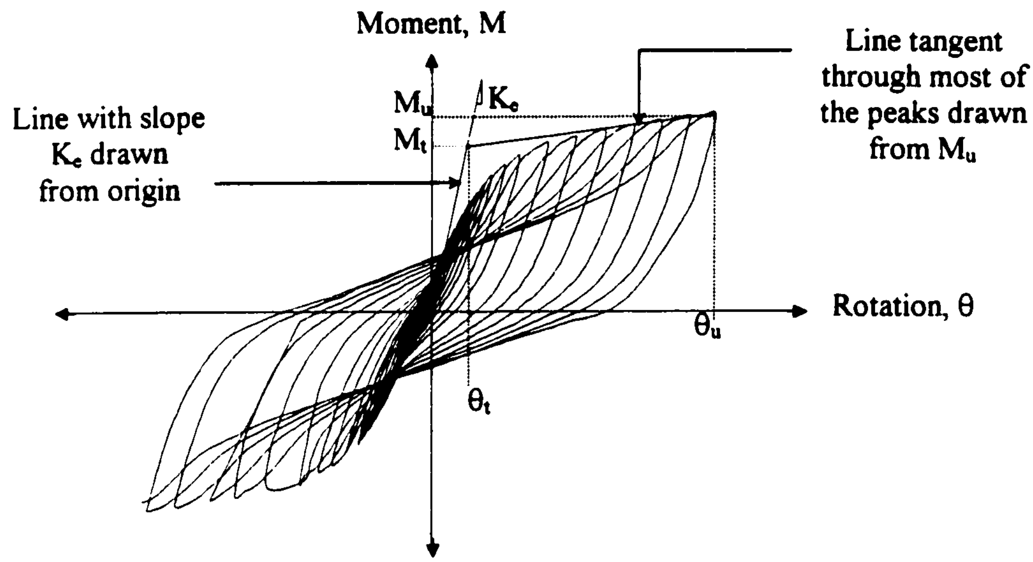

(a)

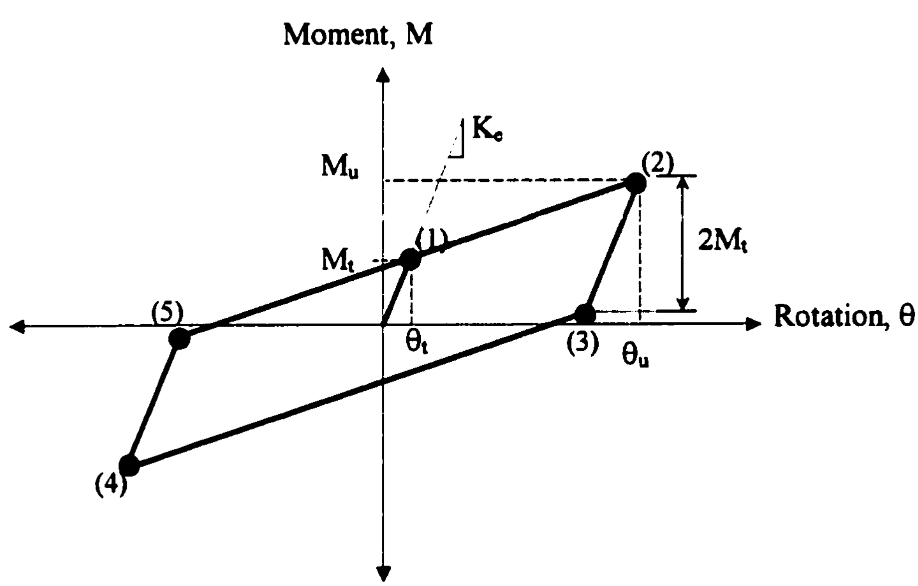

(b)

Fig. 4.3 Typical Bilinear Hysteresis Model:
(a) Details of Transition Moment; (b) Details of Model

is defined as the intersection of a tangent line drawn from the ultimate moment point (with coordinates (θ_u, M_u)) and touching most of the peaks of the hysteresis loops in the first quadrant, and the initial stiffness line passing through origin with a slope of K_e:1 (vertical : horizontal), as shown in Fig. 4.3(a). The method of constructing the bilinear model is similar to that presented for the elasto-plastic model, with the difference being in the definition of the idealized yield moment. Figure 4.3(b) shows an idealized bilinear model for which the method of construction is as follows:

1. Draw a straight line from origin to point (1), with coordinates of (M_t/K_e, M_t). Therefore, point (1) is the intersecting point of a linear line of slope K_e drawn from origin, and a line drawn from the point (2), with coordinates of (θ_u, M_u), and having the slope of

$$K_t = \frac{(M_u - M_t)}{(\theta_u - \theta_t)} \tag{4.1}$$

   where the transition rotation, θ_t, is defined by

$$\theta_t = \frac{M_t}{K_e} \tag{4.2}$$

2. Draw a straight line from point (1) to point (2). This line has a slope of K_t as defined by Eq. (4.1), which represents the post-stiffness of the connection.

3. Locate point (3), which has a coordinate of (θ_u-2M_t/K_e, M_u-2M_t) and draw a straight line from point (2) to point (3). In locating point (3), once again the directional anisotropy is considered, which means that

the yielding in reverse loading occurs at $2M_t$ from the point of unloading (i.e., point (2)).

4. Draw a straight line from point (3) to point (4), which has a coordinate of $(-\theta_u, -M_u)$. This line, which has a slope K_t, as defined by Eq. (4.1), represents the post-stiffness of the connection mechanism after yielding in the reverse cycle occurs.

5. Draw a straight line from point (4) to point (5), which has a coordinate of $(-\theta u+2M_t/K_e, -M_u+2M_t)$. In locating point (5), as done for point (3), the directional anisotropy is considered as the cyclic loading on the connection changes direction from negative to positive loading or unloading to reloading.

6. Draw a line from point (5) to point (1) to complete the model.

Since the bilinear model requires four independent (K_e, M_u, M_t, and θ_u) to describe it, it is a four-parameter hysteresis model.

4.2.3 Modified Bilinear Model

The modified bilinear model proposed in this research use the same formulation as that of bilinear model with the exception that a different approach is used to define the idealized yield moment for the connection. In this model, the Ramberg-Osgood function (1943) is proposed in order to fit the experimental hysteresis loops obtained for a connection. The graphical plot of the Ramberg-Osgood function is shown in Fig. 4.4(a), and the mathematical functions describing the unloading and loading curves shown are, respectively, expressed as follows:

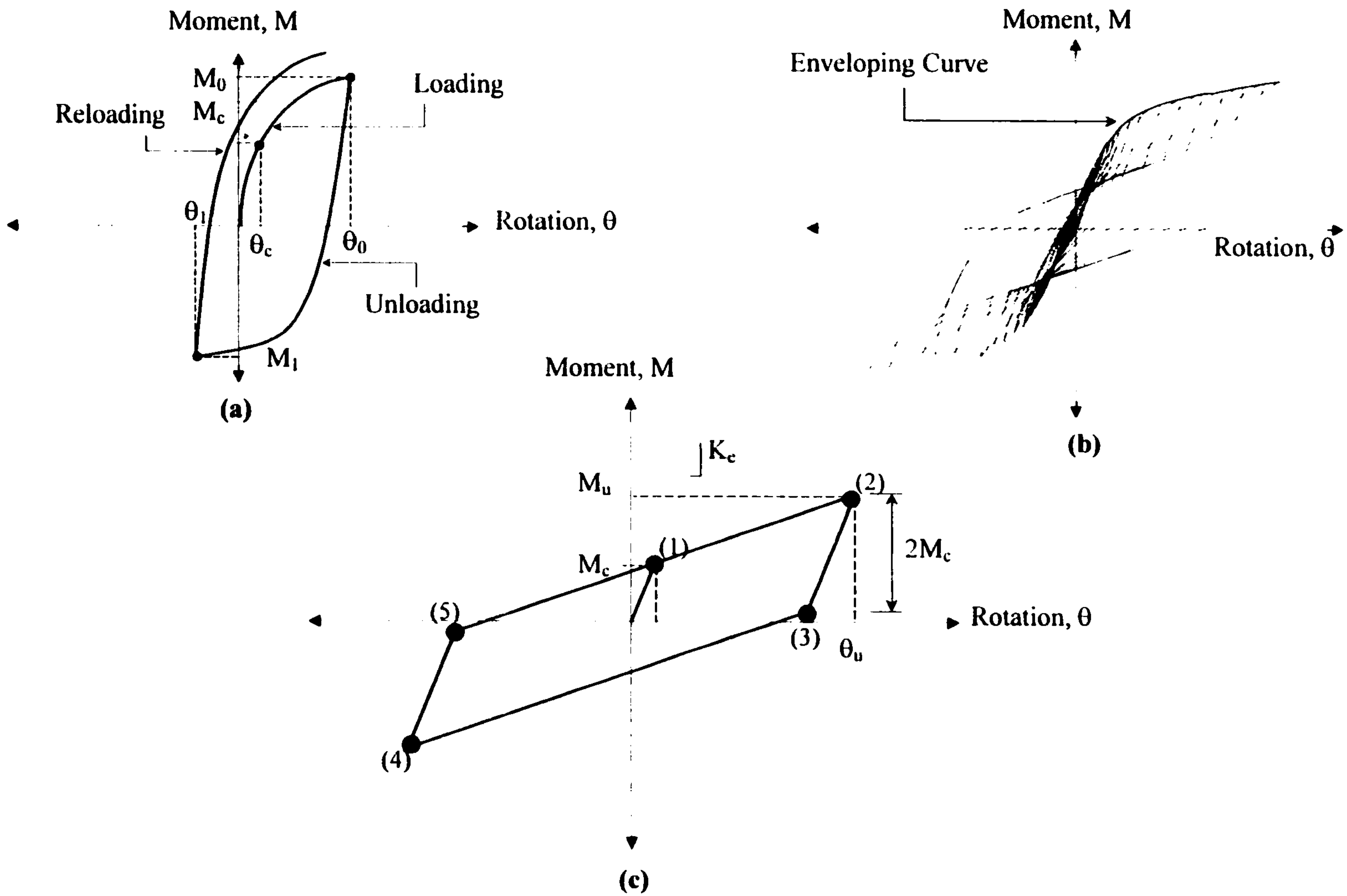

Fig. 4.4 Typical Modified Bilinear Hysteresis Model: (a) Details of Ramberg-Osgood Function; (b) Enveloping Curve; (c) Details of Model

$$\frac{(\theta-\theta_0)}{2\theta_c}=\frac{(M-M_0)}{2M_c}\left(1+\left|\frac{M-M_0}{2M_c}\right|\right)^{r-1} \tag{4.3a}$$

$$\frac{(\theta+\theta_1)}{2\theta_c}=\frac{(M+M_1)}{2M_c}\left(1+\left|\frac{M+M_1}{2M_c}\right|\right)^{r-1} \tag{4.3b}$$

where θ_0 = rotation at the instant of unloading, θ_1 = rotation at the instant of reloading, θ_c = characteristic rotation, M_0 = moment at the instant of unloading, M_1 = moment at the instant of reloading, M_c = characteristic moment, and r = rigidity parameter. Kukreti and Abolmaali (1999) presented a bilinear model for a top and seat angle connection, which used the characteristic moment, M_c, and characteristic rotation, θ_c, as the coordinates of the connection yield point. These values of M_c and θ_c were obtained by fitting the loading Ramberg-Osgood function, Eq. (4.3a), to the enveloping curve defined in Fig. 4.4(b), and using the method of least squares to find the value which best fitted the data. As shown in Fig. 4.4(b), the enveloping curve is a curve drawn passing through the origin and the peaks of each loop in the first quadrant up to the point with coordinates (θ_u, M_u). It should be pointed out that the Ramberg-Osgood function does not model pinching. Therefore, for connections which exhibited pinching at higher load levels, the characteristic moment and rotation were obtained ignoring the pinching effects, which could result in a low value for these parameters, M_c, and θ_c; thus making the formulation model more conservative.

Referring to Figs. 4.4(a) and 4.4(b), the equation for the loading portion of the Ramberg-Osgood function is mathematically obtained when the coordinates (θ_0, M_0) coordinates (θ_1, M_1) are set equal to zero. The Ramberg-Osgood function in terms of hysteresis parameters by substituting coordinates (θ_u, M_u), for (θ_0, $-M_0$).and ($-\theta_u$, $-M_u$) for (θ_1, M_1), for unloading and reloading portions respectively, will become:

$$\frac{(\theta-\theta_u)}{\theta_c}=\frac{(M-M_u)}{M_c}\left(1+\left|\frac{M-M_u}{2M_c}\right|\right)^{r-1} \tag{4.4a}$$

$$\frac{(\theta+\theta_u)}{\theta_c}=\frac{(M+M_u)}{M_c}\left(1+\left|\frac{M+M_u}{2M_c}\right|\right)^{r-1} \tag{4.4b}$$

The modified bilinear model is shown in Fig. 4.4(c) is constructed as follows:

1. Draw a straight line from origin to point (1), with coordinates of (θ_c, M_c). Therefore, a line drawn from origin to point (1) does not have the same slope as initial connection stiffness, K_o. The slope of this line is defined by

$$K_c=\frac{M_c}{\theta_c} \tag{4.5}$$

2. Draw a straight line from point (1) to point (2) with coordinate of (θ_u, M_u). This line has a slope of K_{tc}, which is defined by

$$K_{tc}=\frac{(M_u-M)_c}{(\theta_u-\theta_c)} \tag{4.6}$$

3. Locate point (3), which has a coordinate of (θ_u-$2M_c/K_c$, M_u-$2M_c$), and draw a straight line from point (2) to point (3). In locating point (3), once again the directional anisotropy is considered, which means that the yielding in reverse loading occurs at $2M_c$ from the point of unloading (i.e., point (2)).

4. Draw a straight line from point (3) to point (4), which is defined by coordinate of ($-\theta_u$, $-M_u$). This line, which has a slope K_{tc} defined by Eq. (4.6), represents the post-stiffness of the connection after yielding in the reverse cycle occurs.
5. Draw a straight line from point (4) to point (5), which has a coordinate of ($-\theta u+2M_c/K_c$, $-M_u+2M_c$. In locating point (5), as done for point (3), the directional anisotropy is considered as the cyclic loading on the connection changes direction from negative to positive loading or unloading to reloading.
6. Draw a line from point (5) to point (1) for completion of the enveloping model.

Since the modified bilinear model requires four independent (K_c, M_u, M_c, and θ_u) to describe it, it is a four-parameter hysteresis model.

4.2.4 Trilinear Model

The trilinear model is proposed to idealize moment-rotation hysteresis loops obtained for Type I (all bolted) double web angle connections, in which bearing failure of the beam web material occurs. As presented in Chapter III, for an angle thickness greater than 3/8 in., this failure mode was observed. This failure results in a moment-rotation hysteresis loop that incorporates a rectangular shape segment as shown in Fig. 4.1(b). This rectangle is denoted to have a height of M_b (bearing moment) and a width of θ_b (bearing rotation). It was observed from the experimental results that the area of this rectangle ($\theta_b \times M_b$) increases as the angle thickness increases. It is proposed that for the hysteresis model of all bolted double web angle connections in which beam web bearing failure occurs, initiation of yielding occurs at a moment of $M_b/2$. The proposed hysteresis model is shown in Fig. 4.5. It consists of three independent stiffness values, which are initial stiffness, bearing stiffness (= zero), and post-tangential stiffness. The model is constructed as follows:

1. Draw a line from the origin with slope of K_e to point (1) with coordinates of $(M_b/2K_e\,,\, M_b/2)$. It should be noted that in defining the coordinates of point (1), the effect of beam weight is not considered and therefore, a perfect symmetric hysteresis model is assumed.

2. Draw a line from point (1) to point (2), with coordinates of $(\theta_b/2, M_b/2)$. Point (2) represents the instant at which the bolt shanks touches the beam web and the connection resumes resisting more moment.

3. Draw a line from point (2) to point (3) with coordinates (θ_u, M_u). The connection stiffness between points (2) and (3) is defined by:

$$K_{tb} = \frac{(M_u - M_b/2)}{(\theta_u - \theta_b/2)} \tag{4.7}$$

4. Draw a line with the slope K_e from point (3) to point (4) with coordinates $\{(\theta_u - ((M_u+(M_b/2))/K_e,)), (-M_b/2)\}$. In this model, it is proposed that connection yielding in reverse direction (directional anisotropy) occurs at a moment of $(M_u + M_b/2)$ from the point of unloading (i.e., point (3)).

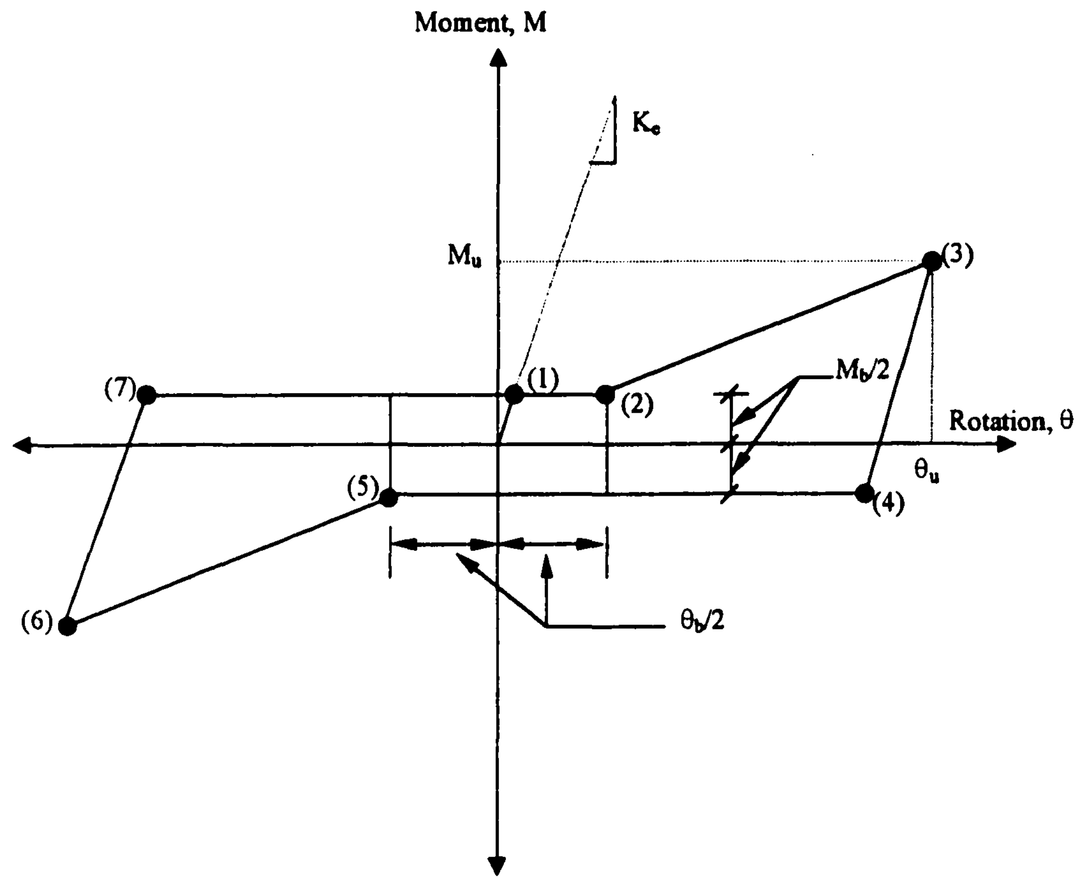

Fig. 4.5 Typical Trilinear Model

5. Draw a line of zero-slope from point (4) to point (5) with coordinates $(-\theta_b, -M_u)$.

6. Draw a line from point (5) to point (6) with coordinates of $(-\theta_u, -M_u)$. This line has a slope equal to K_{tb}, defined by Eq. (4.7), which represents the stiffness of the connection mechanism between points (5) and (6).

7. Draw a line from point (6) to point (7) with coordinates $\{(-\theta_u + ((M_u+(M_b/2))/K_e)), (M_b/2)\}$. This line has a slope equal to initial stiffness, K_e.

8. Draw a line of zero-slope from point (7) to point (1) to complete the construction of the hysteresis model.

Since the trilinear model requires five independent parameters (K_e, M_u, θ_u, M_b, and θ_b) to describe it, it is classified as a five-parameter model. Also, the trilinear model consists of three different stiffness stages to capture the real hysteresis behavior of the double web angle connections with beam web bearing behavior. The connection mechanism starts with initial stiffness until the bearing moment is reached, and then the stiffness vanishes while the bolt shanks are sliding in the egged bolt holes in the beam web. The stiffness of the connection mechanism becomes a finite value when the bolt shanks touches the beam web material at the other side of the egged bolt holes.

4.3 Hysteresis Models for Double Web Angle Connections

4.3.1 "Type I" Double Web Angle with Yielding Behavior

Seven of the "Type I" double web angle connections, Test Specimens (1), (2), (5), (6), (7), (8), and (13), experienced no beam web failure, and their moment-rotation hysteresis behavior can be idealized by the bilinear models such as elasto-plastic, bilinear, and modified bilinear models. The experimental values of the model parameters for these seven test cases are tabulated in columns (3) through (9) of Table 4.1. The values of initial stiffness, K_e, and ultimate moment, M_u, are obtained directly from experimental data. The value of transition moment, M_t, is graphically obtained from the experimental moment-rotation plots, as shown in Fig. 4.3(a). The value of characteristic moment, M_c, characteristic rotation, θ_c, and rigidity parameter, r, is determined by best fitting the loading portion of the Ramberg-Osgood function, Eq. (4.4), to the experimental enveloping curve (refer to Fig. 4.4(b)) by using method of least squares. Figures B-1(a) through B-1(g) of Appendix B presents the comparison of the predicted enveloping curves for the seven double web angle connections with experimental enveloping curves. As shown in these figures, for the test specimens which exhibited less pinching, the Ramberg-Osgood function predicted the enveloping curves more accurately when compared to experimental enveloping curves. This can be observed in Figs. B-1(b), B-1(c), and B-1(d) for Test Specimens (2), (5), and (6), respectively. Figures B-1(e), B-1(f), and B-1(g) show the comparison of the predicted Ramberg-Osgood function with the corresponding experimental enveloping curves for tests which exhibited noticeable pinching. These

Table 4.1 Experimental Hysteresis Parameter Obtained for "Type I" Double Web Angle Connections which Failed Due to Yielding and/or Bolt Fracture

Test No. (1)	Test Designation DW-I-ℓ-t-b_d-g_c-N-d (2)	K_e (kip-in./rad) (3)	M_u (kip-in.) (4)	M_t (kip-in.) (5)	M_c (kip-in.) (6)	θ_c (rad) (7)	θ_u (rad) (8)	r (9)
1	DW-I-4-1/4-3/4-4½-3-16	16,721	105	37	30	0.0008	0.0500	3.29
2	DW-I-4-1/4-3/4-4½-4-16	26,251	184	96	89	0.0038	0.0500	3.36
5	DW-I-4-1/4-3/4-4½-5-21	99,000	288	165	130	0.0016	0.0500	4.52
6	DW-I-4-3/8-3/4-4½-5-21	194,604	540	300	194	0.0018	0.0500	3.21
7	DW-I-4-3/8-3/4-4½-3-16	53,755	166	88	65	0.0033	0.0500	2.71
8	DW-I-4-3/8-3/4-4½-4-16	122,230	342	216	150	0.0024	0.0500	3.57
13	DW-I-5-3/8-5/8-4½-6-24	158,000	900	440	200	0.0021	0.0480	1.90

plots also show that the predicted Ramberg-Osgood function fits the data reasonably well.

The comparison between the actual hysteresis loops obtained from each test specimen and the bilinear models are shown in Figs. B-1(a) through B-1(g) of Appendix B. As shown in these figures, the modified bilinear model is the most conservative of these two models. A comparison between the modified bilinear and bilinear models indicates that the two model predictions are close to one another, with a few exceptions. Figure B-2(b) shows that for Test Specimen (2), the modified bilinear and bilinear models almost overlap. However, Fig. B-2(g) shows that for Test Specimen (13), the predicted modified bilinear model is a much more conservative than the bilinear model; the latter envelops a more area of the enveloping hysteresis loop than the modified bilinear model. The difference between these two models is more noticeable for this test specimen than the other test specimens presented in Figs. B-2(a) through B-2(g) of Appendix B.

Figures B-2(a) through B-2(g) of Appendix B also shows that the elasto-plastic model is the least conservative model when compared to the failure loop obtained from the experimental moment-rotation plots because it envelops a larger area than the experimental failure loop. This is true for all the test specimens shown in Figs. B-2(a) through B-2(g) of Appendix B. Therefore, the only justification in using the elasto-plastic model is that it requires least number of hysteresis parameters (three parameters), and is simple to construct.

4.3.2 "Type I" Double Web Angle with Beam Web Bearing Behavior

The experimental results indicated that when the angle thickness t > 3/8 in. for a "Type I" (all bolted) double web angle connection, the connection fails due to bearing of the bolt shank against the beam web material. This behavior was observed in Test Specimens (3), (4), (9), (10), (11), and (12). For such connections, a trilinear model is proposed, as described in Section 4.2.4. The independent hysteresis parameters defining this model are: K_e, M_u, M_b, θ_b, and θ_u. The experimental values of these parameters obtained for the six tests, which failed due to beam web material bearing failure, are tabulated in Table 4.2.

The comparison between the actual moment rotation hysteresis loops obtained from experiments and that obtained by the trilinear model are presented in Figs. B-3(a) through B-3(g) of Appendix (B). As shown in Figs. B-3(a), B-3(b), B-3(c), and B-3(d) of Appendix B, for Test Specimen (3), (9), (10), and (11), respectively, the proposed trilinear model quite accurately represents the hysteresis behavior, and the area under the failure loop, which is a measure of the energy dissipating capability of the connection.

4.3.3 Type II Double Web Angle Connections

"Type II" double web angle connections are defined in this research as those in which the connection angle is welded to the beam web and bolted to the column flange. The primary failure mode for the connections tested, as discussed in Chapter III, was primarily due to excessive yielding of the angle legs bolted to the column flange, which ultimately resulted in excessive connection rotation. Although bolt

Table 4.2 Experimental Hysteresis Parameter Obtained for "Type I" Double Web Angle Connections which Failed Due to Beam Web Bearing

Test No. (1)	Test Designation DW-I-ℓ-t-b_d-g_c-N-d (2)	K_e (kip-in./rad) (3)	M_u (kip-in.) (4)	M_b (kip-in.) (5)	θ_b (rad) (7)	θ_u (rad) (8)
3	DW-I-4-5/8-3/4-4½-4-16	165,033	561	300	0.0210	0.0500
4	DW-I-5-1/2-3/4-4½-4-21	NRD*	NRD	NRD	NRD	NRD
9	DW-I-5-1/2-5/8-4½-5-24	170,517	707	171	0.0056	0.0450
10	DW-I-5-3/4-3/4-4½-5-24	314,000	814	468	0.0360	0.0440
11	DW-I-4-1/2-3/4-4½-4-24	108,000	442	157	0.0133	0.0440
12	DW-I-5-3/8-5/8-4½-4-24	50,356	325	168	0.0089	0.0440

* No Reliable Data was obtained for this test specimen due to instrumentation malfunction

fracture was observed in some test specimens which included Test Specimens (1) and (3) (refer to Table 3.7). However, this failure was also accompanied with excessive yielding of the angle leg bolted to the column flange. Therefore, the bilinear models, described in Section 4.2, are most suitable to idealize the hysteresis behavior of this type of connection.

Table 4.3 presents the experimental values of the hysteresis parameters required to construct the elasto-plastic, bilinear, and modified bilinear models for this connection. In this table, the values reported for the characteristic moment, M_c, characteristic rotation, θ_c, and rigidity parameter, r, were obtained by best fitting the loading portion of the Ramberg-Osgood function, Eq. (4.4), to the experimental enveloping curve. The comparison of the predicted and experimental enveloping curves for the connections tested are presented in Figs. B-4(a) through B-4(h) of Appendix B.

The comparison between the experimental and the hysteresis behavior models are presented in Figs. B-5(a) through B-5(h) of Appendix B. It can be concluded from these figures that the modified bilinear model best predicts the experimental hysteresis loops, and is the most conservative model. This figure also shows that for Test Specimens (3) and (4) (refer to Figs. B-5(c) and Fig. B-5(e)), the modified bilinear and bilinear models approximated the experimental hysteresis loops with the similar degrees of accuracy. As shown in Figs. B-5(a) through B-5(h), the elasto-plastic model overestimates the energy dissipating capability of the connection (it predicts a larger area for hysteresis loops), and therefore this model will be unconservative for analysis and design. It is important to note that even though the

Table 4.3 Experimental Hysteresis Parameter Obtained for "Type II" Double Web Angle Connections

Test No. (1)	Test Designation DW-II-ℓ-t-b_d-g_c-N-d (2)	K_e (kip-in./rad) (3)	M_u (kip-in.) (4)	M_t (kip-in.) (5)	M_c (kip-in.) (6)	θ_c (rad) (7)	θ_u (rad) (8)	r (9)
1	DW-II-3-1/4-1/2-2½-3-24	47,841	253	192	125	0.0007	0.0316	5.284
2	DW-II-3-1/2-3/4-3½-4-24	252,551	1,061	850	600	0.0002	0.0370	5.324
3	DW-II-4-5/8-3/4-3½-5-24	484,064	2,236	1,844	1,800	0.0043	0.0229	6.220
4	DW-II-4-3/8-3/4-3½-4-24	285,513	819	636	375	0.0011	0.0395	4.482
5	DW-II-5-3/4-3/4-5½-4-24	143,839	1,255	986	1,025	0.0074	0.0396	7.070
6	DW-II-5-1/2-5/8-4½-6-24	394,685	1,819	1,285	1,100	0.0023	0.0321	5.078
7	DW-II-6-3/4-3/4-7½-5-24	276,138	1,807	1,375	1,400	0.0067	0.0376	5.681
8	DW-II-6-1/2-7/8-5½-6-24	402,151	1,792	1,380	700	0.0006	0.0352	4.358

bilinear model is usually less conservative when compared with modified bilinear model, the graphical inspection of all the cases presented in Figs. B-5(a) through B-5(h) indicates that the bilinear model predicts the hysteresis behavior closer to that predicted by the modified bilinear model.

4.4 Hysteresis Models for Top and Seat Angle Connections

The top and seat angle connections studied in this research are of the type in which the top and seat angle are bolted to both the beam and column flanges. The experimental results indicated that excessive yielding of the angle legs was the primary mode for failure. Therefore, the bilinear models, described in Section 4.2, are most suitable to idealize the moment-rotation behavior of this connection.

Table 4.4 presents the experimental values of the hysteresis parameters required for the three bilinear models considered. In this table, the experimental values reported for the characteristic moment, M_c, characteristic rotation, θ_c, and rigidity parameter, r, were obtained by best fitting the loading portion of the Ramberg-Osgood function to the experimental enveloping curve. Figures B-6(a) through B-6(*l*) show these curves for all the test specimens. As can be seen from these figures, the Ramberg-Osgood function predicts the experimental curve quite accurately for all the test specimens.

The results of comparisons of mathematical hysteresis models and experimental moment-rotation hysteresis loops are presented in Figs. B-7(a) through B-7(*l*) of Appendix B for all the test specimens. From this figure, it can be seen that the elasto-plastic model overestimates the energy dissipating capability of all the test

Table 4.4 Experimental Hysteresis Parameter Obtained for Top and Seat Angle Connections

Test No. (1)	Test Designation TS-ℓ_a-ℓ_v-t-b_d-G-g_c-d (2)	K_e (kip-in./rad) (3)	M_u (kip-in.) (4)	M_t (kip-in.) (5)	M_c (kip-in.) (6)	θ_c (rad) (7)	θ_u (rad) (8)	r (9)
1	TS-6-4-3/4-5/8-2½-5-14	247,063	791	684	115	0.0002	0.0229	1.580
2	TS-6-6-3/8-5/8-4½-5-14	73,000	219	153	120	0.0042	0.0450	3.560
3	TS-6-6-3/4-5/8-3½-5-14	168,732	840	555	308	0.0013	0.0420	1.300
4	TS-6-6-3/4-5/8-4½-4-16	177,621	745	607	212	0.0007	0.0450	1.300
5	TS-6-4-3/4-3/4-2½-5-14	428,796	1,221	649	177	0.0002	0.0340	1.490
6	TS-6-4-1/2-3/4-2½-5-14	192,226	813	387	252	0.0011	0.0450	2.830
7	TS-6-4-3/4-3/4-2½-5-16	NRD*	NRD	NRD	NRD	NRD	NRD	NRD
8	TS-6-4-1/2-3/4-2½-4-16	533,178	901	536	220	0.0005	0.0450	2.620
9	TS-6-6-3/4-3/4-3½-4-16	239,845	1,164	729	283	0.0007	0.0440	1.520
10	TS-6-4-3/4-7/8-2½-4-16	602,379	1,665	860	500	0.0005	0.0380	1.550
11	TS-6-6-3/4-7/8-2½-4-16	629,219	1,792	956	248	0.0002	0.0450	1.600
12	TS-6-6-3/4-7/8-4½-4-16	190,132	920	552	195	0.0006	0.0450	1.370

* No Reliable Data was obtained for this test specimen due to instrumentation malfunction

specimens as can be seen in Figs. B-7(a) through B-7(*l*), excluding Fig. B-7(g), for which models are not presented due to instrument malfunction. Figure B-7(h) of Appendix B shows that for Test Specimen (12), the bilinear and modified bilinear models predict the experimental hysteresis loops with about the same degree of accuracy. Figure B-7(f) shows that the bilinear model better predicts the experimental results, and the modified bilinear model is not accurate. For all other test specimens presented in Figs. B-7(a) through B-7(*l*), the modified bilinear model best predicts the hysteresis behavior and is most conservative. Similarly, looking at these plots, it is concluded that the bilinear model can be classified being next to the modified bilinear model, as far as degree of accuracy in predicting experimental results is concerned. Also, these plots show that the elasto-plastic model is the least conservative model for all test specimens. A similar trend was observed for double web angle connections. Therefore, a conclusion may be drawn that the modified bilinear model is usually the most conservative model and the elasto-plastic model is always the least conservative model, with the bilinear model in between the two extremes.

4.5 Hysteresis Models for Flush End-Plate Connections

This section presents the relative predicting capabilities of the different mathematical models for the flush end-plate connection with two rows of bolts in either side of the beam flanges. The failure mode of the connections, as discussed in Chapter III, was primarily excessive yielding. Therefore, the bilinear models described in Section 4.2 are most suitable to idealize the hysteresis behavior of this type of connection.

Table 4.5 presents the experimental values of the hysteresis parameters required to construct the bilinear models. In this table, as before, the experimental values of the characteristic moment, M_c, characteristic rotation, θ_c, and rigidity parameter, r, were obtained by best fitting the Ramberg-Osgood function, Eq. (4.4), to best fit the experimental enveloping curve by the method of least squares. The comparison between the predicted Ramberg-Osgood function and experimental enveloping curves for flush end-plate test specimens are presented in Figs. B-8(a) through B-8(i) in Appendix B. These figures show that very little difference exists between the predicted and experimental curves.

The comparisons of hysteresis models and experimental moment-rotation hysteresis loops are presented in Figs. B-9(a) through B-9(i) of Appendix B. These figures show the predicting capability trends of the three models observed in the case of double web angle and top and seat angle connections. As before, the modified bilinear model best predicts the hysteresis behavior in almost all cases; and the elasto-plastic model is the least conservative model in predicting the hysteresis behavior. Figure B-9(c) shows that for Test Specimen (4) the bilinear and modified bilinear models almost identically predict the energy dissipation capability of the connection.

4.6 Hysteresis Models for Extended-End-Plate Connections

The formulation of the mathematical hysteresis models for the extended end-plate connections of the type discussed in Chapter III is presented in this section. Out

Table 4.5 Experimental Hysteresis Parameter Obtained for Flush End-Plate Connections

Test No. (1)	Test Designation FEP-II-b_p-d_p-t_p-b_d-p_f-p_b-g_c (2)	K_e (kip-in./rad) (3)	M_u (kip-in.) (4)	M_t (kip-in.) (5)	M_c (kip-in.) (6)	θ_c (rad) (7)	θ_u (rad) (8)	r (9)
1	FEP-II-6-18-3/8-3/4-1⅝-3-3	NMV*	1,979	1,450	1,650	0.0026	0.0116	6.480
2	FEP-II-6-18-1/2-3/4-1⅝-3-3	458,357	2,209	1,500	1,800	0.0032	0.0122	3.380
3	FEP-II-6-18-5/8-3/4-1⅝-3-3	498,330	2,228	1,750	2,000	0.0034	0.0070	4.541
4	FEP-II-8-18-3/8-1-1⅞-3½ -3½	699,191	2,257	1,500	1,300	0.0012	0.0152	3.661
5	FEP-II-8-18-1/2-1-1⅞-3½ -3½	935,306	3,434	2,700	2,750	0.0021	0.0188	9.835
6	FEP-II-8-18-3/4-1-1⅞-3½ -3½	NMV	4,036	3,050	4,000	0.0085	0.0203	6.848
7	FEP-II-6-22-3/8-3/4-1⅝-3-3	599,077	2,227	1,470	2,000	0.0038	0.0098	3.788
8	FEP-II-6-22-1/2-3/4-1⅝-3-3	616,329	2,766	1,900	2,300	0.0028	0.0108	3.675
9	FEP-II-6-22-5/8-3/4-1⅝-3-3	725,965	2,892	2,050	2,500	0.0035	0.0084	3.384
10	FEP-II-8-22-3/8-1-1⅞-3½ -3½	915,236	2,870	1,720	2,100	0.0026	0.0097	4.747
11	FEP-II-8-22-1/2-1-1⅞-3½ -3½	973,722	UM**	2,610	3,500	0.0040	UM	6.000
12	FEP-II-8-22-3/4-1-1⅞-3½ -3½	1,311,543	4,906	3,700	4,500	0.0040	0.0140	6.671

* No Meaningful Value was obtained

** Ultimate Moment was not reached due to testing apparatus malfunction of the eight experimental tests conducted for extended end-plate connections, only five specimens could be tested to failure due to limitations of actuator capacity. The failure mode for these five tests was primarily excessive yielding. Therefore, the bilinear models, described in Section 4.2, are most suitable to idealize the hysteresis behavior of this type of connection.

The experimental values of the hysteresis parameters required to construct the three bilinear models are tabulated in Table 4.6. In this table, the values of hysteresis parameters are presented for the test cases in which failure resulted, which includes Test Specimens (1), (2), (3), (4), and (8). The experimental values of the characteristic moment, M_c, characteristic rotation, θ_c, and rigidity parameter, r, presented in this table were obtained by fitting the Ramberg-Osgood function, Eq. (4.4), to the experimental enveloping curve using the method of least squares. The comparison between the predicted Ramberg-Osgood function and the experimental enveloping curves for the five failed test specimens are presented in Figs. B-10(a) through B-10(e) of Appendix B. As shown in the plots presented in this figure, with the exception of Test Specimen (2) (refer to Fig. B-10(b)), the predicted enveloping Ramberg-Osgood curve is very close to the experimental enveloping curve.

The predictions obtained by the three bilinear hysteresis models are compared with the experimental moment-rotation hysteresis loops for each test case in which failure occurred in Figs. B-11(a) through B-11(e) of Appendix B. The graphical plots presented in this figure show that the modified bilinear model most accurately and conservatively predicts the energy dissipation capability of extended end-plate connections. Figure B-11(c) shows that both the bilinear and modified bilinear

Table 4.6 Experimental Hysteresis Parameter Obtained for Extended End-Plate Connections

Test No. (1)	Test Designation EEP-b_p-d_p-t_p-b_d-p_f-g_c (2)	K_e (kip-in./rad) (3)	M_u (kip-in.) (4)	M_t (kip-in.) (5)	M_c (kip-in.) (6)	θ_c (rad) (7)	θ_u (rad) (8)	r (9)
1	EEP-7-22½-1/2-3/4-1⅜-3½	1,129,937	2,758	2,052	1,350	0.0005	0.0084	3.875
2	EEP-8-22½-5/8-7/8-1½-5½	2,035,000	3,535	2,279	1,700	0.0004	0.0085	2.700
3	EEP-9-22½-1/2-1⅛-1⅞-3½	1,200,516	3,460	2,540	2,500	0.0018	0.0134	5.480
4	EEP-10-22½-1/2-7/8-1⅜-4½	2,058,229	3,165	2,841	2,349	0.0012	0.0132	6.468
5	EEP-9-31-7/8-1-1¾-3½	3,470,945	UM*	UM	UM	UM	UM	UM
6	EEP-10-31-3/4-1⅛-1¼-7½	4,857,958	UM	UM	UM	UM	UM	UM
7	EEP-9-31-5/8-1-1⅞-7½	1,675,542	UM	UM	UM	UM	UM	UM
8	EEP-10-31-1/2-1⅛-1⅛-3½	3,235,654	6,218	3,760	3,000	0.0003	0.0145	3.200

* Ultimate Moment was not reached due to testing apparatus malfunction

models for Test Specimen (3) predict similar behavior. Finally, the graphical plots of Figs. B-11(a) through B-11(e) show that the elasto-plastic model is the least conservative model, which is consistent with observation made for the case of double web angle, top and seat angle, and flush end-plate connections investigated in this research.

4.7 Chapter Summary

This chapter presented the different mathematical hysteresis models that can be used to idealize the experimentally recorded moment-rotation hysteresis behavior of semi-rigid connections of the types studied in this research. Two basic types of mathematical hysteresis models are proposed, the bilinear and trilinear models, depending whether the connection failure results due to excessive yielding of the connection elements or due to beam web material bearing failure. Typical moment-rotation hysteresis loops obtained for a connection which fails due to excessive yielding was shown in Fig. 4.1(a), whereas the hysteresis loops of a connection in which beam web bearing failure occurs was shown in Fig. 4.1(b). The only type of connection tested which exhibited beam web bearing failure was the "Type I" (all bolted) double web angle connections with angle thickness $t > 3/8$ in.

Three different bilinear models, which vary in degree of simplicity and predicting capability, are proposed in this research. These include the elasto-plastic, bilinear, and modified bilinear models. Parameters defining the elasto-plastic model are: initial stiffness, K_e, ultimate moment, M_u, and ultimate rotation, θ_u. Hysteresis parameters defining the bilinear model, are: K_e,, M_u, transition moment, M_t, and θ_u.

Parameters defining the modified bilinear model are: K_c, characteristic moment, M_c, M_u, and θ_u. Therefore, the elasto-plastic model is a three-parameter model whereas the bilinear and modified bilinear models each require four independent parameters for their formulations.

The trilinear model proposed for the connections which exhibit beam web bearing behavior requires five independent hysteresis parameters, which are: K_e, bearing moment, M_b, bearing rotation, θ_b, M_u, and θ_u

Comparisons between the mathematical models and the experimentally recorded moment-rotation loops are presented in Appendix B. The graphical plots presented in this appendix show that the elasto-plastic model, though the simplest model to construct, is the least conservative in idealizing the energy dissipating capability of the connection. This was expected, because in this model the idealized yield moment was considered to be the ultimate moment and no strain hardening behavior is considered after initial yielding. The bilinear model, on the other hand, estimated the energy dissipation capability of the connection in a more realistic and conservative manner. Finally, the modified bilinear model was usually the most accurate and conservative model for the test specimens considered. From the graphical plots shown in Appendix B, it was concluded that in most of the cases considered, the bilinear and modified bilinear models were fairly close, and sometimes almost identical. Even though both bilinear and modified bilinear models are four-parameter models, the transition moment parameter defined for the bilinear model is based on an arbitrary graphical procedure, whereas the characteristic moment, used in its place in the modified bilinear model, has a mathematical definition, as defined by the Ramberg-Osgood function. The selection of a mathematical model for incorporating the material nonlinearly of the connection into a dynamic frame analysis computer program will depend on the judgement of the structural designer.

Finally, for the limited cases in which beam web bearing failure occurred, the trilinear model proposed was observed to predict the moment-rotation hysteresis loops for "Type I" (all bolted) double web angle connections reasonably accurate (refer to Figs. B-3(a) through B-3(d) of Appendix B). However, this needs to be further researched using more test data before this can be generalized; but the results are promising. Also, for this connection there is a need to investigate the basic yield failure mechanism, and develop empirical relationships which predict the likely type of failure that would occur for a given connection configuration, i.e., will it fail by excessive rotation caused by angle yielding, or by bolt fracture, or by beam web material bearing failure? Due to limited test data available in the present study, this could not be investigated.

CHAPTER V

DYNAMIC ANALYSIS OF STEEL FRAMES WITH SEMI-RIGID CONNECTIONS

5.1 General

The ultimate objective of this research is to develop an algorithm and associated computer program for dynamic analysis of planar steel frames that considers the hysteresis behavior of semi-rigid connections. As done for static analysis of steel frames with semi-rigid connections in Chapter II, the connections will be modeled by a moment spring with a known moment-rotation behavior. The hysteresis models developed for different types of semi-rigid connections (i.e., double web angle, top and seat angle, flush end plate, and extended end plate connections) in Chapter IV will be used to characterize the connection moment-rotation hysteresis behavior. These models are classified in two categories: elasto-plastic and bilinear (including modified bilinear). The computer program developed will incorporate options to analyze a frame with either one of these models.

In this chapter, Section 5.2 will briefly present the nonlinear dynamic analysis procedures used. In Section 5.3, the details of the algorithm developed for dynamic analysis of frames with semi-rigid connections will be presented, followed by verification of the algorithm in Section 5.4. Next, in Section 5.5, results of a parametric study undertaken to investigate the effect of connection hysteresis parameters, model types, and different earthquake ground motion records on the overall frame behavior are presented. Finally, in Section 5.6 the chapter findings are summarized.

5.2 Nonlinear Dynamic Response Procedures Used

The general equation of motion for a discretized (finite element method used) inelastic multi-degree of freedom system without damping and subjected to base motion is given by

$$[M]\{\ddot{u}\}+f_s(u,\dot{u})=-[M]\{\ddot{u}_g\} \tag{5.1}$$

where $[M]$ is the mass matrix, $\{f_s(u,\dot{u})$ is the inelastic resisting force vector, which depends on the prior displacement history and velocity of the system; $\{\ddot{u}_g\}$ is ground acceleration vector; and $\{u\}$, $\{\dot{u}\}$, and $\{\ddot{u}\}$ represent nodal displacement, velocity, and acceleration vectors, respectively. In Eq. (5.1) the damping matrix is not incorporated, though the energy dissipating capability of semi-rigid connections is expected to introduce damping in the system. Furthermore, the structural damping matrix is commonly considered to be linearly related to the mass and stiffness (considering only frame beam and column members) matrices, and, if desired, can be incorporated at a later date.

An analytical solution of Eq. (5.1) at any arbitrary time is not possible to be constructed if the applied force (which depends on ground acceleration) varies arbitrarily with time or if the system is nonlinear, which is the case for the problem studied. Hence, a numerical marching time stepping method is needed to solve Eq. (5.1), and obtain answers for response subject to the initial conditions, $\{u\} = \{u(0)\}$ and $\{\dot{u}\} = \{\dot{u}(0)\}$. The applied earthquake forcing function is usually given as a set of discrete values, and is expressed as $\{P_{eff}(t_i)\} = -[M]\{\ddot{u}_g(t_i)\}$ within each time interval, $\Delta t_i = t_{i+1} - t_i$, which is generally taken to be constant over the whole response analysis. The response is then determined at each time step i.

Time stepping procedures can be classified as: (1) methods based on interpolation of the excitation function, (2) methods based on finite difference expressions of velocity and acceleration, and (3) methods based on an assumed variation of acceleration. In this research the method based on an assumed variation of acceleration over each time step was adopted. In particular, the average variation of acceleration over each time step is used (e.g., Newmark-β method with $\gamma = \frac{1}{2}$ and $\beta = \frac{1}{4}$), which is shown to be unconditionally stable for linear elastic systems. Muraleetharan et al. (1994) suggested that in structural dynamics problems, many of the high frequency modes actually correspond to spurious artifacts of the discretization process instead of representing physical behavior of the actual continuous system. Therefore, numerical dissipation capable of damping out spurious participation of the higher modes was suggested to be desirable. In Newmark-β method numerical dissipation can be controlled by a parameter other than time step. For example, for $\gamma \geq \frac{1}{2}$ and $\beta = \left(\frac{1}{4}\gamma + \frac{1}{2}\right)^2$, the amount of numerical dissipation for a fixed time step increases with increasing γ. When $\gamma = \frac{1}{2}$ Newmark-β method does not introduce any numerical dissipation in a dynamic system, which could be a drawback. Muraleetharan et. al. (1994) suggested the three-parameter α-method proposed by Hilber et al. (1977) to compensate for defects inherent in the Newmark-β algorithm. The concerns of Muraleetharan et. al. (1994) with regard to the nonlinear dynamic problem of the saturated porous media using finite element continuum discretization was well justified. However, for the dynamic problem studied in this research, material nonlinearity occurs at the connection elements joining the beam and column nodes. Thus, the nonlinearity is localized, unlike that of the saturated porous media investigated by Muraleetharan et. al. (1994), in which it is dispersed throughout the continuum. Therefore, the Newmark-β average acceleration method is expected to produce acceptable results in this research.

5.3 Nonlinear Dynamic Program Algorithm

The nonlinear inelastic program algorithm developed in this study is an extension of the coupled nonlinear static finite element program presented in Chapter II. In this computer program, the beam-to-column connection is modeled as a discrete moment spring with a specified analytical moment-rotation hysteresis relationship. The step-by-step procedure proposed for dynamic response analysis is as follows:

1. Formulate element stiffness matrices for beam and column members, $[K^{e}]$, for time step i (refer to Eqs. (2.7), (2.8), and (2.9) of Chapter II).

2. Formulate the connection element stiffness matrix, $\left[K_n^{\,c}\right]$, for the n^{th} spring element using initial elastic stiffness, K_e, of the connection (refer to Eq. (2.10) of Chapter II).

3 Formulate element consistent mass matrices for beam and column members using

$$\left[M^e\right] = \left[M^a\right] + \left[M^b\right] \tag{5.2}$$

where $\left[M^a\right]$ is the axial consistent mass matrix defined by

$$\left[M^a\right] = \frac{ml}{6}\begin{bmatrix} 2C^2 & 2CS & 0 & CS & CS & 0 \\ 2CS & 2S^2 & 0 & CS & S^2 & 0 \\ 0 & 0 & 0 & 0 & 0 & 0 \\ CS & CS & 0 & 2C^2 & 2CS & 0 \\ CS & S^2 & 0 & 2CS & 2S^2 & 0 \\ 0 & 0 & 0 & 0 & 0 & 0 \end{bmatrix} \tag{5.3}$$

and $\left[M^b\right]$ is the beam consistent mass matrix defined by

$$\left[M^b\right] = \frac{ml}{420}\begin{bmatrix} 156S^2 & -156CS & -22Sl & 54S^2 & -54CS & 13Sl \\ -156CS & 156C^2 & 22Cl & -54CS & 54C^2 & -13Cl \\ -22Sl & 22Cl & 4l^2 & -13Sl & 13Cl & -3l^2 \\ 54S^2 & -54CS & -13Sl & 156S^2 & -156CS & 22Sl \\ -54CS & 54C^2 & 13Cl & -156CS & 156C^2 & -22Cl \\ 13Sl & -13Cl & -3l^2 & 22Sl & -22Cl & 4l^2 \end{bmatrix} \tag{5.4}$$

in which m is the member mass, l is the member length, and S and C are the sine and cosine functions defined in Fig. 2.2 of Chapter II.

4. Assemble the system (global) stiffness matrix, $[K]$, and system mass matrix, $[M]$.

5. Input the earthquake ground acceleration variation record, direction of the earthquake, and select the time increment used to perform the dynamic analysis. The direction of the earthquake needs to be input in the global X and Y direction of the structural model. The earthquake record needs to be normalized with respect to units of g (acceleration due to gravity). The algorithm presented has the capability of reducing the time increment (time step) until convergence is achieved.

6. Initialize the system displacement and acceleration vectors, $\{u(0)\}$ and $\{\ddot{u}(0)\}$. If initial conditions other than zero are specified, the program algorithm is capable of considering such conditions.

7. Input the hysteresis parameters for each spring element. The input parameters for each spring element vary based on the hysteresis model used. The following three models are considered:

   (i) For the elasto-plastic model, input initial stiffness, K_e, ultimate moment, M_u, and ultimate rotation, θ_u.

   (ii) For the bilinear model, input K_e, transition moment, M_t (idealized yield moment, refer to Chapter IV), M_u, and θ_u.

   (iii) For the modified bilinear model, input enveloping characteristic moment, M_c (idealized yield moment, refer to Chapter IV), enveloping characteristic rotation, θ_c (idealized yield rotation, refer to Chapter IV), M_u, and θ_u.

   It should be noted that both the bilinear and modified bilinear models are four parameter models, and differ only in the definition of the idealized yield moment. Actually, both are different forms of a bilinear or two linear segment model.

8. Calculate dynamic load vector $\{P_{eff}\}$ for each time step, i, by multiplying the system mass matrix with the input ground acceleration vector for the earthquake record, i.e.,

$$\{P_{eff}\}_i = \{P_{eff}(t_i)\} = -[M]\,\{\ddot{u}_g(t_i)\}_i \tag{5.5}$$

It should be noted that the system mass matrix will be banded and symmetric; a subroutine was developed for multiplying a banded symmetric matrix and a column matrix appearing on the right hand side of Eq. (5.5).

9. Calculate Newmark-β matrices $[a]$ and $[b]$ using the following expressions:

$$[a] = \frac{4}{\Delta t}[M] \tag{5.6}$$

$$[b] = 2[M] \tag{5.7}$$

Start of the time step iteration i:

10. Calculate incremental effective dynamic load vector, $\{\Delta\overline{P}\}$ using

$$\{\Delta\overline{P}\}_i = (\{P_{eff}\}_{i+1} - \{P_{eff}\}_i) + [a]\{\dot{u}\}_i + [b]\{\ddot{u}\}_i \tag{5.8}$$

where $\{\dot{u}\}_i$ and $\{\ddot{u}\}_i$ represent the incremental velocity and acceleration vectors, respectively, for time step i.

11. Calculate the dynamic system banded stiffness matrix $[\overline{K}]_i$ for each time step i, using

$$[\bar{K}]_i = [K]_i + \frac{4}{\Delta t^2}[M] \tag{5.9}$$

where $[K]_i$ is the current system banded stiffness matrix and $[M]$ is the system banded mass matrix.

12. Solve the system dynamic equilibrium equation

$$[\bar{K}]_i \{\Delta u\}_i = \{\Delta \bar{P}\}_i \tag{5.10}$$

for the incremental displacement vector $\{\Delta u\}_i$ using the Guass-elimination and back substitution method.

13. Using the solution of Eq. (5.10), calculate the incremental velocity and acceleration vectors, $\{\Delta \dot{u}\}_i$ and $\{\Delta \ddot{u}\}_i$, for each time step using the following equations, respectively:

$$\{\Delta \dot{u}\}_i = \frac{2}{\Delta t}\{\Delta u\}_i - 2\{\dot{u}\}_i \tag{5.11}$$

$$\{\Delta \ddot{u}\}_i = \frac{4}{(\Delta t)^2}\{\Delta u\}_i - \frac{4}{\Delta t}\{\dot{u}\}_i - 2\{\ddot{u}\}_i \tag{5.12}$$

14. Update the system displacement, velocity, and acceleration vectors for the next time step using the following expressions, respectively:

$$\{u\}_{i+1} = \{u\}_i + \{\Delta u\}_i \tag{5.13}$$

$$\{\dot{u}\}_{i+1} = \{\dot{u}\}_i + \{\Delta \dot{u}\}_i \tag{5.14}$$

$$\{\ddot{u}\}_{i+1} = \{\ddot{u}\}_i + \{\Delta \ddot{u}\}_i \tag{5.15}$$

Iteration for connection (spring) element starts:

15. Identify connection elements.

16. From the system displacement vector, extract the rotational degrees of freedom corresponding to each spring element (i.e., extract the spring element two nodal rotations, θ_j and θ_k) for next time step, and calculate the relative rotation for the n^{th} spring element. If absolute value of θ_j is greater than absolute value of θ_k then relative rotation is calculated using

$$(\theta_n)_{i+1} = (\theta_j)_{i+1} - (\theta_k)_{i+1} \tag{5.16}$$

Otherwise, compute the relative rotation using

$$(\theta_n)_{i+1} = (\theta_k)_{i+1} - (\theta_j)_{i+1} \tag{5.17}$$

17. Calculate the incremental relative rotation for the n^{th} spring element between time steps i and $i+1$ as follows:

$$(\Delta\theta_n)_i = (\theta_n)_{i+1} - (\theta_n)_i \tag{5.18}$$

18. Calculate the incremental relative rotational velocity for the n^{th} spring element between time steps i and $i+1$ from

$$(\Delta\dot{\theta}_n)_i = \frac{2}{\Delta t}(\Delta\theta_n)_i - 2\{\dot{\theta}_i\} \tag{5.19}$$

19. Calculate the rotational velocity at time step $i+1$ from

$$(\dot{\theta}_n)_{i+1} = (\dot{\theta}_n)_i + (\Delta\dot{\theta}_n)_i \tag{5.20}$$

20 Check the direction of the connection element rotational velocity, $(\dot{\theta})_i$, for the present time step. If the direction of velocity has reversed since

the previous load step, $(\dot{\theta})_{i+1}$, it means that either unloading or reloading occurs. If this happens, set the connection stiffness equal to the initial stiffness of the connection, K_c, for the elasto-plastic and bilinear models, or M_c/θ_c for the modified bilinear model. Reformulate the connection element stiffness matrix, $[K_n{}^c]_{i+1}$ for the n^{th} connection element corresponding to its value for the next time step, $i+1$. Reassemble the updated system stiffness matrix.

21. Locate the unloading or reloading reference rotation, $(\theta_0)_n$, for the n^{th} connection element, as shown in Fig. 5.1. The reference rotation is located only if the unloading or reloading occurs after a yield event. This means that the connection element has experienced yielding prior to load reversal.

22. Locate the yield rotation, $(\theta_1)_n$ for the n^{th} connection element for the next time step. In locating such yield point three conditions exist, which include:

    (i) If during an unloading event the direction of incremental rotational velocity, $(\Delta\dot{\theta})_i$, is the same as the direction of incremental rotational velocity for the previous time step, $(\Delta\dot{\theta})_{i-1}$, then the unloading event continues. Then, the yield rotation $(\theta_1)_n$ for next time step is calculated considering Bauschinger's effect from the following equation:

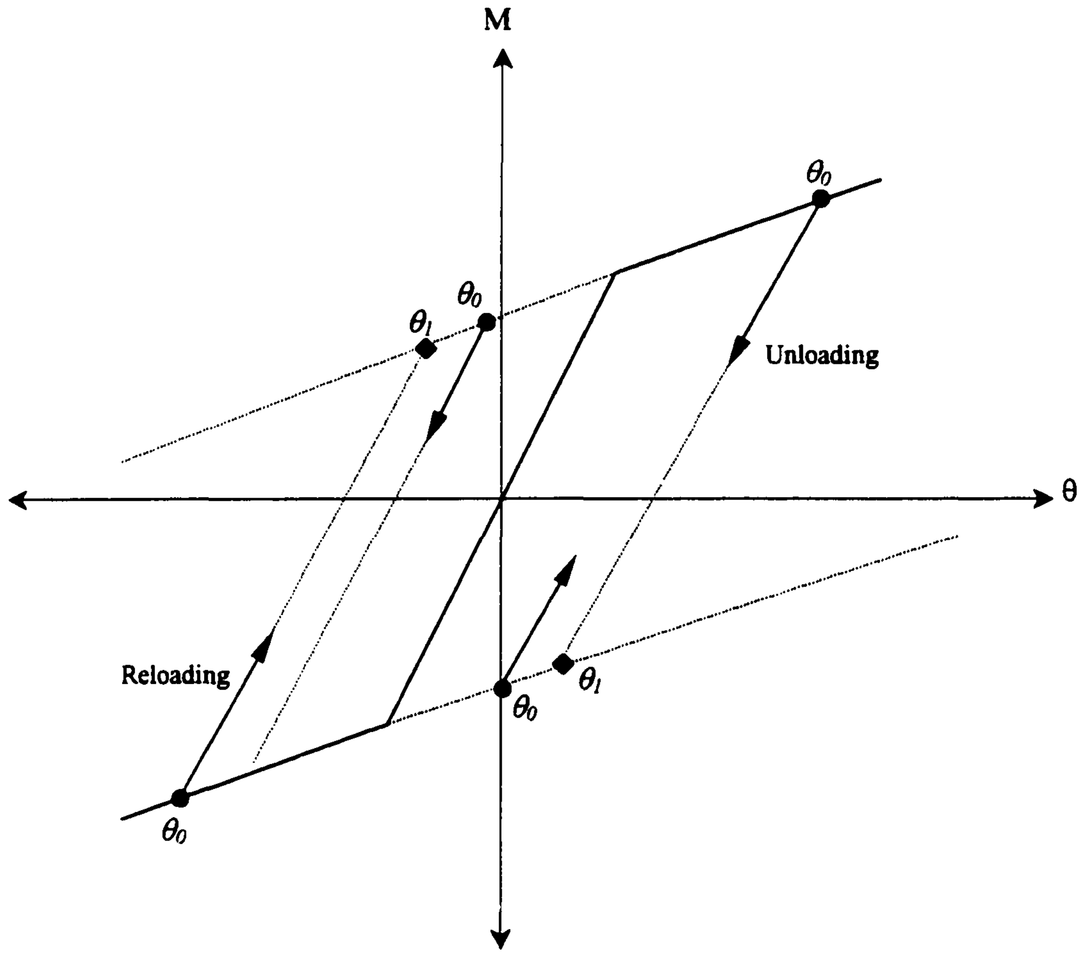

Fig. 5.1 Moment-Rotation Hysteresis Behavior of a Connection Showing Unloading or Reloading Events

$$(\theta_1)_n = (\theta_0)_n - \left(\frac{2M_y}{K_e}\right) \tag{5.21}$$

Then, the yield rotation $(\theta_1)_n$ for next time step is calculated considering Bauschinger's effect from the following equation:

$$(\theta_1)_n = (\theta_0)_n - \left(\frac{2M_y}{K_e}\right) \tag{5.21}$$

where $(\theta_0)_n$, is the rotation at the point of unloading, M_y is the n^{th} connection yield moment, and K_e is the n^{th} connection initial stiffness.

(ii) If during a reloading event the direction of incremental rotational velocity, $(\Delta\dot{\theta})_i$, is the same as the direction of incremental rotational velocity for the previous time step, $(\Delta\dot{\theta})_{i-1}$, then the reloading event continues. Then, the yield rotation $(\theta_1)_n$ for the next time step is calculated using

$$(\theta_1)_n = (\theta_0)_n + \left(\frac{2M_y}{K_e}\right) \tag{5.22}$$

(iii) If the direction of incremental rotational velocity, $(\Delta\dot{\theta})_i$, is not the same as the direction of incremental rotational velocity for the previous time step, $(\Delta\dot{\theta})_{i-1}$, then the yield rotation $(\theta_0)_n$ for the next time step is the rotation at the point of unloading or reloading.

23. Check the n^{th} spring rotation $(\theta_n)_{i+1}$ against the yield rotation $(\theta_0)_n$ or $(\theta_1)_n$. If the connection element yields, which occurs when $|(\theta_n)_{i+1} - (\theta_0)_n| > \varepsilon$ or $|(\theta_n)_{i+1} - (\theta_1)_n| > \varepsilon$ (where ε is the tolerance, which is taken equal to 0.00005), divide the time step into two, and repeat Steps (9) to (23).

24. If the n^{th} connection element yields, which occurs when $|(\theta_n)_{i+1} - (\theta_0)_n| \leq \varepsilon$ or $|(\theta_n)_{i+1} - (\theta_1)_n| \leq \varepsilon$, then update the n^{th} connection element stiffness matrix using tangential stiffness given by

$$(K_t)_n = \frac{(M_u)_n - (M_y)_n}{(\theta_u)_n - (\theta_y)_n} \tag{5.23}$$

25. Assemble the updated system stiffness matrix, $[K]_i$, for the next time step.

26. Calculate the moment $(EM_n)_i$ in each connection element for time step i. If the connection element is in the elastic region, then it is given by

$$(EM_n)_i = (\Delta\theta_n)_i (K_e)_n \tag{5.24}$$

If connection element has yielded, then it is given by

$$(EM_n)_i = (\Delta\theta_n)_i (K_t)_n + (\theta_y)_n (K_e)_n \tag{5.25}$$

Connection iteration terminates.

27. Calculate member end-forces, $\{f_s\}_i$ for frame members,

$$\{f_s\}_i = [K^*]\{\delta^*\} \tag{5.26}$$

where $\{f_s\}_i$ is the local beam/column member force vector, at time step i, $[K^e]$ is the elastic stiffness matrix of the frame member, and $\{\delta^e\}_i$ is the local member displacement vector at time step i.

Time step iteration ends

5.4 Verification of the Computer Program

No analytical and/or experimental results are available in the literature for dynamic response of steel frames with semi-rigid connections considered in this study when subjected to an earthquake ground motion. Nader and Astaneh (1996) conducted shaking table tests on rigid, semi-rigid, and flexible steel frames to obtain the dynamic behavior of such frames. The semi-rigid connections used in this study were a combination of top and seat angle and double web angle connections, and the frames had lateral braces. Therefore, the type of connection considered was different than the ones studied in this research. Also, the hysteresis loops obtained from this study had the effect of lateral braces and the ultimate rotation was shown to be less than 0.01 rad. The semi-rigid connection of this study behaved elastic. Hence, the results of the aforementioned study could not be used for comparison purposes.

Thus, to verify the prediction capabilities of the computer program developed to automate the algorithm presented in Section 5.2, it was not possible to choose example problems analyzed by other researchers and directly compare the results. However, an attempt has been made in this study to verify the computer program developed by analyzing frame examples with different time step size adopted to march the numerical solution and show that the results converge to a solution as the time step size is made smaller and smaller. The results obtained are presented in this section.

In this study two frames, a two-story one-bay and a two-story two-bay frame, which are shown in Fig. 5.2 as Frame 1 and Frame 2, respectively, were analyzed when subjected to 7 sec of the 1940 El-Centro Earthquake ground motion. Both frames consist of 12 ft. high W12×96 columns and 20 ft. long W14×96 beams, and connections with the following values for the bilinear moment-rotation hysteresis model parameters: initial stiffness K_o = 500,000 kip-in./rad, yield rotation θ_y = 0.003 rad, yield moment M_y = 1,500 kip-in., ultimate moment M_u = 3,000 kip-in., and ultimate rotation θ_u = 0.03 rad. In both frames, all connections are assumed to be identical, and are modeled using a bilinear moment-rotation hysteresis model using the aforementioned model parameter values. It should be noted that the intent for choosing Frame 2 was to check if the computer program modeled correctly an interior beam-to-column joint with multiple connections, shown as joints labeled 1 and 2 in Fig. 5.2 (b). Both the frames were analyzed by decreasing the time step size, until the response solution obtained for roof (top story) sway did not change much up to the significant decimal places considered. The solution thus obtained was labeled as the "converged result."

The response history predicted for the roof sway for Frame 1 for time step sizes of Δt = 0.0060, 0.0040, 0.0033, and 0.0025 sec are shown in Fig. 5.3. A converged solution was obtained for Δt = 0.0025 sec. It should be noted that for approximately the first 2.8 sec, the response history obtained for all the time step sizes is about the same. This is so because the frame connections remain elastic

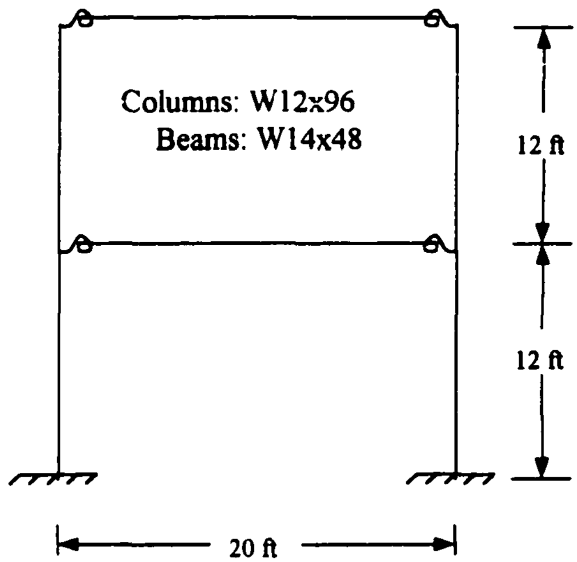

(a)

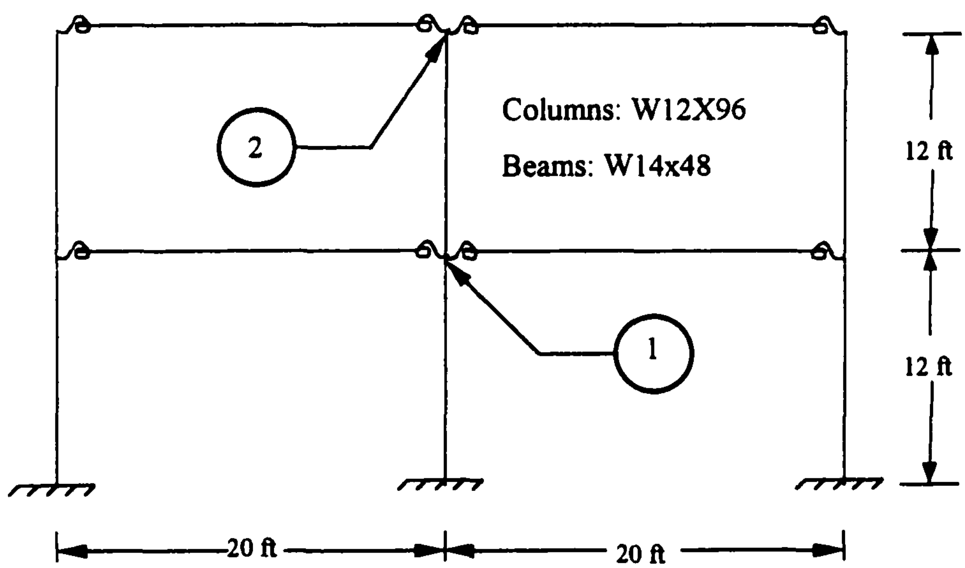

(b)

Fig. 5.2 Frames Used for Verification and Parametric Study: (a) Frame 1; (b) Frame 2

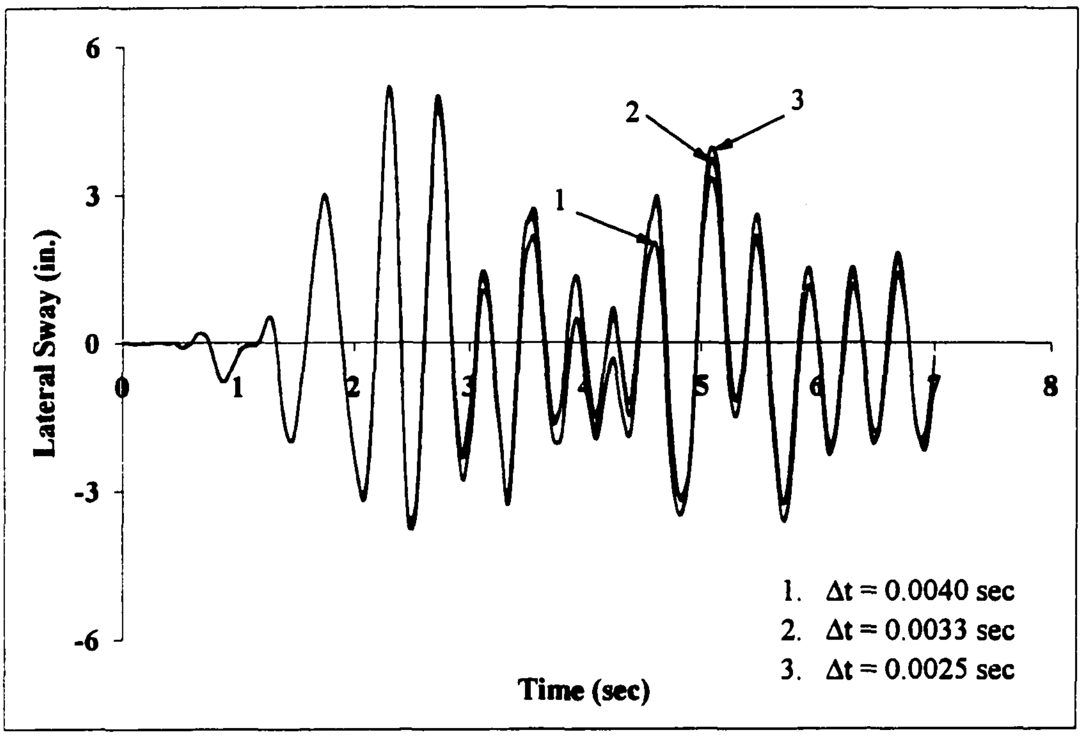

Fig. 5.3 Convergence of Roof Sway History for Frame 1 Subjected to El-Centro Earthquake

during this time duration. It is interesting to note that the peak sway occurs during this time duration. The results shown in Fig. 5.3 also show that the convergence trend is one way—peak displacements increase as the time step size is refined. The peak sway responses predicted by changing the size of Δt do not show any phase shift. A comparison of the converged roof sway response history for Frame 1 with a similar frame with rigid joints is presented in Fig. 5.4.

It can be seen that the two solutions differ significantly in both magnitudes of the peak sway values and also at the times when they occur. The response of the semi-rigid frame has larger amplitudes and longer periods of response, as expected from a more flexible structure.

The moment-rotation hysteresis loop predicted by the computer program for the left bottom story connection element of Frame 1 is shown in Fig. 5.5. This figure shows that the computer program produces the hysteresis loops correctly for the connection element. The corners of the loops are modeled accurately. This figure also confirms that due to ground motion acceleration and resulting dynamic forces on the system (frame), the hysteresis loops obtained do not follow the loops in a sequential manner. For example during unloading, prior to reaching the unloading yield point, reloading may occur and the loops will reverse in direction, due to reversal in velocity. This phenomenon is observed in Fig. 5.5.

The member-end shear forces and bending moments predicted for Frame 1 after 5 sec of the earthquake record are shown in Figs. 5.6 and 5.7, respectively. As can be checked, the internal forces created in the members satisfy perfect equilibrium within each member. However, it was found that the moment transferred by each

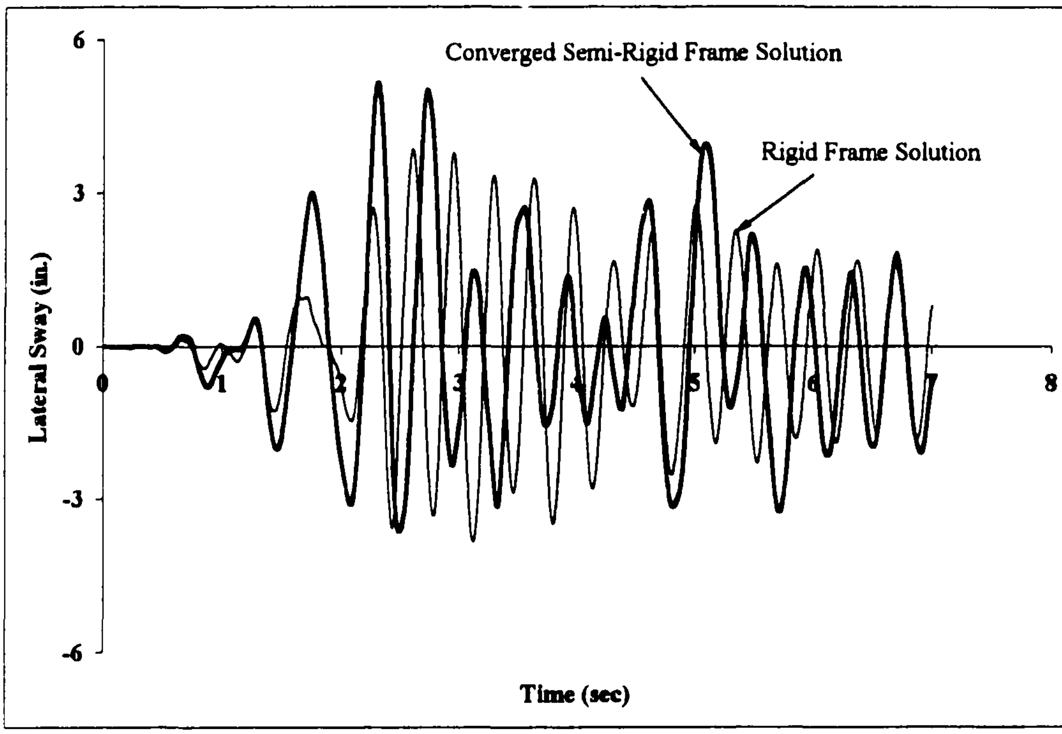

Fig. 5.4 Comparison of Roof Sway History Considering Semi-Rigid and Rigid-Joint Behavior for Frame 1 Subjected to El-Centro Earthquake

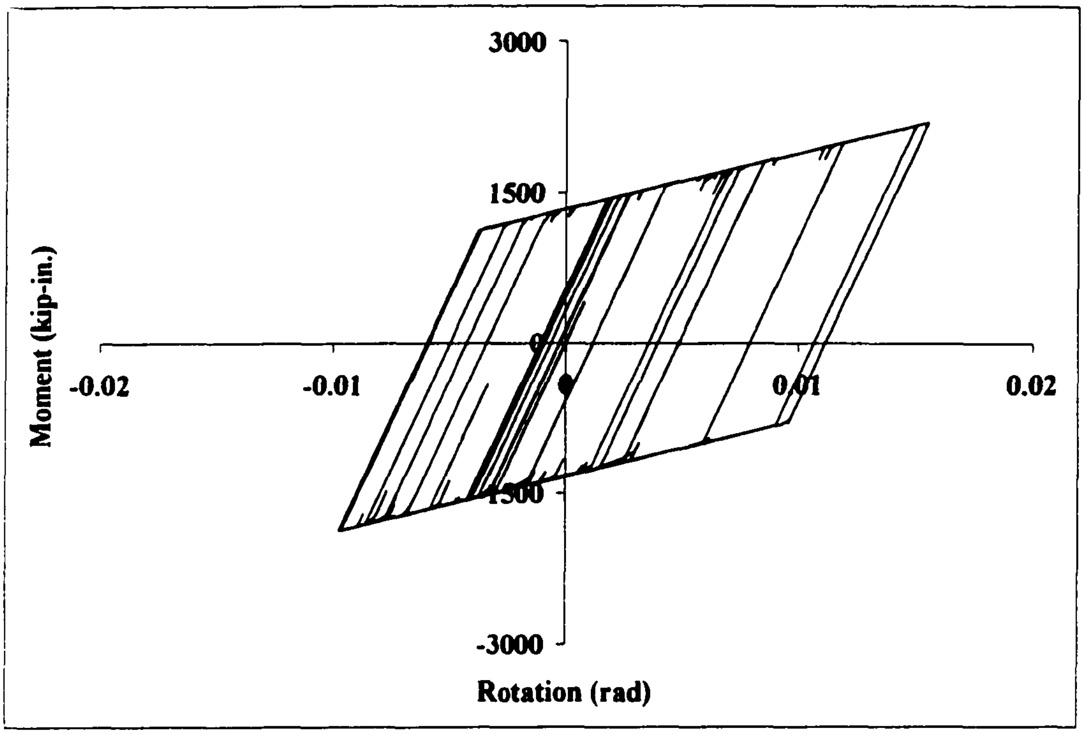

Fig 5.5 Bilinear Moment-Rotation Hysteresis Loops Obtained from the Dynamic Frame Computer Program for a Typical Spring of Frame 1

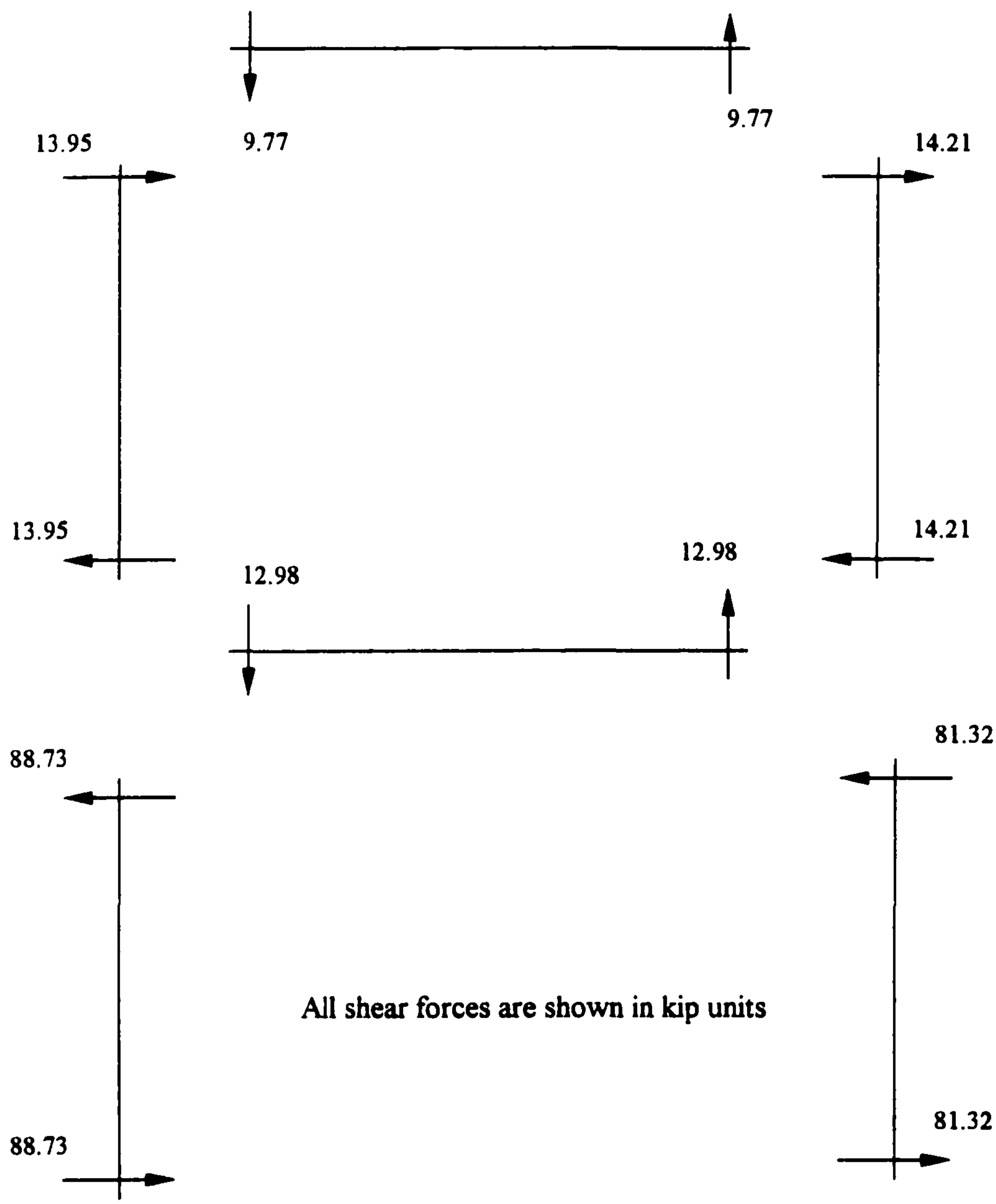

Fig 5.6 Members Shear for Frame 1 at 5 Seconds of the El-Centro Earthquake Record

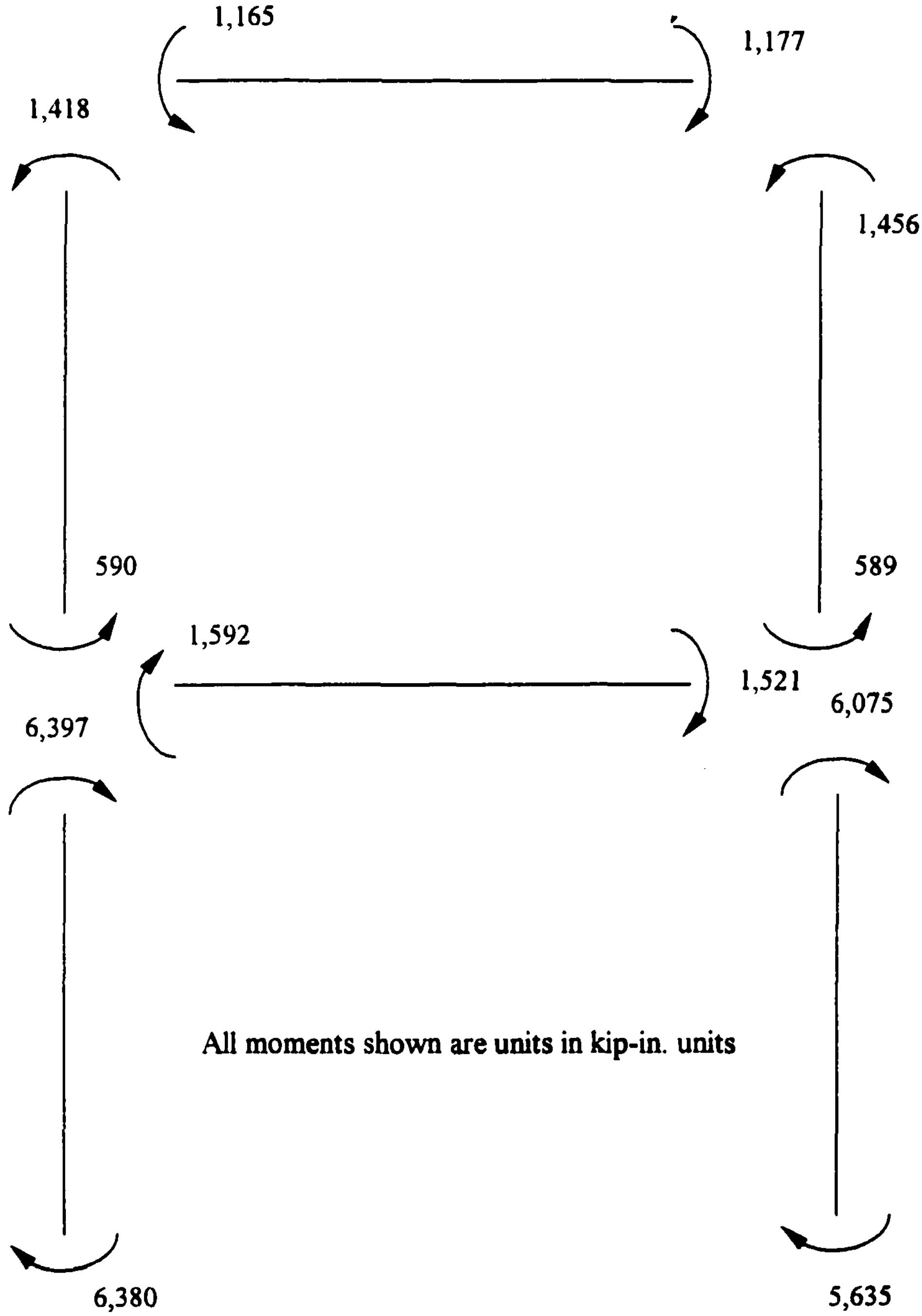

Fig 5.7 Members End Moments for Frame 1 at 5 Seconds of the El-Centro Earthquake Record

member end onto the joint it is connected to is not exactly equal and opposite to the internal moment created in the spring. One reason for this is the lack of inertial moments from the consistent mass matrix shown on the bending moment diagram. This was found to be true for each connection spring.

The response history predicted for the roof sway for Frame 2 for time step sizes of Δt = 0.010, 0.0040, and 0.0033 sec are shown in Fig. 5.8. A converged solution was obtained for Δt = 0.0033 sec. It should be noted that for approximately the first 3.3 sec, the response history obtained for all the step sizes is about the same. This is so because the frame connections remain in the elastic domain during this time duration. The results shown in Fig. 5.8 also show that the convergence trend is one way—peak displacements increase as the time step size is refined. The peak sway responses predicted by changing the size of Δt do not show any phase shift.

A comparison of the converged roof sway response history for Frame 2 with a similar frame with rigid joints is presented in Fig. 5.9. It can be seen that the two solutions differ significantly in both magnitudes of the peak values and also at the times when they occur. Once again the semi-rigid frame solution exhibits a longer period response than the elastic solution. The reduced amplitude of the semi-rigid frame solution after 5 sec is attributed to the longer period of the frame and the lack of low frequency content in this portion of the El-Centro record.

The moment-rotation hysteresis loop predicted by the computer program for the lower left connection element of Frame 2 is shown in Fig. 5.10. This figure shows that the computer program produces the hysteresis loops correctly for the connection element. The corners of the loops are modeled accurately. This figure

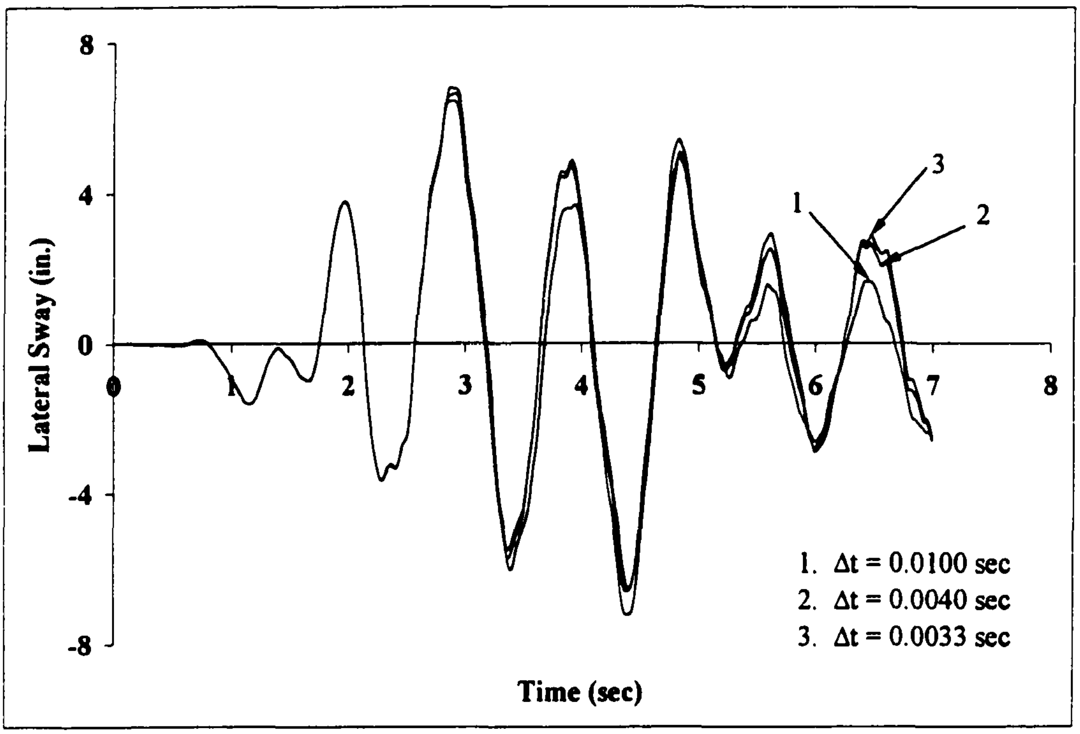

Fig. 5.8 Convergence of Roof Sway History for Frame 2 Subjected to El-Centro Earthquake

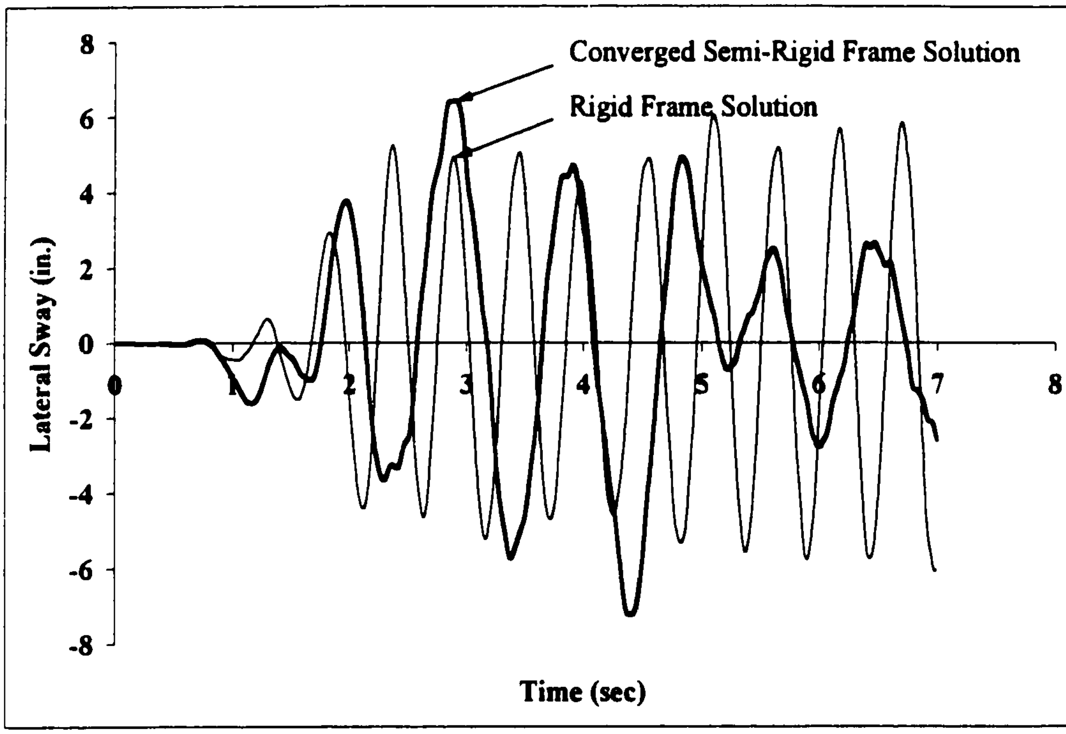

Fig. 5.9 Comparison of Roof Sway History Considering Semi-Rigid and Rigid-Joint Behavior for Frame 2 Subjected to El-Centro Earthquake

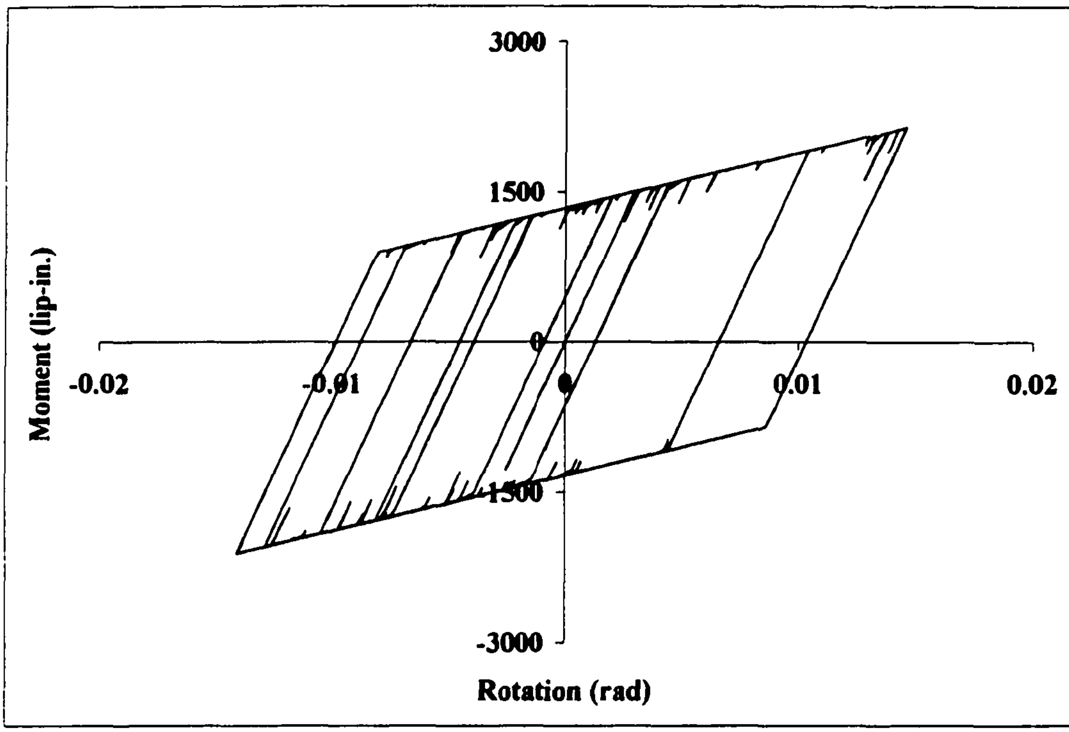

Fig 5.10 Bilinear Moment-Rotation Hysteresis Loops Obtained from the Dynamic Frame Computer Program for a Typical Spring of Frame 2

also confirms that due to ground motion acceleration and resulting dynamic forces on the system (frame), the hysteresis loops obtained do not follow the loops in a sequential manner. The member-end shear forces and bending moments predicted for Frame 2 after 3 sec of the earthquake record are shown in Figs. 5.11 and 5.12.

As can be checked, the internal forces created in the members satisfy perfect equilibrium within each member. However, it was found that the disbalanced moment transferred by each member end onto the joint it is connected to is not exactly equal and opposite to the internal moment created in the spring. This was found to be true for each connection spring. As stated for Frame 1, this is attributed to the lack of inertial moments from the consistent mass matrix.

5.5 Parametric Study

In this section the findings of a parametric study conducted to investigate the effects of varying the hysteresis parameters, hysteresis models, and earthquake records on the overall displacement response history of semi-rigid frames is presented. For this parametric study, Frame 1 of Fig. 5.2 (a) is used to conduct the dynamic analysis, and the roof sway was considered as the main response quantity in evaluating the frame's performance. The purpose of this study was additional verification of the computer program, as an exhaustive parametric study of multiple such nonlinear structures is beyond the scope of this study.

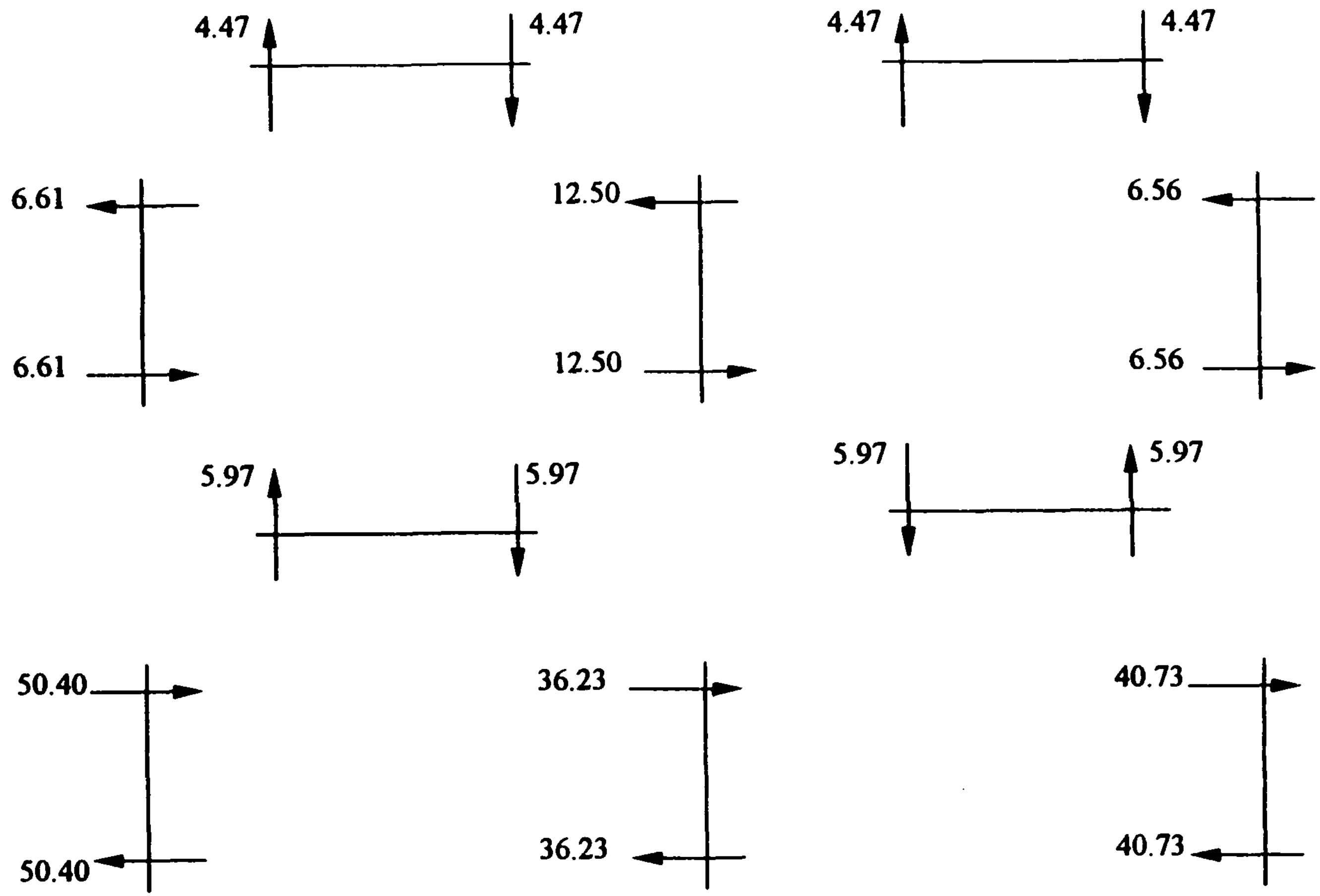

All shear forces are in kip units

Fig 5.11 Members Shear Forces for Frame 2 at 3 Seconds of the El-Centro Earthquake Record

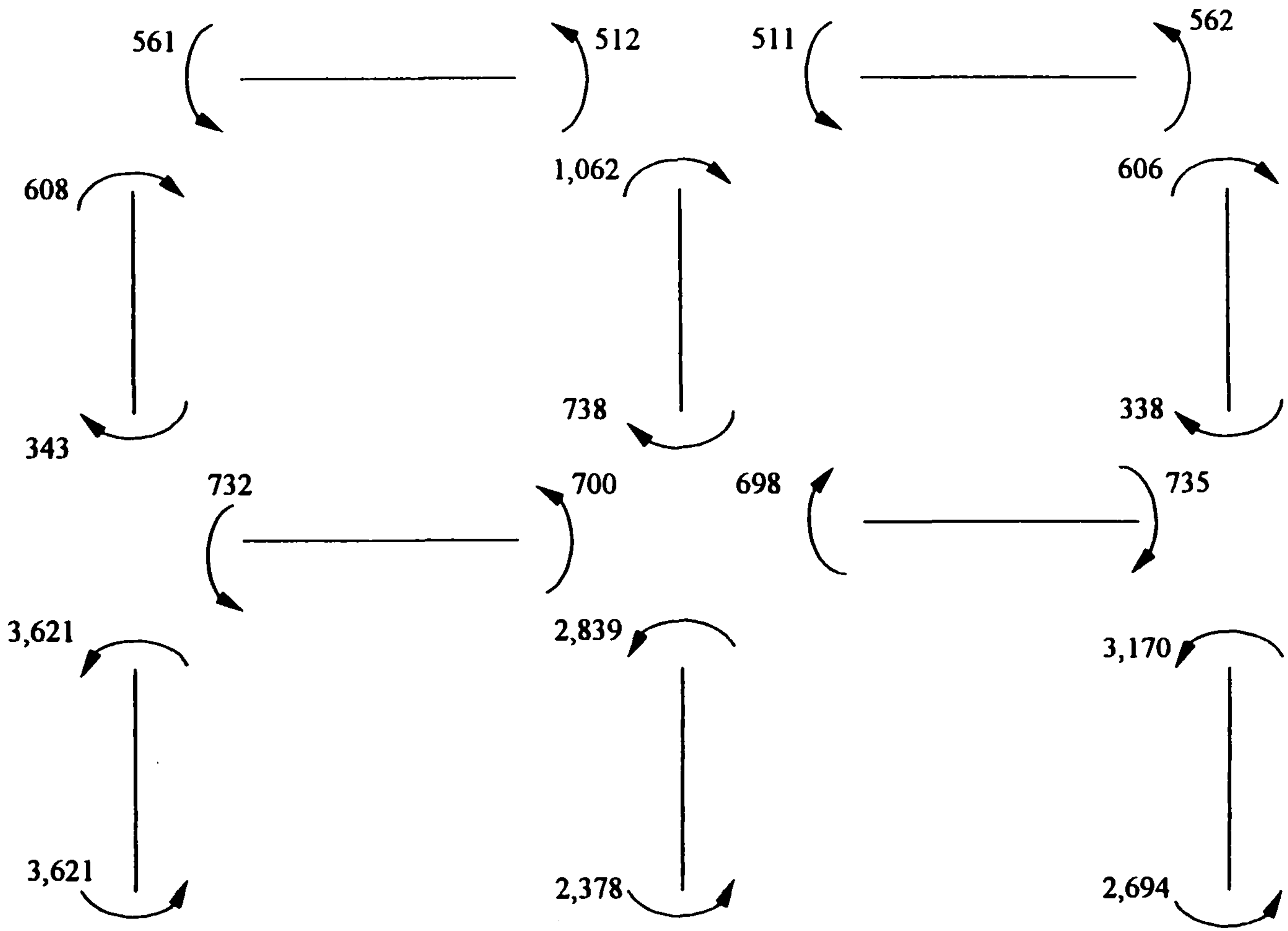

All moments shown are in kip-in. units

Fig 5.12 Members End Moments for Frame 2 at 3 Seconds of the El-Centro Earthquake Record

5.5.1 Effect of Hysteresis Model Parameters

The moment-rotation hysteresis model parameters for the elasto-plastic model bilinear model, and modified bilinear model which uses Ramberg-Osgood parameters, were presented in Chapter IV. The parameters common to all models include the following: initial elastic stiffness, K_e, ultimate moment capacity, M_u, and ultimate rotation capacity, θ_u. The definition of the so-called "yield moment" differs in the three models. For the elasto-plastic moment, the yield moment is taken equal to M_u; for the bilinear model, the yield moment is taken equal to the transition moment, M_t; and for the modified bilinear model, the yield moment is taken equal to the Ramberg-Osgood characteristic moment, M_c. However, both M_t and M_c depend on K_e and M_u of a connection. The tests conducted in this study, results for which were reported in Chapter III, clearly indicated that a connection with a high initial elastic stiffness, K_e, usually has a high ultimate moment capacity, M_u. Thus, the initial elastic stiffness, K_e, cannot be varied independently, because the selection of an improper value for K_e, corresponding to the value chosen for M_u, could distort the actual moment-rotation behavior significantly. In fact, in the bilinear and modified bilinear models it would also effect the value of the post-yielding stiffness, which was defined as the tangential stiffness, K_t , as shown in Figs. 4.3 and 4.4 of Chapter IV. The tangential stiffness, K_t, can be defined by

$$K_t = \frac{M_u - M_y}{\theta_u - \theta_y} \qquad (5.27)$$

It should be noted that for a given M_u and θ_u, an increase in M_y or a decrease in θ_y would decrease K_t. Hence, in the parametric study for the hysteresis parameters, an increase in K_e was accompanied by an increase in M_u. By varying M_u and keeping other parameters constant, the variation of tangential stiffness, K_t, is automatically accounted for by Eq. (5.27).

Effect of Initial Elastic Stiffness

In this study, the following cases were first considered for the connection parameters of Frame 1 subjected to the first 7 seconds of the El-Centro Earthquake ground motion:

1. Case #1: K_e = 400,000 kip-in./rad, θ_y = 0.003 rad, M_y = 1,200 kip-in., M_u = 3,000 kip-in., and θ_u = 0.03 rad.
2. Case #2: K_e = 700,000 kip-in./rad, θ_y = 0.003 rad, M_y = 2,100 kip-in., M_u = 5,000 kip-in., and θ_u = 0.03 rad.

These values were chosen based on the values obtained for the different connections tested in this study, which were reported in Chapter III. The roof story sway response obtained for these two cases are compared in Fig. 5.13. From this figure, it can be seen that K_e effects both the magnitudes of the peak displacements and the times they occur at. During the first 7 seconds of the earthquake record, it is seen that the maximum sway of 6.2 in. occurs at 2.34 sec with K_e = 400,000 kip-in./rad.

Next, a series of analyses were performed by varying K_e from 5×10^5 to 10^8 kip-in./rad, and keeping the following parameters as constants to: M_y =1,500 kip-in., M_u = 3,000 kip-in., and varying θ_y such that $\theta_y = M_y/K_e$ for the aforementioned values of K_e. Based on the experimental results reported in Chapter III, it was seen that the value of θ_y usually was about 10% of θ_u. Keeping this in mind, the values of

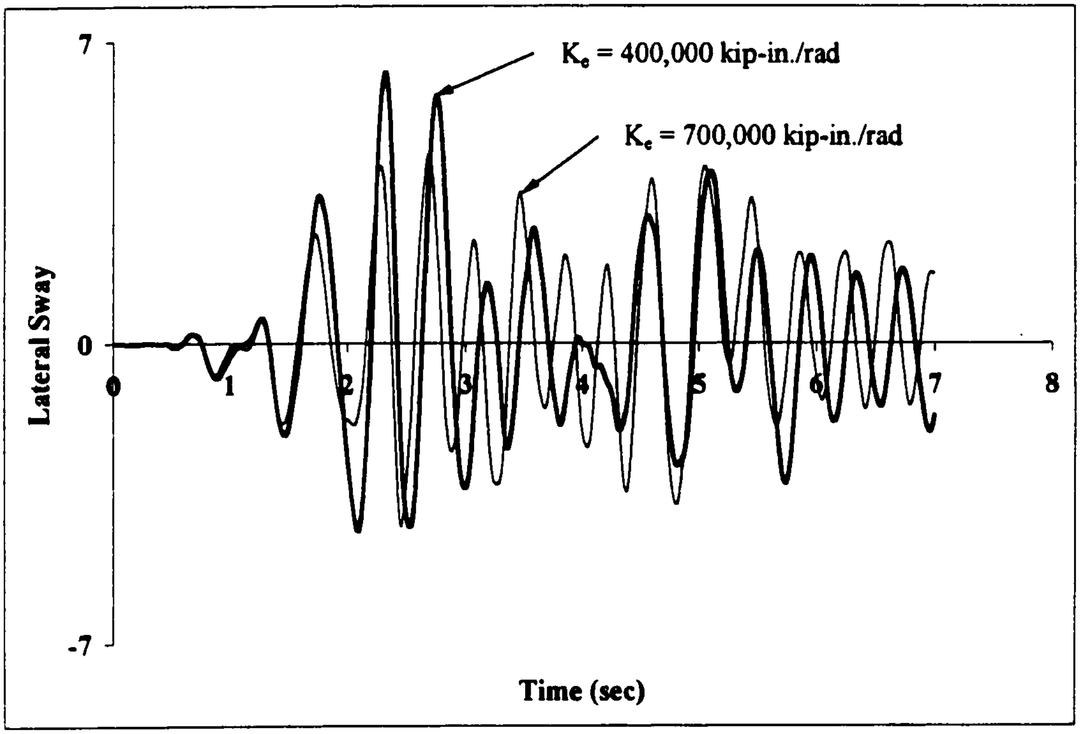

Fig 5.13 Effect of Connection Stiffness on Roof Sway of Frame 1

θ_u for each case was also varied such that $\theta_u = 10\theta_y$. The maximum sway obtained from dynamic response analysis for the first 3 seconds of the El-Centro Earthquake record was plotted versus K_e. Both the maximum sway when the whole system is elastic, and when some of the connection springs become inelastic during this time duration were looked at. The variation of these maximum sway values with respect to the initial stiffness values chosen are shown in Fig. 5.14. In this figure, the maximum sway value obtained from rigid-joint analysis is also shown by the horizontal dashed line. As can be seen from this figure, for small values of K_e, the resulting sway is large. The connections basically behave more like pinned-connections with little transfer of moments. Also, for very high values of K_o (i.e., $K_o > 10^7$ kip-in./rad), the frame behaves as one with rigid connections.

Effect of Ultimate Moment Capacity

In this study, the following cases were first considered for the connection parameters of Frame 1 subjected to the first 7 seconds of the El-Centro Earthquake ground motion:

1. Case #1: $\theta_y = 0.003$ rad, $M_y = 1{,}500$ kip-in., $M_u = 2{,}000$ kip-in., and $\theta_u = 0.03$ rad.
2. Case #2: $\theta_y = 0.003$ rad, $M_y = 1{,}500$ kip-in., $M_u = 4{,}000$ kip-in., and $\theta_u = 0.03$ rad.

The roof story sway response obtained for these two cases are compared in Fig. 5.15. It can be seen that larger peak sways are obtained for connections with higher M_u, but there is practically no phase shift in the peak displacements obtained for the two solutions. During the first 7 seconds of the earthquake record, it is seen that the

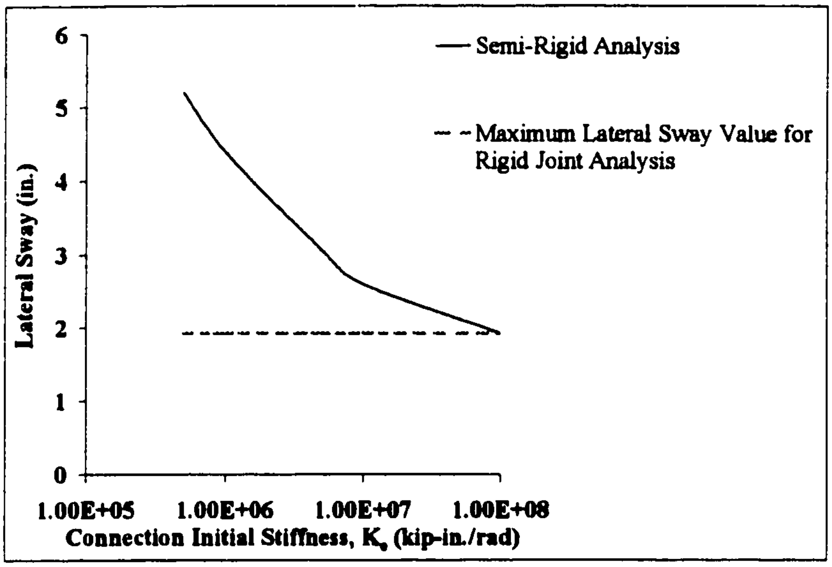

(a)

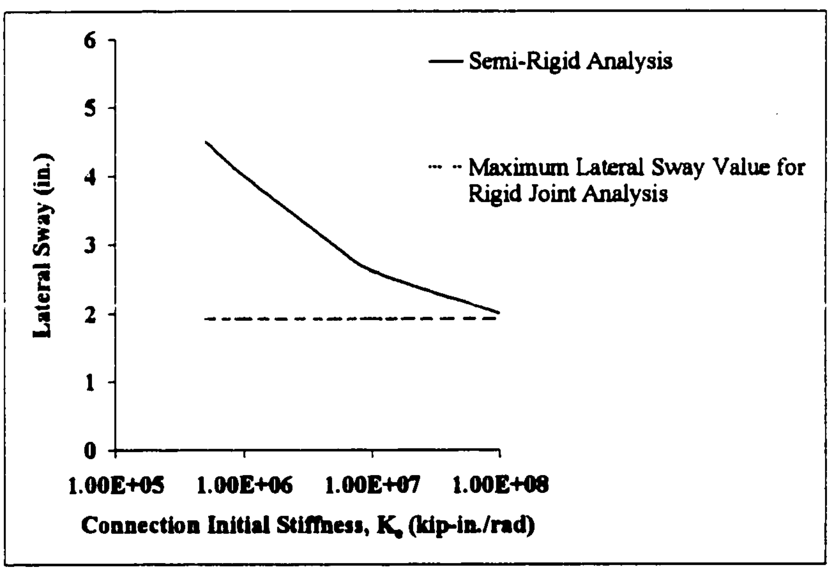

(b)

Fig. 5.14 Variation of the Roof Sway Versus Connection Initial Stiffness for El-Centro Earthquake Record: (a) Plot for Maximum Elastic Sway at 2.32 Seconds; (b) Plot for Maximum Inelastic Sway at 2.80 Seconds

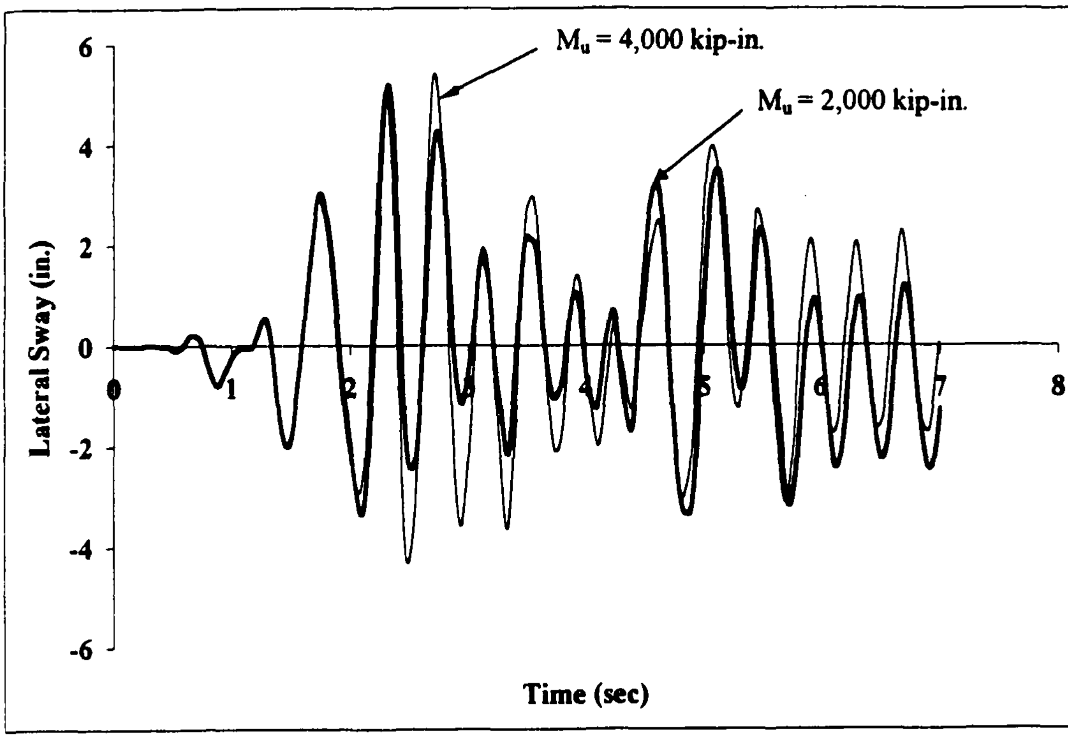

Fig 5.15 Effect on Connection Ultimate Moment Capacity on Roof Sway of Frame 1

maximum sway of 5.3 in. occurs at 2.73 sec with M_u = 4,000 kip-in./rad. Next, a series of analyses were performed by varying M_u from 2,000 to 5,000 kip-in., and for each case holding K_o to values of 10^5, 10^6, 10^7, and 10^8 kip-in./rad. The other parameters were held constants to: M_y =1,500 kip-in., $\theta_y = M_y/K_o$, and $\theta_u = 10\theta_y$. The maximum sway obtained for the first 3 seconds of the El-Centro Earthquake record was plotted versus M_u for each K_o value. The variations of maximum elastic and inelastic sway with respect to M_u are shown in Fig. 5.16. In this figure, the maximum sway value obtained from rigid-joint analysis is also shown by the horizontal dashed line. As can be seen from this figure, for frames with very low ultimate moment capacity connections, the sway predicted is larger. The connections basically behave as shear connections, and with the absence of braces, result in high lateral sway. As the connection moment increases, lateral sway decreases. However, the result of variation of M_u on frame behavior is less pronounced in this case (dynamic analysis), as was observed for the static analysis in Chapter II.

Effect of Ultimate Rotation

In this study, the following cases were first considered for the connection parameters of Frame 1 subjected to the 7 sec of the El-Centro Earthquake ground motion:

1. Case #1: θ_y = 0.003 rad, M_y = 1,500 kip-in., M_u = 3,000 kip-in., and θ_u = 0.02 rad.
2. Case #2: θ_y = 0.003 rad, M_y = 1,500 kip-in., M_u = 3,000 kip-in., and θ_u = 0.05 rad.

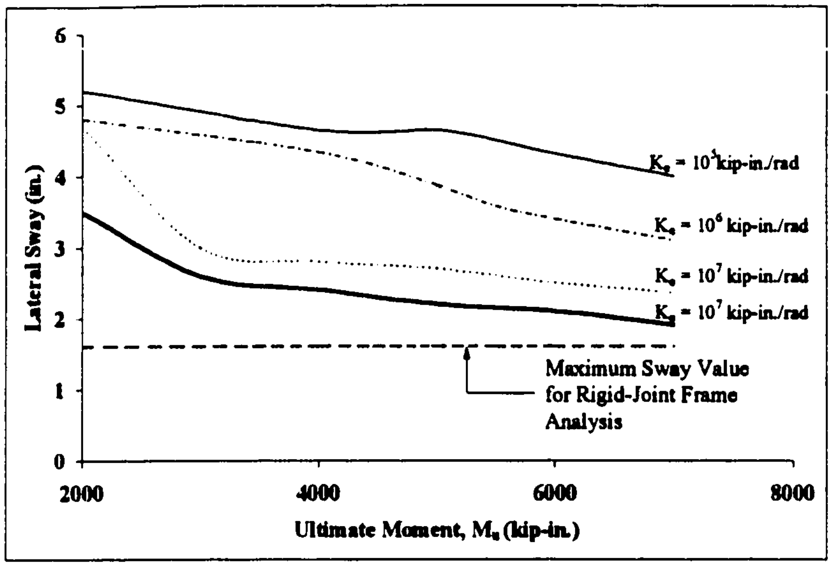

(a)

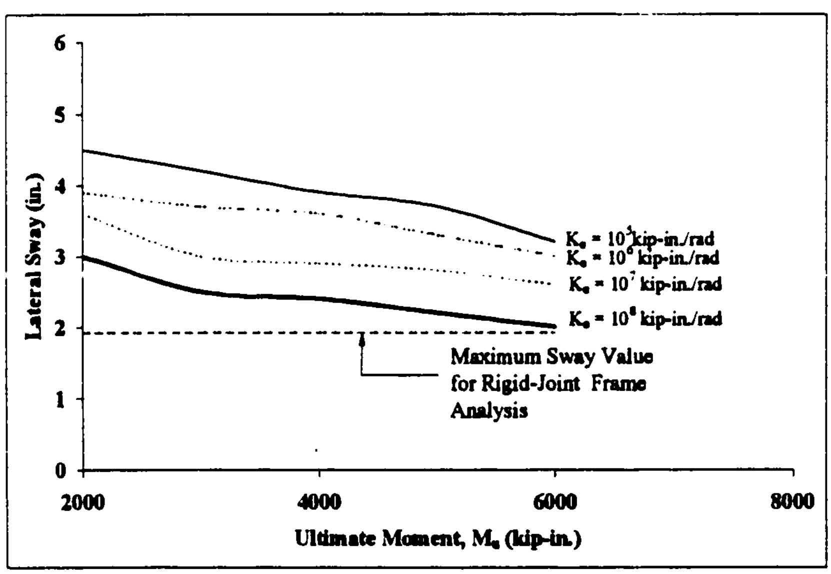

(b)

Fig. 5.16 Variation of the Roof Sway Versus Ultimate Moment Capacity for El-Centro Earthquake Record: (a) Plot for Maximum Elastic Sway at 2.32 Seconds; (b) Plot for Maximum Inelastic Sway at 2.80 Seconds

The roof story sway response obtained for these two cases are compared in Fig. 5.17. It can be seen that the two response histories vary in both amplitudes of peak values, and also for at the times at which they occur. It appears that the frame with a larger θ_u (and more flexible connections), responds much quicker in attaining its maximum sway (5.2 in. at 2.33 sec for $\theta_u = 0.05$ rad versus 4.3 in. at 2.73 sec for $\theta_u = 0.02$ rad). This may be due to the large low frequency content early in the El-Centro record.

Next, a series of analyses were performed by varying θ_u from 0.02 to 0.05 rad, and keeping the other parameters as constants to: $\theta_y = 0.1\theta_u$ rad, M_y =1,500 kip-in., $K_e = M_y/\theta_y$, and M_u = 3,000 kip-in. The maximum sway obtained for the 3 seconds of the El-Centro Earthquake record was plotted versus θ_u. The variation of maximum elastic and inelastic sway with respect to θ_u are shown in Fig. 5.18. From this plot, it can be seen at as θ_u increases, the frame sway would increase, which is the expected behavior since a large θ_u corresponds to a more flexible and ductile connection.

5.5.2 Effect of Hysteresis Model Chosen

Frame 1 is analyzed using the elasto-plastic and bilinear models for the connections with the following model parameter values: $\theta_y = 0.003$ rad, M_y = 1,500 kip-in., M_u = 3,000 kip-in., and $\theta_u = 0.03$ rad. The roof sway response obtained for the frame subjected to the first 7 seconds of the El-Centro Earthquake ground motion for the two connection models are compared in Fig. 5.19. The sway predicted by the bilinear model is generally higher than that predicted by the elasto-plastic model. In the beginning, the amplitudes of the peak displacements differ, but as the solution progresses, both phase shift and more damping occurs when the elasto-plastic

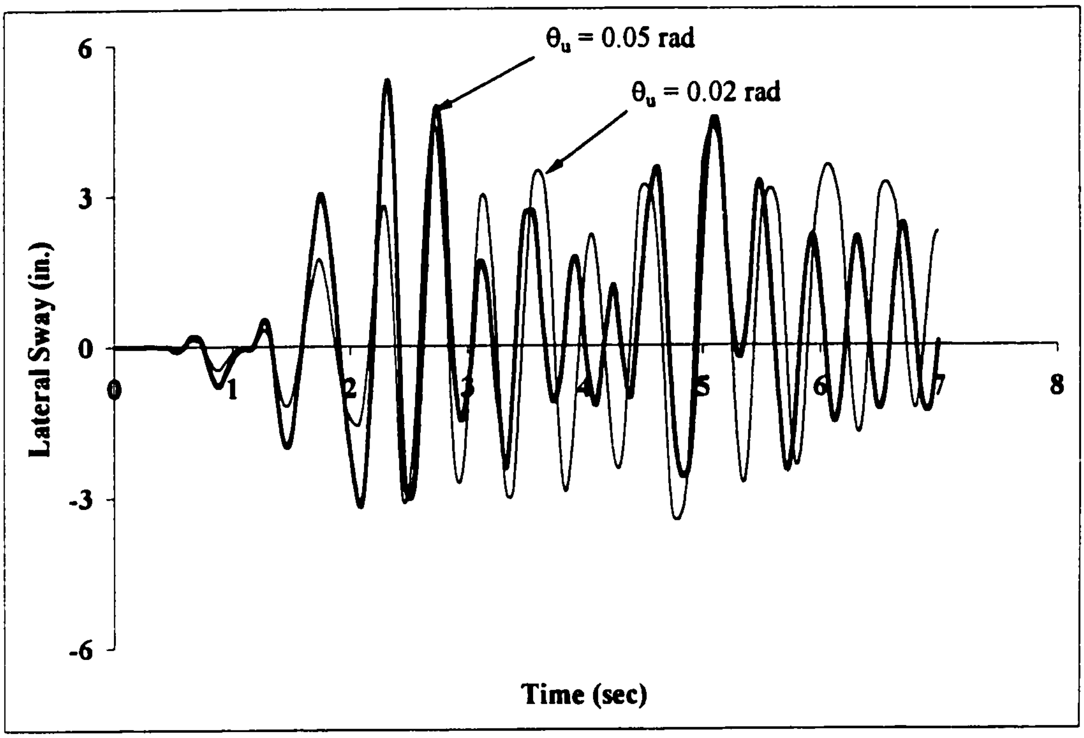

Fig 5.17 Effect of Connection Ultimate Rotation on Roof Sway of Frame 1

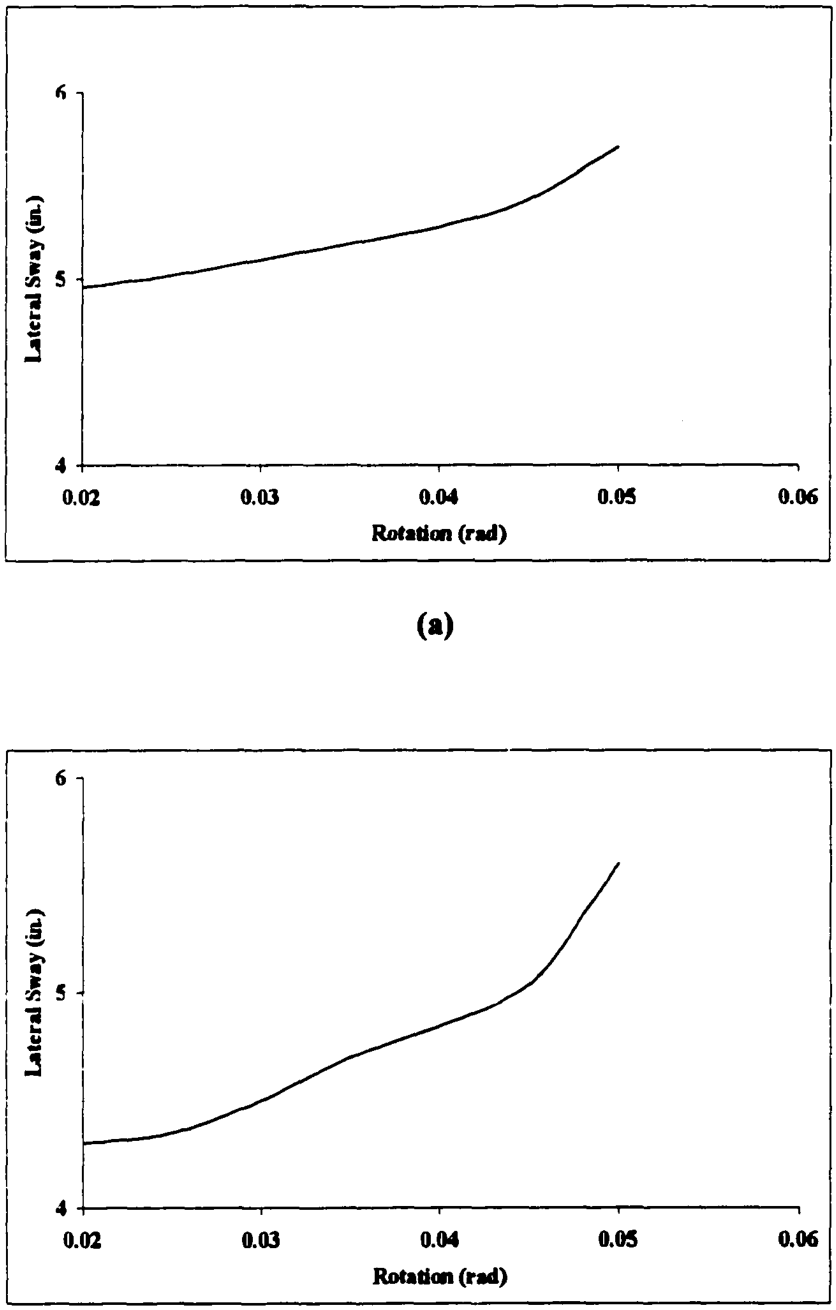

(a)

(b)

Fig. 5.18 Variation of Roof Sway Versus Ultimate Rotation for El-Centro Earthquake Record: (a) Plot for Maximum Elastic Lateral Sway at 2.32 Seconds; (b) Plot for Maximum Inelastic Lateral Sway at 2.80 Seconds

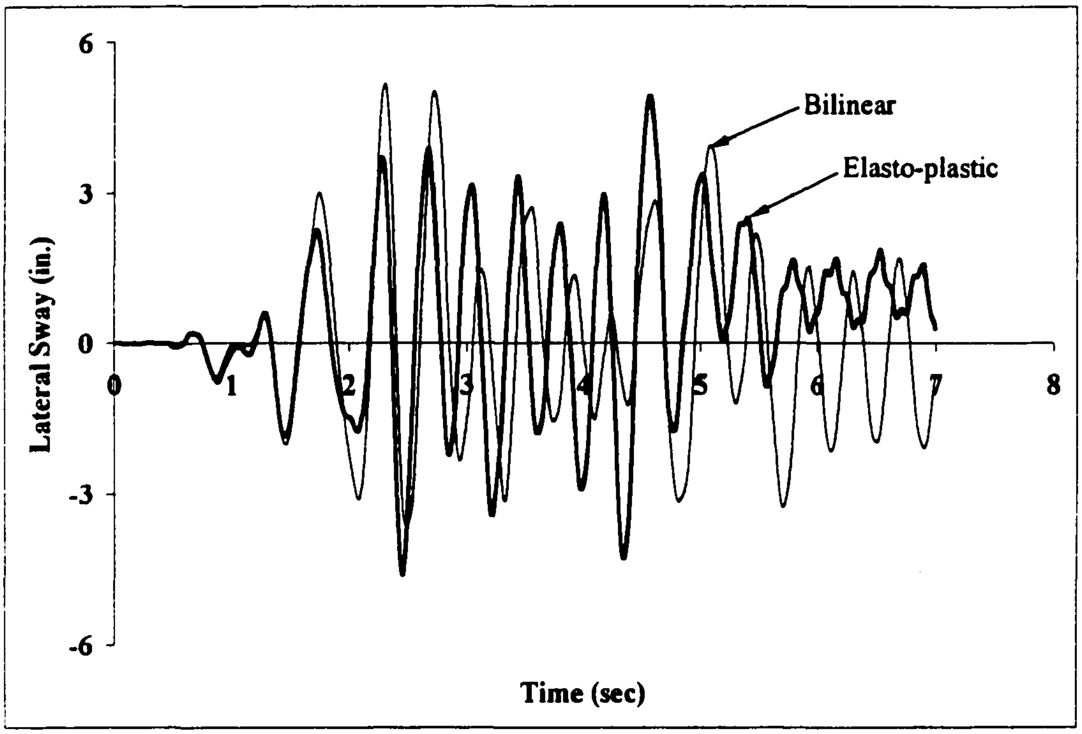

Fig 5.19 Comparison of Roof Sway Results Predicted when the Elasto-Plastic and Bilinear Hysteresis Models are Used for Frame 1

connection model is used. This should have been expected because the area under the elasto-plastic hysteresis loop, which represents the energy dissipated by the connection, is much more than that for the bilinear model. In Fig. 5.19 another interesting result can be seen—the response predicted when the elasto-plastic model is used for the connections shifts away from the time axis after about 4.00 sec. This may be due to a combination of reasons. It may be due to a random end of the large yielding cycles. It is also interesting to note that for the elasto-plastic model more connections experience yielding. In the bilinear model, the two bottom story connections yield, whereas when the elasto-plastic model was used all the four connections yielded. The elasto-plastic loop predicted by the computer program for one of the connection springs of Frame 1 of Fig. 5.2 (a) is shown in Fig. 5.20. The hysteresis loops follow the prediction model with a good degree of accuracy; there is some minor truncation at corner points, which is not significant.

5.5.3 Effect of Earthquake Record Used

An earthquake can be broadly categorized as being either a 'high frequency' earthquake or a 'low frequency' earthquake. The El-Centro and Taft earthquakes are examples of 'high frequency' earthquakes and their energy spectral ordinates are at low natural periods. Soft soils and other factors may alter the frequency response of an earthquake so that more of the energy is transmitted at low frequencies. The Mexico City earthquake is an example of a 'low frequency' earthquake whose power content is associated with the low frequency of its energy spectra.

Keeping these factors in mind, in the parametric study the effects of the following three Earthquake records on the sway response of Frame 1 is studied: El-

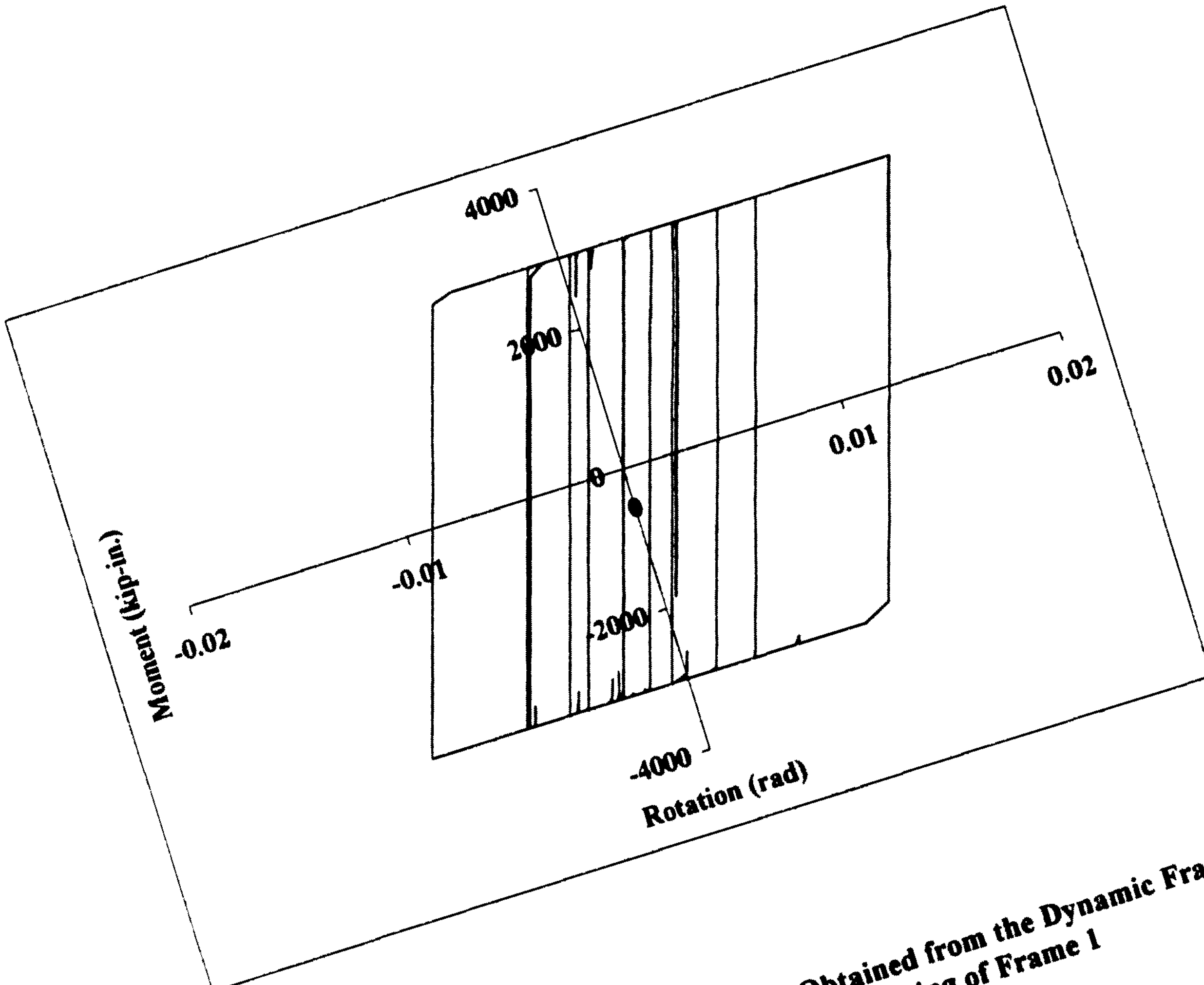

Fig 5.20 Elasto-Plastic Hysteresis Loops Obtained from the Dynamic Frame Computer Program for a Typical Spring of Frame 1

Centro, 1940; Taft, 1952; and Mexico City, 1985. Figure 5.21 shows the acceleration time history of these records. As can be seen from this figure, the maximum peak acceleration for El-Centro, Taft, and Mexico City earthquakes are 0.3g, 0.18g, and 0.17g, respectively, and they occur at 2.02, 5.70, and 60.08 sec, respectively.

The dynamic computer program developed was used to analyze Frame 1 using the aforementioned earthquake records. A bilinear moment-rotation hysteresis model was considered for each connection, with following values for the connection parameters: K_e = 500,000 kip-in./rad, θ_y = 0.003 rad, M_y =1,500 kip-in., M_u = 3,000 kip-in., and θ_u = 0.03 rad. In these analyses, 20 sec of El-Centro, 25 sec of Taft, and 60 sec of Mexico City records were used. A time step of Δt = 0.0033 sec was used for all the analyses, since this produced a converged solution. It should be pointed out that the purpose of this study is to further verify if the dynamic analysis computer program predicts sway behavior consistent with the input ground motion. It is not an exhaustive parametric study in which variation of connection types and building configurations (i.e., number of stories) are also considered along with variations in ground motion records. The roof story sway response obtained for all the three earthquake records is shown in Fig. 5.22. As can be seen from Fig. 5.22, the magnitude of the maximum sway predicted and the time at which it occurs varies: due to El-Centro Earthquake a 5.2 in. sway occurs at 2.32 sec, due to Taft Earthquake a 4 in. sway occurs at 10.2 sec., and due to Mexico City Earthquake a sway of 1.2 in. occurs at 59.2 sec. These predictions are consistent with the occurrence of the peak accelerations in the different earthquake records considered, as described in the previous paragraph. Due to the El-Centro and Taft Earthquakes, left and right bottom

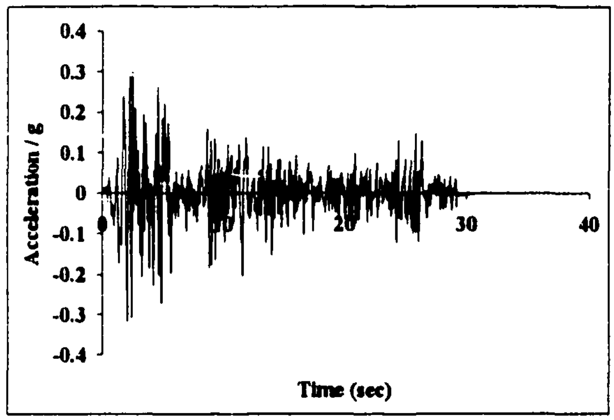

(a)

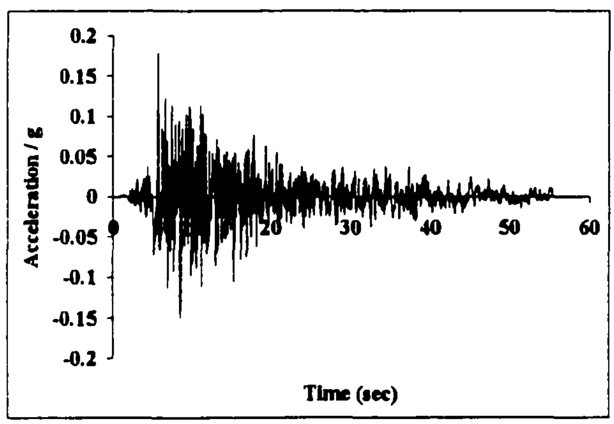

(b)

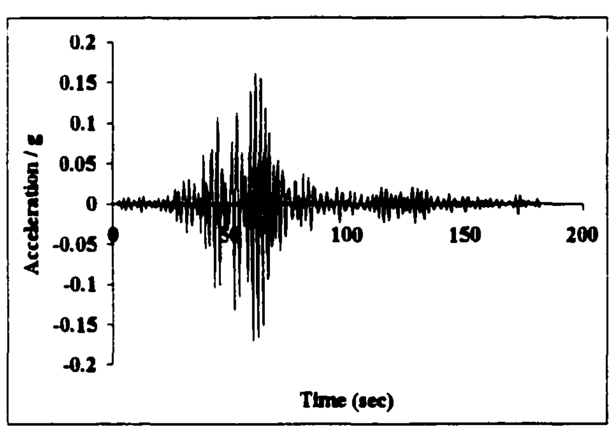

(c)

Fig 5.21 Earthquake Records Used in the Parametric Study: (a) El-Centro, 1940; (b) Taft, 1952; (c) Mexico City, 1985

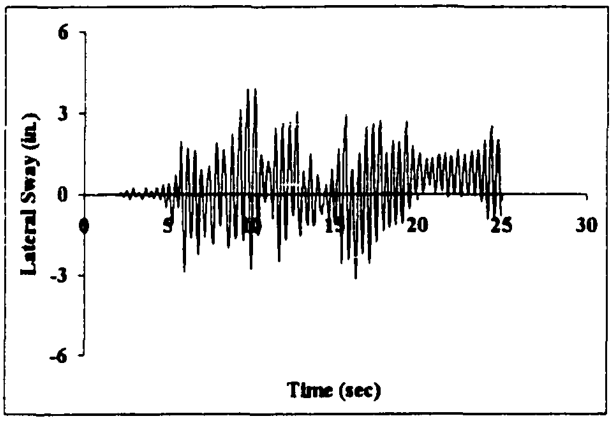

(a)

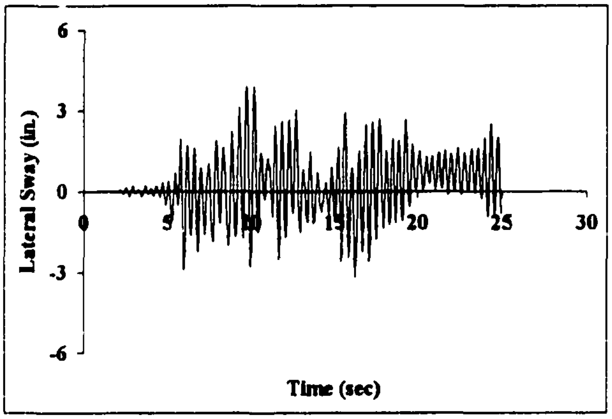

(b)

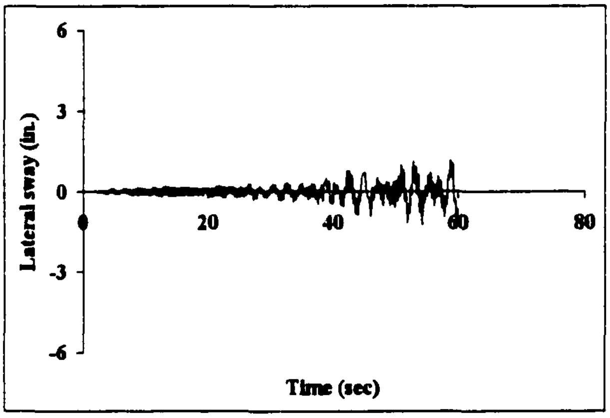

(c)

Fig. 5.22 Comparisons of Roof Lateral Sways Obtained from Semi-Rigid Analysis for Frame 1 Using Following Earthquake Records: (a) El-Centro; (b) Taft; (c) Mexico City

story spring connections of Frame 1 (refer to Fig. 5.2) yield early-on (after 2.80 sec for El-Centro and 10.20 sec for Taft), whereas the Mexico City Earthquake caused only the left bottom story spring connection to yield and that too at a much later time (after 50.50 sec). Thus, the connections of the frame undergo more yielding during the total earthquake record for the El-Centro and Taft Earthquakes, and this causes a shift in the response away from the time axis to occur, as can be seen in Figs. 5.22 (a) and 5.22 (b). Such a shift is not evident in Fig. 5.22 (c) for the Mexico City Earthquake. Thus, the response of the frame with semi-rigid connections depends on the dominant frequency of the earthquake's energy spectra relative to that of the structural system.

To really investigate the magnification of sway, if any, due to semi-rigid connections, one needs to compare the results obtained when the connections are treated as rigid joints. The response of Frame 1 considering all joints to be rigid due to the three earthquake records considered is shown in Fig. 5.23. It can be seen in this figure, throughout the response history the frame remains elastic. The results for maximum sway and the time at which it occurs is as follows: due to El-Centro Earthquake a 2.90 in. sway occurs at 2.32 sec, due to Taft Earthquake a 3.00 in. sway occurs at 8.80 sec., and due to Mexico City Earthquake a sway of 0.75 in. occurs at 59.00 sec. Comparing these sway predictions with those obtained when modeling the connections as semi-rigid joints, the magnification factors for the three earthquakes are as follows: 1.62 for El-Centro, 1.40 for Taft, and 1.60 Mexico City. Thus, for Frame 1, it is concluded that magnitude of magnification of sway due to connection rigidity depends on the dominant frequency of the earthquake's energy spectra

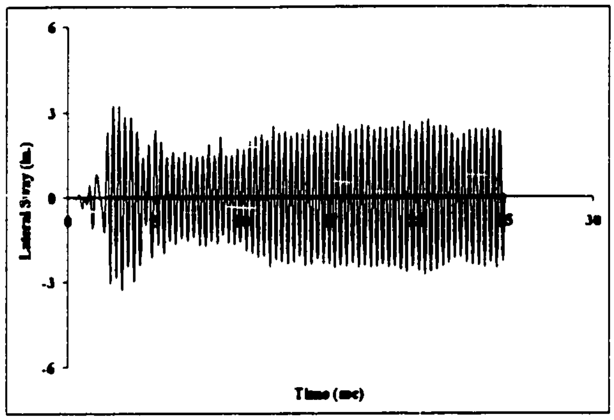

(a)

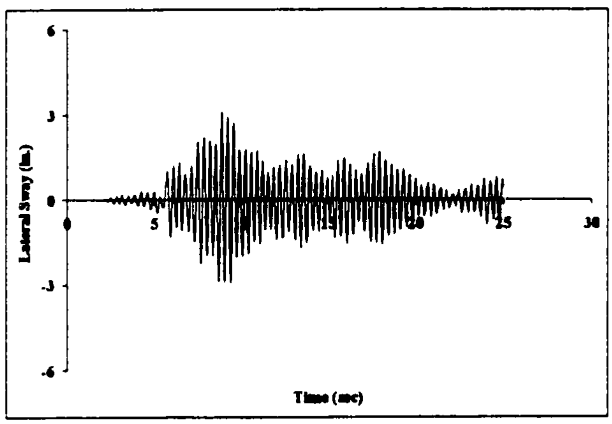

(b)

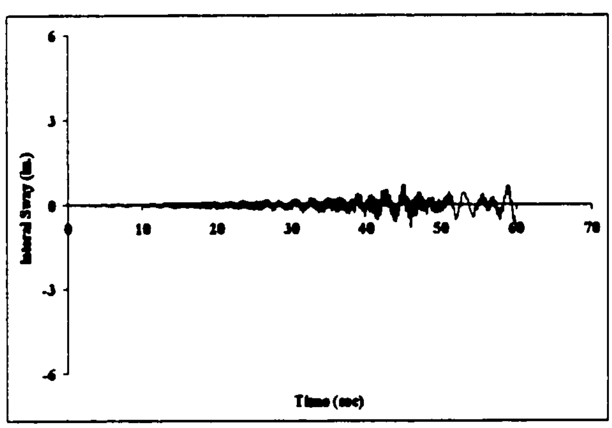

(c)

Fig. 5.23 Comparisons of Roof Lateral Sways Obtained from Rigid-Joint Analysis for Frame 1 Using Following Earthquake Records: (a) El-Centro; (b) Taft; (c) Mexico City

relative to that of the structural system. But, it is concluded that connection rigidity does have a significant effect.

5.6 Chapter Summary

In this chapter an algorithm for dynamic response analysis of planar steel frames with semi-rigid connections is presented. The connections are modeled as moment spring elements, each with a specified bilinear moment-rotation hysteresis model. The frame members are assumed to remain elastic. In the solution algorithm, the differential equations of motion for the discretized system (finite element method used to discretize the system) are solved in its original form by subdividing the total time into equal size time steps, and assuming a constant acceleration variation in each time step. An iterative algorithm is developed to predict the response at the end of each time step. A Newton-Raphon scheme is used to march along the moment-rotation curve of each connection in each iterative cycle. The algorithm presented in this chapter, and the computer program developed to automate it, is shown to give a convergent solution as the time step, used to march the solution, is refined. Results for two frame examples are presented.

A parametric study was conducted to further validate the program and investigate the effect of variation of the hysteresis parameters, hysteresis models, and different earthquake records on the sway response history of the parametric study frame. The hysteresis parameters for the connection considered were: initial stiffness of, K_e, yield moment, M_y, yield rotation, θ_y, ultimate moment, M_u, and ultimate rotation, θ_u. To investigate the effect of each parameter one at a time, it was realized that some of these parameters are inter-related. Based on the experimental results reported in Chapter III, the following rules were adopted to select the cases considered for this parametric study: $K_e = M_y/\theta_y$ and $\theta_u = 10\theta_y$. The results of the parametric study indicated that small values of initial stiffness results in large sway. The connections basically behave as pinned connections with little transfer of moments. For values of $K_e > 10^7$ kip-in./rad, the connection behaves like a rigid joint. Connection with low ultimate capacity basically behave as shear connections, and with the absence of braces result in high lateral sway. Of course, the use of connections with higher ultimate moment capacity would decrease the sway, but the gain is less pronounced under dynamic loads as was observed for static loads. A connection with larger ultimate rotation capacity will generally be more ductile and will increase the frame sway. The use of the elasto-plastic hysteresis model for the frame connections can underestimate the sway in comparison to that obtained if a bilinear hysteresis model was used for the connection. The effect of an earthquake on the frame depends on the dominant frequency of its energy spectra relative to that of the structural system. In general, as the rigidity of the connections decreases, the sway increases. The question is: how much? For the frame example analyzed in this study, for the three earthquake records (El-Centro, Taft, and Mexico City), it was found that dynamic analysis of Frame 1 with semi-rigid connections magnified the maximum sway by 40% to 62% relative to that obtained for Frame 1 with rigid-joints. A more exhaustive parametric study in which connection types, number of stories in a building, and input ground motion record are varied needs to be conducted before any general conclusion can be made regarding the contribution of semi-rigid connections on the magnification of sway relative to a rigid-joint analysis.

CHAPTER VI

SUMMARY, CONCLUSIONS, AND RECOMMENDATIONS

6.1 Summary

The main objective of this research was to develop a dynamic analysis algorithm and associated computer program for planar steel frames with semi-rigid connections. To accomplish this objective, the research was divided into the following four related phases: (1) development of an analysis procedure and associated computer program for steel frames with semi-rigid connections subjected to static loads; (2) an experimental testing program to record moment-rotation hysteretic behavior of a family of commonly used semi-rigid connections; (3) develop mathematical models idealizing the actual observed hysteresis behavior; and (4) finally modify the static frame analysis program to possess dynamic response analysis capability which incorporates the hysteresis models for the semi-rigid connections.

In the first phase of this study a finite element analysis computer program algorithm was developed for planar frames with semi-rigid beam-to-column connections (joints). The connections were modeled as nonlinear rotational spring elements, with material nonlinearity of these spring elements being described by an exponential moment-rotation (M-θ) function. This moment-rotation function requires specification of three parameters, which are: the initial elastic stiffness, K_e, ultimate moment capacity, M_u, and rigidity parameter, α, which defines the shape of the curve. The connection springs are considered as zero length elements, the ends of which are connected to a beam and column member end. A Newton-Raphson technique was used to march along the exponential moment-rotation function, which used the updated tangent stiffness of the connection in each iteration cycle to compute the unbalanced load needed to be applied to satisfy equilibrium. The secondary (P-Δ) effects for frame members were coupled with the modeling of the nonlinear spring behavior in the analysis procedure. Since for the exponential moment-rotation function, the tangent stiffness at the origin (at rotation $\theta = 0°$) is not bounded, it was proposed to compute its value at an infinitesimal rotation ($\theta = 10^{-6}$ rad) away from the origin. This value of tangent stiffness was taken equal to the initial elastic stiffness of the connection. Two frame examples were selected, which were also analyzed by other researchers (King and Chen, 1993; Bhatti and Hingtegen, 1995). The results obtained for lateral sway and column end-moments were validated when compared to those reported in the literature. Also, a parametric study was conducted to investigate the effect of the three moment-rotation model parameters, K_e, M_u, and α, on the lateral sway response of the frame.

The second phase of the study, which was the experimental program, included the cyclic testing of the following four types of semi-rigid connections: (1) two types of double web angle (all bolted , and welded to beam web and bolted to column flange), (2) top and seat angle, (3) flush end-plate, and (4) extended-end-plate connections. The basic configuration of the test set up used for all types of connections tested was similar, and consisted of: (1) an actuator to apply the force to the beam test specimen; (2) a beam of a reaction frame to support the actuator; and (3) a column of a reaction frame to support the column test specimen. The beam test specimen was attached to the column specimen using the desired connection, and the actuator applied a cyclic load to the beam specimen end. Lateral braces were provided at the beam-end connected to the actuator swivel to prevent out-of-plane buckling of the test specimen. The instrumentation used for all the test specimens consisted of an actuator with built-in load cell and displacement transducer to measure, respectively, load and displacement (cyclic) applied, two LVDTs to calculate the relative connection rotation, two wire potentiometers to measure displacements at two points along the beam specimen span, and strain gauged bolts to measure bolt forces. Similar loading history was applied to all the test specimens. The loading of all test specimens started with three cycles of 1 kip, three cycles of 2 kip, and three cycles of 3 kip actuator load. The specimen was loaded in this manner (called load control) until yielding of the connection was noticed, at this time the loading was switched to displacement control. The moment-rotation hysteresis loops and mode of failure were recorded for each type of connection tested. A total of 55 connections were tested. From the data recorded, the values of the connection initial stiffness, ultimate moment capacity, and ultimate rotation capacity were determined.

In the third phase of this study mathematical hysteresis models were developed to idealize the experimentally recorded moment-rotation hysteresis behavior of semi-rigid connections. Two basic types of mathematical hysteresis models were proposed, the bilinear and trilinear models, depending on whether the connection failure results due to excessive yielding and/or fracture of just the connection elements or due to beam web material bearing failure. The only type of connection, among the connections tested, which exhibited beam web bearing failure was the "Type I" all bolted double web angle connections with angle thickness $t > 3/8$ in.

Three different bilinear models, which vary in degree of simplicity and predicting capability, are proposed in this research. These include the elasto-plastic, bilinear, and modified bilinear models. The parameters defining the elasto-plastic model are: initial stiffness, K_e, ultimate moment, M_u, and ultimate rotation, θ_u. Hysteresis parameters defining the bilinear model are: K_e, M_u, transition moment, M_t, and θ_u. The transition moment was defined as the moment at the intersection of the tangent drawn from the ultimate point, with coordinates (θ_u, M_u), to the peaks of the hysteresis loops in the first quadrant and the line of initial stiffness. The parameters defining the modified bilinear model are: characteristic moment, M_c, characteristic rotation, θ_c, M_u, and θ_u, where M_c and θ_c are determined by fitting a Ramberg-Osgood function to the experimental enveloping curve. The enveloping curve is defined as the curve passing through the peaks of the moment-rotation hysteresis loops in the first quadrant, i.e., the loading portion. Therefore, the elasto-plastic model is a three-parameter model, whereas the bilinear and modified bilinear models each require four independent parameters for their formulations. A trilinear model is proposed for connections which exhibit beam web bearing failure. This model requires five independent hysteresis paramcters, which are: K_e, bearing moment, M_b, bearing rotation, θ_b, M_u, and θ_u. The values of θ_b and M_b depend on the angle leg thickness; higher the thickness, larger will be the value of θ_b and M_b. In this model, initiation of yielding occurs at a moment of $M_b/2$, then the connection behaves as a perfectly plastic spring up to a rotation of $\theta_b/2$, and after that strain hardening occurs till the ultimate point, with coordinates (θ_u and M_u), is reached. Thus, the model consists of three independent stiffness segments, which are initial elastic stiffness, bearing stiffness (slope = zero), and post-tangential stiffness.

The fourth and final phase of this research was to develop a dynamic analysis computer program for frames with semi-rigid joints subjected to an earthquake ground motion. In this part of the research, the static computer program developed in the first phase was extended to add the dynamic analysis capability. In this formulation, the connection was again modeled as a rotational spring element, but now with a prescribed hysteresis moment-rotation model. Both the elasto-plastic and bilinear (which includes the modified bilinear) hysteresis models were incorporated in the program developed. The differential equations of motion were solved numerically using the constant acceleration (Newmark-β) method, and the Newton Raphson scheme was used to march along the moment-rotation hysteresis model of the connection. Two frame examples were analyzed for a given earthquake ground motion history to obtain sway response histories and member forces. Convergence trends of the results are presented. To further verify the computer program, a parametric study was conducted to determine the effect of variation of the hysteresis parameters, different hysteresis models, and different earthquake records on the displacement history of a selected frame. Finally, the graphical results of the parametric study for the sway response of the frame are presented.

6.2 Conclusions

The conclusions of the four phases of the study are presented in this section.

The static program developed for the analysis of planar frames with semi-rigid connections in **Phase I** predicted results that were comparable with results available in the literature. The exponential model proposed to model the monotonic (static) moment-rotation curve of the connection proved to be a valid model. The results obtained from this study showed that by using a value of 0.8 for the rigidity parameter, α, the lateral sway of the frame and its member end moments were in close agreement with those reported by Bhatti and Hingtegen (1995); whereas for α = 0.9 the results were in close agreement with those results reported by King and Chen (1993).

The results of the parametric study conducted in the first phase indicated that as the connection initial stiffness, K_e, increases, the frame behaves as one with rigid joints. The example frame chosen with rigid joints has a maximum lateral sway less than $H/400$, where H is the inter-story lateral load. For a low value of the connection moment capacity, M_u, the frame behaves as one with shear connections and no lateral braces, and in which the lateral load is primarily resisted by columns acting as cantilever beams. As the ultimate moment of the connection was increased, the frame sway decreased depending on the value of the initial elastic stiffness, K_e, and rigidity parameter, α, used. For low values of α (i.e., $\alpha = 0.5$), the results are similar to a frame with rigid joints; whereas for high values of α (i.e., α = 0.9 to 1.0), the results are similar to a frame with semi-rigid joints. It was also concluded that if P-Δ effects are significant, the rate of decay of the tangential stiffness of the spring connection elements is very rapid.

In the experimental investigation undertaken as **Phase II** of this research, the following observations were made:

1. For the *Type I Double Web Angle Connection*, in which both the angle legs were bolted, two failure modes were observed, which included failure due to excessive rotation caused by yielding of the angle and beam web bearing failure. The excessive rotation failure mode was observed for specimens with an angle thickness $t \leq 3/8$ in., whereas the beam web bearing failure was identified for test specimens with an angle thickness $t > 3/8$ in. The ultimate rotation for the former failure mode was about 0.005 rad, and for the latter about 0.045 rad. The moment-rotation hysteresis loops for this type of connection exhibited pinching for both failure modes. For the case of beam web bearing failure, the pinching of the hysteresis loops had a very well defined flat plateau, where deformation occurred under constant moment, followed by a hardening region where rotation increased with increase in moment. The width of this flat plateau was larger for higher angle thickness. The

overall behavior of these connections, where the bolts were pre-tensioned to proof load, showed that these connections are capable of dissipating energy, and for certain combinations of geometric variables significant moment transfer across the connection is possible before failure.

2. For the *Type* II *Double Web Angle Connection*, in which one angle leg was welded to the beam web and the other bolted to the column flange, the moment-rotation hysteresis loops showed significant ductility, and pinching at higher load levels. The failure modes were either excessive yielding of angle or tensile fracture failure of bolts connected to the column flange. An ultimate moment capacity as high as 2,236 kip-in. and an initial stiffness as high as 484,064 kip-in./rad were recorded, which were comparable to the range of strength and stiffness values recorded for some flush end-plate connection test specimens. However, a comparison between the ultimate rotation of 0.02289 rad obtained for a Type II double web angle connection, and an ultimate rotation of 0.00707 rad obtained for the flush an end-plate connection, shows that the former connection provides the same stiffness and strength, but possesses better ductility.

3. For the *Top and Seat Angle Connection*, the moment-rotation hysteresis loops showed pinching at higher cyclic load levels. The modes of failure observed were excessive angle yielding and tensile fracture of bolts connected to the column flange. The connection's initial stiffness for

one of the test specimen was as high as 629,219 kip-in./rad, which is comparable to a value of 616,329 kip-in./rad obtained for a flush end-plate connection tested. Again, as in the case of "Type II" double web angle connections, the ultimate rotation of the top and seat angle connection specimen was 0.045 rad, whereas the ultimate rotation for the flush end-plate connection specimen was 0.01083 rad. This indicates that top and seat angle connections with fully pre-tensioned bolts could provide high stiffness as some traditional moment connections and also possess more ductility.

4. For the *Flush End-Plate Connection*, the primary modes of failure were end-plate yield failure, rupture of the end-plate, and tensile fracture failure of the bolts. The ductility observed in the moment-rotation hysteresis loops was not as large as those observed for other connections tested with fully pre-tensioned bolts with similar strength and stiffness. A flush end-plate connection test specimen, Test Specimen (12), which had an initial stiffness of 1,311,543 kip-in./rad, an ultimate rotation capacity of 0.00823 rad, and an ultimate moment capacity of 4,622 kip-in., compared with the stiffness and strength of an extended end-plate connection test specimen, Test Specimen (1), which possessed an initial stiffness of 1,129,937 kip-in./rad, an ultimate rotation capacity of 0.00840 rad, and an ultimate moment capacity of 2,758 kip-in. It is interesting to note that the values of ultimate rotation and initial stiffness are very close (almost the same) for the two aforementioned test

specimens; however, the flush end-plate test specimen possessed more strength. This shows that with proper choice of values of the connection's geometric variables, it is possible to design a semi-rigid connection to possess sufficient stiffness and moment capacity as some typical moment-type connections, and which possesses higher ductility desirable in seismic conditions. This aspect needs to be further studied.

5. For the *Extended End-Plate Connection*, the failure modes for the test specimens were excessive end-plate yielding and tensile fracture failure of the bolts. The moment-rotation hysteresis loops for these test specimens showed that the connection possessed good energy dissipation capability. This type of connection was the stiffest connection studied in this research.

Among the mathematical hysteresis models developed in **Phase III**, it was concluded that the elasto-plastic model, though the simplest model to construct, is the least conservative in idealizing the energy dissipating capability of the connection. This was expected, because in this model the idealized yield moment was considered to be the ultimate moment of the connection. The bilinear model, on the other hand, estimated the energy dissipation capability of the connection in a more realistic manner. Finally, the modified bilinear model was consistently the most accurate and conservative model for most of the test specimens considered. Also, it was concluded that in most of the cases considered, the bilinear and modified bilinear models were fairly close, and sometimes identical. Even though both bilinear and modified bilinear models are four-parameter models, the transition moment parameter defined for the bilinear model is based on an arbitrary graphical procedure, whereas the characteristic moment, used in its place in the modified bilinear model, has a mathematical definition, as defined by the Ramberg-Osgood function. Finally, for the limited cases in which beam web bearing failure occurred, the trilinear model proposed in this study was observed to predict the moment-rotation hysteresis loops for "Type I" double web angle connections reasonably accurately. However, this needs further investigation.

The dynamic analysis program developed to analyze planar frames with semi-rigid connections in **Phase IV**, produced convergent response solutions. The dynamic solution obtained satisfied equilibrium conditions exactly for member-end shears and moments. However, the joints (moment springs) did not satisfy equilibrium perfectly. One reason for this is the lack of the inertial moments from the consistent mass matrix on this diagram. This may also be due to the fact that damping effects are not considered in calculating the member forces. The results for two frames analyzed show that the semi-rigid frame analysis produced higher maximum sway values when compared with the dynamic analysis of similar frames with rigid joints. Also comparing the shapes of the displacement (sway response) histories indicated that the converged semi-rigid solution obtained has some phase shift. The sway response history showed that the response shifts away from the time axis when more connections yield. This shift is a characteristic property observed in nonlinear dynamic problems in which yielding occurs.

In an attempt to further verify the predicting capabilities of the dynamic program developed, a limited parametric study was conducted to investigate the effect of variation of the hysteresis parameters, different hysteresis models, and different earthquake records on the sway response history of a frame. The hysteresis parameters for the connection were: K_c, yield moment, M_y, yield rotation, θ_y, ultimate moment, M_u, ultimate moment, and ultimate rotation, θ_u. To investigate the effect of each parameter one at a time, it was realized that some of these parameters are inter-related. Based on the experimental results reported in Chapter III, the following rules were adopted to select the cases considered for this parametric study: $K_c = M_y/\theta_y$ and $\theta_u = 10\theta_y$. The following general observations were made from the parametric study:

1. Small values of initial connection stiffness, K_c, result in large sway. Such connections basically behave as pinned connections with little transfer of moments. For values of $K_c > 10^7$ kip-in./rad, the connection behaves like a rigid joint. However, the semi-rigid frame analysis solutions differ significantly in both magnitudes of peak displacements and also at the times they occur. The semi-rigid frame solution exhibits a longer period response than the elastic solution obtained from a rigid joint analysis.
2. For frames with very low ultimate capacity connections, the sway predicted will be larger. Such connections basically behave as shear connections, and with the absence of braces, result in large lateral sway.
3. Larger ultimate rotational capacity of a connection indicates that the connection possesses more ductility. Such connections will result in larger frame sways if the ductility is utilized.

4. If the elasto-plastic model is used to characterize the behavior of a semi-rigid joint in a frame, the sway will be underestimated. The bilinear model for the semi-rigid connections predicts better results.

5. The dominant frequency of earthquake's energy spectra relative to that of the frame considered will greatly influence how much the rigidity of the connections affects the sway predictions.

6.3 Recommendations

The following recommendations are made based on the observations made in this study:

1. Further studies need to be conducted to study the ductility behavior of certain shear type connections with fully pre-tensioned bolts, which can offer similar strength and stiffness as traditional moment connections. There is a need to investigate the basic yield failure mechanism, and develop empirical relationships which predict the likely type of failure that would occur in a given connection configuration, i.e., will it fail by excessive rotation caused by significant yielding and/or bolt fracture, or by any other failure such as beam web bearing failure in all bolted double web angle connections.

2. Extend the dynamic analysis computer program to account for plastic hinge formation in the frame members.

3. Conduct a study to investigate the effect of considering different approximations to numerically solve the equations of motion, for

example, methods based on finite difference expressions of velocity, the linear acceleration or α-method, etc.

4. Use the computer program to analyze frames with both dead loads and earthquake loads acting. This would first require a static analysis for the dead loads, followed by a dynamic analysis for the earthquake base motion.

5. It is recommended that an extensive parametric study be performed using the dynamic analysis computer program developed for semi-rigid frame analysis by varying not only the connection parameters but also building story heights and bays. This would give better insight into the contributions of the rigidity of the connection towards frame behavior

6. Conduct shake table tests on full-scale frame models with standard semi-rigid connections, and compare response results recorded with those predicted by the dynamic analysis computer program.

7. Use Fourier time series analysis to march the solution, which is a time series analysis. Even though, Fourier series analysis is traditionally used for linear problems, it would be an interesting research.

BIBLIOGRAPHY

American Institute of Steel Construction. (1994). ***Manual of Steel Construction: Load and Resistance Factor Design***, Vol. 2, Second Ed.

Astaneh, A., Nader, M.N., and Malik, L. (1989). "*Cyclic behavior of double web angle connections*, " **Journal of Structural Engineering**, ASCE, Vol. 115, No. 5, pp. 1101-1118.

Barakat, M., and Chen, W.F. (1991). "Design analysis of semi-rigid frames: evaluation and implementation," **Engineering Journal**, ASIC, Vol. 28, No. 2, pp. 55-64.

Bhatti, M.A., and Hingtegen, J.D. (1995). "*Effects of connection stiffness and plasticity on the service load behavior of unbraced steel frames*," **Engineering Journal**, ASCE, Vol. 32, No. 1, pp. 21-33.

Chen, W.F., and Lui, E.M. (1991). "***Stability Design of Steel Frames***", CRC Press, Boca Raton, Florida.

Clough, R W., and Benuska, k. L. (1967). "*Nonlinear earthquake behavior of tall Buildings*", **Journal of Engineering Mechanics**, ASCE, Vol. 93, No. EM3, pp. 129-146.

Davison, J.B., Kirby, P.A., and Nerthercot, D.A. (1987). "*Effect of lack of fit on connection resistance*" A Chapter in **Joint Flexibility in Steel Frames**, Editor: W.F. Chen, Elsevier Applied Science Publishers, London, pp. 17-54.

Driscoll, G.C., and Lu, L.W. (1989). "*Top and seat angle connection and end-plate connection: snug versus fully pretensioned bolts*," **ATLSS Report No. 89-06**, submitted to NSF, Lehigh University, Bethlehem, Pennsylvania.

Goto, Y., and Chen, W.F. (1987). "*On the computer-based design analysis for flexibly jointed frames*, " A Chapter in **Joint Flexibility in Steel Frames**, Editor: W.F. Chen, Elsevier Applied Science Publishers, London, pp. 203-231

Hartman, J. (1999). "*Cyclic Performance of Flush End Plate Connections*," A Thesis submitted as partial fulfillment of the requirement for degree of Mater of Science, Department of Civil Engineering, University of Oklahoma, Norman, Oklahoma.

Hetchman, R.A., and Johnston, B.G. (1947). "*Riveted semi-rigid beam-to-column building connection*," **Progress Report No. 1, submitted to AISC**, Lehigh University, Bethlehem, Pennsylvania.

Hibler, H.M., Hughes, T.J.R., and Taylor, R.L. (1977). "*Improved numerical dissipation for time integration algorithms in structural dynamics,*" **Journal of Earthquake Engineering**, Structural Dynamic Division, JSCE, Vol. 5, pp. 283-292.

Lionberger, S. R., and Weaver, W. (1969). "*Dynamic response of frames with non-rigid connections,*" **Journal of Engineering Mechanics**, ASCE, Vol. 95, No. EM1, pp. 95-114.

King, W.S., and Chen, W.F. (1993). "*LRFD analysis for semi-rigid frame design,*" **Engineering Journal**, AISC, Vol. 30, No. 4, pp. 130-140.

Kishi, N., and Chen, W.F. (1986). "*Data base of steel beam to column connections,*" **Structural Engineering Report No. CE-STR-86-26**, School of Civil Engineering, Purdue University, West Lafayette, Indiana.

Kishi, N., and Chen, W.F. (1987a). "*Moment rotation of top and seat angle connections,*" **Structural Engineering Report No. CE-STR-87-4**, School of Civil Engineering, Purdue University, West Lafayette, Indiana.

Kishi, N., and Chen, W.F. (1987b). "*Moment rotation of top and seat angle connections,*" **Structural Engineering Report No. CE-STR-87-29**, School of Civil Engineering, Purdue University, West Lafayette, Indiana.

Kukreti, A.R., and Abolmaali, A. (1999). "*Moment-rotation hysteresis behavior for top and seat angle connections,*" **Journal of Structural Engineering**, ASCE, Vol. 125, No. 8, pp. 810-820.

Kukreti, A.R., and Abolmaali, A. (1998). "*Analysis of steel frames with semi-rigid joints and considering P-delta,*" submitted for publication, **Engineering Journal**, AISC.

Kukreti, A.R., Ghassemeh, M., and Murray, T.M. (1990). "Behavior and design of large-capacity moment-endplates." **Journal of Structural Engineering**, ASCE, Vol. 116, No. 3, pp. 809-828.

Lui, E.M., and Chen, W.F. (1987). "*Steel frame analysis with flexible joints,*" A Chapter in **Joint Flexibility in Steel Frames**, Editor: W.F. Chen, Elsevier Applied Science Publishers, London, Vol. 8, pp. 161-202.

Mander, J.B., Chen, S.S., and Pekan, G. (1994). "*Low cycle fatigue behavior of semi-rigid top and seat angle connections,*" **Engineering Journal**, AISC, Vol. 31 No. 3, 3rd Quarter, pp. 111-122.

Marley, M.J., and Gerstle, K.H. (1982). "*Analysis and tests of flexibility-connected steel frames,*" **Report for Project No. 199**, submitted to AISC, Research done at University of Colorado, Bolder, Colorado.

Mazroi, A. (1990). "*Moment-rotation behavior of beam-to-column end-plate connections in multi-story frames*," Ph.D. Dissertation submitted as partial fulfillment for degree of Doctor of Philosophy, School of Civil and Environmental Engineering and Environmental Science, University of Oklahoma, Norman, Oklahoma.

Muraleetharan, K.K., Mish, K.D., and Arulanandan, K. (1994). "*A fully coupled non-linear dynamic analysis procedure and its verification using centrifuge test results*," **International Journal for Numerical and Analytical Methods in Geomechanics**, Vol. 18, No. 21, pp. 305-325.

Nader, M.N., and Astaneh-Asl, A. (1996). "*Shaking table tests of rigid, semi-rigid, and flexible steel frames*," **Journal of Structural Engineering**, ASCE, Vol. 122, No. 6, pp. 201-589-596

Tsai, K.C., Wu, S., and Popov, E.P. (1995). "*Experimental performance of seismic steel beam-column moment joints*," **Journal of Structural Engineering**, ASCE, Vol. 121, No. 6, pp. 925-931.

Popov, E.P., and Bertero,.P. (1973). "*Cyclic loading of steel beams and connections*," **Journal of the Structural Division,** ASCE, Vol. 99, No. ST6, pp. 1189-1204.

Popov, E.P., and Pinkey, R.B. (1968). "*Cyclic loading of steel beams and connections subjected to inelastic strain reversals*," **Bulletin No. 13,** AISI

Ramberg, W., and Osgood, W.R. (1943). "*Description of stress-strain curves by three parameters*," **Monograph No. 4, Publicazione Italsider**, Nuvoa Italsider, Genova.

Rathbun, J.C. (1936). "*Elastic properties of riveted connections*," **Paper No. 1933**, ASCE, Vol. 101, pp. 524-563.

Sarraf, M., and Bruneau, M. (1996). "*Cyclic testing of existing and retrofitted riveted stiffened seat angle connections*," **Journal of Structural Engineering**, ASCE, Vol. 122, No. 7, pp. 762-775

Vayas, I., Pasternak, H., and Schween, T. (1995). "*Cyclic behavior of beam-to-column steel joints with slender web panels*," **Journal of Structural Engineering**, ASCE, Vol. 121, No. 2, pp. 240-248

APPENDIX A

Experimental Moment-Rotation Hysteresis Loops
Obtained for:
Double Web Angle Connections
Top and Seat Angle Connections
Flush End-Plate Connections
Extended End-Plate Connections
(Figures A-1 Through A-5)

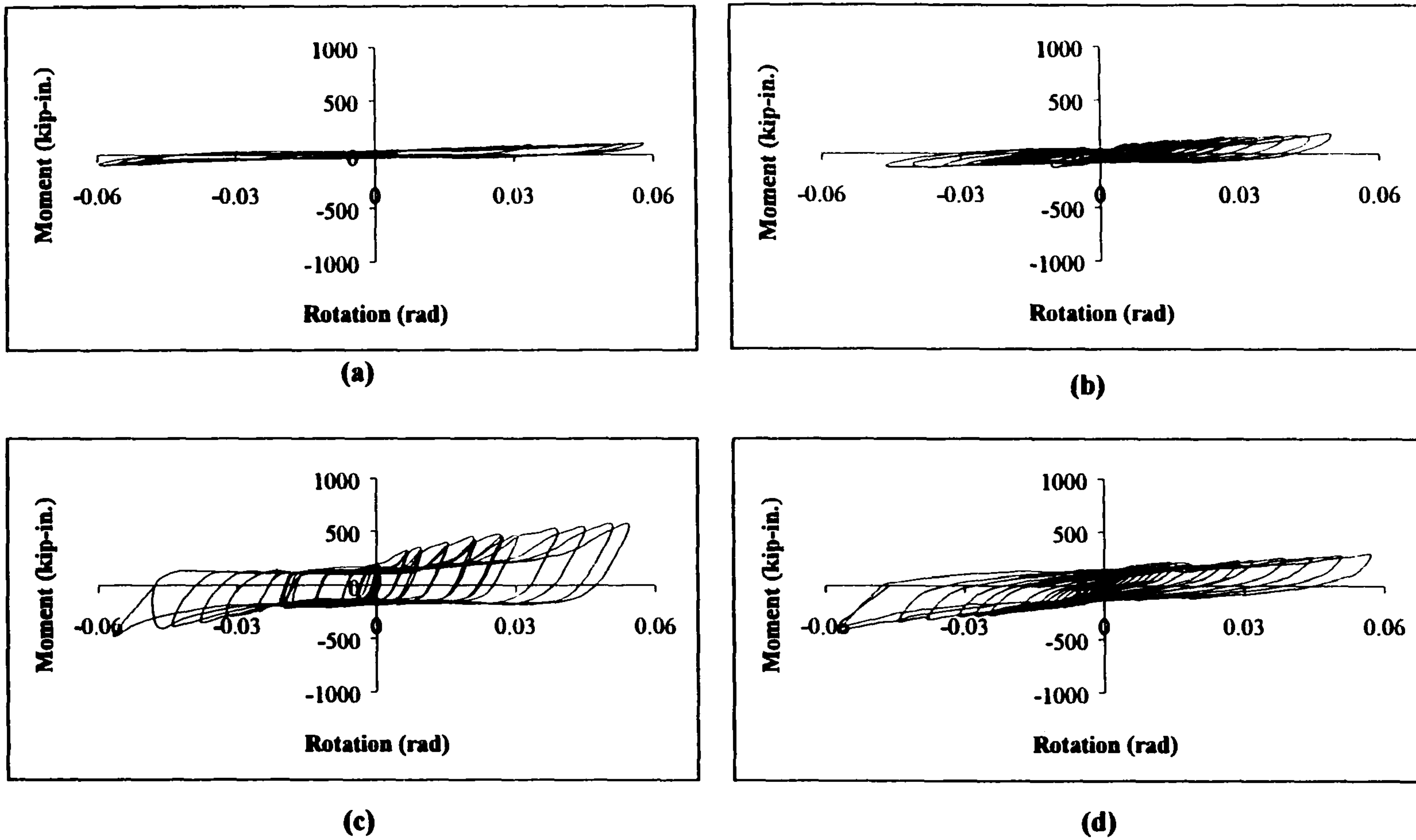

Fig. A-1 Moment-Rotation Hysteresis Loops for "Type I" Double Web Angle Connections (Continued):
(a) Test Specimen No. 1 (DW-*I*-4-1/4-3/4-4½-3-16); (b) Test Specimen No. 2 (DW-*I*-4-1/4-3/4-4½-4-16);
(c) Test Specimen No. 3 (DW-*I*-4-5/8-3/4-4½-4-16); (d) Test Specimen No. 5 (DW-*I*-4-1/4-3/4-4½-5-21)

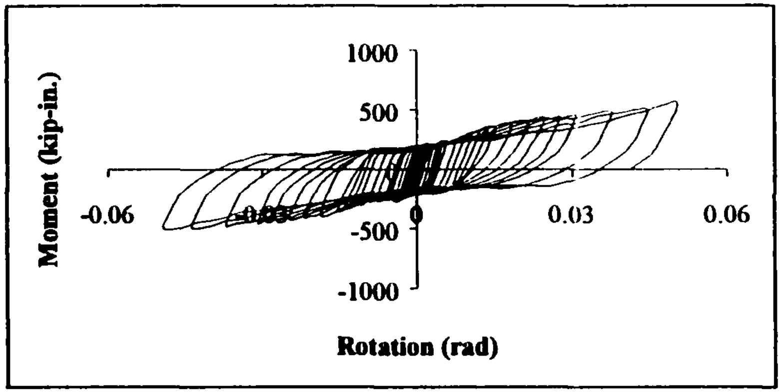

(e)

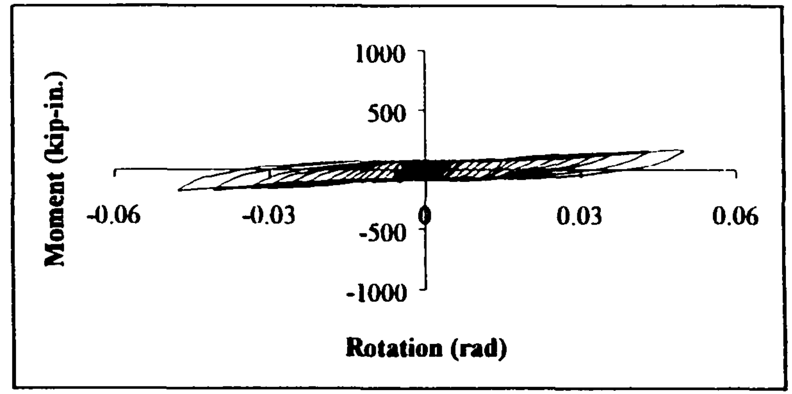

(f)

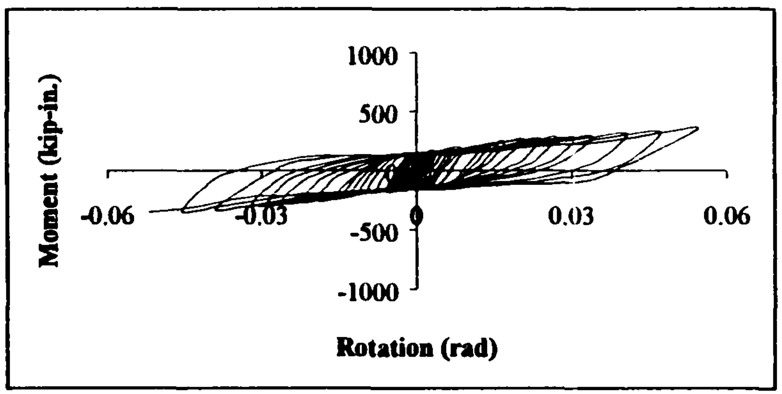

(g)

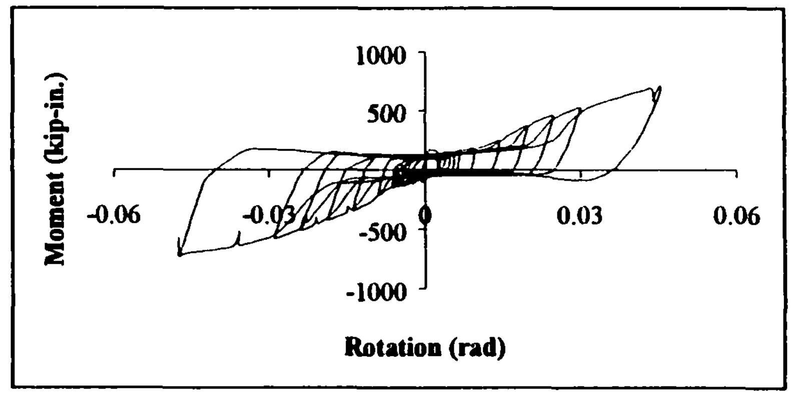

(h)

Fig. A-1 Moment-Rotation Hysteresis Loops for "Type I" Double Web Angle Connections (Continued): (e) Test Specimen No. 6 (DW-*I*-4-3/8-3/4-4½-5-21); (f) Test Specimen No. 7 (DW-*I*-4-3/8-3/4-4½-3-16); (g) Test Specimen No. 8 (DW-*I*-4-3/8-3/4-4½-4-16); (h) Test Specimen No. 9 (DW-*I*-5-1/2-5/8-4½-5-24)

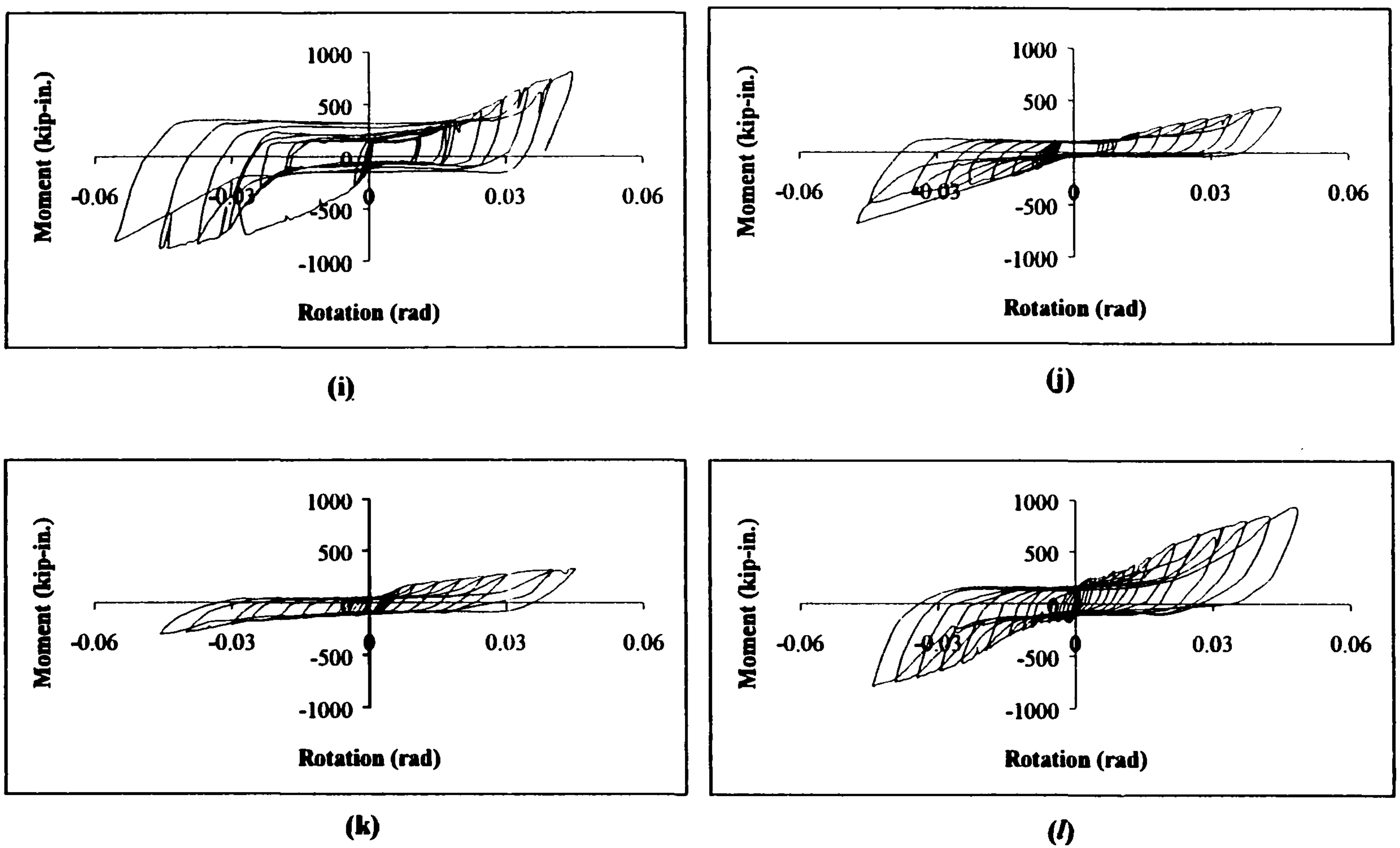

Fig. A-1 Moment-Rotation Hysteresis Loops for "Type I" Double Web Angle Connections:
(i) Test Specimen No. 10 (DW-*I*-5-3/4-3/4-4½-5-24); (j) Test Specimen No. 11 (DW-*I*-4-1/2-3/4-4½-4-24);
(k) Test Specimen No. 12 (DW-*I*-5-3/8-5/8-4½-4-24); (*l*) Test Specimen No. 13 (DW-*I*-5-3/8-5/8-4½-6-24)

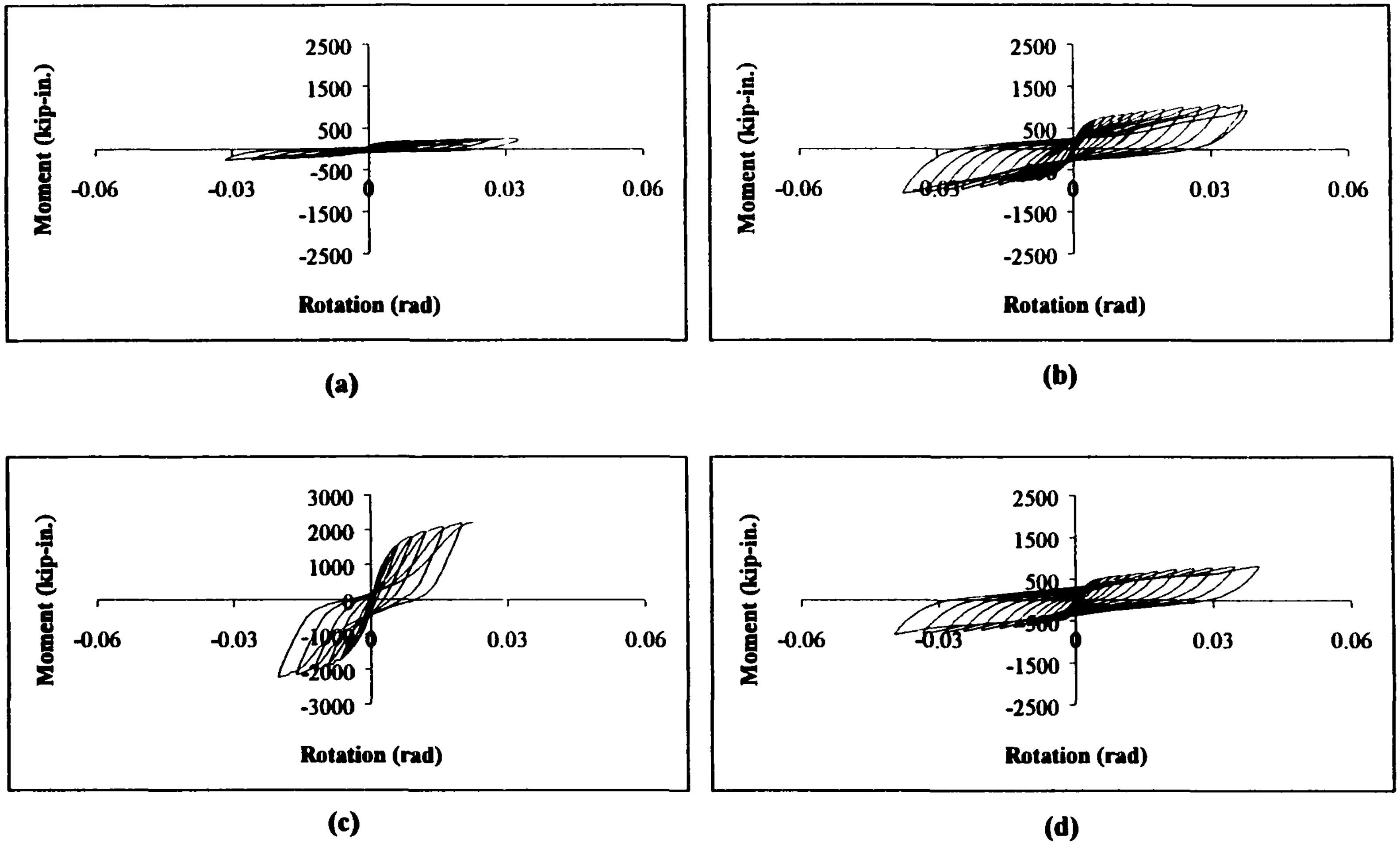

Fig. A-2 Moment-Rotation Hysteresis Loops for "Type II" Double Web Angle Connections (Continued): (a) Test Specimen No. 1 (DW-*II*-3-1/4-1/2-2½-3-24); (b) Test Specimen No. 2 (DW-*II*-3-1/2-3/4-3½-4-24); (c) Test Specimen No. 3 (DW-*II*-4-5/8-3/4-3½-5-24); (d) Test Specimen No. 4 (DW-*II*-4-3/8-3/4-3½-4-24)

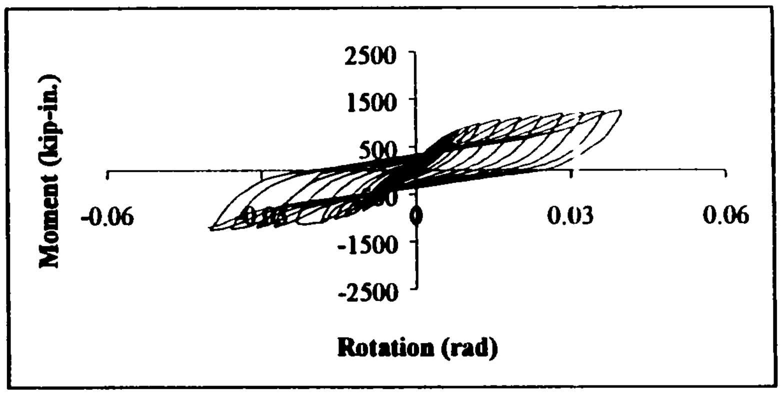

(e)

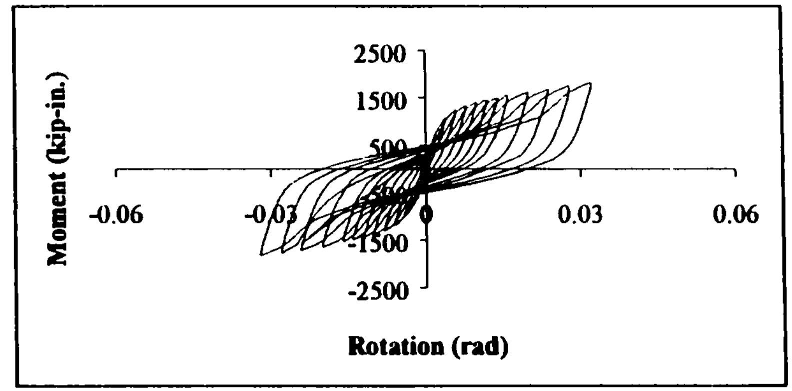

(f)

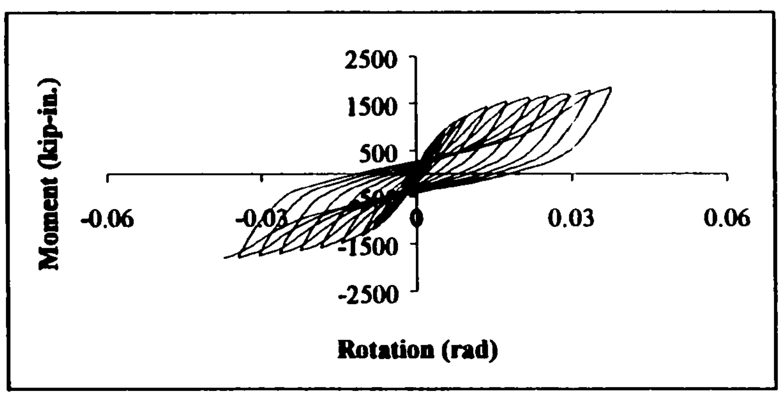

(g)

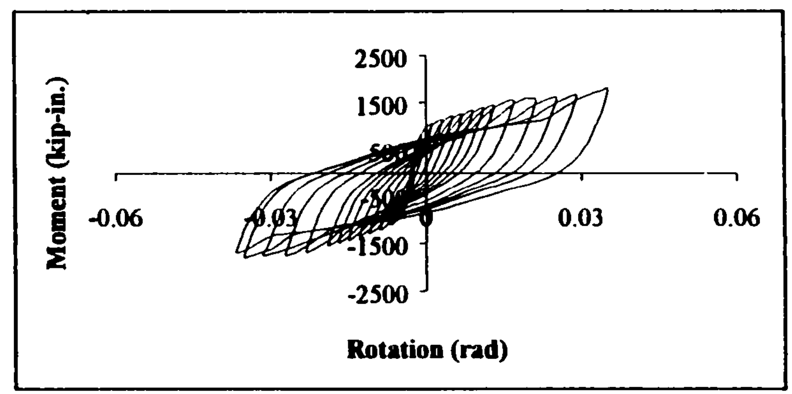

(h)

Fig. A-2 Moment-Rotation Hysteresis Loops for "Type II" Double Web Angle Connections:
(e) Test Specimen No. 5 (DW-*II*-5-3/4-3/4-5½-4-24); (f) Test Specimen No. 6 (DW-*II*-5-1/2-5/8-4½-6-24);
(g) Test Specimen No. 7 (DW-*II*-6-3/4-3/4-7½-5-24); (h) Test Specimen No. 8 (DW-*II*-6-1/2-7/8-5½-6-24)

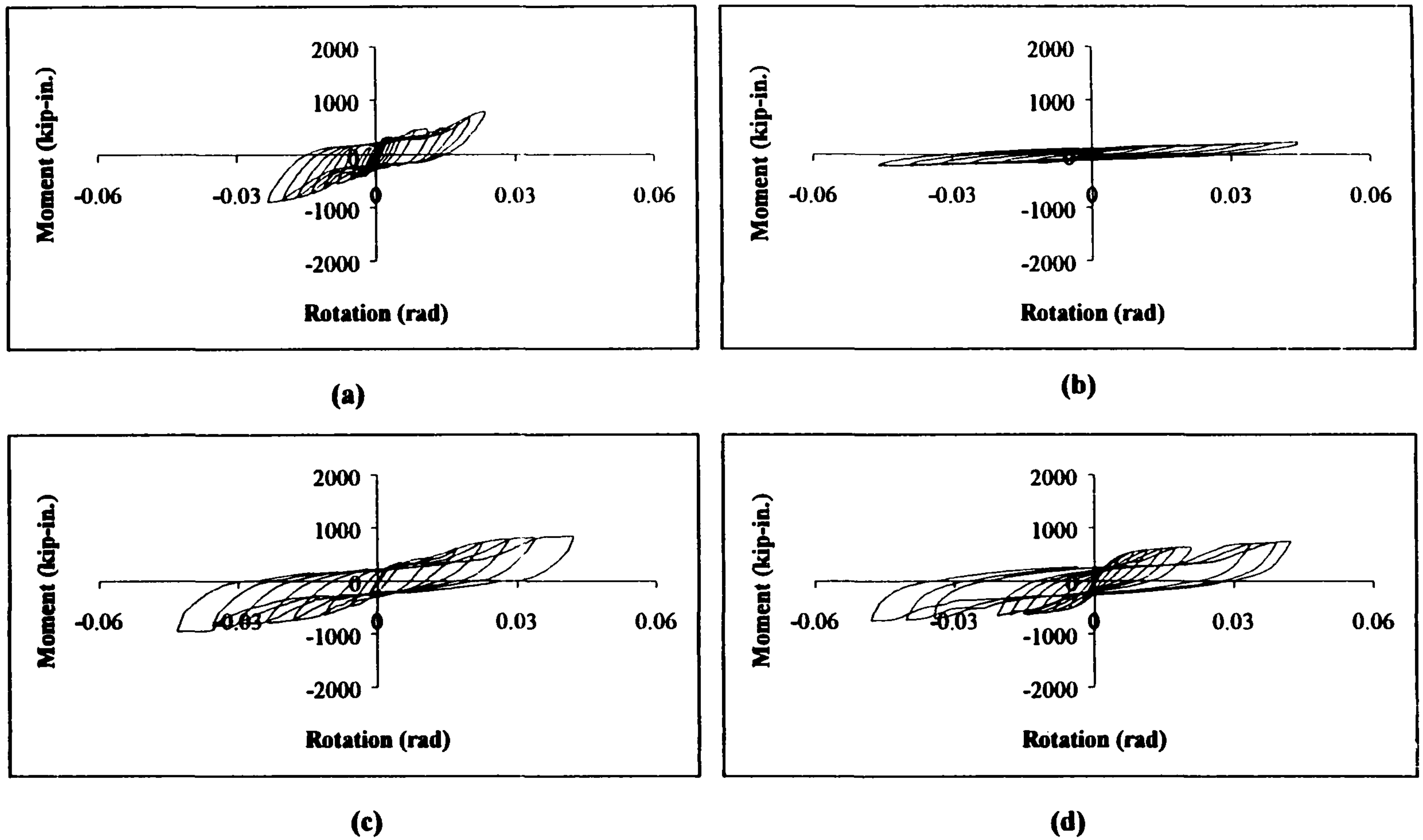

Fig. A-3 Moment-Rotation Hysteresis Loops for Top and Seat Angle Connections (Continued): (a) Test Specimen No. 1 (TS-6-4-3/4-5/8-2½-5-14); (b) Test Specimen No. 2 (TS-6-6-3/8-5/8-4½-5-14); (c) Test Specimen No. 3 (TS-6-6-3/4-5/8-3½-5-14); (d) Test Specimen No. 4 (TS-6-6-3/4-5/8-4½-4-16)

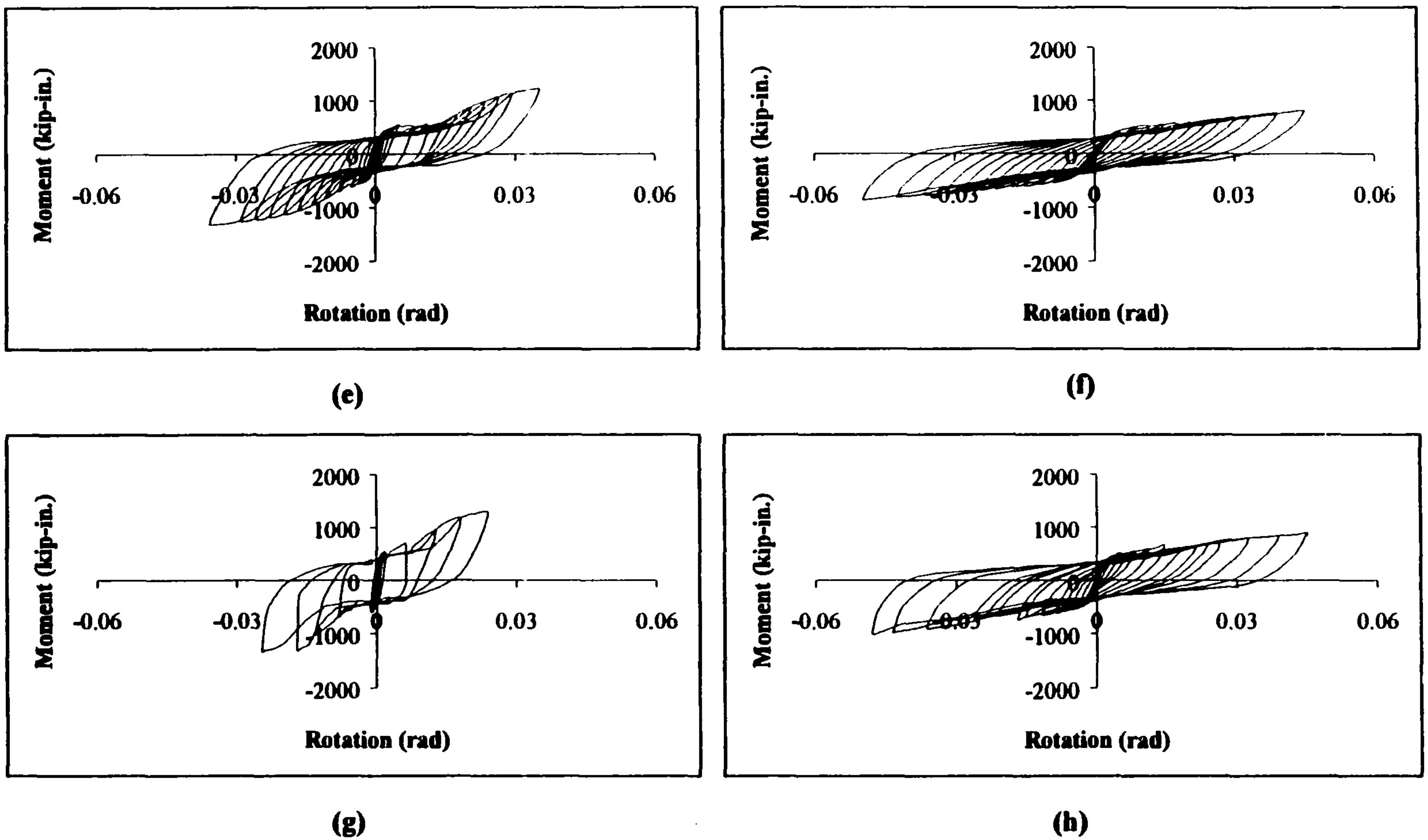

Fig. A-3 Moment-Rotation Hysteresis Loops for Top and Seat Angle Connections (Continued): (e) Test Specimen No. 5 (TS-6-4-3/4-3/4-2½-5-14); (f) Test Specimen No. 6 (TS-6-4-1/2-3/4-2½-5-14); (g) Test Specimen No. 7 (TS-6-4-3/4-3/4-2½-5-16); (h) Test Specimen No. 8 (TS-6-4-1/2-3/4-2½-4-16)

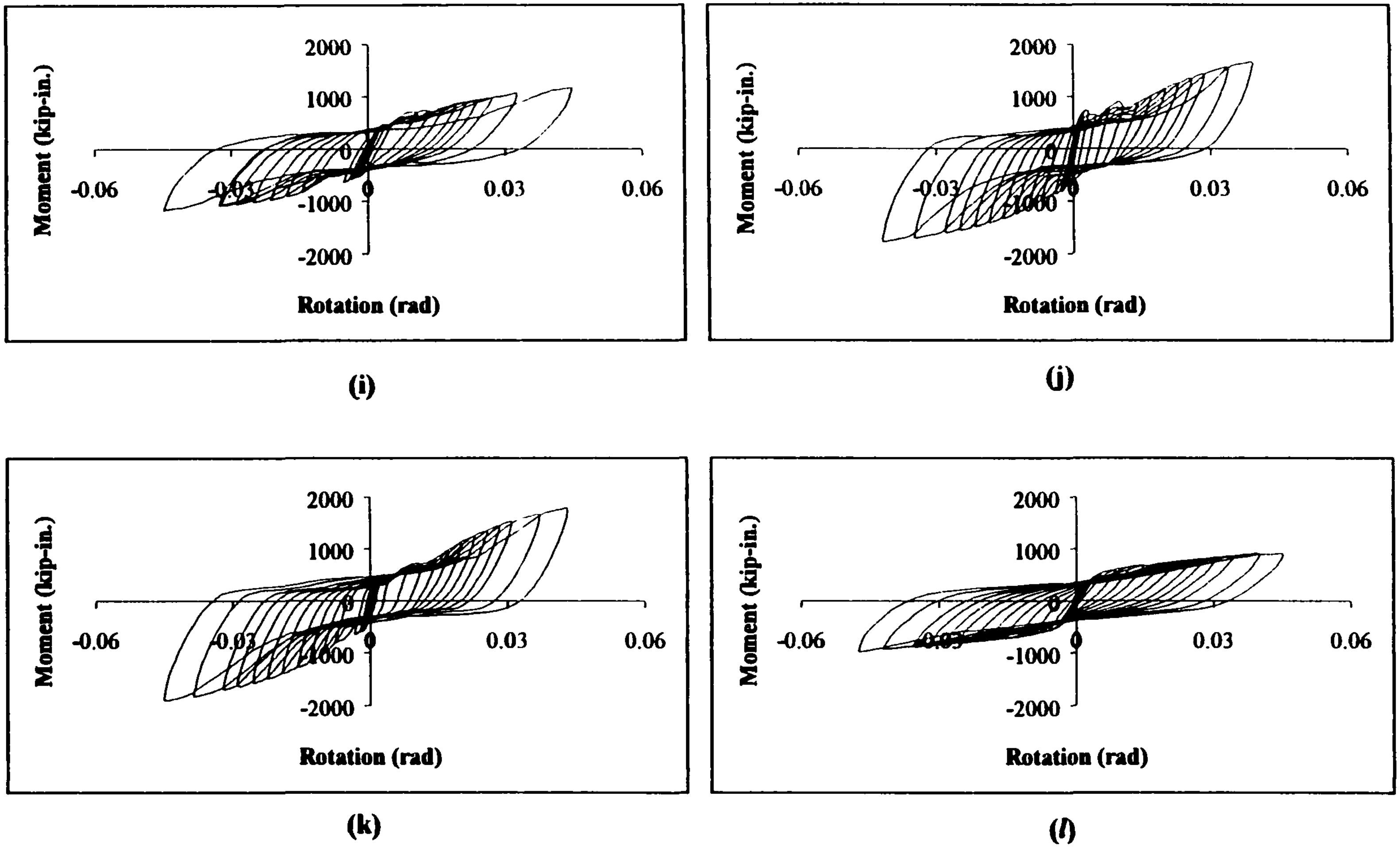

Fig. A-3 Moment-Rotation Hysteresis Loops for Top and Seat Angle Connections:
(i) Test Specimen No. 9 (TS-6-6-3/4-3/4-3½-4-16); (j) Test Specimen No. 10 (TS-6-4-3/4-7/8-2½-4-16);
(k) Test Specimen No. 11 (TS-6-6-3/4-7/8-2½-4-16); (*l*) Test Specimen No. 12 (TS-6-6-3/4-7/8-4½-4-16)

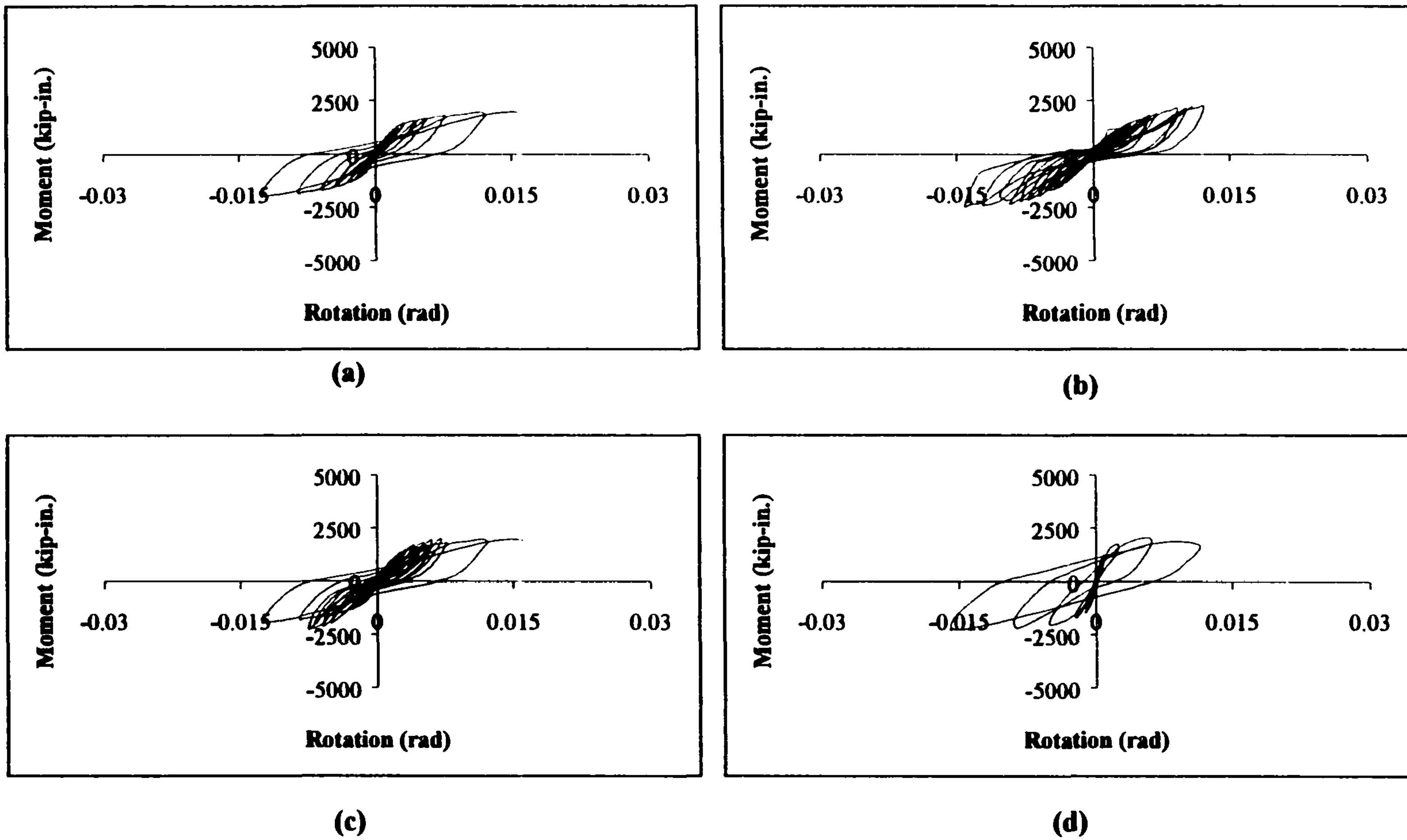

Fig. A-4 Moment-Rotation Hysteresis Loops for Flush End-Plate Connections (Continued):
(a) Test Specimen No. 1 (FEP-II-6-18-3/8-3/4-$1^5/_8$-3-3); (b) Test Specimen No. 2 (FEP-II-6-18-1/2-3/4-$1^5/_8$-3-3);
(c) Test Specimen No. 3 (FEP-II-6-18-5/8-3/4-$1^5/_8$-3-3); (d) Test Specimen No. 4 (FEP-II-8-18-3/8-1-$1^7/_8$-3½-3½)

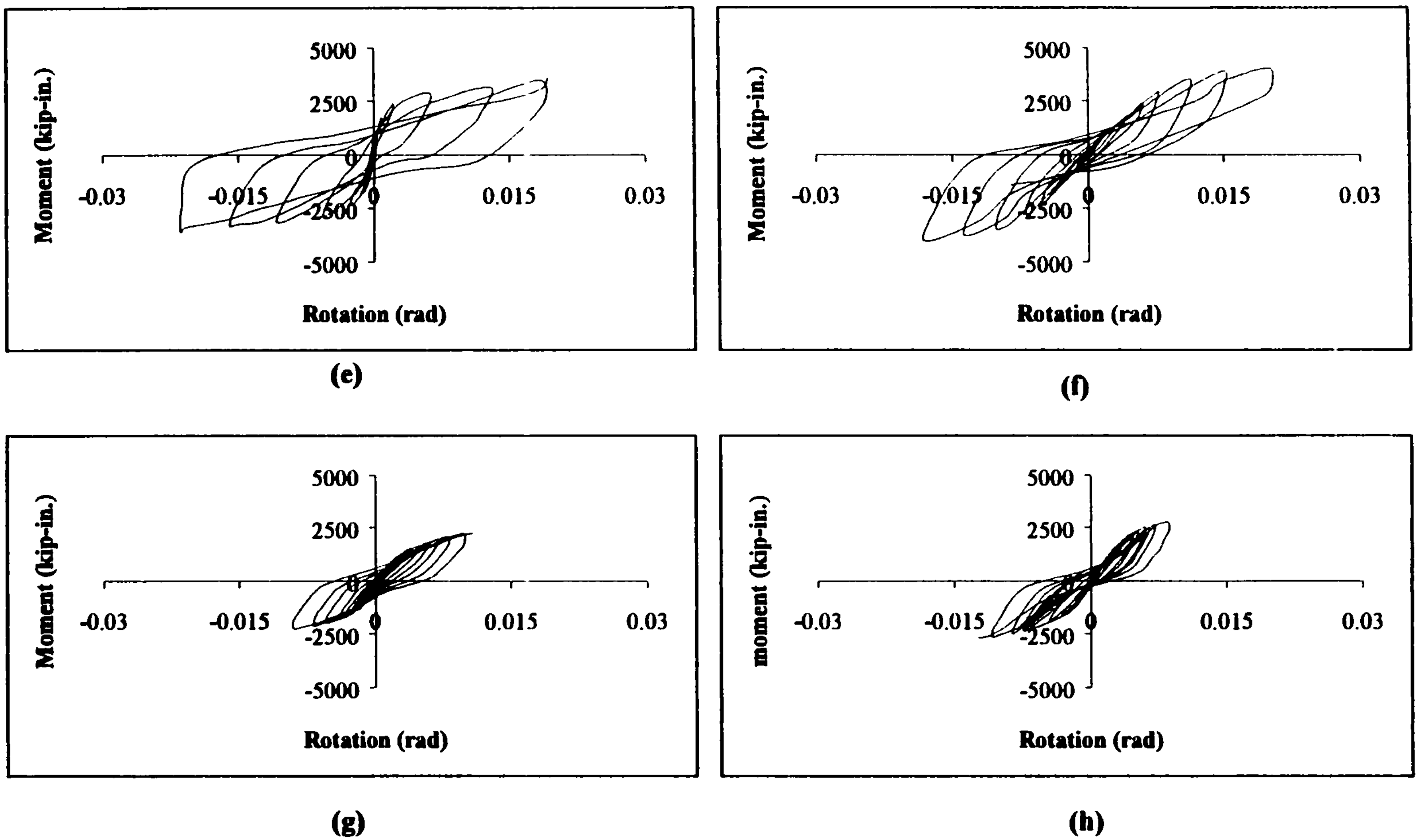

Fig. A-4 Moment-Rotation Hysteresis Loops for Flush End-Plate Connections (Continued):
(e) Test Specimen No. 5 (FEP-II-8-18-1/2-1-1$^7/_8$-3½-3½); (f) Test Specimen No. 6 (FEP-II-8-18-3/4-1-1$^7/_8$-3½-3½);
(g) Test Specimen No. 7 (FEP-II-6-22-3/8-3/4-1$^5/_8$-3-3); (h) Test Specimen No. 8 (FEP-II-6-22-1/2-3/4-1$^5/_8$-3-3)

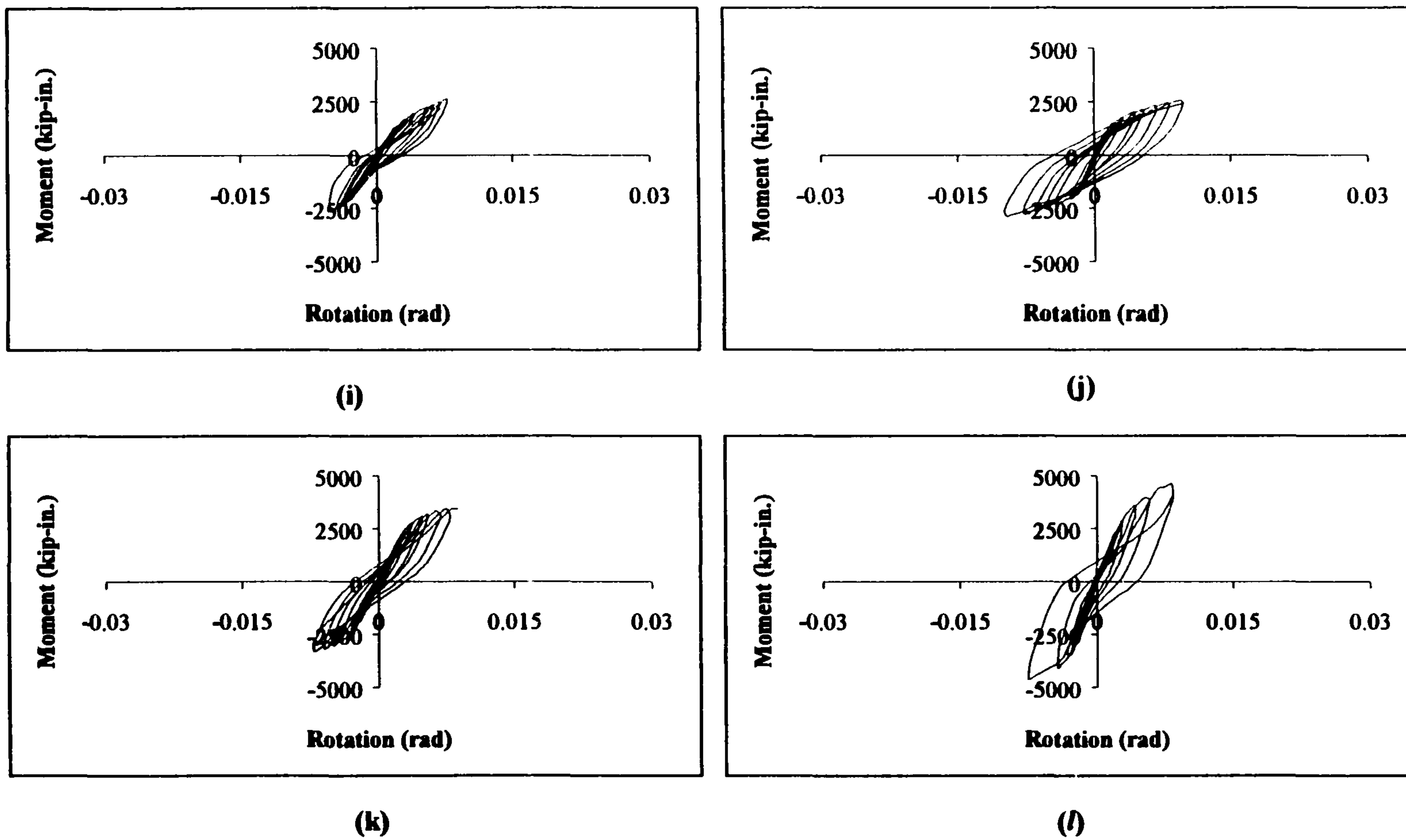

Fig. A-4 Moment-Rotation Hysteresis Loops for Flush End-Plate Connections:
(i) Test Specimen No. 9 (FEP-II-6-22-5/8-3/4-1$^{5}/_{8}$-3-3); (j) Test Specimen No. 10 (FEP-II-8-22-3/8-1-1$^{7}/_{8}$-3½-3½);
(k) Test Specimen No. 11 (FEP-II-8-22-1/2-1-1$^{7}/_{8}$-3½-3½); (*l*) Test Specimen No. 12 (FEP-II-8-22-3/4-1-1$^{7}/_{8}$-3½-3½)

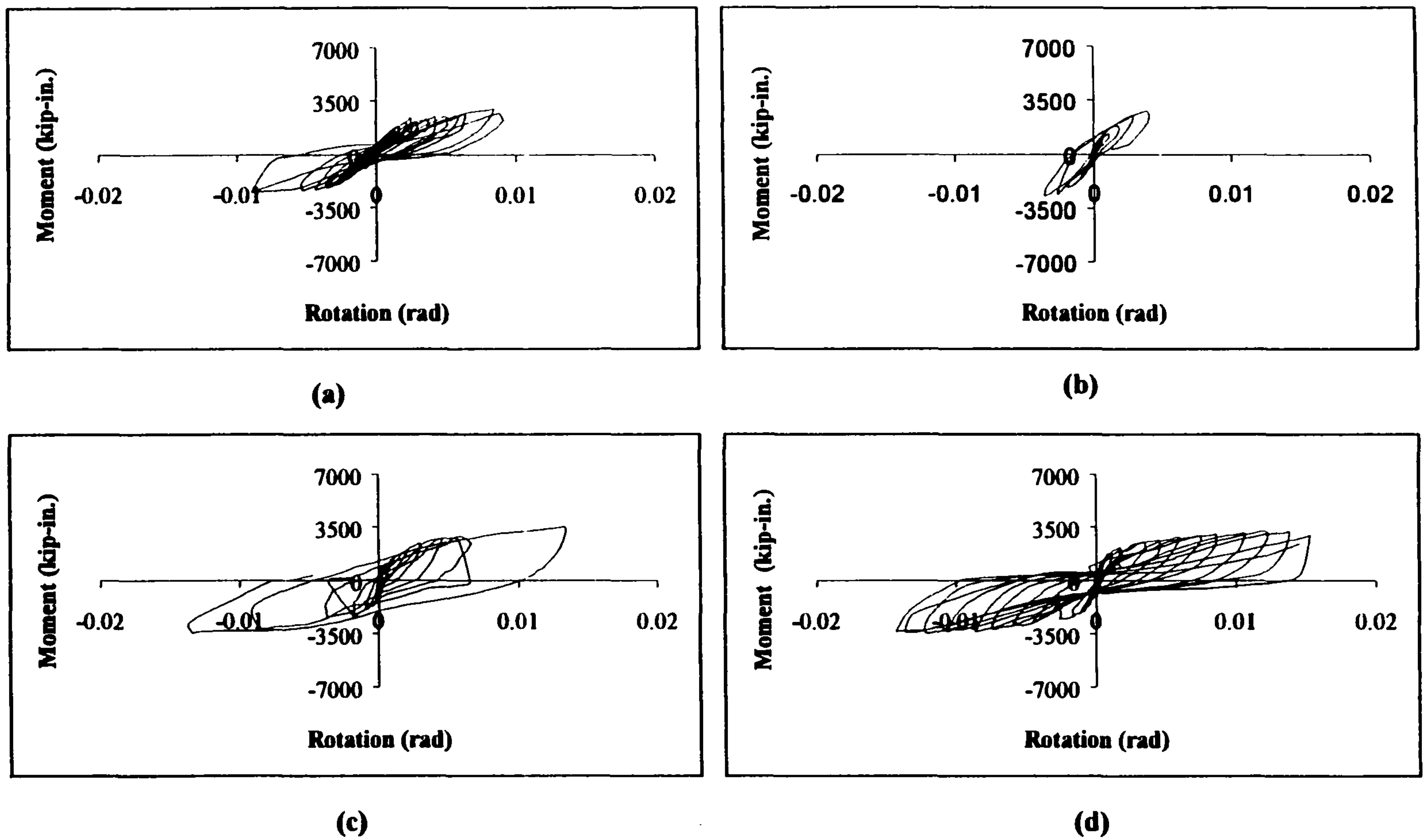

Fig. A-5 Moment-Rotation Hysteresis Loops for Extended End-Plate Connections (Continued):
(a) Test Specimen No. 1 (EEP-7-22½-1/2-3/4-$1\frac{3}{8}$-3½); (b) Test Specimen No. 2 (EEP-8-22½-5/8-7/8-$1\frac{1}{2}$-5½)
(c) Test Specimen No. 3 (EEP-9-22½-1/2-$1\frac{1}{8}$-$1\frac{7}{8}$-3½); (d) Test Specimen No. 4 (EEP-10-22½-1/2-7/8-$1\frac{3}{8}$-4½)

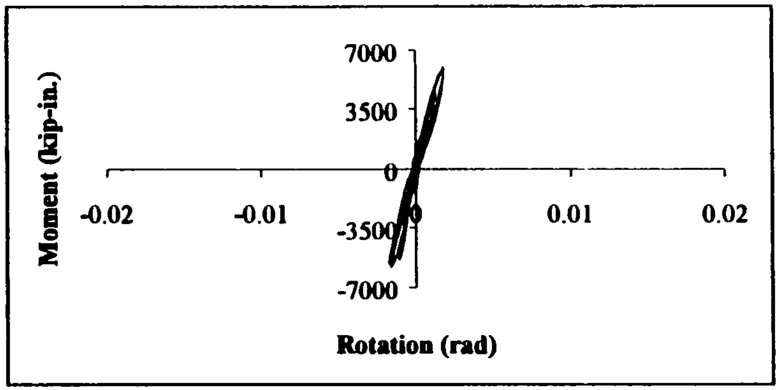

(e)

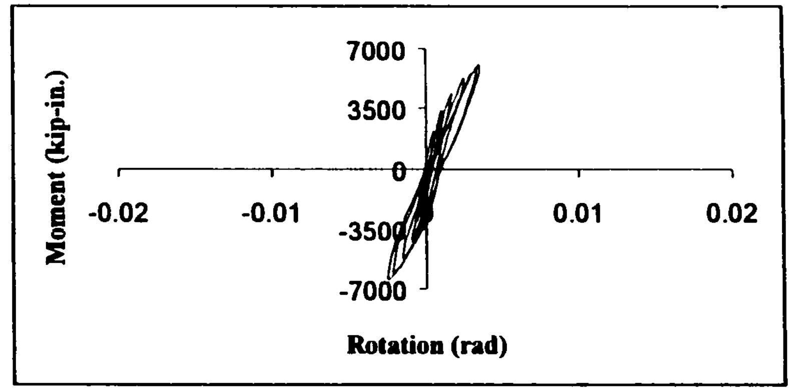

(f)

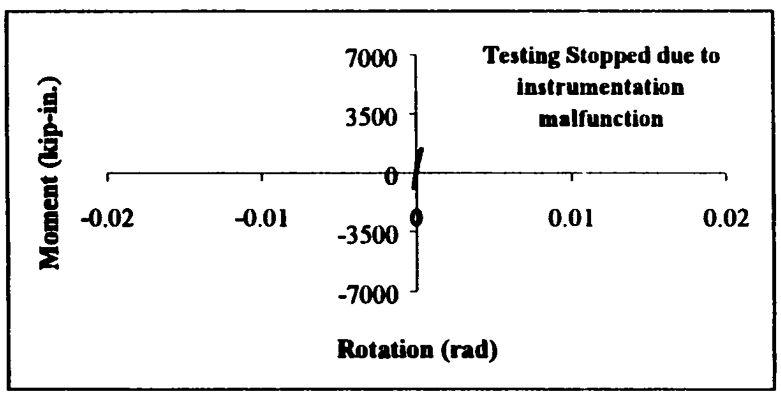

(g)

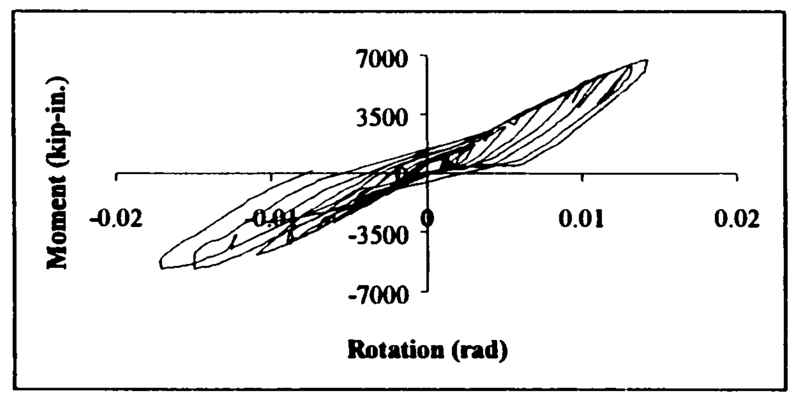

(h)

Fig. A-5 Moment-Rotation Hysteresis Loops for Extended End-Plate Connections:
(e) Test Specimen No. 5 (EEP-9-31-7/8-1-1$^{3}/_{4}$-3½); (f) Test Specimen No. 6 (EEP-10-31-3/4-1$^{1}/_{8}$-1$^{1}/_{4}$-7½);
(g) Test Specimen No. 7 (EEP-9-31-5/8-1-1$^{7}/_{8}$-7½); (h) Test Specimen No. 8 (EEP-10-31-1/2-1$^{1}/_{8}$-1$^{1}/_{8}$-3½)

APPENDIX B

Comparisons of Experimental Moment-Rotation Hysteresis Loops with Hysteresis Models Obtained for:

Double Web Angle Connections

Top and Seat Angle Connections

Flush End-Plate Connections

Extended End-Plate Connections

(Figures B-1 Through B-11)

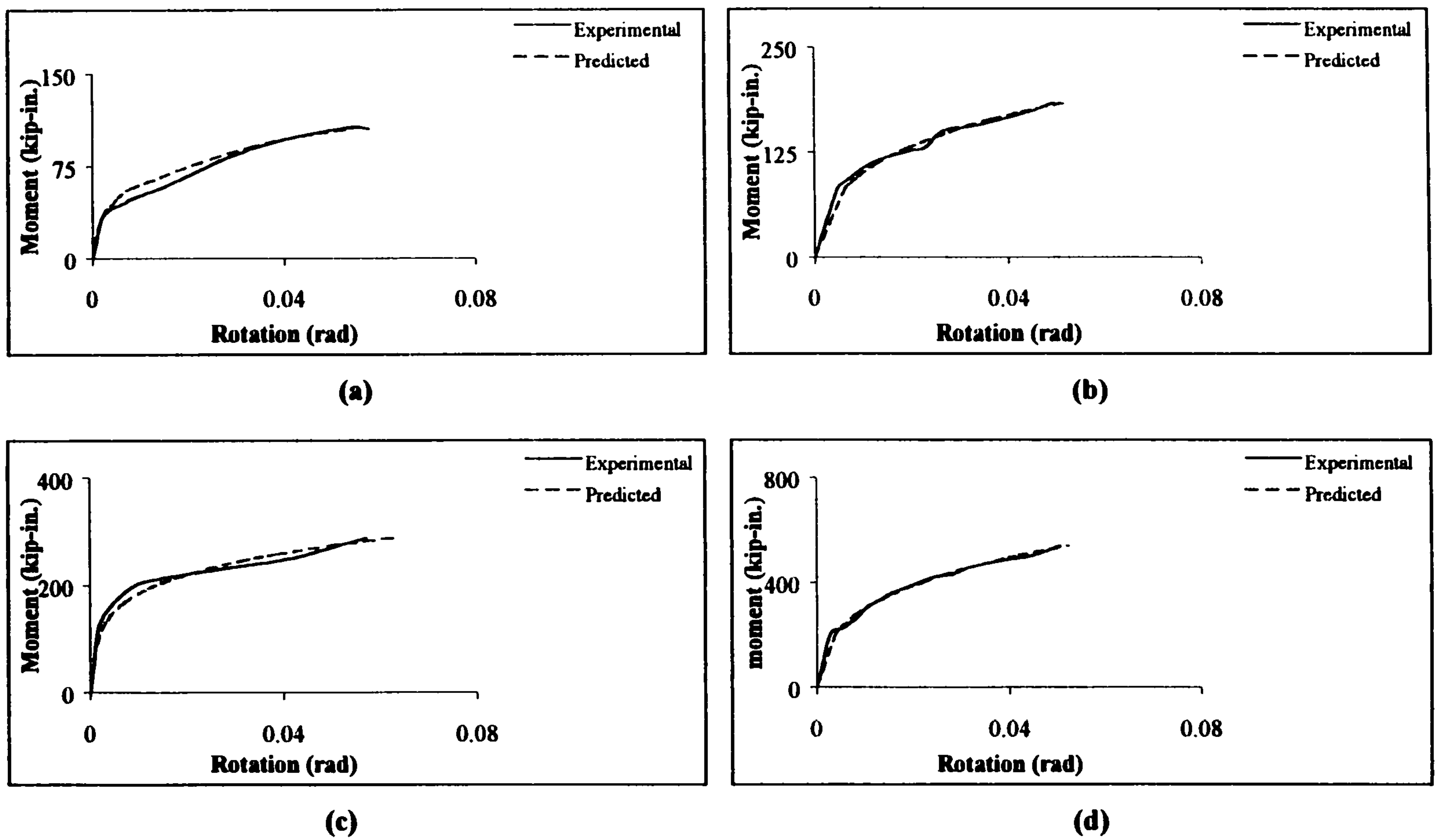

Fig. B-1 Comparison of Predicted and Experimental Moment-Rotation Enveloping Curves for "Type I" Double Web Angle Connections with Angle Yielding Failure (Continued): (a) Test Specimen No. 1 (DW-I-4-1/4-3/4-4½-3-16); b Test Specimen No. 2 (DW-I-4-1/4-3/4-4½-4-16); (c) Test Specimen No. 5 (DW-I-4-1/4-3/4-4½-5-21); (d) Test Specimen No. 6 (DW-I-4-3/8-3/4-4½-5-21)

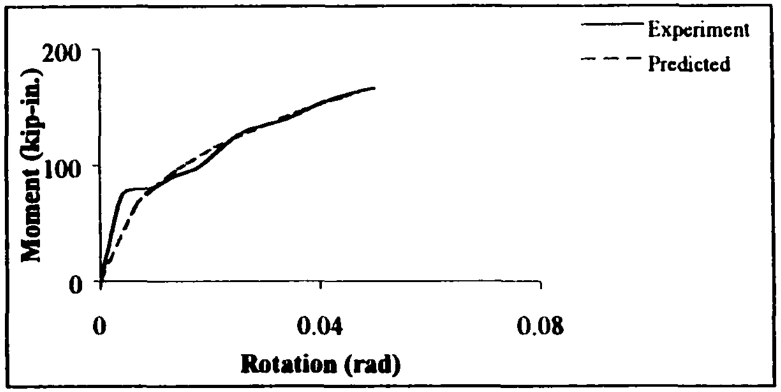

(e)

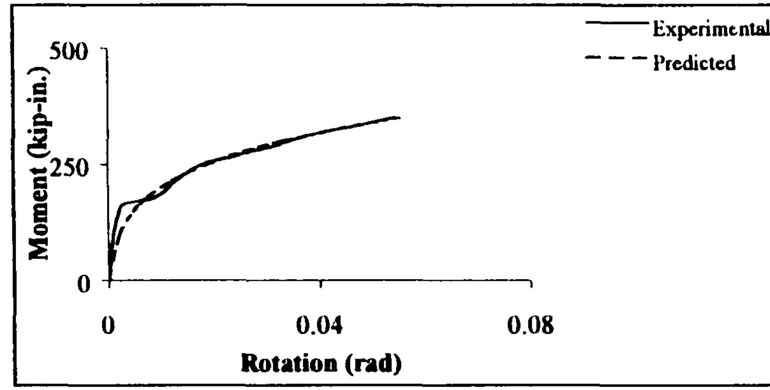

(f)

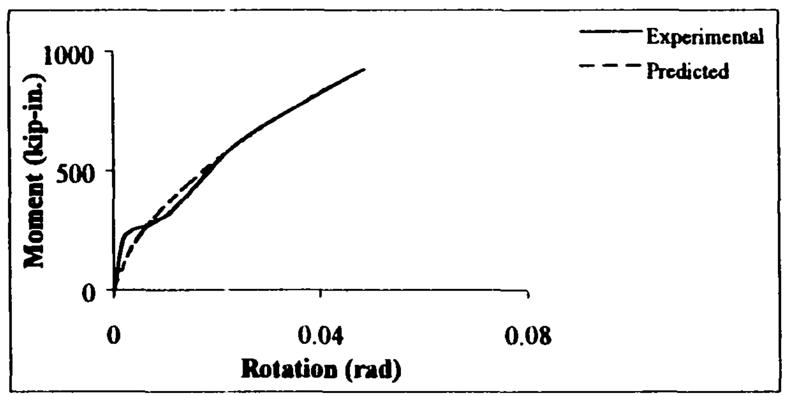

(g)

**Fig. B-1 Comparison of Predicted and Experimental Moment-Rotation Enveloping Curves for "Type I" Double Web Angle Connections with Angle Yielding Failure:
(e) Test Specimen No. 7 (DW-I-4-3/8-3/4-4½-3-16); (f) Test Specimen No. 8 (DW-I-4-3/8-3/4-4½-4-16);
(g) Test Specimen No. 13 (DW-I-5-3/8-5/8-4½-6-24)**

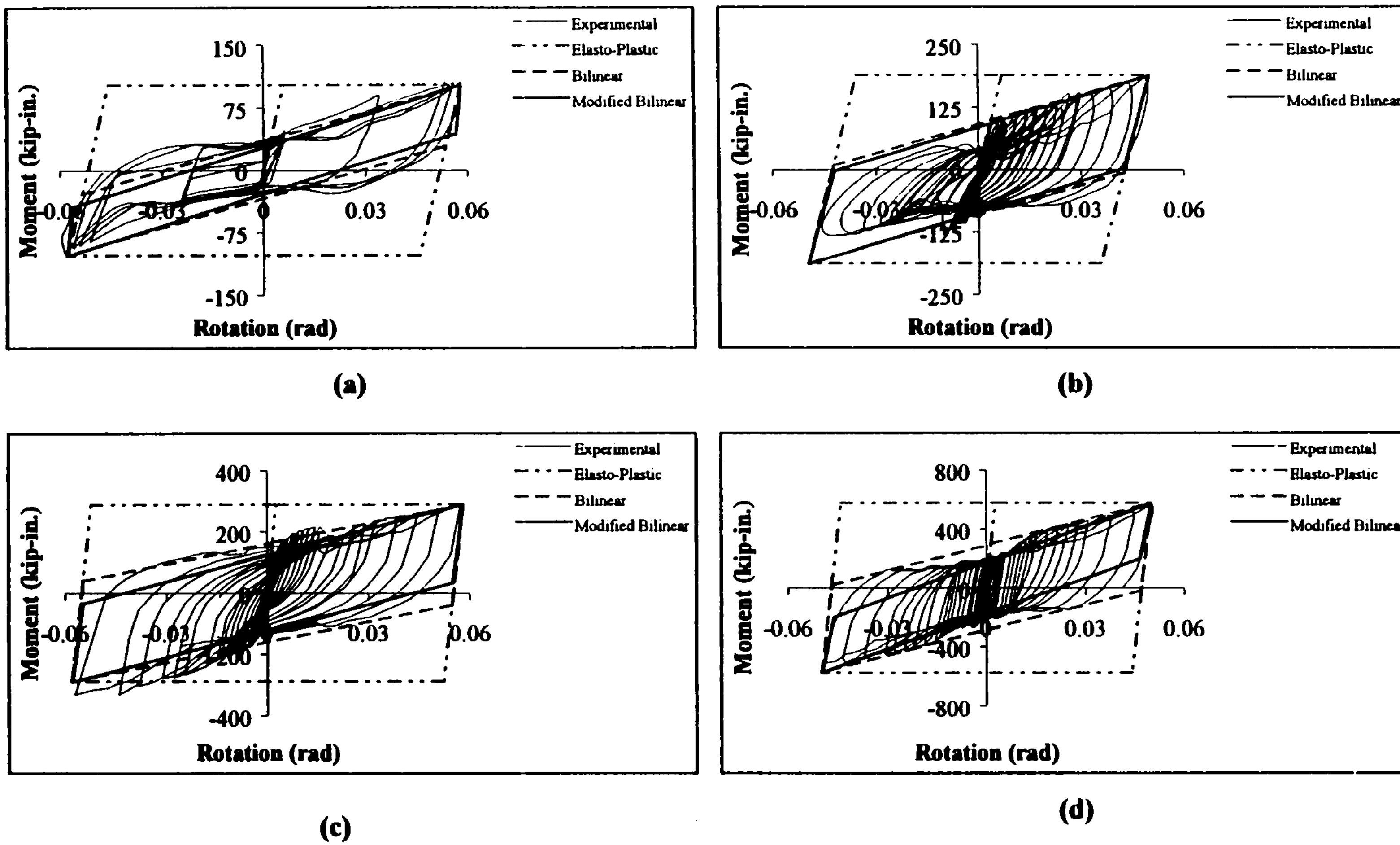

Fig. B-2 Comparison of Experimental Models and Moment-Rotation Hysteresis Loops for "Type I" Double Web Angle Connections with Angle Yielding Failure (Continued): (a) Test Specimen No. 1 (DW-I-4-1/4-3/4-4½-3-16); (b) Test Specimen No. 2 (DW-I-4-1/4-3/4-4½-4-16); (c) Test Specimen No. 5 (DW-I-4-1/4-3/4-4½-5-21); (d) Test Specimen No. 6 (DW-I-4-3/8-3/4-4½-5-21)

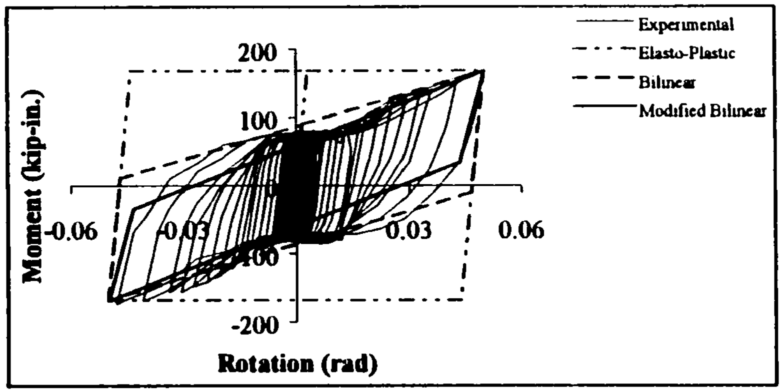

(e)

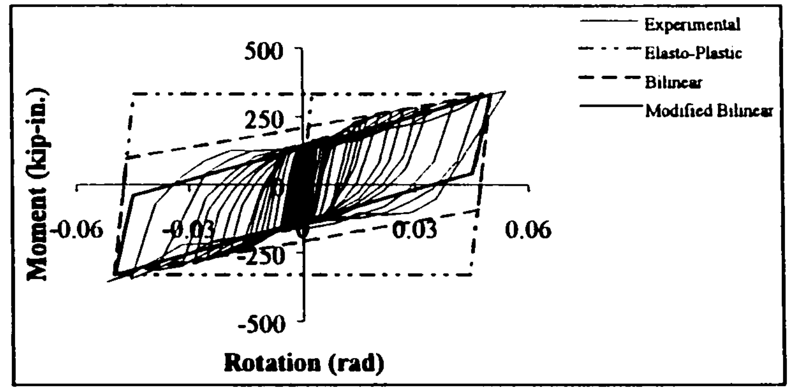

(f)

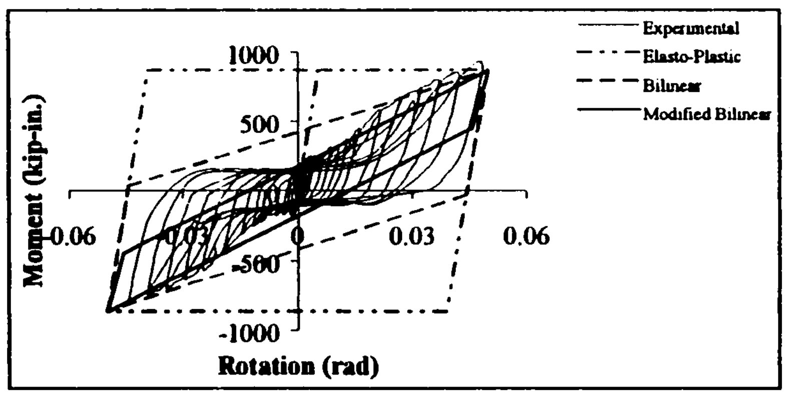

(g)

Fig. B-2 Comparison of Experimental Models and Moment-Rotation Hysteresis Loops for "Type I" Double Web Angle Connections with Angle Yielding Failure: (e) Test Specimen No. 7 (DW-I-4-3/8-3/4-4½-3-16); (f) Test Specimen No. 8 (DW-I-4-3/8-3/4-4½-4-16); (g) Test Specimen No. 13 (DW-I-5-3/8-5/8-4½-6-24)

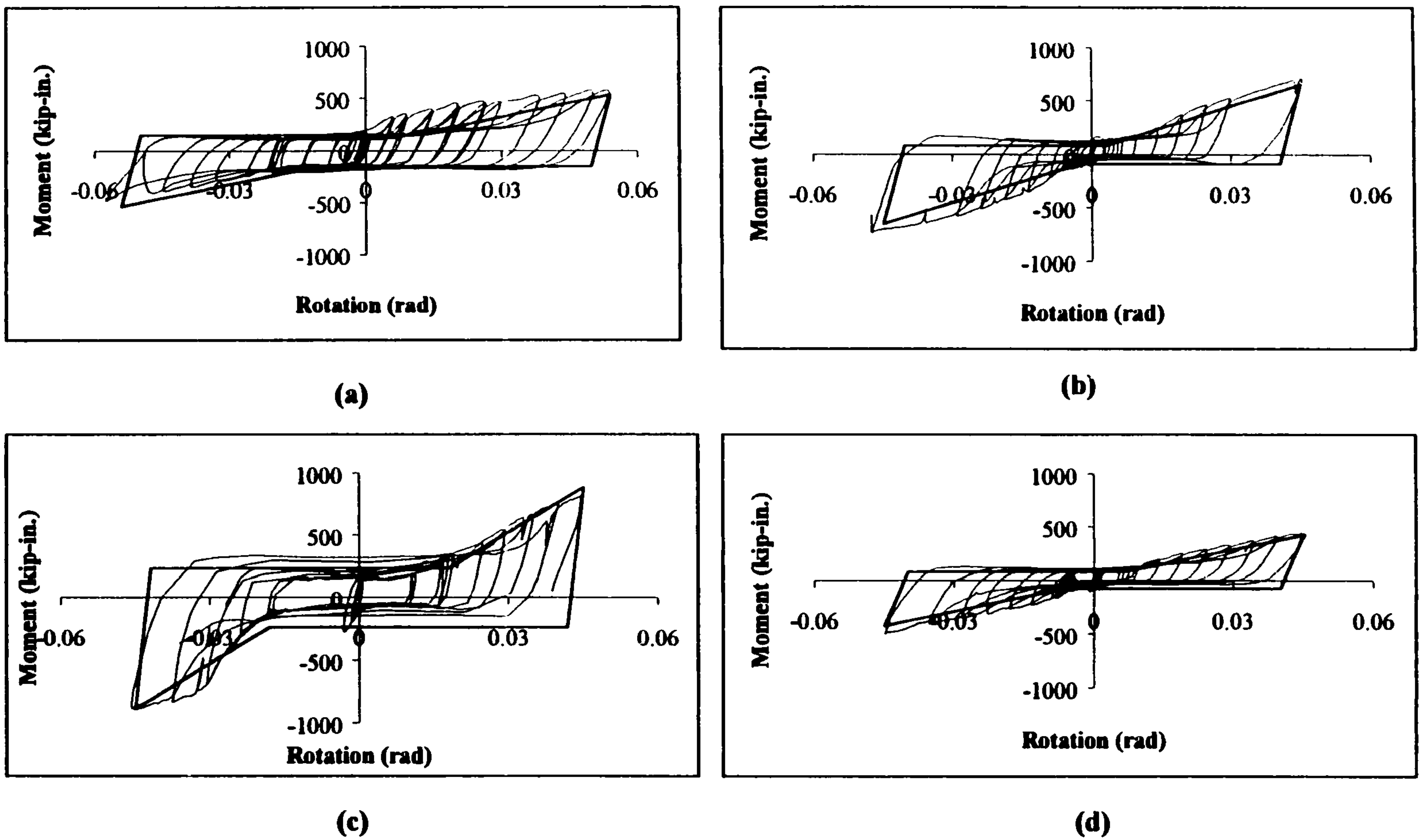

Fig. B-3 Comparison of Experimental Trilinear Model and Moment-Rotation Hysteresis Loops For "Type I" Double Web Angle Connections with Beam Web Bearing Failure: (a) Test Specimen No. 3 (DW-I-4-5/8-3/4-4½-4-16); (b) Test Specimen No. 9 (DW-I-5-1/2-5/8-4½-5-24); (c) Test Specimen No. 10 (DW-I-5-3/4-3/4-4½-5-24); (d) Test Specimen No. 11 (DW-I-4-1/2-3/4-4½-4-24)

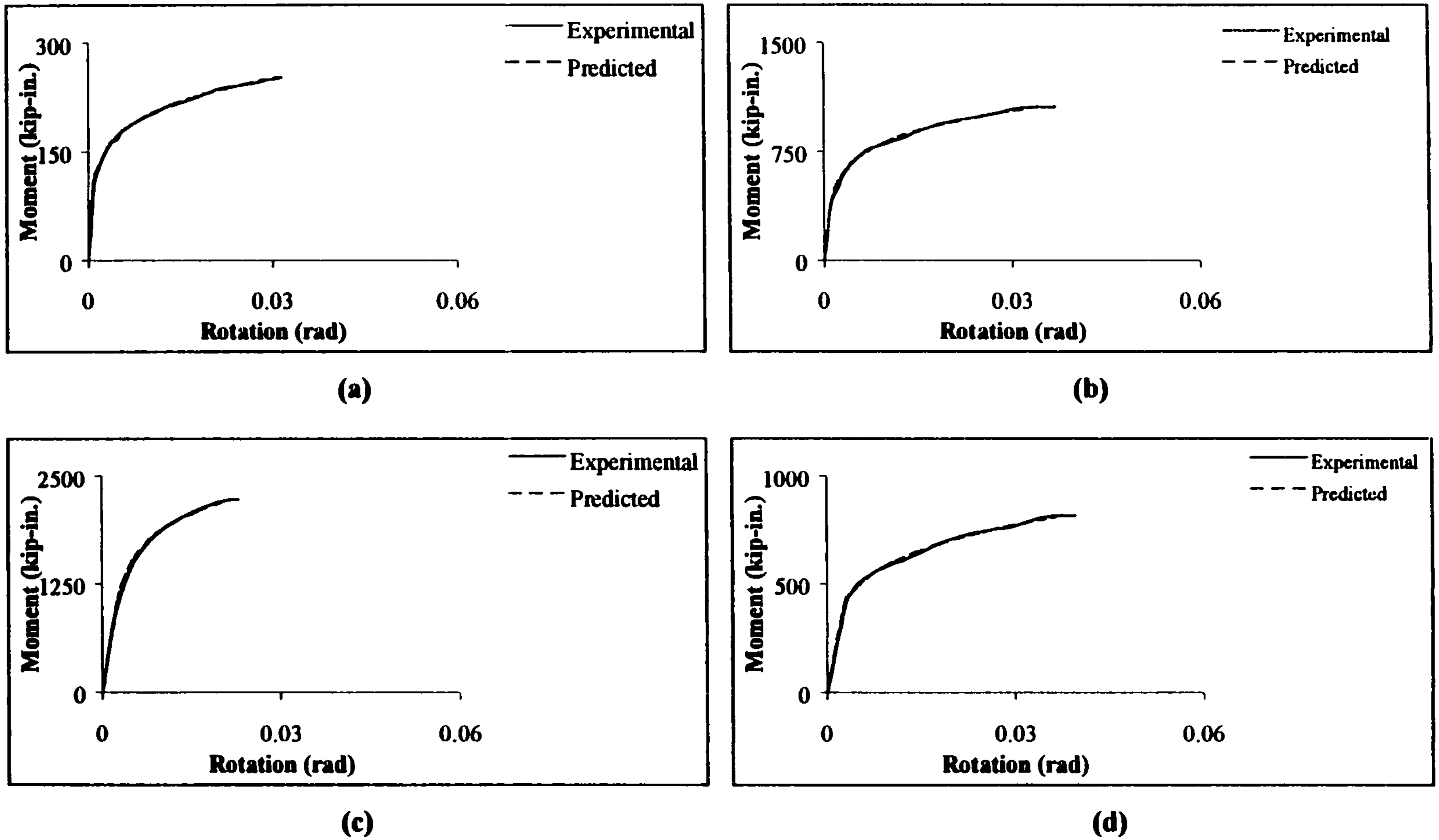

Fig. B-4 Comparison of Predicted and Experimental Moment-Rotation Enveloping Curves for "Type II" Double Web Angle Connections (Continued): (a) Test Specimen No. 1 (DW-II-3-1/4-1/2-2½-3-24); (b) Test Specimen No. 2 (DW-II-3-1/2-3/4-3½-4-24); (c) Test Specimen No. 3 (DW-II-4-5/8-3/4-3½-5-24); (d) Test Specimen No. 4 (DW-II-4-3/8-3/4-3½-4-24)

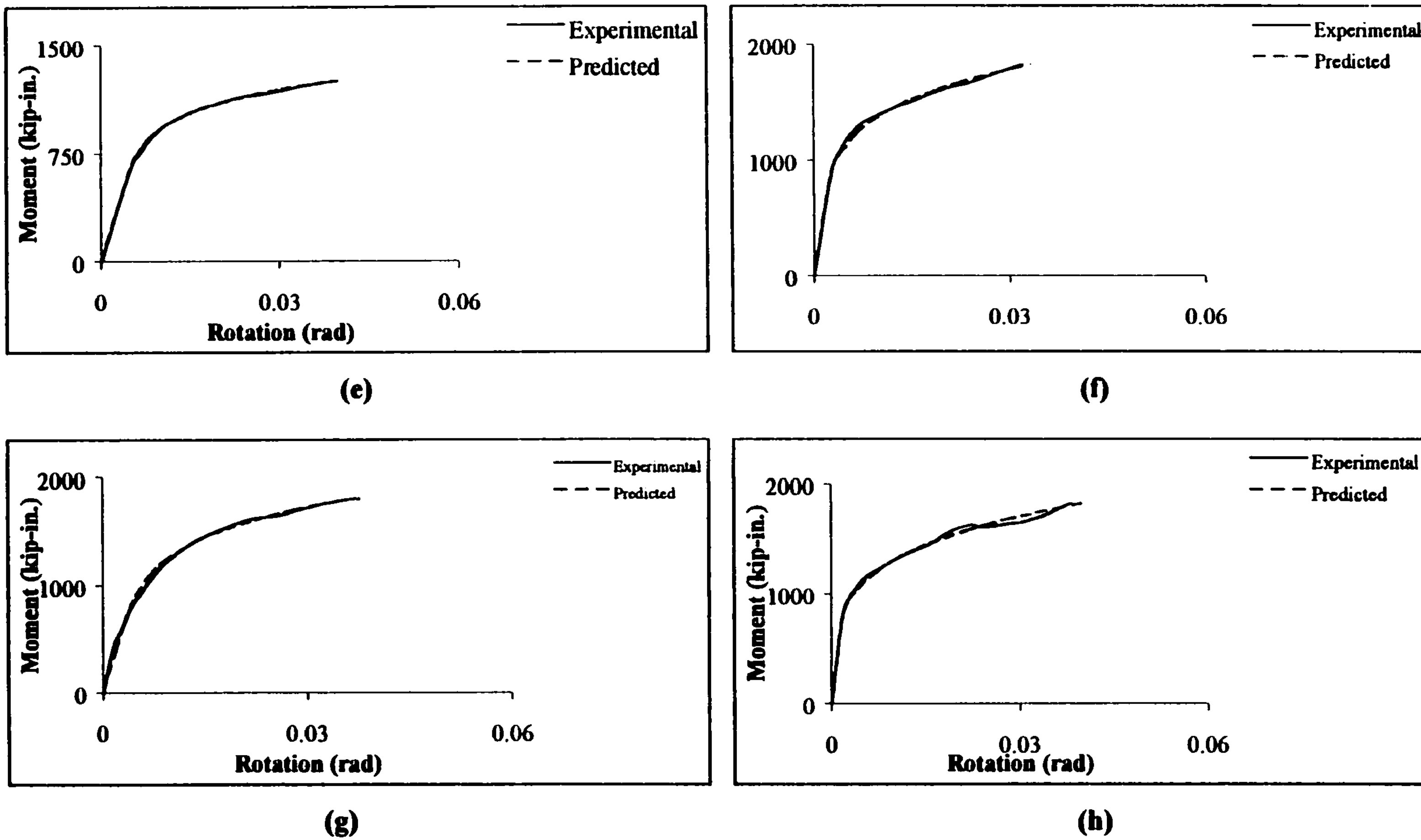

Fig. B-4 Comparison of Predicted and Experimental Moment-Rotation Enveloping Curves for "Type II" Double Web Angle Connections:
(e) Test Specimen No. 5 (DW-II-5-3/4-3/4-5½-4-24); (f) Test Specimen No. 6 (DW-II-5-1/2-5/8-4½-6-24);
(g) Test Specimen No. 7 (DW-II-6-3/4-3/4-7½-5-24); (h) Test Specimen No. 8 (DW-II-6-1/2-7/8-5½-6-24)

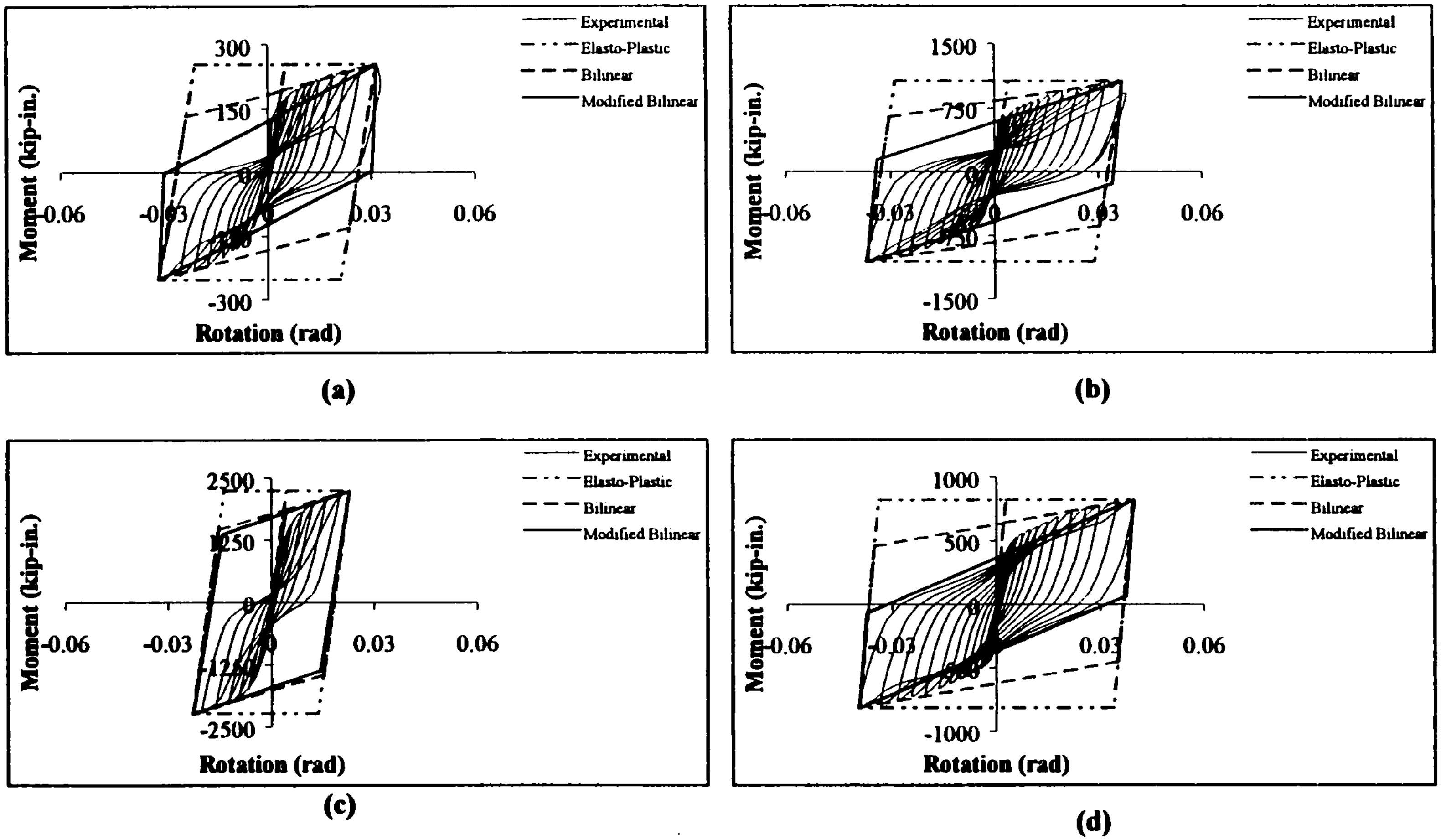

Fig. B-5 Comparison of Experimental Models and Moment-Rotation Hysteresis loops for "Type II" Double Web Angle Connections (Continued):
(a) Test Specimen No. 1 (DW-II-3-1/4-1/2-2½-3-24); (b) Test Specimen No. 2 (DW-II-3-1/2-3/4-3½-4-24); (c) Test Specimen No. 3 (DW-II-4-5/8-3/4-3½-5-24); (d) Test Specimen No. 4 (DW-II-4-3/8-3/4-3½-4-24)

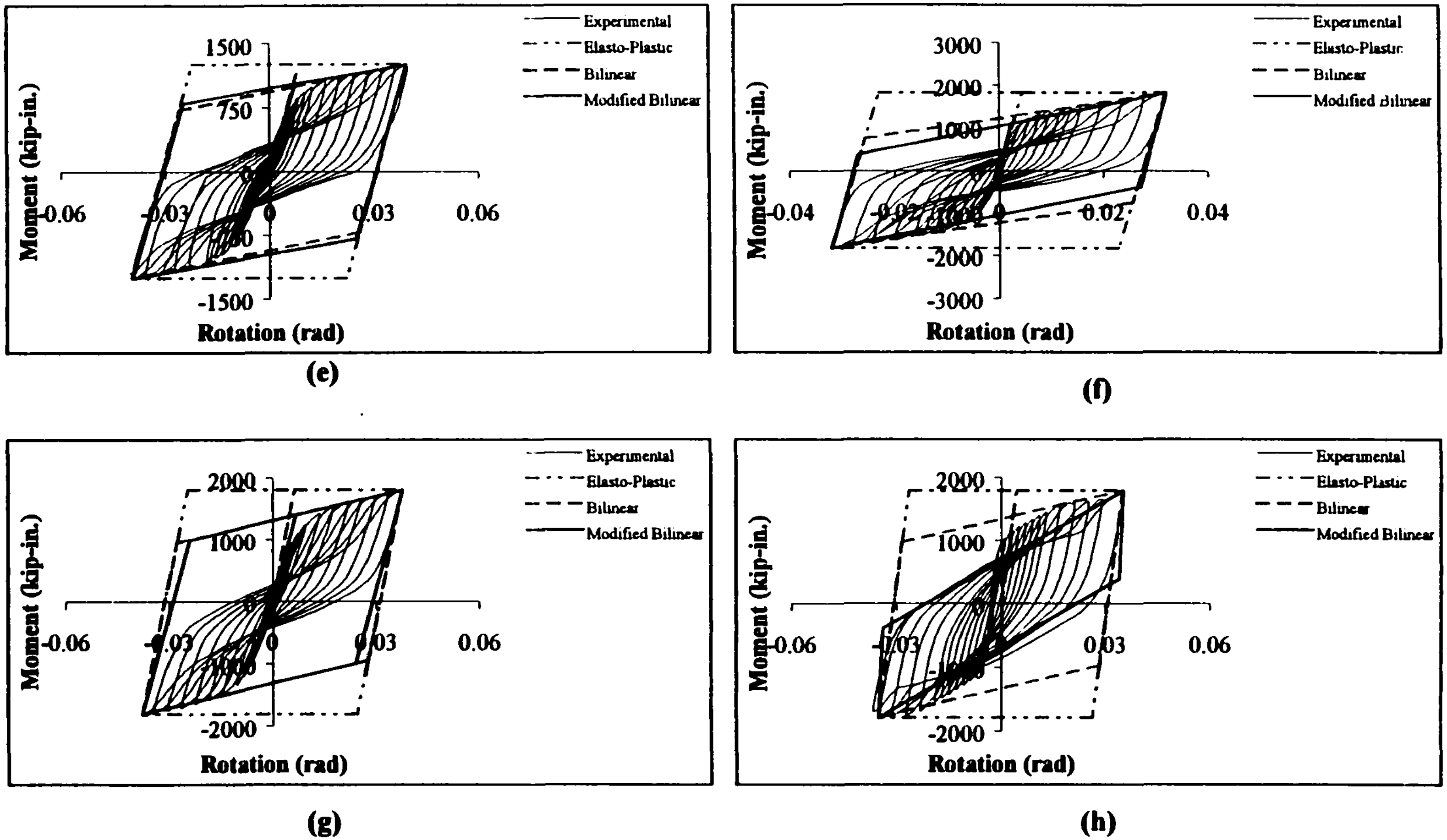

Fig. B-5 Comparison of Experimental Models and Moment-Rotation Hysteresis loops for "Type II" Double Web Angle Connections:
(e) Test Specimen No. 5 (DW-II-5-3/4-3/4-5½-4-24); (f) Test Specimen No. 6 (DW-II-5-1/2-5/8-4½-6-24);
(g) Test Specimen No. 7 (DW-II-6-3/4-3/4-7½-5-24); (h) Test Specimen No. 8 (DW-II-6-1/2-7/8-5½-6-24)

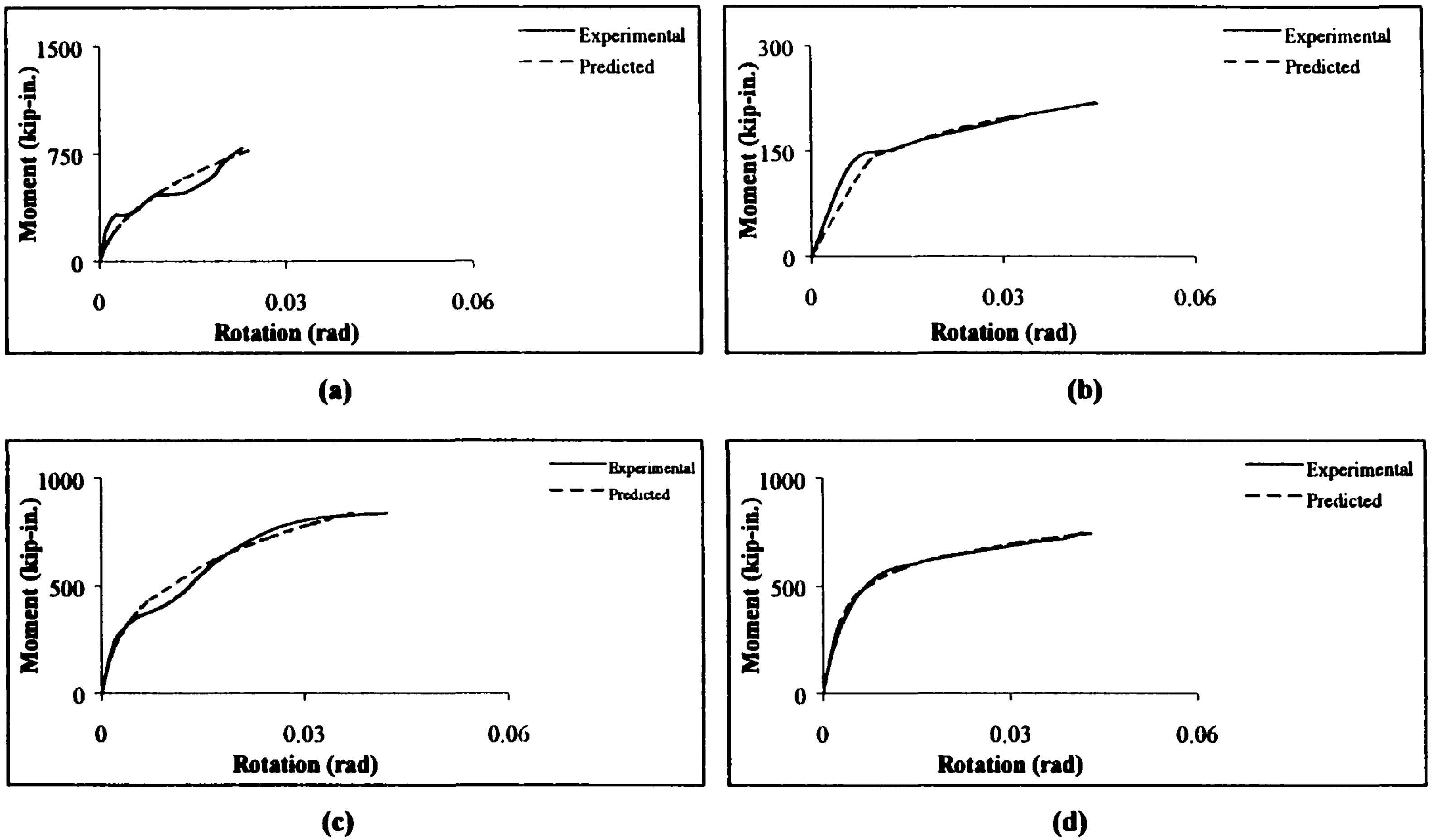

Fig. B-6 Comparison of Experimental Models and Moment-Rotation Enveloping Curves for Top and Seat Angle Connections (Continued): (a) Test Specimen No. 1 (TS-6-4-3/4-5/8-2½-5-14); (b) Test Specimen No. 2 (TS-6-6-3/8-5/8-4½-5-14); (c) Test Specimen No. 3 (TS-6-6-3/4-5/8-3½-5-14); (d) Test Specimen No. 4 (TS-6-6-3/4-5/8-4½-4-16)

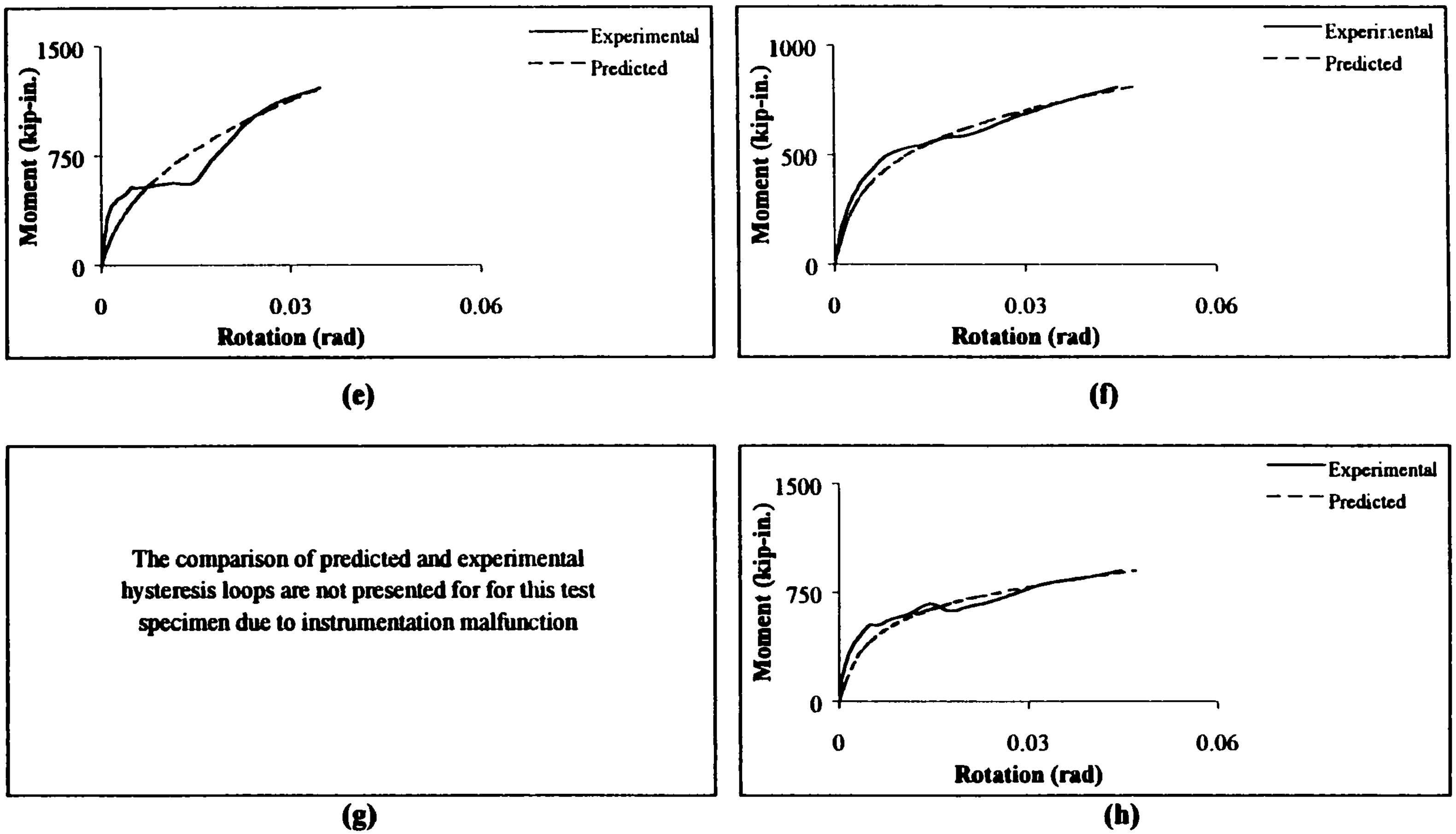

Fig. B-6 Comparison of Experimental Models and Moment-Rotation Enveloping Curves for Top and Seat Angle Connections (Continued):
(e) Test Specimen No. 5 (TS-6-4-3/4-3/4-2½-5-14); (f) Test Specimen No. 6 (TS-6-4-1/2-3/4-2½-5-14);
(g) Test Specimen No. 7 (TS-6-4-3/4-3/4-2½-5-16); (h) Test Specimen No. 8 (TS-6-4-1/2-3/4-2½-4-16)

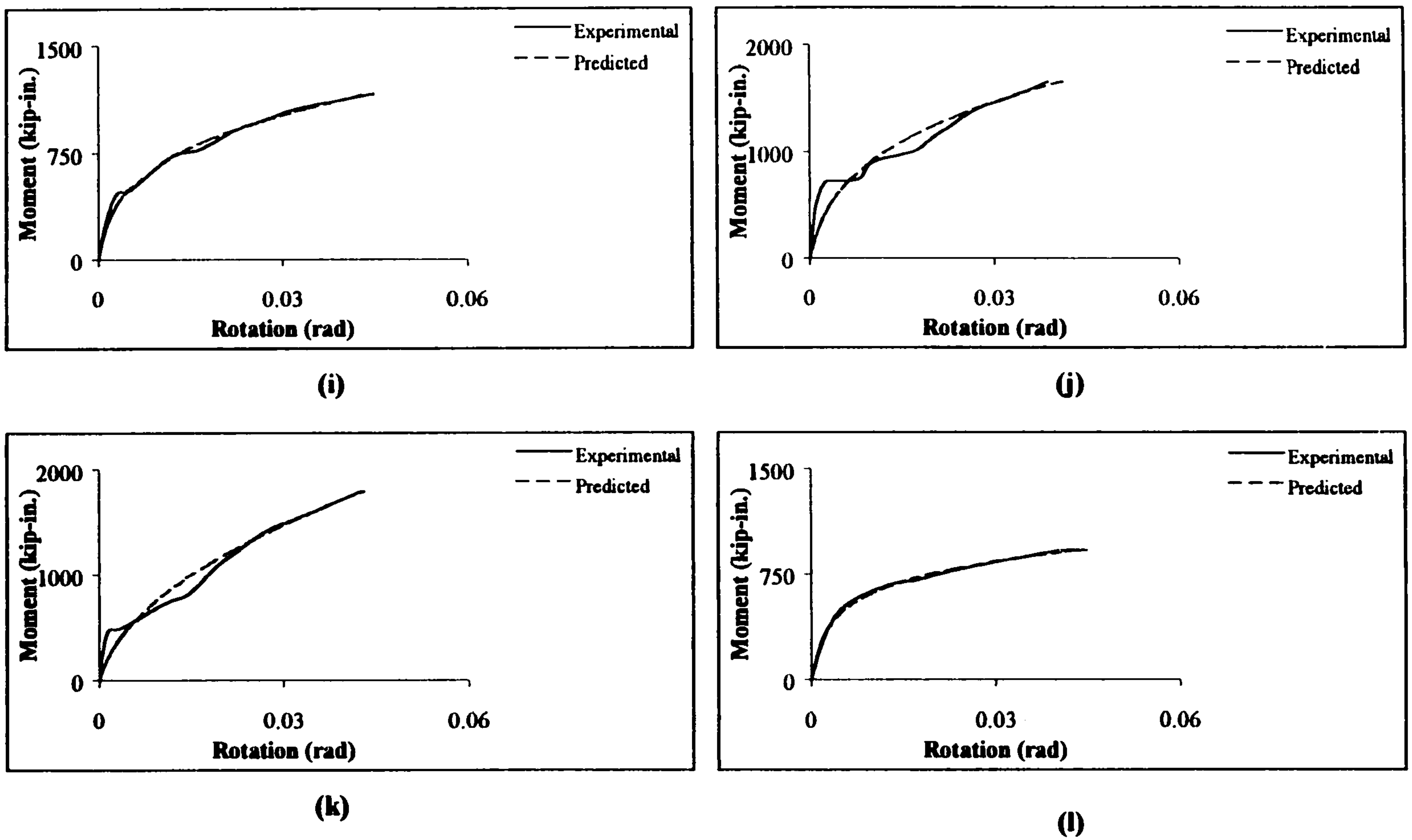

Fig. B-6 Comparison of Experimental Models and Moment-Rotation Enveloping Curves for Top and Seat Angle Connections:
(i) Test Specimen No. 9 (TS-6-6-3/4-3/4-3½-4-16); (j) Test Specimen No. 10 (TS-6-4-3/4-7/8-2½-4-16);
(k) Test Specimen No. 11 (TS-6-6-3/4-7/8-2½-4-16); (*l*) Test Specimen No. 12 (TS-6-6-3/4-7/8-4½-4-16)

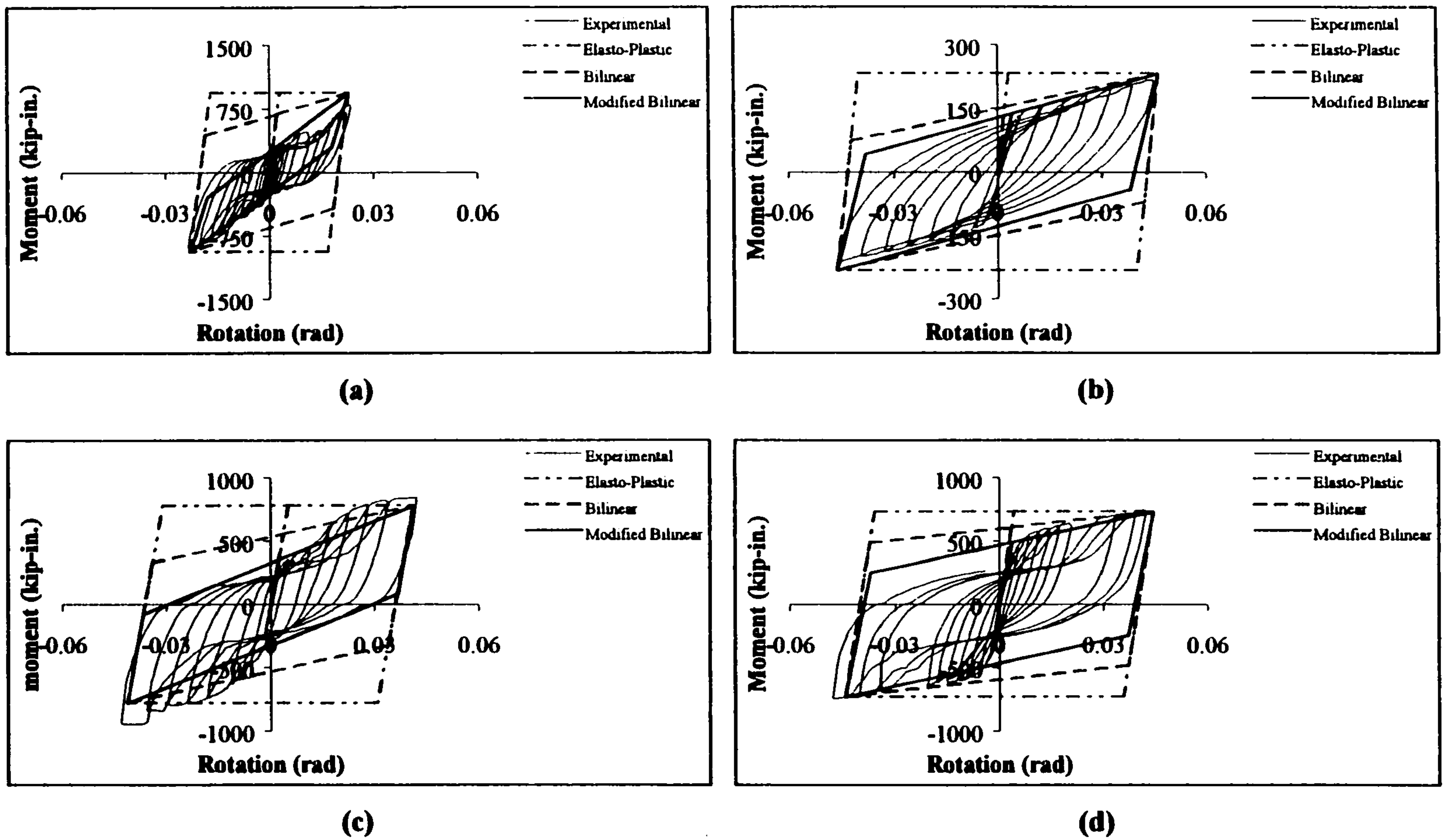

Fig. B-7 Comparison of Experimental Models and Moment-Rotation Hysteresis Loops for Top and Seat Angle Connections (Continued):
(a) Test Specimen No. 1 (TS-6-4-3/4-5/8-2½-5-14); (b) Test Specimen No. 2 (TS-6-6-3/8-5/8-4½-5-14); (c) Test Specimen No. 3 (TS-6-6-3/4-5/8-3½-5-14); (d) Test Specimen No. 4 (TS-6-6-3/4-5/8-4½-4-16)

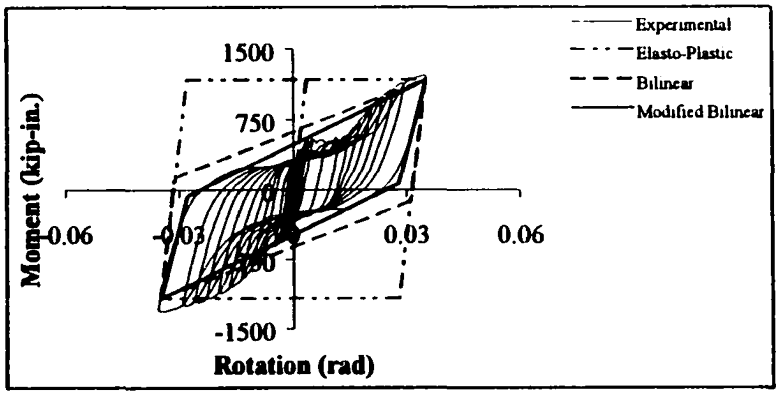

(e)

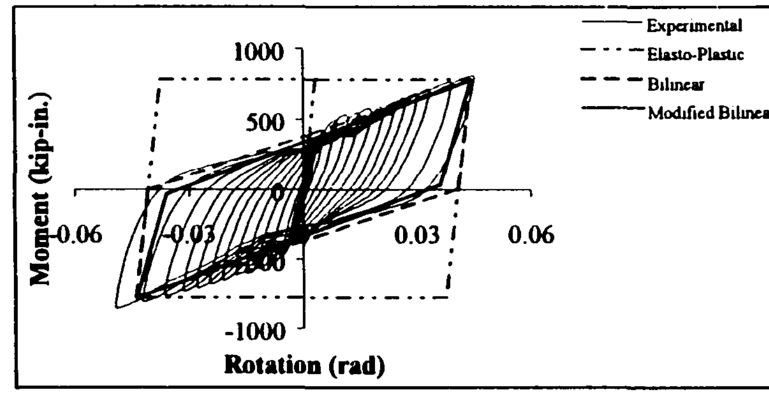

(f)

The comparison of predicted and experimental hysteresis loops are not presented for for this test specimen due to instrumentation malfunction

(g)

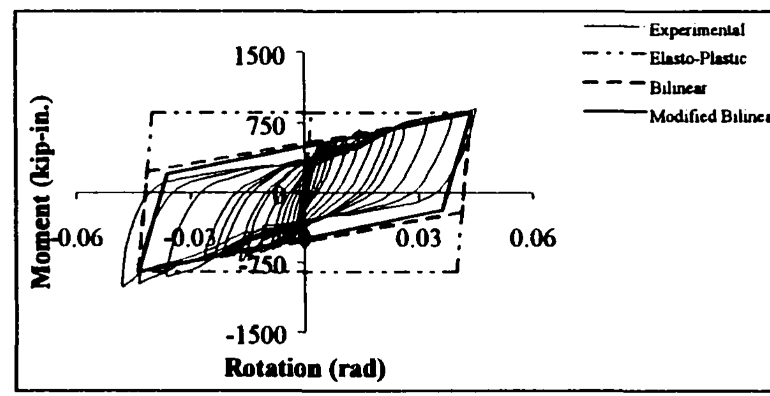

(h)

Fig. B-7 Comparison of Experimental Models and Moment-Rotation Hysteresis Loops for Top and Seat Angle Connections (Continued):
(e) Test Specimen No. 5 (TS-6-4-3/4-3/4-2½-5-14); (f) Test Specimen No. 6 (TS-6-4-1/2-3/4-2½-5-14);
(g) Test Specimen No. 7 (TS-6-4-3/4-3/4-2½-5-16); (h) Test Specimen No. 8 (TS-6-4-1/2-3/4-2½-4-16)

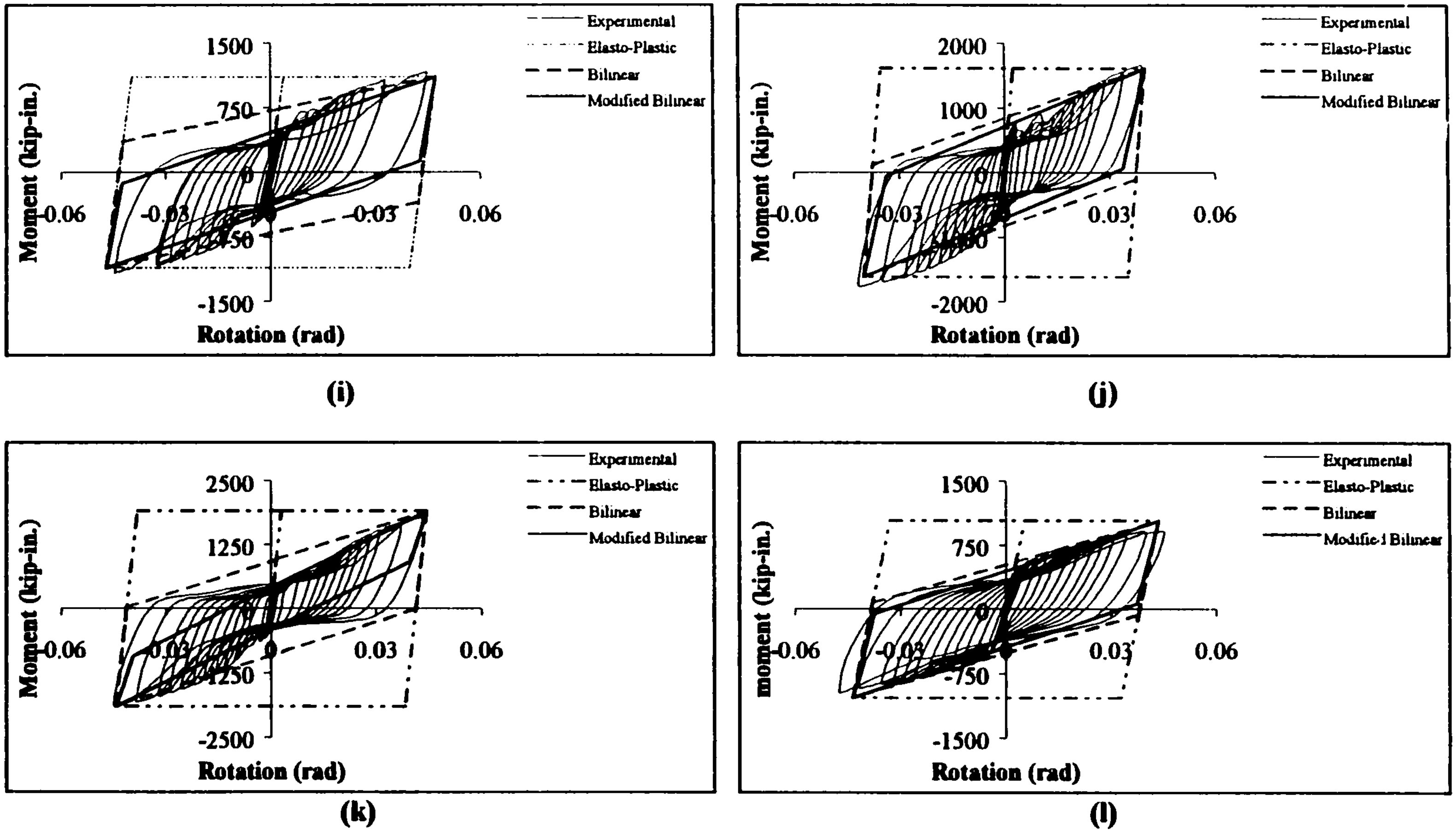

Fig. B-7 Comparison of Experimental Models and Moment-Rotation Hysteresis Loops for Top and Seat Angle Connections:
(i) Test Specimen No. 9 (TS-6-6-3/4-3/4-3½-4-16); (j) Test Specimen No. 10 (TS-6-4-3/4-7/8-2½-4-16); (k) Test Specimen No. 11 (TS-6-6-3/4-7/8-2½-4-16); (*l*) Test Specimen No. 12 (TS-6-6-3/4-7/8-4½-4-16)

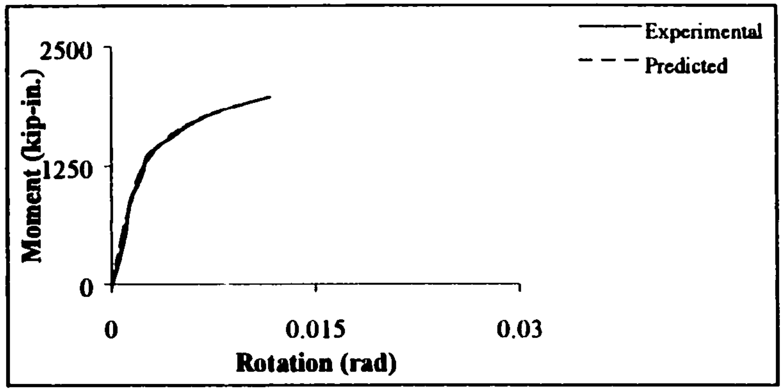

(a)

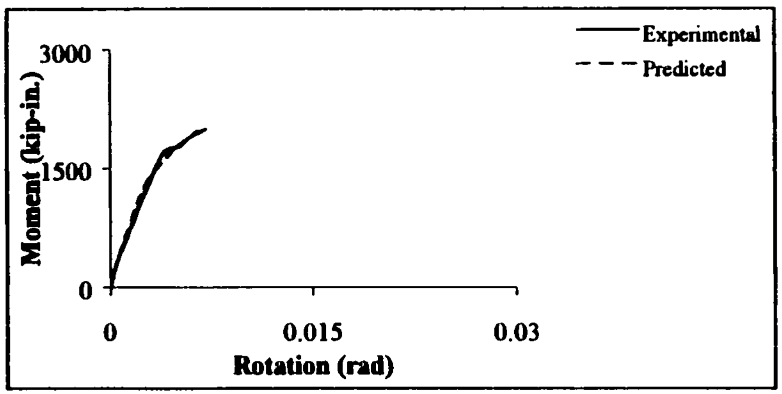

(b)

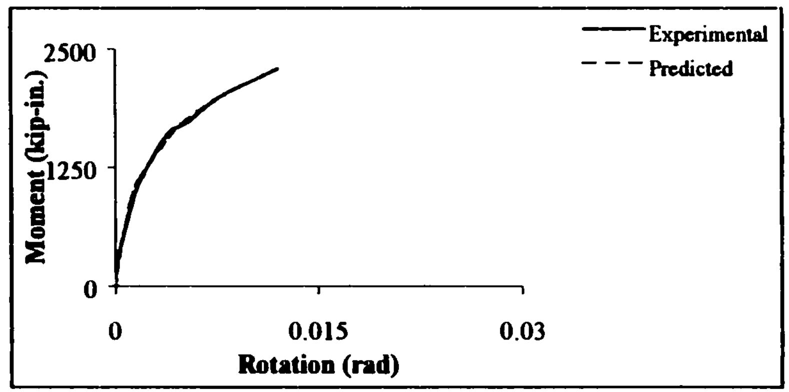

(c)

Fig. B-8 Comparison of Predicted and Experimental Moment-Rotation Enveloping Curves for Flush End-Plate Connections (Continued):
(a)Test Specimen No. 2 (FEP-II-6-18-1/2-3/4-$1^{5}/_{8}$-3-3); (b))Test Specimen No. 3 (FEP-II-6-18-5/8-3/4-$1^{5}/_{8}$-3-3);
(c) Test Specimen No. 4 (FEP-II-8-18-3/8-1-$1^{7}/_{8}$-3½-3½)

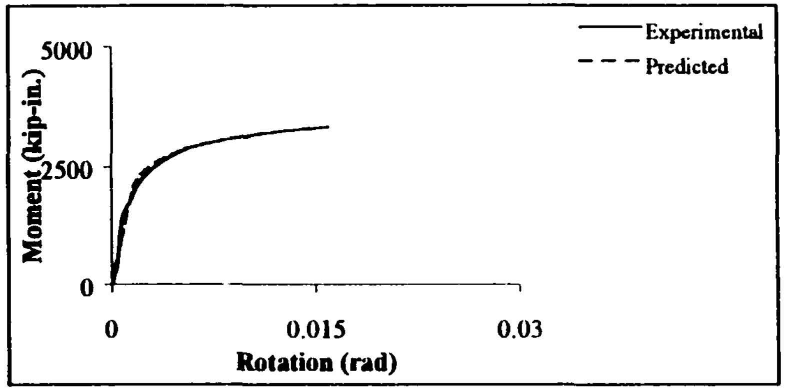

(d)

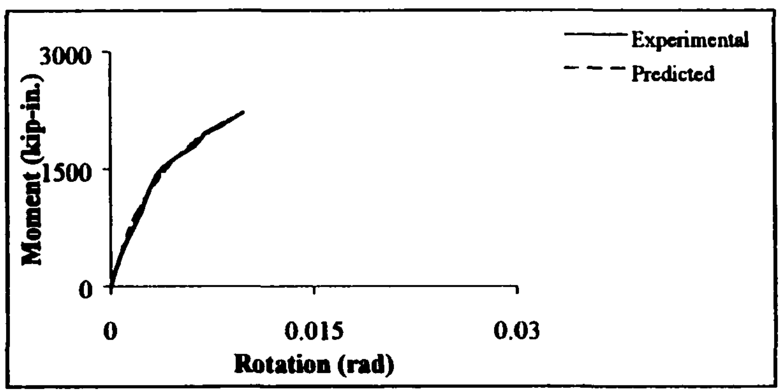

(e)

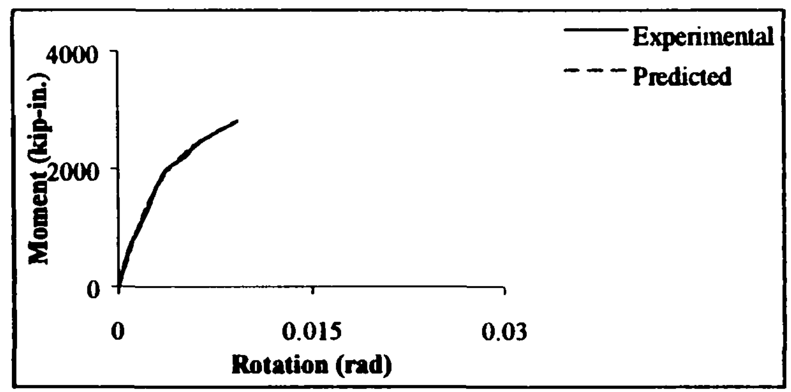

(f)

Fig. B-8 Comparison of Predicted and Experimental Moment-Rotation Enveloping Curves for Flush End-Plate Connections (Continued): (d) Test Specimen No. 5 (FEP-II-8-18-1/2-1-$1^{7}/_{8}$-3½-3½); (e) Test Specimen No. 7 (FEP-II-6-22-3/8-3/4-$1^{5}/_{8}$-3-3) (f) Test Specimen No. 8 (FEP-II-6-22-1/2-3/4-$1^{5}/_{8}$-3-3)

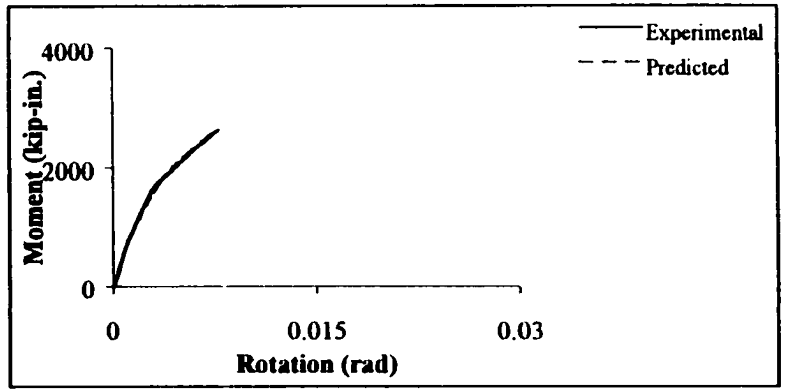

(g)

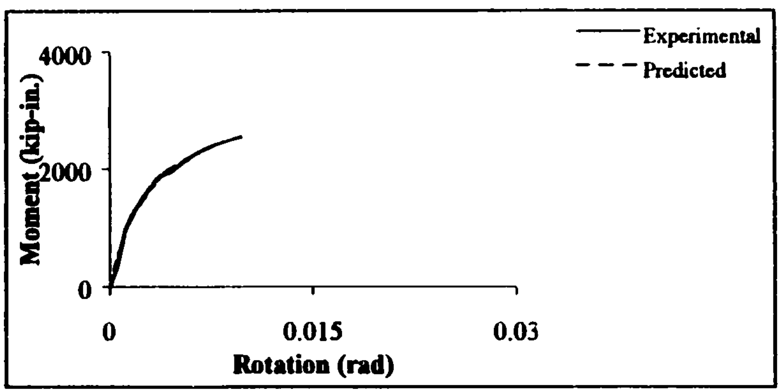

(h)

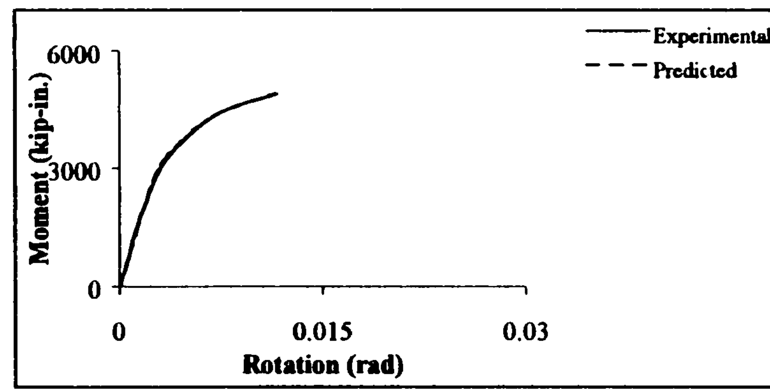

(i)

Fig. B-8 Comparison of Predicted and Experimental Moment-Rotation Enveloping Curves for Flush End-Plate Connections:
(g) Test Specimen No. 9 (FEP-II-6-22-5/8-3/4-$1^{5}/_{8}$-3-3); (h) Test Specimen No. 10 (FEP-II-8-22-3/8-1-$1^{7}/_{8}$-3½-3½);
(i) Test Specimen No. 12 (FEP-II-8-22-3/4-1-$1^{7}/_{8}$-3½-3½)

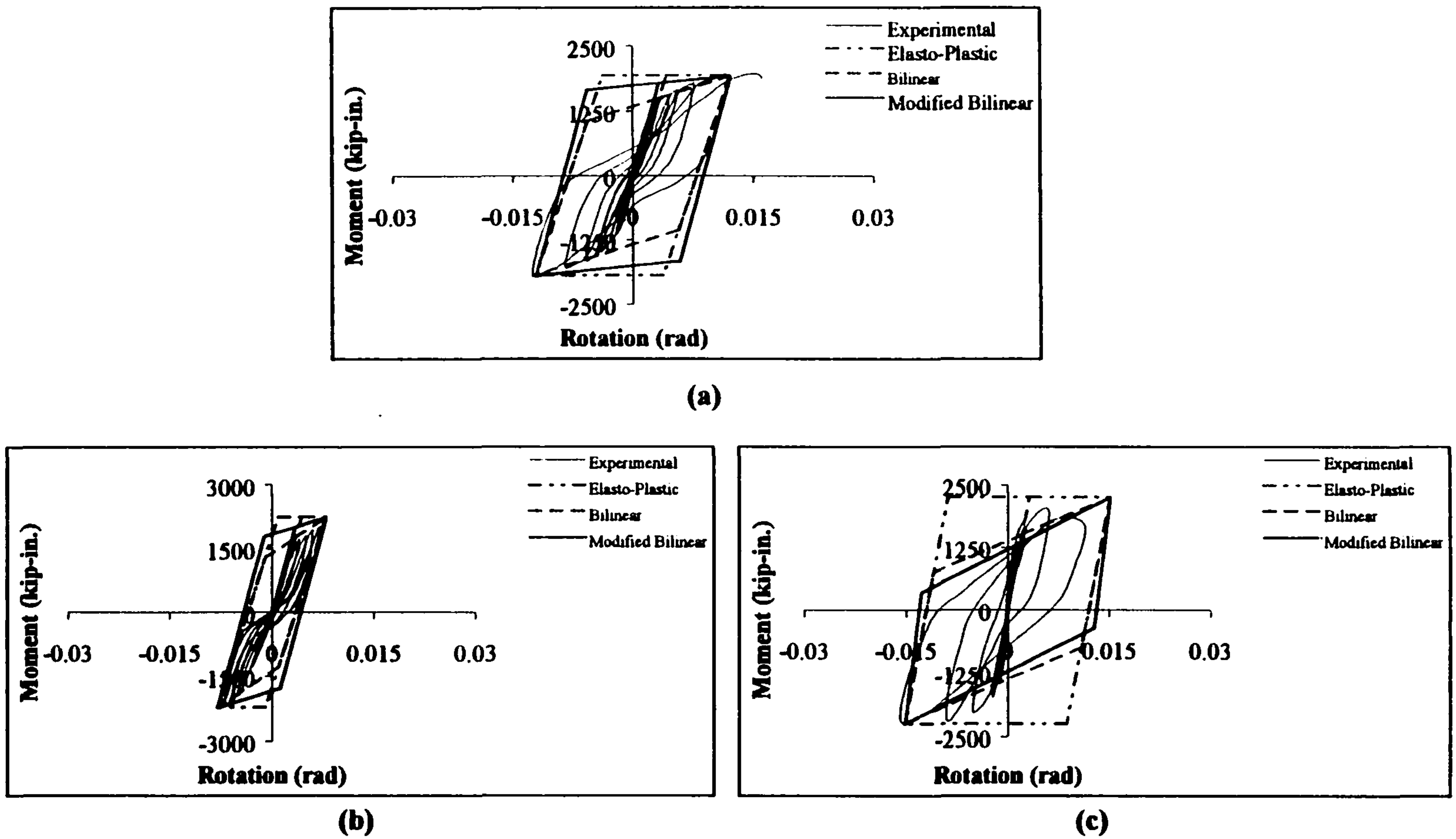

Fig. B-9 Comparison of Experimental Models and Moment-Rotation Hysteresis Loops for Flush End-Plate Connections (Continued): (a) Test Specimen No. 2 (FEP-II-6-18-1/2-3/4-1$^5/_8$-3-3); (b) Test Specimen No. 3 (FEP-II-6-18-5/8-3/4-1$^5/_8$-3-3); (c) Test Specimen No. 4 (FEP-II-8-18-3/8-1-1$^7/_8$-3½-3½)

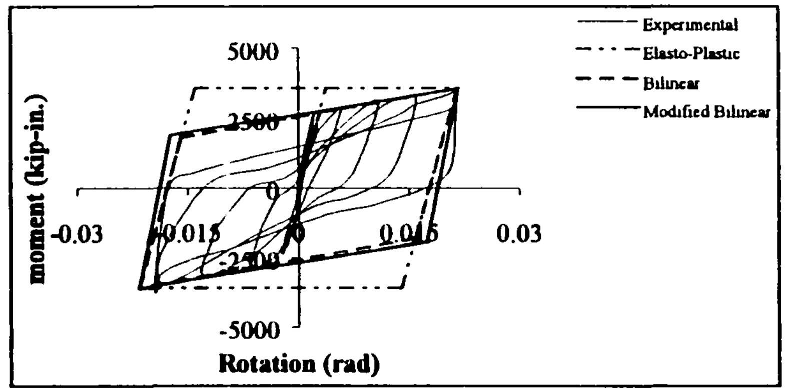

(d)

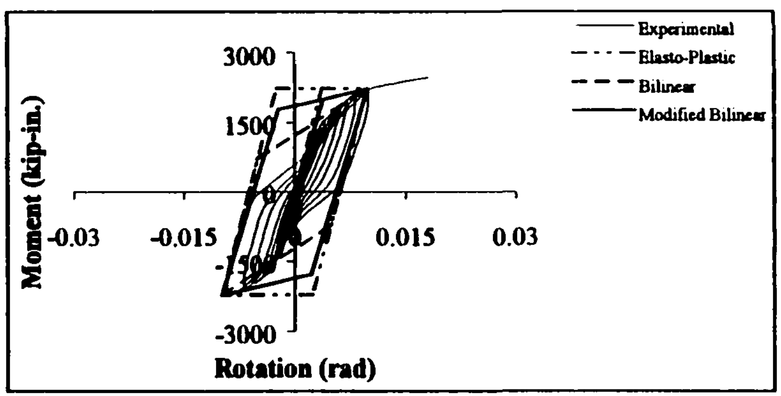

(e)

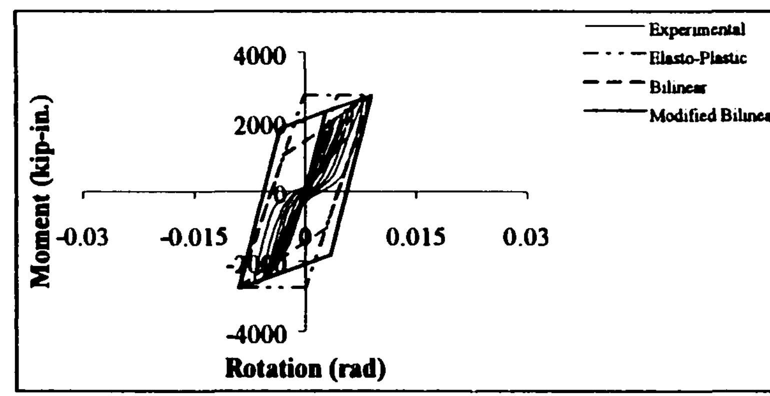

(f)

Fig. B-9 Comparison of Experimental Models and Moment-Rotation Hysteresis Loops for Flush End-Plate Connections (Continued): (d) Test Specimen No. 5 (FEP-II-8-18-1/2-1-1$^7/_8$-3½-3½); (e) Test Specimen No. 7 (FEP-II-6-22-3/8-3/4-1$^5/_8$-3-3); (f) Test Specimen No. 8 (FEP-II-6-22-1/2-3/4-1$^5/_8$-3-3)

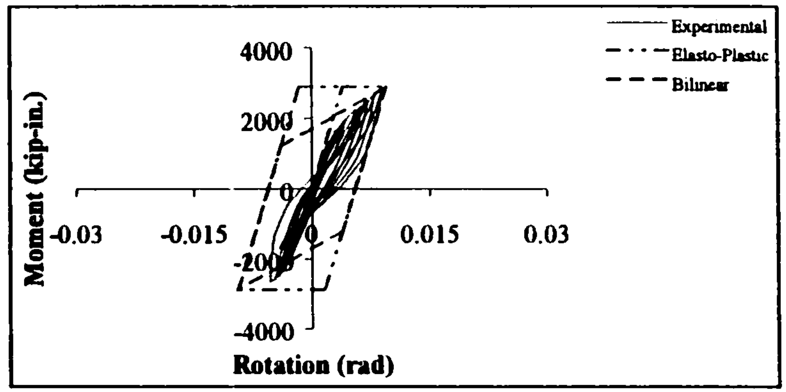

(g)

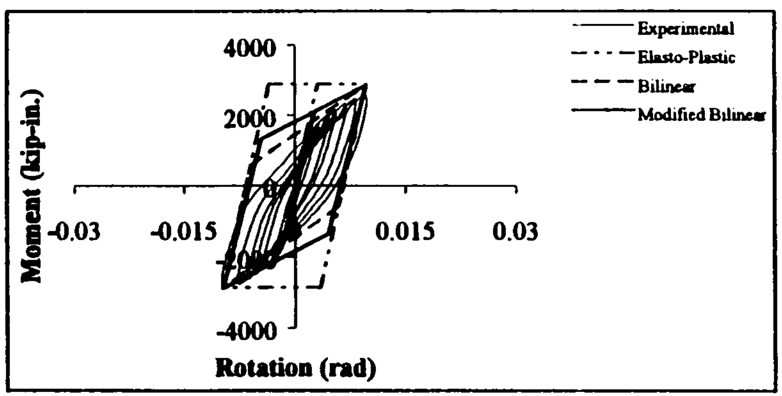

(h)

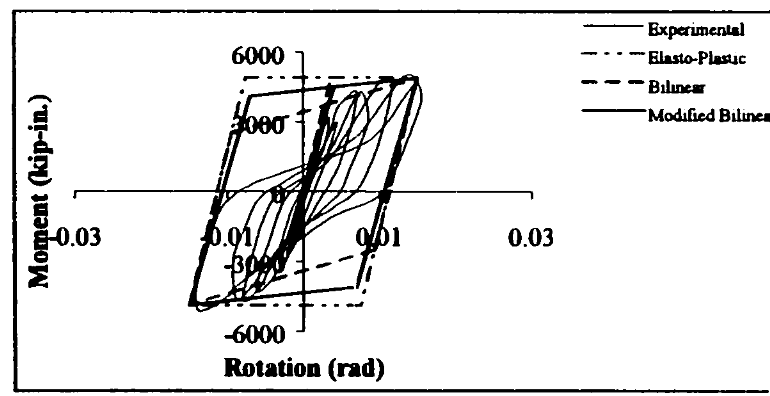

(i)

Fig. B-9 Comparison of Experimental Models and Moment-Rotation Hysteresis Loops for Flush End-Plate Connections:
(g) Test Specimen No. 9 (FEP-II-6-22-5/8-3/4-1$^5/_8$-3-3); (h) Test Specimen No. 10 (FEP-II-8-22-3/8-1-1$^7/_8$-3½-3½);
(i) Test Specimen No. 12 (FEP-II-8-22-3/4-1-1$^7/_8$-3½-3½)

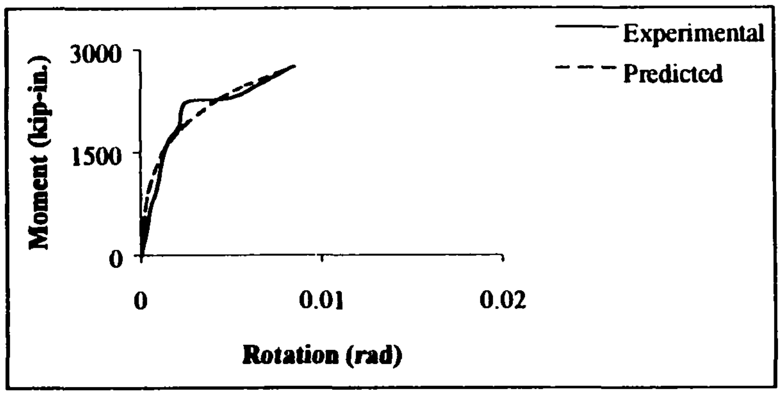

(a)

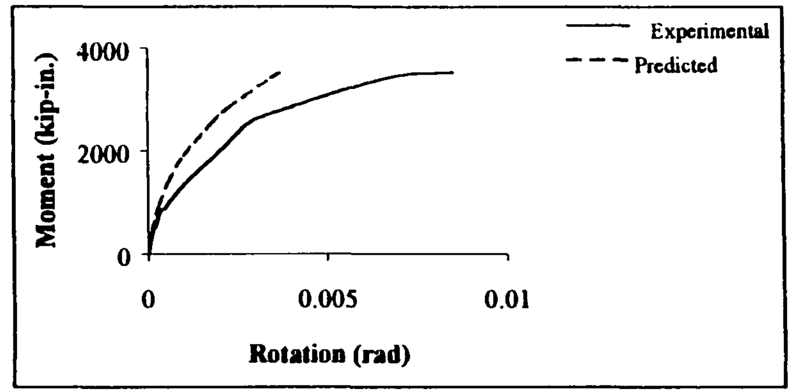

(b)

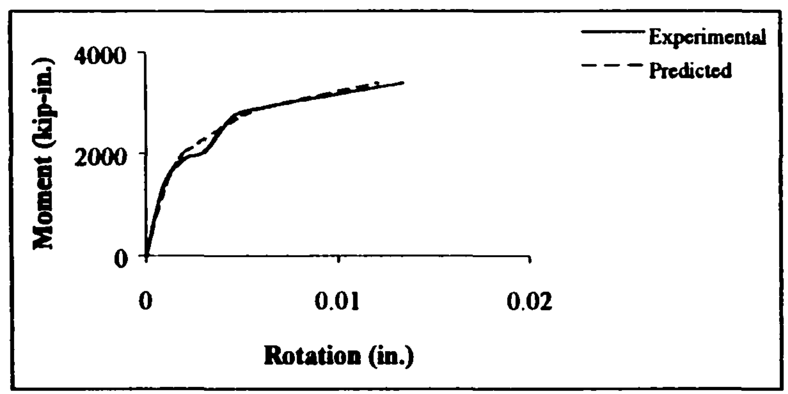

(c)

Fig. B-10 Comparison of Experimental Models and Moment-Rotation Enveloping Curves for Extended End-Plate Connections (Continued): (a)Test Specimen No. 1 (EEP-7-22½-1/2-3/4-1$^{3}/_{8}$-3½); (b) Test Specimen No. 2 (EEP-8-22½-5/8-7/8-1$^{1}/_{2}$-5½); (c) Test Specimen No. 3 (EEP-9-22½-1/2-1$^{1}/_{8}$-1$^{7}/_{8}$-3½)

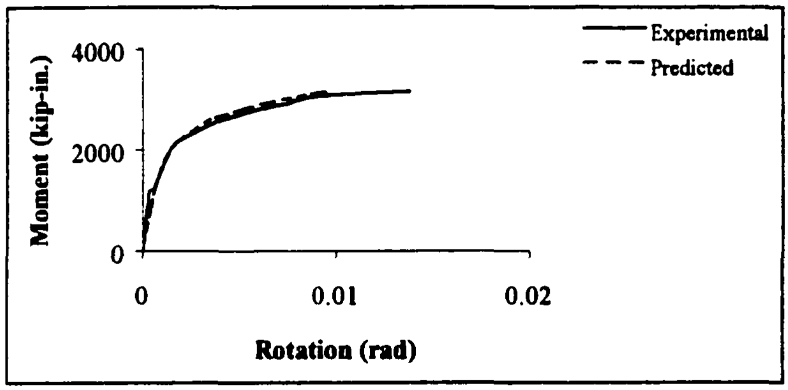

(d)

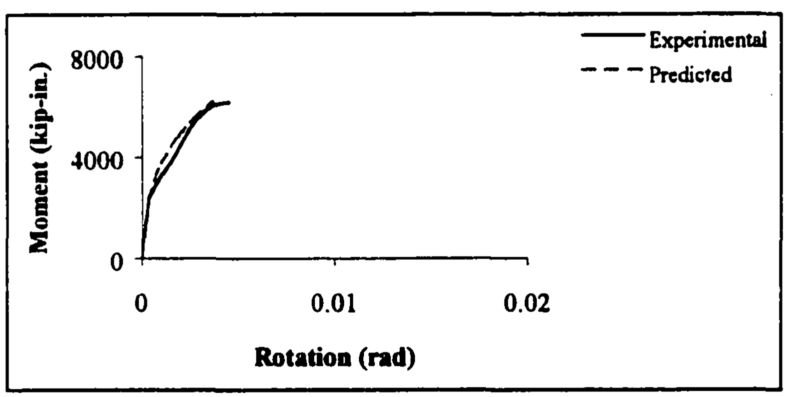

(e)

Fig. B-10 Comparison of Experimental Models and Moment-Rotation Enveloping Curves for Extended End-Plate Connections: (d) Test Specimen No. 4 (EEP-10-22½-1/2-7/8-1$^{3}/_{8}$-4½); (e) Test Specimen No. 8 (EEP-10-31-1/2-1$^{1}/_{8}$-1$^{1}/_{8}$-3½)

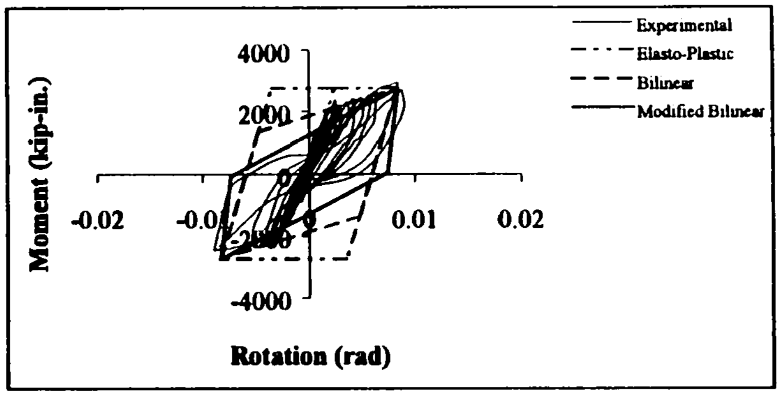

(a)

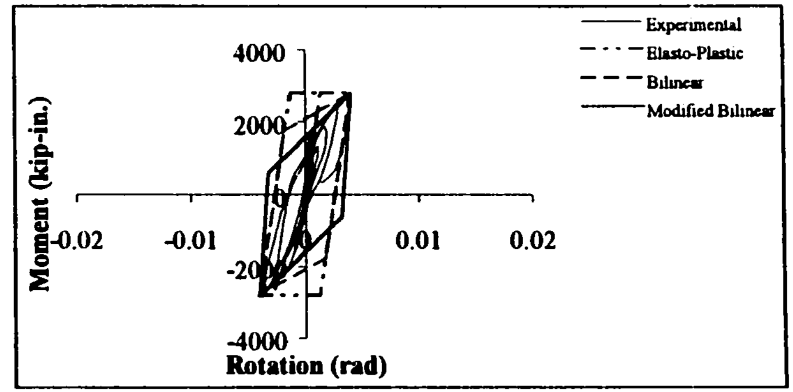

(b)

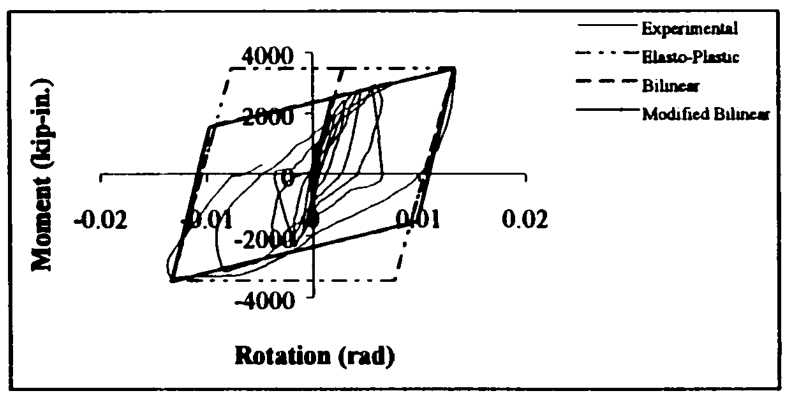

(c)

Fig. B-11 Comparison of Experimental Models and Moment-Rotation Hysteresis Loops for Extended End-Plate Connections (Continued): (a) Test Specimen No. 1 (EEP-7-22½-1/2-3/4-$1\frac{3}{8}$-3½); (b) Test Specimen No. 2 (EEP-8-22½-5/8-7/8-$1\frac{1}{2}$-5½); (c) Test Specimen No. 3 (EEP-9-22½-1/2-$1\frac{1}{8}$-$1\frac{7}{8}$-3½)

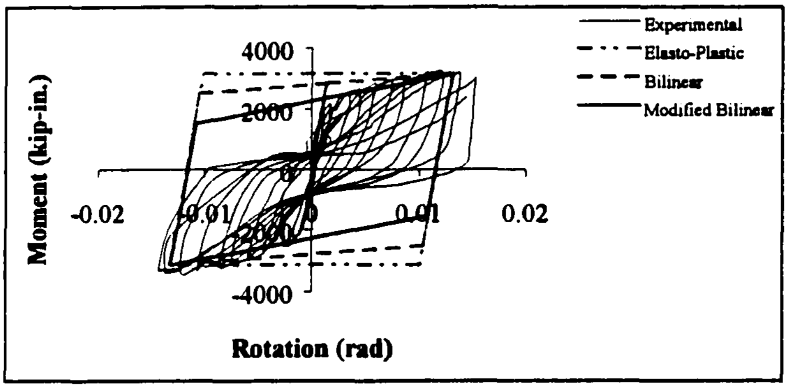

(d)

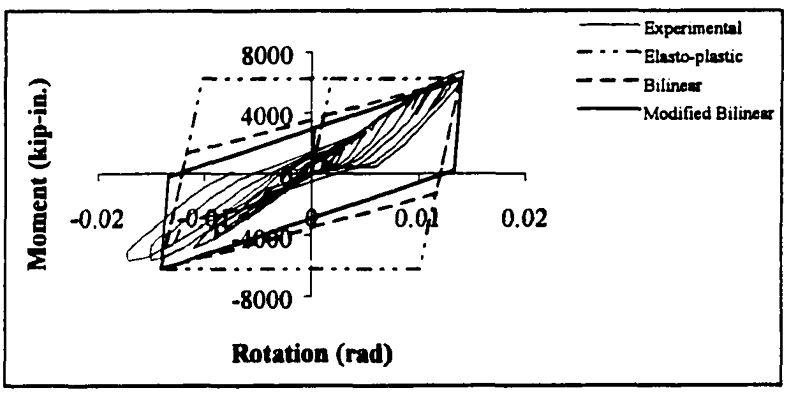

(e)

Fig. B-11 Comparison of Experimental Models and Moment Rotation Hysteresis Loops for Extended End-Plate Connections: (d) Test Specimen No. 4 (EEP-10-22½-1/2-7/8-1$^3/_8$-4½); (e) Test Specimen No. 8 (EEP-10-31-1/2-1$^1/_8$-1$^1/_8$-3½)